Preparation of benzoboroxole–modified gold surfaces for selective oligosaccharide and glycoprotein recognition

By Yazmin Kaur Tagger

A thesis submitted to The University of Birmingham
for the Degree of DOCTOR OF PHILOSOPHY
School of Chemical Engineering
College of Physical Sciences and Engineering
The University of Birmingham
Submitted November 2020

ABSTRACT

Recognition of oligosaccharides is associated with very limited specificity due to their strong solvation in water and the high degree of subtle structural variations between them. Here, oligosaccharide recognition sites are created on material surfaces with unmatched, binary on–off binding behaviour, sharply discriminating a target oligosaccharide over closely related carbohydrate structures. The basis for the superselective binding behaviour relies on the highly efficient generation of a pure, high order complex of the oligosaccharide target with synthetic carbohydrate receptor sites, in which the spatial arrangement of the multiple receptors in the complex is preserved upon material surface incorporation. The synthetic binding scaffolds can be easily tailored to recognise different oligosaccharides and glycoconjugates, opening up a realm of possibilities for their use in a wide field of applications, ranging from life sciences to diagnostics.

In this thesis, a modular synthetic approach is to be created that can harness both the construction of high–yield, complex oligosaccharide–synthetic carbohydrate receptor assemblies and the precise generation of surface–confined templated binding sites. Therefore, recognition sites of unparalleled oligosaccharide discrimination are to be created.

The synthesis and characterisation of various self–assembled monolayers (SAMs) and oligosaccharide–synthetic carbohydrate receptor complexes are to be described alongside molecular imprinting studies which will determine the binding of various saccharides. Surface plasmon resonance (SPR) is to be used and from these

experiments, the selectivity and sensitivity of the binding can be calculated. An overview of the thesis layout comprising the sections of this work is listed below.

Chapter 1 – A Review of Oligosaccharide and Glycoprotein Sensing Systems

This chapter presents an:

a) Introduction to glycosylation and its role in the development of diseases such as cancer.

b) Introduction to self–assembled monolayers (SAMs) and their application in fabricating biosensors such as molecular imprinted surfaces using radical polymerisation processes.

c) The improvements in imprinting biomolecules such as glycoproteins.

Chapter 2 – Surface Characterisation Techniques.

Outlines the background theory behind each of the surface characterisation techniques and protein analysis techniques used in this work.

Chapter 3 – Results I: The formation and characterisation of the DSA SAM and the cross–linking of AABOB onto a DSA SAM.

This chapter explores the characterisation of the initial surface along with the conditions for the cross–linking of benzoboroxole carbohydrate receptors to the initial

surface. X–ray photoelectron spectroscopy (XPS), contact angle and ellipsometry data is used to determine the surface properties.

Chapter 4 – Results II: Complexation and Molecular Imprinting

This chapter examines all the surface plasmon resonance (SPR) data of the molecular imprinting, with binding affinities calculated too. The binding affinties were calculated using Sigmaplot, version 13 to give the selectivity of the surfaces and different sugars were used to detect the selectivity.

Chapter 5 – Conclusions and Future Work

Provides and overview of each chapter alongside the future studies that could be undertaken from the basis of this thesis.

Chapter 6 – Experimental Procedures, Protocols and Synthesis.

Describes the experimental procedures used during the investigations performed in this work.

Chapter 7 – References

Chapter 8 – Appendix

The journal publication mentioned in the thesis.

ACKNOWLEDGMENTS

This thesis is the outcome of three years research carried out at the School of Chemical Engineering, University of Birmingham and this work would have not been possible without the great supervision and support of Prof. P. M. Mendes and my fellow colleagues.

Prof. Paula Mendes has been an extremely encouraging supervisor throughout my time here in the group and has helped me achieve the most from my research. Throughout her sabbatical, she was always an email or skype call away, and I never felt unsupported. Her continued optimism helped me through the difficult moments during my research and always allowed for experiences and opportunities to improve my work and research outcome. Paula is definitely an inspiration to many in the field, including women in research. It goes without saying, thank you Paula.

Along with Paula, Dr Stefano Tommasone, my co–supervisor for my research, and a research fellow within the group that has been a very important driver for the progression of the research. He has given me the reassurance and encouragement throughout for my research, the numerous Costa trips and I can only say thank you Stefano.

I would also like to thank the other Post Doc researchers who helped me during my PhD. Thank you to Dr Eduardo Anaya–Plaza and Dr Marcos Fernandez–Villamarin, who were available and willing to help with the chemistry of the project. Without their aid, I do not think the research could develop to where it has. Also, Dr Josh Gibson

has been an amazing help with the XPS analysis, allowing my knowledge of the technique and the analysis aid to develop a meaningful understanding of the surface science developed quickly and thoroughly within my research.

Special thank you must go to the members of the Mendes group past and present, namely Barbara Gomes, Philippa Mitchell, Giuseppe Di Palma, Kamlesh Patel, Joshua Norman, Francia Allabush, Barbara Simoes, Alice Di Pasquale, Pushpa Patel, Laura Brooks and Laura Buccoli.

Many thanks are in order to the technical staff of Science City, Chemical Engineering at Birmingham, who have made working in the laboratories a delight and willing to sort out any issues there may have been.

Finally, thank you to the people who have dealt with me the longest, my family and friends. Mum, Dad and Arun, I am eternally grateful for your support throughout my life and believe this could not have been possible without you all. Mum, thank you for constantly supporting me, both educationally and personally. Just know that the tears were for the progression of the project and the thesis submission. Jemma, my best friend, thank you for your irreplaceable company and friendship over the years, you are always able to help me get out of a negative sight and are always a call away if I needed you. Thank you to Kate and Rita, definitely a call or meet up away whenever I need someone to listen to me. I also would like to thank my selected family members that are forever supporting my academic goals, regardless of the hurdles that come in the way.

Therefore, I would like to dedicate my thesis to my fallen angels that I lost far too soon. Without your undivided love for me throughout my childhood and early adult life, I would not be the person I am today. As your eldest grandchild, I can only imagine how proud you two would have been to see my academic achievements. Love you always, Manjit Kaur and Tarsem Singh.

LIST OF ABBREVIATIONS

- APS: Ammonium persulfate
- ATRP**:** Atom transfer radical polymerization
- AUC: Area under the ROC curve
- BOB: Benzoboroxole
- DSA: Disulphide acrylamide – N, N' bis(acryoyl) cystamine
- MBA: N,N'–Methylenebisacrylamide
- MIP: Molecularly imprinted polymer
- NMR: Nuclear magnetic resonance
- PCa: Prostate cancer
- PSA: Prostate specific antigen
- SAM: Self assembled monolayer
- SPP: Surface plasmon polaritons
- SPW: Surface plasmon wave
- SPR: Surface plasmon resonance
- TIR: total internal reflection
- XPS: X–ray photoelectron spectroscopy
- UHP: Ultra high purity

TABLE OF CONTENTS

LIST OF TABLES

LIST OF FIGURES

CHAPTER 1 – A REVIEW OF GLYCOPROTEIN SENSING SYSTEMS

Abstract: *This chapter presents a review of the literature that covers a broad range of topics, providing the reader an understanding of the history and recent advances in recognising glycoproteins. The chapter begins by introducing carbohydrates and the role they play in nature, before discussing glycans and the process of glycosylation. The process of aberrant glycosylation in disease is discussed, with cancer briefly mentioned. The glycan–binding entities mentioned in this section include natural receptors; antibodies and lectins. As well as natural receptors, synthetic receptors are explored in the review, such as aptamers, boronic acids and benzoboroxoles.*

The latter half of the chapter introduces how nanotechnology has been employed to develop recognition platforms with a focus on use of self–assembled structures as the basis of a sensor. Self–assembled monolayers (SAMs) have been used to develop newer recognising platforms such as molecular imprinting. These are discussed as well as the different forms of polymerisation that can be employed in the fabrication of synthetic receptors. A variety of molecular imprinting systems have been reported recently for glycoproteins. Particular attention is paid to the systems that have boron functionalities incorporated within their design to target saccharide chains of biomolecules. The review is concluded by summarising any challenges faced on oligosaccharide and glycoprotein detection and the aim of the research conducted in this thesis.

1.1 Introduction to carbohydrates

Carbohydrates are fundamental components which are used in nature for multiple physiological processes. Carbohydrates, also called saccharides show a broad array of structural sizes and complexities, which range from the most basic monosaccharide (examples include glucose, fructose and galactose) to larger, more complex structures found at cell interfaces. Their varied characteristics enable them to be used in a variety of functions and it is advised that a certain amount of carbohydrate–containing foods must be consumed regularly to maintain normal blood glucose levels [1] and to supply the brain with sufficient amounts of glucose. Inadequate amounts of glucose may lead to adverse effects including a decline in normal brain functions, demonstrated by impaired outcomes in tests of memory and cognition [2]. Inherently fundamental to biological systems, the demand for suitable detection methods that are able to provide information on the type of saccharide and the concentrations are required.

1.1.1 Monosaccharides

The monosaccharide is the most basic unit of any saccharide structure, with each unit comprised of a carbon backbone with hydroxy moieties spaced at distinct intervals along the length of the chain. The typical empirical formula of a saccharide for each unit is $(C–H_2O)n$, with n between 3 and 7 [3].

Saccharides can be presented in many different ways, with the most commonly used projections, Fischer or Haworth, shown in fig. 1. Respectively, saccharides are presented in its open chain or cyclic form. The Fischer projection has the advantage

where the carbon stereo centres are more clearly observed, whereas Haworth cyclic projection provides a presentation of the spatial arrangements of the hydroxyl moieties better. An example of both configurations are shown in fig. 1 a) using the D–glucose molecule as an example b) shows the L–configuration and D–configuration for glucose [4, 5].

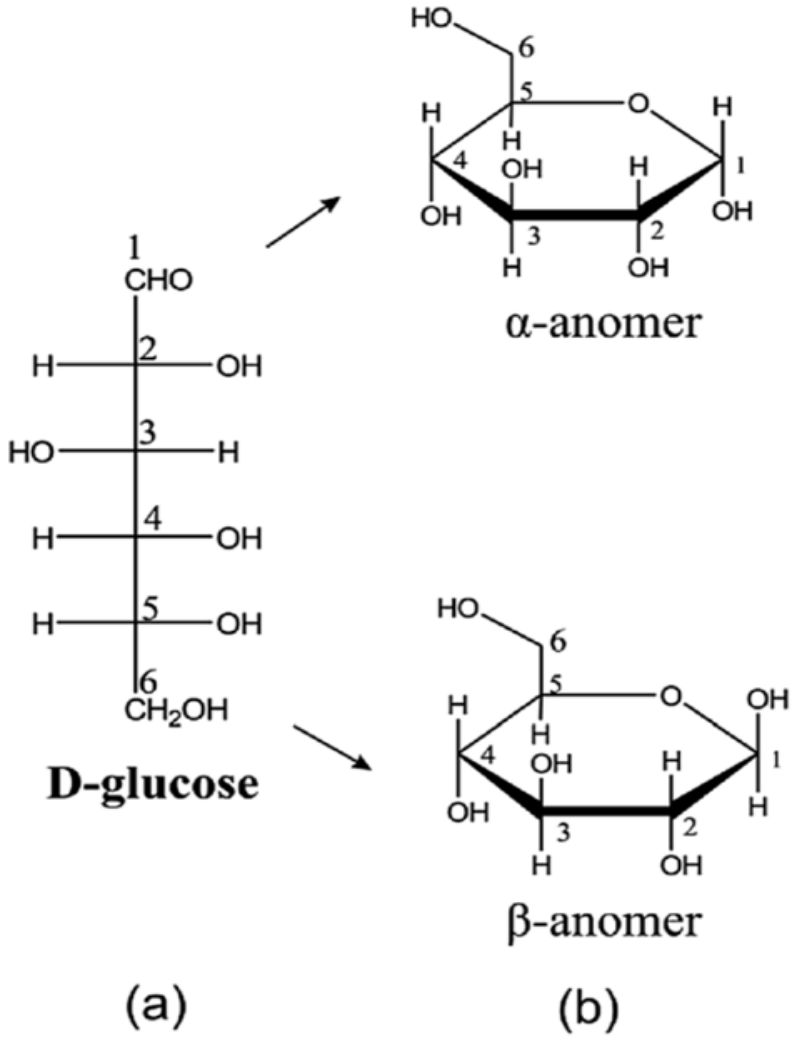

Figure 1: Configurations of monosaccharides, a) Fischer and b) Haworth as well as demonstrating the L– and D–configuration.

Monosaccharides are inherently heterogenic in their chemical nature and this is due to the high number of chiral carbons along the length of each molecule. This has led to the development of methods that enable the distinction between subtle differences in the position of hydroxyl moieties of the molecules [6].

1.1.2 Di–, oligo– and polysaccharides

Disaccharides are carbohydrates that are made up of two monosaccharide subunits. Sometimes, the disaccharides are also used as an alternative to monosaccharides as they share various common properties. Examples of disaccharides are sucrose, maltose and lactose, structure of sucrose is shown below.

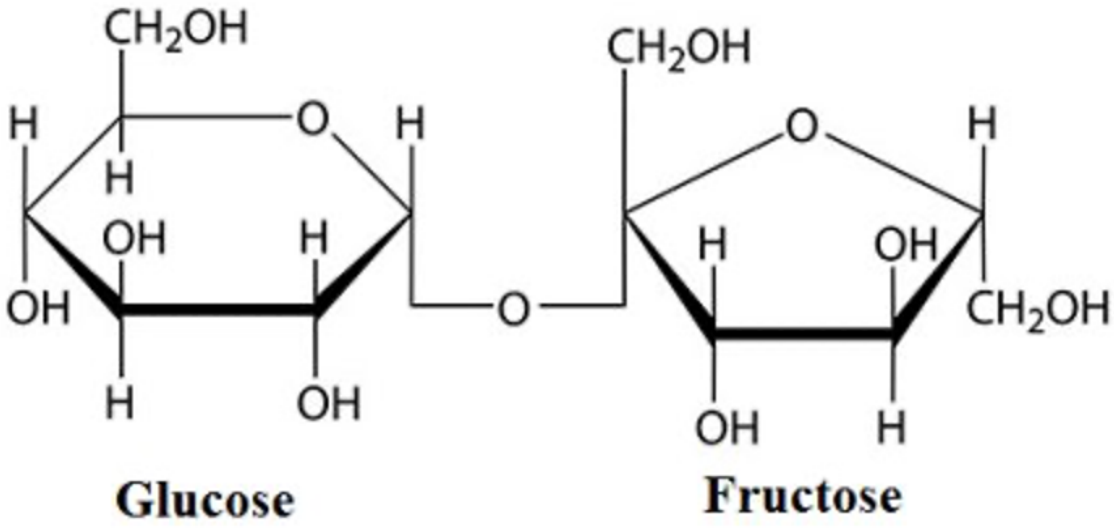

Figure 2: Chemical structure of disaccharide sucrose [image taken from [7].

Sucrose is the most important carbohydrate belonging to the class of disaccharides. Sucrose is made up of a glucose and a fructose unit, has shown in fig. 2. Joined

together by a glycosidic bond between carbon 1 of the glucose unit and carbon 2 of fructose.

Other examples of disaccharides include lactose and maltose. Lactose has the same formula as sucrose ($C_{12}H_{22}O_{11}$) and is made up of a galactose and glucose unit. The glycosidic bond is present of the first carbon of glucose and the forth carbon of galactose, creating a C1–C4 glycosidic bond. Maltose also has a 1–4 glycosidic bond, with two of the glucose units bound. However, the orientation of the two glucose molecules are different, with the first glucose molecule in its alpha orientation and the second glucose remaining in its aldehyde functional group, which can be either an alpha or a beta orientation.

Three to ten monosaccharide units that are bound together are considered oligosaccharides. The glycosidic linkage between two monosaccharide units is achieved by condensation reactions between the anomeric carbon (glycoside) and a hydroxyl group on opposing saccharide (aglycone). The wide array of these linkages in concert with the wide variety of monosaccharides and their many isomeric forms makes complex carbohydrates information–rich molecules [8].

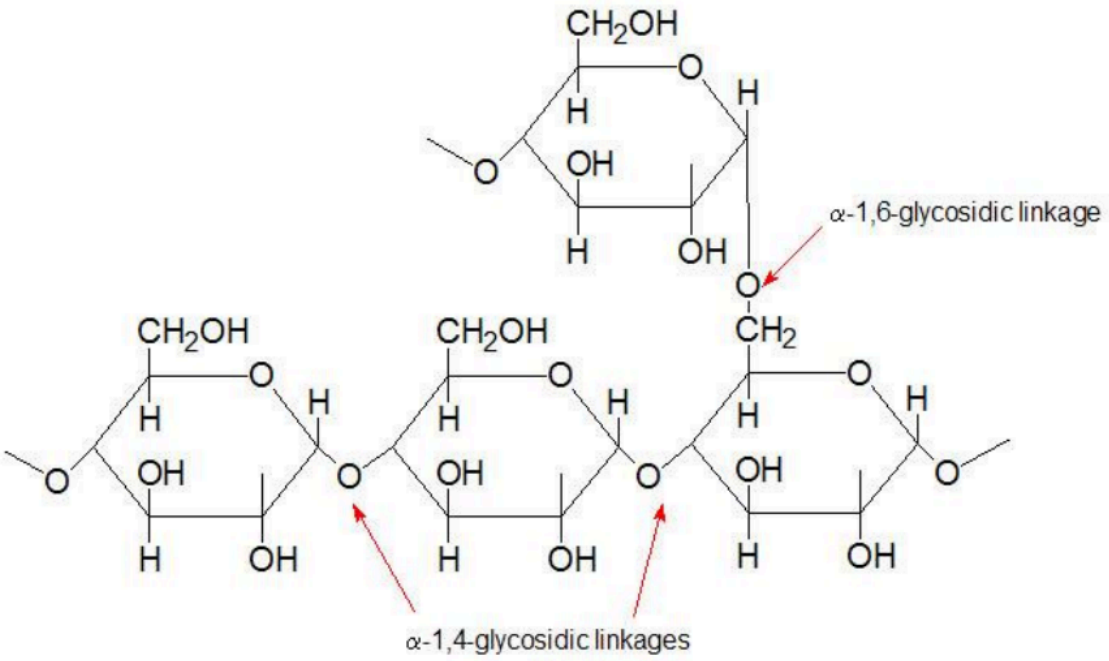

Figure 3: Chains of glucose molecules joined by α–1,4–glycosidic bonds are linked by an α–1,6–glycosidic bond to create a branch point.

Oligosaccharides are involved in many fundamental biological processes. However, relatively little is known about the precise molecular mechanism of action of these macromolecules, because the complexity of these structures impeded their synthesis by chemical methods analogous to those employed to create oligonucleotides and peptides [9].

A long–chain carbohydrate that is made up of monosaccharides is known as a polysaccharide, connected by glycosidic bonds. A typical polysaccharide is between 200 and 2500 monosaccharides long. The chemical formula of a polysaccharide is typically $(C_6H_{10}O_5)_n$, where n is normally larger than 40, shown in fig.4.

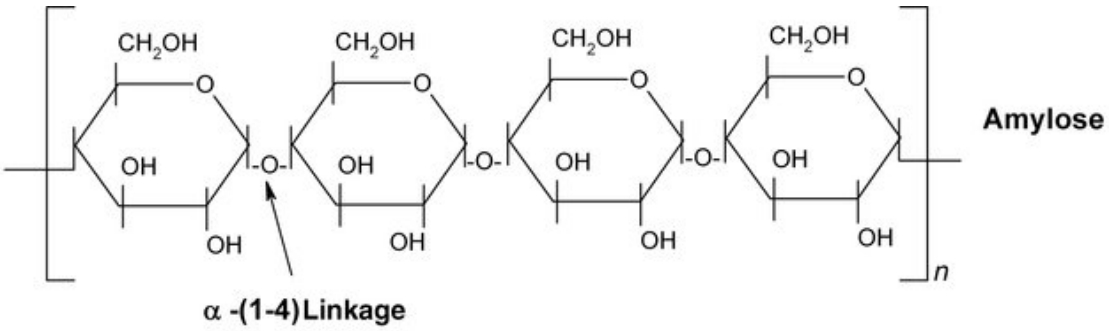

Figure 4: Generic structure of the polysaccharide, starch [image taken from [10].

1.2 Glycans

Glycans occur as free polysaccharides or as mono, oligo or polysaccharides conjugated to a wide variety of biological molecules, including glycoproteins, glycolipids and peptidoglycans [11], with examples shown in fig. 5 [12]. In contrast to RNA, DNA and protein synthesis, glycan biosynthesis is not a template–driven process. The assembly of glycans occurs by the expression and activity levels of a series of enzymes present in cells via glycosylation [13]. Glycans are generated from a limited number of monosaccharides. Glycans are characterised by a remarkable structural diversity due to the nature and sequence of the constituent units, the possible branching of the carbohydrate chains and the configuration and position of glycosidic linkages. Monosaccharides have multiple hydroxyl moieties that can serve as linking groups, with the glycosidic bond at the anomeric carbon having either α or β stereochemistry and lead to a wide range of potential linkages between two monosaccharide units [14]. In addition, glycans can be further diversified by a range of modifications, including phosphorylation, sulfation, and acetylation [15]. Playing important roles in various physiological and pathophysiological events, glycans are present in cell growth, cell signalling, cell–cell interactions, differentiation and tumour growth [16].

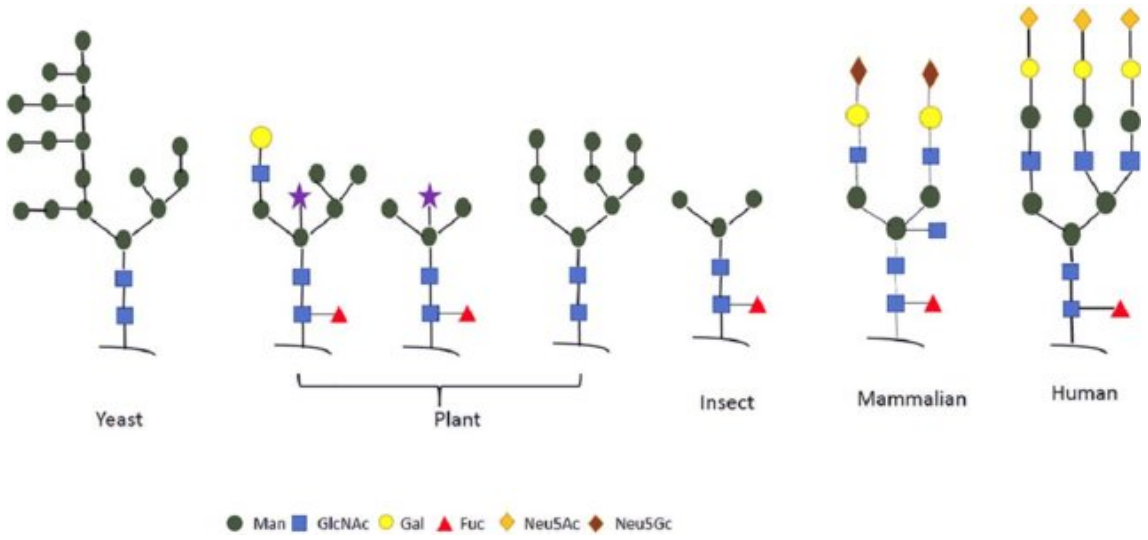

Figure 5: Examples of glycans that can be found in nature, ranging from those glycans which are present in plants, yeast and insects followed by humans and animals [image taken from [17]].

During the development and progression of diseases such as cancer, glycan expression can be altered, leading in changes glycan structures that can potentially be used to accurately identify the disease at an early stage. In addition to their clinical value in disease diagnosis and management, glycans are ideal markers for identifying and isolating specific cell types, including stem cell lineages for therapeutic transplantation [18], an emerging class of therapeutics [19]. Amongst other facets, glycans are key targets in drug discovery [20] and are present on the surface of a variety of pathogens and malignant cells, making them ideal targets for vaccines.

1.3 Lewis antigens

Lewis antigens (Le^a and Le^b) are synthesized by two independent fucosyltransferases. Le^a is a precursor molecule for the synthesis of Le^b, shown in fig.6 [21].

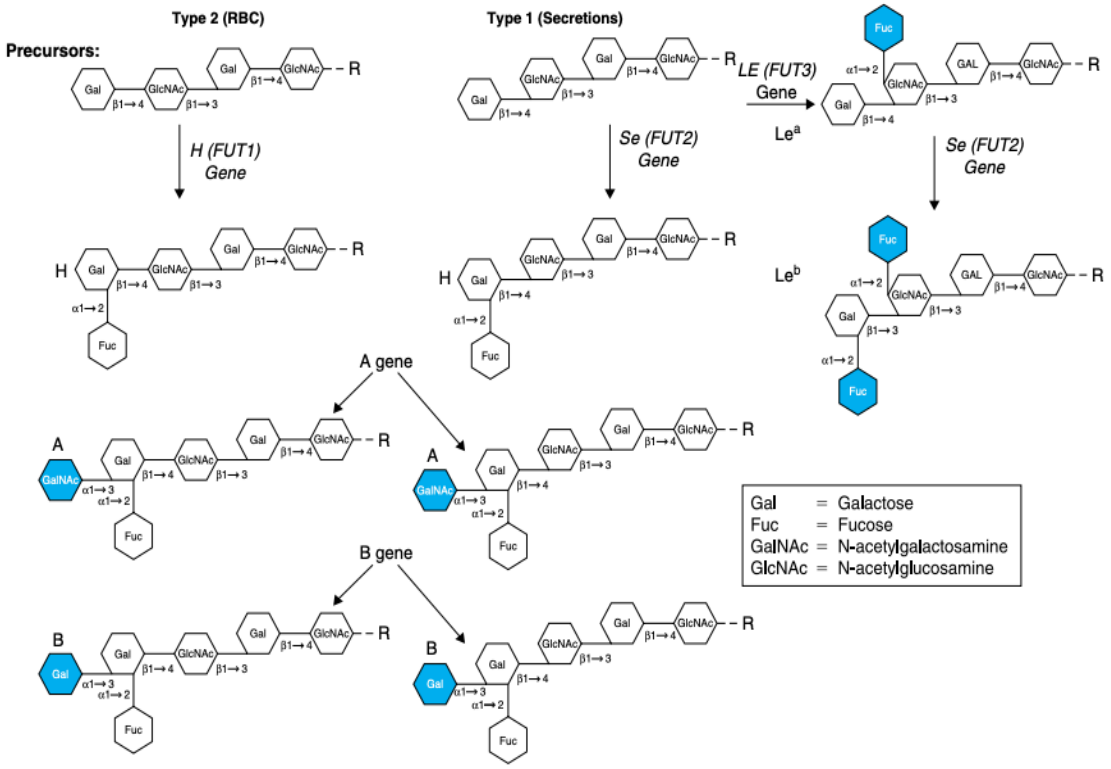

Figure 6: Synthesis of Lewis antigens [image taken from [22]].

Fig. 6 shows the oligosaccharide precursor core type 1 and type 2 and how the structures differ. The structures only differ in the linkage between the terminal galactose (Gal) and the N–acetylglucosamine (GkNAc). The area in blue demonstrates the terminal carbohydrates that define the antigens.

Not intrinsic to the red blood cell membrane, Lewis antigens are synthesised by the intestinal epithelial cells, circulated in the plasma free or bound to lipoproteins and then passively adsorbed onto the red blood cell membrane [23].

Le^a and Le^b are synthesized in a stepwise fashion by two separate fucosyltransferase. Fucosyltransferase adds fucose to GlcNAC (N–acetylglucosamine), and Se(FUT2), which adds fucose on the Gal (galactose) moiety. The enzyme encoded by LE(FUT3) is responsible for synthesis of Le^a resulting in the Le(a+b–) phenotype [24].

1.4 Introduction to Glycosylation

Glycosylation plays a critical role in the determination of protein structure, function and stability [25]. Structurally, glycosylation is known to affect the three dimensional configuration of proteins. This is particularly important when considering protein–protein interactions such as those that occur between protein ligands and their cognate receptors or in the creation of other large macromolecular complexes [26]. Secreted proteins include hormones and cytokines and they are glycosylated, showing to impact in determining their activity when bound to receptors [27].

Protein glycosylation is thought to have multiple functions in the cell, with the monitoring of protein folding found to occur in the ER. The correctly folded proteins are then trafficked to the Golgi. Sugar moieties on soluble proteins can be bound by specific receptors in the trans Golgi network to facilitate their delivery to the correct destination. These sugars are able to act as ligands for receptors on the cell surface,

mediating the cell attachment or stimulating signal transduction pathways [28]. Oligosaccharides are very large and bulky, affecting protein–protein interactions by either preventing proteins binding to cognate interaction domains or facilitating these proteins [29]. Glycoproteins are found in almost all living organism, with eukaryotes having the greatest range of organisms shown to express glycoproteins, from single–celled to complex multicellular organisms [30]. As one of the most relevant and complex post–translational modifications in the cell, protein glycosylation is thought to influence almost half of all proteins in nature [31]. The process of glycosylation consists of a covalent interaction between a glycosyl donor of a glycan and a glycosyl acceptor amino acid side chain of a protein.

Glycosylation can be modified, facilitating the diversity of glycoproteins. These aspects include; the glycosidic linkage – the site of glycan binding, the composition of glycans, the structure of the glycan – whether there are branched or unbranched chains and the glycan length. The glycopeptide bonds are characterised dependent on the nature of the sugar–peptide bond and the oligosaccharide attached. These groups are N–, O– and C–glycosylation along with glypiation and phosphoglycosylation.

1.4.1 N–linked glycosylation

N–linked glycosylation refers to the attachment of oligosaccharides to a nitrogen atom, typically at the N4 atom of asparagine residues [32]. N–linked glycosylation, a commonly observed protein modification is fundamental to the structure, stability, function and pharmacology of glycoproteins [33, 34]. The N–linked glycosylation

process has two key principal phases, 1) the assembly of lipid–linked oligosaccharides (LLO) and 2) the transfer of the oligosaccharide to selected asparagine residues present on the polypeptide chain. Taken place at both ends of the endoplasmic reticulum (ER) membrane, biosynthesis of the LLO involves a series of specific glycosyltransferases that catalyse the assembly of the branched oligosaccharide in a highly defined way [35]. The enzyme, oligosaccharyltransferase (OST), selects the Asn–X–Ser/Thr consensus sequence on polypeptide chains, generating the N–glycosidic linkage between the side–chain amide of asparagine and the oligosaccharide [36]. N–linked glycosylation, a commonly observed protein modification is fundamental to the structure, stability, function and pharmacology of glycoproteins [33, 34]. It is estimated that over 50% of serum proteins are N–glycosylated at one or more asparagine (Asn) residue(s).

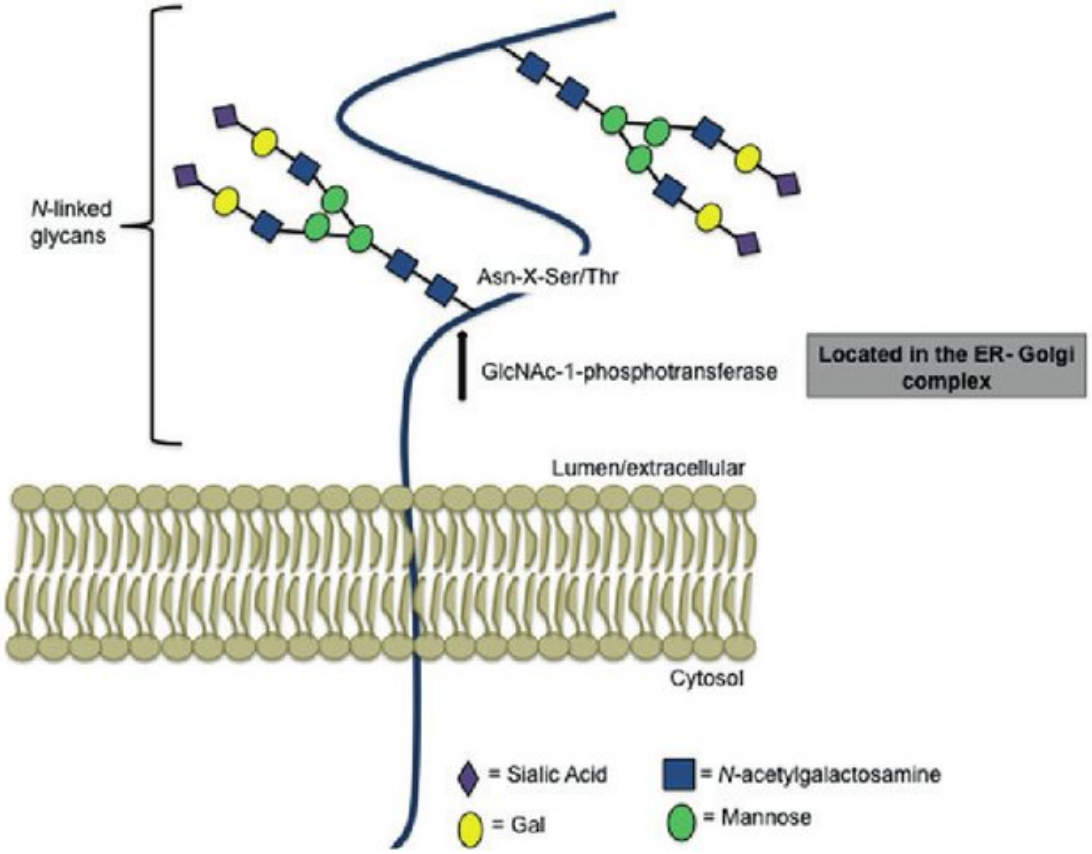

Figure 7: Schematic depiction of N–linked glycosylation. N–linked glycosylation is mainly linked to asparagine residues of proteins, specifically the Asn–X–Ser/Thr motif.

The N–linked protein glycosylation pathway in eukaryotes can be divided into two different processes; 1) the assembly of the lipid–linked oligosaccharide at the membrane of the endoplasmic reticulum and 2) the transfer of the oligosaccharide from the lipid anchor dolichyl pyrophosphate (Dol–PP) to selected asparagine residues of nascent polypeptides [37]. There are three characteristics of N–linked protein glycosylation, these are 1) the use of Dol–PP as carrier for the oligosaccharide assembly, 2) the transfer of the completely assembled $Glc_3Man_9GlcNAc_2$ oligosaccharide only and 3) the recognition of asparagine residues which are characterised by the sequence asparagine–X–serine/threonine (where X

can be any amino acid except proline [38]) and are highly conserved in eukaryotes. Initially, the pathway of N–linked glycosylation was described based on experiments performed with higher eukaryotic cells [39-41]. Later, it was confirmed that these basic principles are also conserved in lower eukaryotic cells, such as Saccharomyces cerevisiae [42-44].

1.4.2 O–linked glycosylation

O–linked glycosylation regulates protein conformation as well as facilitating reversible multimeric protein assembly and stability [45, 46]. O–linked glycosylation is characterised by the interaction of a sugar with the hydroxyl group of a serine or threonine [47]. O–linked glycosylation commonly occurs on glycoproteins. As well as the different linkage, O–glycosylation differs in the mechanism of glycosylation, and is not as complex as the N–glycosylation mechanism. Proteins trafficked into the Golgi are most often O–glycosylated by N–acetylgalactosamine (GalNAc) transferase, which transfers a single GalNAc residue to the β–OH group of serine or threonine [35]. N–acetylgalactosamine transferase has not been consensually sequenced, although structural motifs have been characterised. Some proteins are shown to be O–glycosylated with examples including fucose, GlcNAc, galactose, mannose and xylose, dependent on both the cell and species. Sugar nucleotides are used as the monosaccharide donors for O–glycosylation with highly variable number of sugars consecutively added to the growing glycan chain. In addition, O–glycosylation can also occur in the cytosol and nucleus to regulate gene expression or signal transduction through other glycosyltransferases (Gtfs).

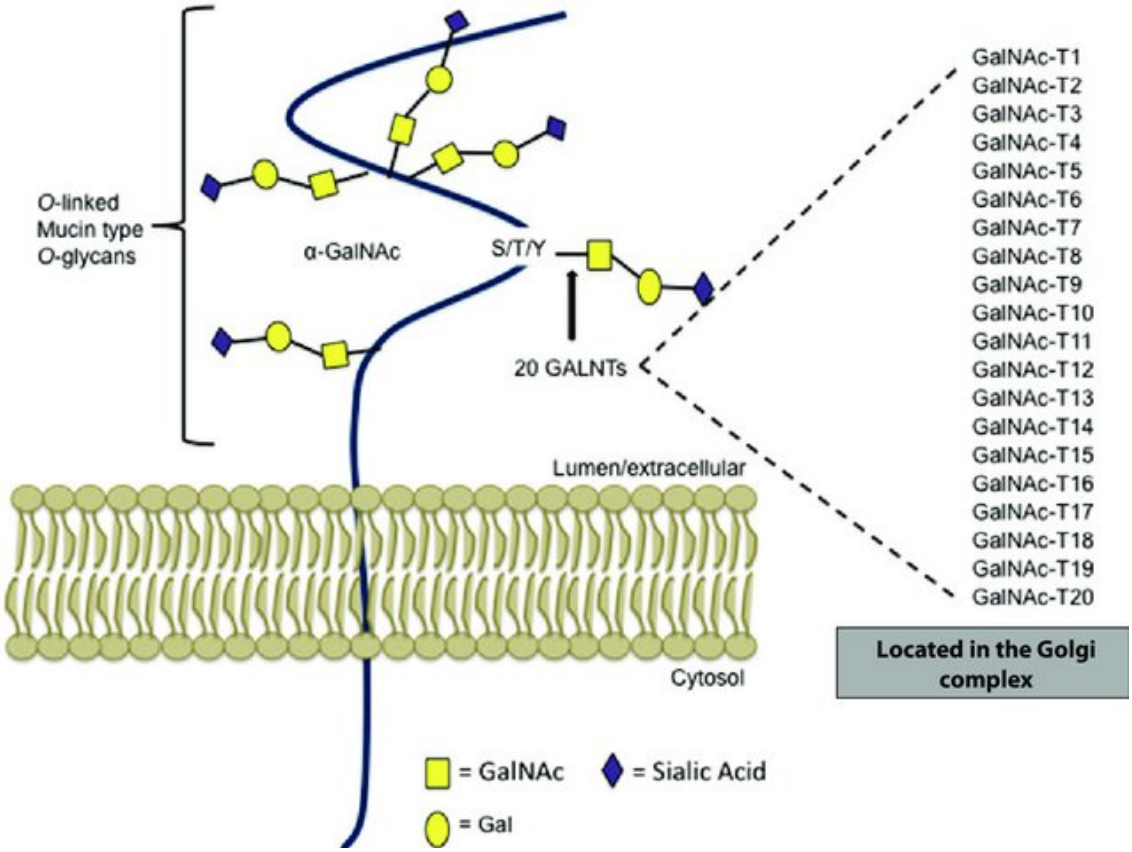

Figure 8: Schematic depiction of O–linked glycosylation. O–linked glycosylation is mainly linked to Ser/Thr and Tyr residues.

1.4.3 C–glycosylation

A novel type of protein glycosylation, C–Mannosylation differs fundamentally from previously described types of glycosylation as it involves covalent attachment of an a–mannopyranosyl residue to the indole C2 carbon atom of tryptophan via a C–C link [48]. Representing a different approach to glycosylation, c–mannosylation forms carbon–carbon bonds, instead of carbon–nitrogen or carbon–oxygen bonds. C–mannosyltransferase links C1 of mannose to C2 of the indole ring of tryptophan. C–

mannosyltransferase recognizes the specific sequence Trp–X–X–Trp and then transfers a mannose residue from dolichol–P–Man to the first Trp in the sequence. C–mannosylation has been detected in multiple cell lines, such as RAW264.7 [49]. RAW264.7 cells are monocyte/macrophage like cell linage, originating from Abelson leukemia virus transformed the cell linage derived from BALB/c mice [50]. Specific C–glycosylated proteins include Trp2 in RNAse, IL–12B and the erythropoietin receptor.

1.4.4 Glypiation

Glypiation is the addition by covalent bonding of a glycosylphosphatidylinositol (GPI) anchor. GPI anchors consist of the attachment of glycophosphatidyl–inositol near to the C–terminal of a protein chain anchoring the protein to the membrane and are attached to the protein in the endoreticulum by the process of transamidation [51].
GPI anchors consist of a:

- Phosphoethanolamine linker that binds to the C–terminus of target proteins
- Glycan core structure
- Phospholipid tail that anchors the structure in membrane

GPI biosynthesis begins on the cytoplasmic leaflet of the ER. The biosynthesis of the GPI anchors is completed on the luminal side [52]. 3–4 Man and various other sugars (e.g., GlcNAc and Gal) are built onto a phosphatidylinositol (PI) molecule embedded in the membrane using sugars donated from sugar nucleotides and dolichol–P–mannose outside and inside the ER. In addition, 2–3 phosphoethanolamine (EtN–P)

linker residues are donated from phosphatidylethanolamine in the ER lumen to facilitate binding of the anchor to proteins [53].

Proteins destined to be glypiated have 2 signal sequences:

- An N–terminal signal sequence that directs co–translational transport into the ER
- A C–terminal signal sequence that is recognized by a GPI transamidase (GPIT)

GPIT does not have a consensus sequence but instead recognizes a C–terminal sequence motif that enables it to covalently attach a GPI anchor to an amino acid in the sequence [54]. This C–terminal sequence is embedded in the ER membrane immediately after translation, and the protein is then cleaved from the sequence and attached to a preformed GPI anchor [55].

1.4.5 Phosphoglycosylation

Phosphoglycosylation is the enzymatic attachment of a sugar to the polypeptide chain through a phosphodiester bridge [56]. Examples of the glycosylation was investigated in *Dictyostelium* and *Leishmania* [57]. The GlcNAc–1–phosphotransferase was partially purified from *Dictyostelium* and localized to light membranes that are believed to represent the Golgi compartment [58]. Subsequently, studies had indicated that the enzyme recognizes Ser–containing peptides of various *Dictyostelium* proteins among which cysteine proteinases are the most prominent [59]. No single specific motif was observed in the peptide acceptor, however transfers occur in Ser–rich domains in

which the flanking Ala residues preferentially influence phosphoglycosylation were observed. *Man–1–phosphotransferase* has been characterized in *Leishmania mexicana* promastigotes and it is believed to be situated in the *cis*–Golgi compartment [60]. The enzyme adds Man–α–1–phosphate to Ser residues in domains rich in this amino acid; it does not act on Thr and its action is promoted by flanking Asp and Glu residues.

A study had shown the accelerating rate in the discovery human glycosylation disorders, with the enrolled patients showing unexplained intellectual development disorders, along with metabolic pathways. It was shown that most genetic defects were hypomorphic states of genes with complete loss being lethal [61].

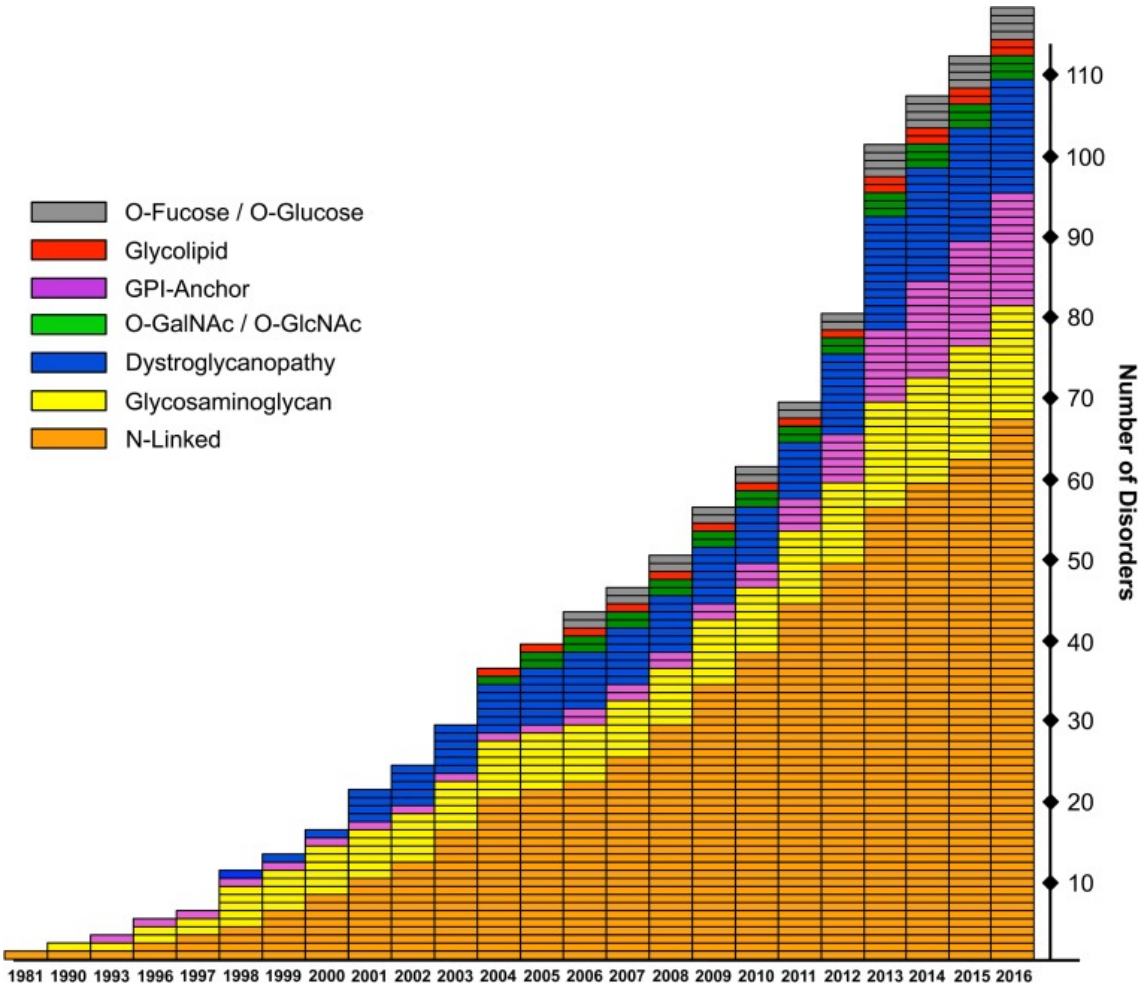

Figure 9: Accelerating progress in the discovery of human glycosylation disorders [image taken from [61]].

1.5 Aberrant glycosylation in diseases

Carrying information in biological systems makes glycans an important source of biomarkers for a wide range of diseases, including neurodegenerative diseases, hereditary disorders, immune deficiencies, cardiovascular diseases and many types of cancers [62, 63]. Changes in glycosylation can modulate inflammatory responses and enable viral immune escape, promote cancer cell metastasis or regulate apoptosis [16]. Cancer and autoimmune diseases are just a few defects that are researched for the glycosylation of proteins. A few examples are tabulated below, with the reported

glycosylation defect or alteration [64]. Defects are found in the activation, presentation, and transport of sugar precursors, in the glycosidases and glycosyltransferases involved in glycan synthesis and processing, and in proteins that control the traffic of components of the glycosylation machinery within the cell [65].

Table 1: Autoimmune diseases and the glycosylation defects involved.

Autoimmune disease	Reported glycosylation defects/alteration
Rheumatoid arthritis	N–glycans of serum IgG are missing terminal galactose (IgG G0) when compared with healthy controls.
Autoimmune haemolytic anaemia	G(0) glycoforins of IgG decreased below normal levels on IgG eluted from erythrocytes
HIV–associated autoimmune phenomena	Reduced sialylation of CD43

Aberrant glycosylation is recognised in Alzheimer's disease [66]. In Alzheimer's disease, the most studied post–translational modification is phosphorylation, although very little research is conducted on the process of glycosylation in the brain [67]. Altered glycosylation of tau [68], presenilin [69], and transferrin [70] have been

described in the disease with the suggestion of aberrant changes in glycosylation which occurs in Alzheimer's disease [71].

Glycosylation is one of the molecular changes which accompanies malignant transformation. N–glycans as well as Lewis antigen sequences are observed to increase in some cancers [72]. Cancer is characterized by aberrations in glycolipid and glycoprotein content; both at the structural and concentration level [73, 74]. However, these changes are acute and manifesting as a by–product of oncogene expression providing disturbed glycosyltransferase transcriptional signalling [75].

The multitude of glycan biomarkers are produced and are used to diagnose many diseases which are as a result of abnormal cell growth. Before the discussion of current glycan detection methods, an example of a disease with altered glycosylation should be described.

1.6 Prostate cancer and PSA

Predicted to become the most prevalent of all cancers in the UK by 2030, prostate cancer (PCa) kills one man every hour. The worldwide count of new prostate cancer diagnosed is set to increase to a staggering 1.7 million with a projected increase of almost 500,000 deaths [76].

Currently, prostate specific antigen (PSA) is the only biomarker approved by the US Food and Drug Administration (FDA) for the detection and prognosis of prostate cancer [77]. A serine protease secreted by prostate epithelial cells, PSA is primarily involved

in the liquefying of human sperm through a proteolytic mechanism [78]. The initial implementation of PSA was used in clinical practice to lead the increased detection of men with early–stage prostate cancer [79]. More studies were continued to develop a prostate cancer staging method based on the level of PSA detection, thus used as a marker for prognostic purposes [80].

However, PSA has shown to have serious limitations and inconsistency as both a diagnostic and prognosis marker for prostate cancer. In fact, PSA is revealed to be an organ–specific marker not as cancer–specific marker. PSA is produced by prostatic epithelium at low levels in normal conditions with dramatic increase from benign prostatic hyperplasia to prostate cancer and further cancer advancing [81]. Reducing the sensitivity of PSA detection, men aged over 60 years have an increased production of PSA, thus affecting the diagnosis of prostate cancer. On the other hand, men who are treated with specific therapeutic agents with anti–androgenic effects, such as 5–α reductase inhibitors, are found to have reduced levels of PSA [82]. Taking into account these drawbacks, the clinical utility of serum PSA for prostate cancer screening and prognosis is regrettably reduced, thus the search for novel markers for prostate cancer continues.

In patients with PCa, the terminal N–glycan structure of PSA is rich in sialic acid α2,3–linked galactose, whereas the terminal N–glycan structures of PSA from healthy patients are predominantly α2,6–linked [83] (Fig. 10).

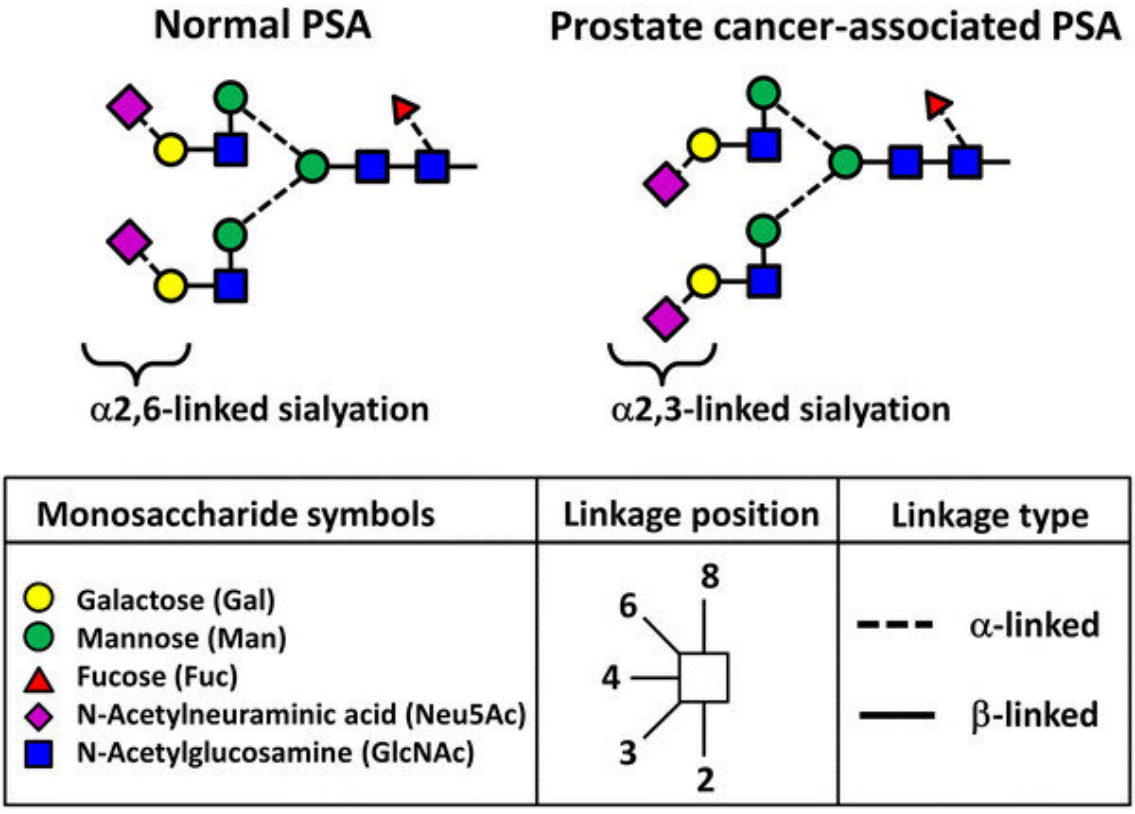

Figure 10: Aberrant glycosylation of PSA N–glycans (S2, 3PSA) in PCa. In healthy patients, the terminal sialic acid of PSA is predominantly α2,6–linked to galactose residues. In patients with PCa, the terminal sialic acid is predominantly α2,3–linked to galactose residues [image taken from [84]].

From this finding, a successful novel assay with the use of a magnetic microbead–based immunoassay to detect α2,3–linked sialylation on free PSA (S2, 3PSA) was developed [85]. The preliminary study was small, however the accuracy was 0.84 AUC (Area under the ROC curve) and sensitivity was demonstrated as 95% whilst the specificity was 72%. The results found had suggested that assays measuring cancer–associated glycan alterations in serum S2, 3PSA might improve the accuracy of early PCa detection and reduce unnecessary prostate biopsies.

One of the issues with the enzyme–linked immunosorbent assay (ELISA) is its failure to effectively discriminate between various PSA glycoforms [86]. The PSA glycoprotein has a single N–linked glycan which is composed of a N–acetyl–lactosamine bound to an α2–3–linked sialic acid, shown in fig. 10 [87, 88].

Previous studies have assumed that this glycan structure did not vary between individuals, however it is now known that the changes to the core fucosylation and sialyation of the PSA glycans are common in prostate cancer. The sialyation patterns of the glycan in prostate cancer patients have been shown to be more heterogeneous when compared to the glycans of non–cancerous patients [89-91].

To summarise, recent studies of PSA collectively conclude that research should focus on the change in targeting of the sialyation and fucosylation of the N–linked PSA glycan, producing a more specific test which is capable of discriminating between a range of PSA glycoforms [89, 92, 93]. Lectin assays is another technique that can selectively detect α2–6 sialic acid linkages of the PSA glycan. It has been explored to improve the detection of prostate cancer [94].

1.7 Natural recognition receptors

In the heart of current and further developments in glycan–related basic research is the recognition of glycans by other molecules with high affinity and exquisite specificity. There are unique challenges associated with such recognition processes due to the glycan–binding entities needed to be able to discriminate between a large repertoire of

carbohydrate structures, including closely related isomers. The selective recognition is very hard to achieve because of subtle differences, such as the stereochemistry of a single hydroxyl group. Currently, natural and artificial receptors are used for the recognition of glycans. Natural receptors include anti–glycan antibodies along with lectins before introducing examples of artificial receptors, such as aptamers and boronic acid derivates.

1.7.1 Lectins

Present in plants, animals and microorganisms, lectins are carbohydrate–binding proteins with non–immune origin. Lectins are involved in numerous physiological events, playing a crucial role as tools for glycan probing, purification of glycoproteins, cell labelling, carriers in targeted therapies and detection of cancer and other diseases [95-97]. Lectins display relevantly weak affinities for monosaccharides and the dissociation constants (K_D) are in the millimolar range. For oligosaccharides, affinities are in the micromolar range, despite opportunity for multiple contacts with the lectin surface. The affinities are lower due to the shallow binding pockets present on the lectin surface which are exposed to competitive solvent interactions. Without deeper binding pockets, poor selectivity for individual sugars could be a possible reason for lower affinities. On the other hand, in biological settings, some lectins can assemble into homo–oligomeric structures with multiple binding sites in order achieving superior affinity and selectivity. Therefore, an oligomer can interact in an effective manner with different arms of a branched oligosaccharide or to different glycan sites of the same glycoprotein. In such oligomeric arrangements, a high degree of multivalency can be reached, contributing to affinities in the nanomolar range [98-102].

Lectins and glycans interact primarily via a network of hydrogen bonds between the ring oxygen atom and multiple hydroxyl groups of the carbohydrate residues and oxygen atoms, as well as through van der Waals contacts [101-103]. The CH–π interactions between the carbohydrate backbone and aromatic amino acids such as phenylalanine, tyrosine, or tryptophan also make an important contribution to the overall binding [104, 105].

The Ralstonia solanacearum (RSL) lectin is able to establish CH–π contacts with the C3, C4, C5 and C6 carbons of α–l–Me–fucoside via the indole ring of a tryptophan residue, with the dispersion interactions contributing to the binding with an energy between 7 and 8 kcal mol^{-1} [106]. Lectins are becoming relevant for the recognition of charged carbohydrate residues and electrostatic interactions for negatively charged sialic acids. In this example, positively–charged arginine residues are often involved in sialic acid interaction processes [107]. A study reported the investigation of the complexation of Siglec–8 lectin and its target, 6′–sulfo sialyl Lewis X (6′S sLe^x) (fig. 11) and found examples of intermolecular contacts between lectins and glycans at the binding site [108].

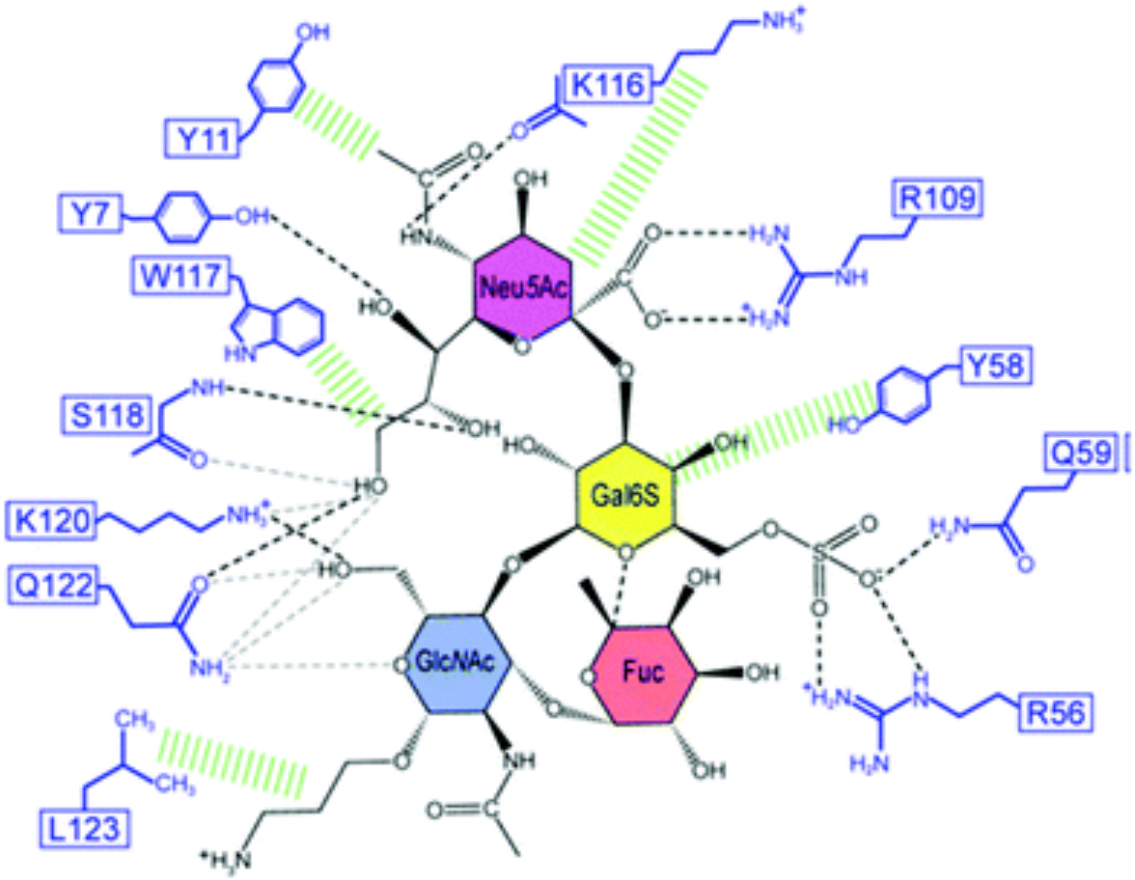

Figure 11: Schematic illustration of the Siglec–8–6′S sLex interaction network. Black dashed lines indicate hydrogen bonds in the depicted structure; grey dashed lines indicate hydrogen bonds abundantly observed in other structures of the ensemble [image taken from [108]].

The carboxyl group of the sialic acid residue makes a salt bridge with the guanidinium group of Arg109 and is among several other interactions between the lectin and the glycan. Furthermore, Lys116 and Ser118 engage in a network of hydrogen bonds with the N–acetyl amide and the O8 and O9 hydroxyl groups of the glycerol chain. The binding described is promoted by hydrophobic contacts with the surrounding aromatic rings of other amino acid residues such as Tyr11 and Trp117. The binding of the Gal6S is mediated by

the side chains of three residues (Arg56, Tyr58, and Gln59), together with a salt bridge and the guanidinium group of Arg56 and/or a hydrogen bond with the amino group of Gln59. C–type lectins have carbohydrate binding activity and are involved in many cell surface recognition events which are mediated by Ca^{2+} ions, coordinating carboxylate residues [109, 110]. A type of C–type lectin specific for high–mannose glycans, Dectin–2, can trigger a defence response against pathogens in a Ca^{2+}–dependent process [111, 112].

Several hundred lectins have currently been identified and approximately 100 lectins are commercially available. The use of lectins for glycan recognitions is a major breakthrough and came from the development of lectin microarrays. Lectin microarrays rely on the immobilisation of a panel of lectins, allowing for high–throughput analysis of complex carbohydrates included in serum glycoproteins, whole cells and bacteria [95, 113, 114]. Over other glycan characterisation techniques such as NMR spectroscopy and liquid chromatography, lectin microarrays have the advantage of possibly rapidly obtaining a broad profile or fingerprint of the glycans present in a crude sample, with minute sample consumption and reduced cost. The general information about the glycosylation pattern can be determined, such as whether it is N– or O– glycosylated, high mannose, core fucosylated, or if the glycosylation is fully or partially sialylated, with potential applications in the development of disease–related biomarkers [113, 115-118].

The benefits associated with lectin microarray don't surpass the inherent low affinity and specificity of lectins, hindering the detection performances. To improve their binding properties, lectin engineering has been researched [119-123]. There are several types of

lectins which can be used as scaffolds, examples include L–type, F–type, R–type and Galectins with different engineering procedures available, including site–directed mutagenesis, random mutagenesis and DNA shuffle are just a few [123]. The engineering of a bacterial F–type lectin domain (FLD) from Streptosporangium roseum, namely SrFLD was recently researched, showing significantly improved binding towards multivalent fucosylated glycoconjugates [124]. The engineered lectin, SrDupFLD, contained a partial duplication of the original FLD sequence, possibly affording two L–fucose binding pockets.

Binding studies conducted have shown that the engineered lectin had a stronger binding for multivalent fucosylated glycoconjugates, with a dissociation constant 12–fold lower than the wild–type lectin SrFLD. Analogously, lectins in which the l–fucose binding residues of the N–terminal partial FLD region and the complete FLD region were mutated, respectively SrDup$_{TM}$FLD and SrDupFLD$_{TM}$, were expressed and purified, with increased binding avidity observed for SrDup$_{TM}$FLD. Against its original hypothesis, the study revealed the increased affinity of the engineered lectins may not be mediated by additional l–fuctose binding sites in the Dup partial FLD region, instead the study suggested that it may be ascribed to an increased tendency of the lectins for oligomerization.

An example of how artificial lectin can be created is reported by Ribeiro et al [125]. Engineering the first chimeric and bispecific lectin, with two rationally oriented and distinct recognition surfaces, they were able to bind both fucosylated and sialylated glycoconjugates (fig. 12). FS–Janus lectin, a chimeric lectin, was obtained by fusing sequences from the lectin of Ralstonia solanacearum (RSL), which displays strong affinity

for fucose, as well as a sequence from the NanI sialidase of Clostridium perfringens ATCC13124 (CBM40_NanI), with strong affinity for sialylated oligosaccharides. The binding ability towards fucose, 3′–sialyllactose (3′–SL) and 6′–sialyllactose (6′–SL) functionalised surfaces was evaluated using surface plasmon resonance (SPR). The Janus lectin showed nanomolar avidity for fucosylated and sialylated surfaces, with the latter being an important achievement since classic lectins usually display low affinity for sialylated epitopes.

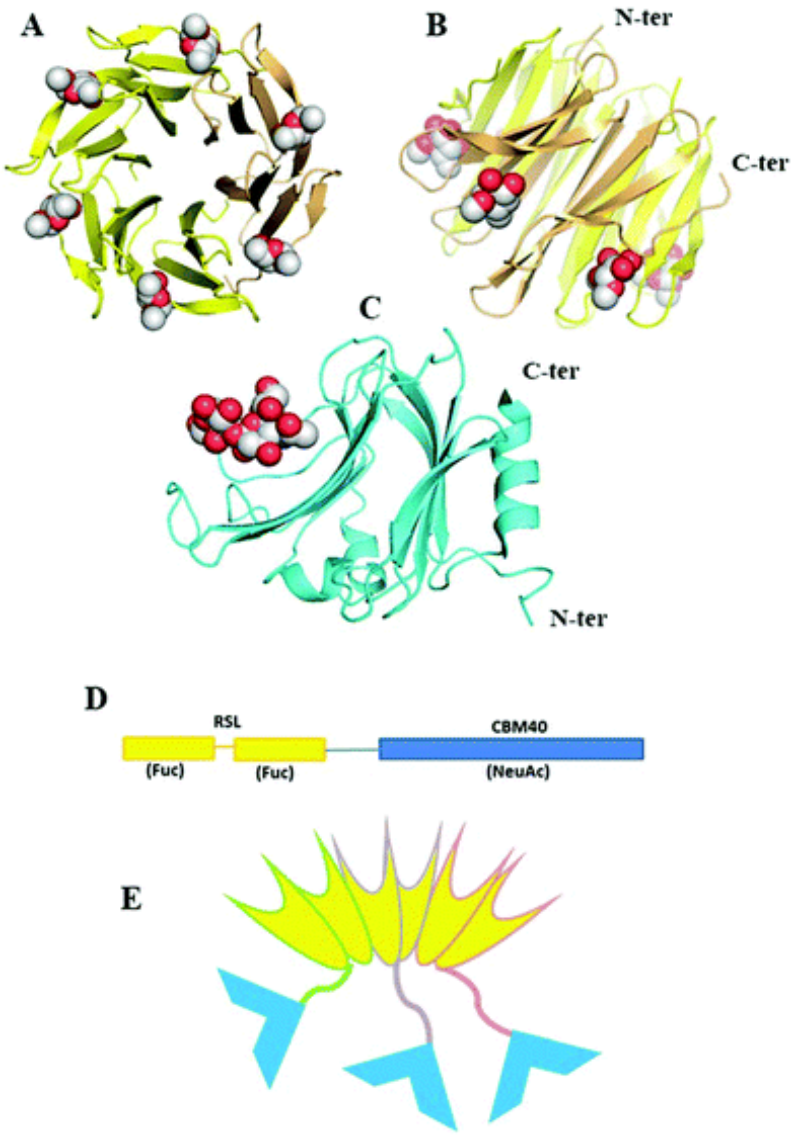

Figure 12: A Janus lectin with two rationally oriented and distinct recognition surfaces, which are able to bind independently to fucosylated and sialylated glycoconjugates. (A and B) Two views of crystal structure of RSL–trimer complexed with six fucose ligands [image taken from [125]].

There are many challenges associated with lectin engineering, including the selection of template lectin, construction of a mutagenesis library and high–throughput screening

methods. However, as these challenges are overcome, lectins with superior binding properties will broaden the range of applications.

1.7.3 Anti–Glycan Antibodies

An antibody, a large Y–shaped protein, are produced by the immune system in response to a foreign molecule, namely antigen, entering the body. A given antibody binds specifically only to a small site on its antigen, called an epitope, which usually consists of a few amino acids or monosaccharide units. Antibodies should provide specificity along with avidity for its antigen. In contrast, glycans alone pose a serious challenge to antibody development. The development of a highly selective anti–glycan antibody is hindered by inherently poor immunogenicity of carbohydrates, labour intensive antigenic material production and the similarity between various carbohydrate sequences [126]. Due to the wide variety of complex glycans intrinsically produced in standard host organism, there are observed difficulties in generating anti–glycan antibodies.

A large collection of anti–glycan antibodies (AGAs) are present in human serum, playing critical functions in many immune processes. The expression of AGA is dependent on the exposure to both the sequences from the “self” of the same species and the foreign carbohydrate sequences. Some AGAs exhibit affinity for naturally occurring glycans, despite this AGAs cannot be considered true auto–antibodies due to apparent lack of selectivity for native carbohydrate sequences [127]. Naturally occurring AGAs in human sera also include those to foreign glycan epitopes, such as galactose–α–1,3–galactose (α–Gal) and N–glycolylneuraminic acid (Neu5GC). These antigens are responsible for the

rejection of xenotransplanted organs in humans from pigs [128, 129]. In addition, extensively studied AGAs include the anti–blood group antibodies against A, B and rare 'Bombay' type O antigens. Highly specific, anti–blood group antibodies are able to differentiate differences between the glycan structures [130]. Natural AGAs have been associated to various different human diseases, such as Crohn's disease, cystic fibrosis and malignant cancers [131-136]. This creates a useful biomarker to be a successful diagnostic tool for these diseases.

It is typical for glycan–binding antibodies to exhibit lower affinities (with equilibrium dissociation constant (K_D) values in the micromolar range for monovalent interactions) when compared with protein–specific antibodies (with K_D values in the nanomolar range) [137, 138]. Affinities can be enhanced, by the generation of antibodies with two or more glycan binding sites or the non–covalent assembly into oligomers with multiple binding sites. [139, 140]. Multivalent complexes can result in high affinities as well as enhanced selectivities [141, 142]. An example of this includes the human antibody 2G12 which was found to bind strongly to HIV–1 glycoprotein gp120 (K_D of 5.6 nM) via the formation of a dimer establishing multiple complex interactions with the oligomannose epitope of the glycoprotein [143, 144].

A growing understanding of the immunological mechanisms by which the immune system refines its antibodies, together with recent technological advances in carbohydrate chemistry and bioconjugation are also enabling the production of high–affinity anti–glycan antibodies [138, 145]. Qβ virus–like particles (VLPs) have been used and are

conjugated via copper–catalyzed azide–alkyne cycloaddition with short synthetic glycans. As a result, anti–glycan IgG antibodies with nanomolar affinity were produced (fig. 13) [138].

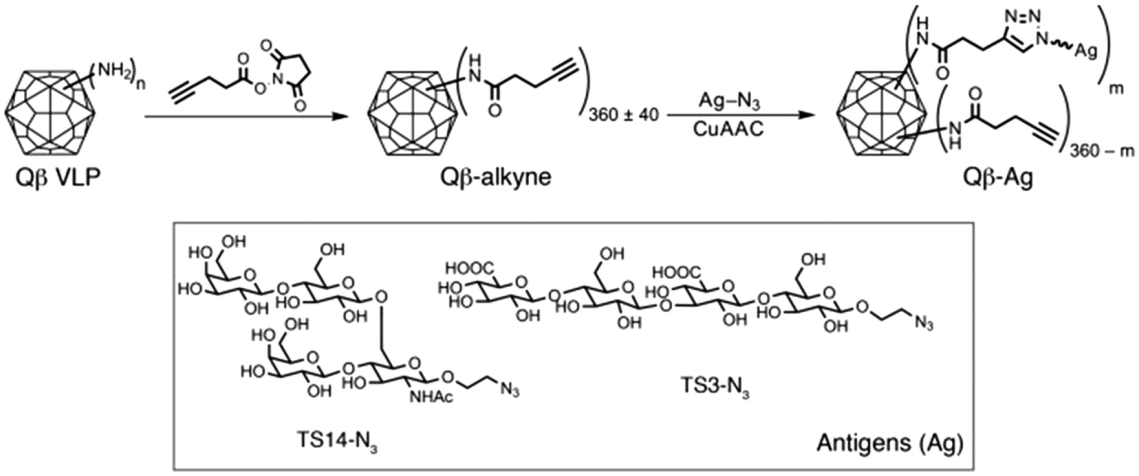

Figure 13: Synthetic scheme illustrating the functionalization of Qβ VLPs with two oligosaccharide antigens (Ag), TS14 and TS3; m represents the number of antigens per VLP [image taken from [145]].

AGA–carbohydrate complexes are held together by hydrogen bonds, van der Waals, CH–π and electrostatic interactions [146, 147]. Antibodies are able to accommodate long glycan epitopes in their binding sites and can generally interact with all monosaccharide units. Specific recognition can be detected with the enveloping capacity of the antibody binding sites [148, 149].

Experimental techniques have been key to elucidate molecular structural features for modulating glycan–antibody recognition. These techniques include synthetic chemistry, NMR, antibody engineering and microarray technology [150-152]. Molecular modelling, along with antibody engineering, have been applied to demonstrate that the affinity and

specificity mostly rely on CH–π interactions in both pyranoside– and furanoside–antibody systems [153]. Pyranosides are six–membered sugars whilst furanoside are five–membered sugar rings [154]. Ionic interactions are shown to play a key role in the binding of charged glycans and the recognition of neutral glycans by AGAs with hydrophobic stacking interactions and hydrogen bonds being more prevalent [155].

Recent improvements in glycan microarray–based technology have now caused well–defined validated specificities [156, 157]. Over 100 AGAs have been reported with many of the AGAs targeting the same glycan structure. The Thomsen–Friedenreich (TF) antigen (Galβ1–3GalNAcα1–Ser/Thr) and tumour associated carbohydrates, i.e. the Tn (GalNAcα1–Ser/Thr), have been particularly targeted for AGA development [158]. A good number of AGAs have been studied for ABH blood group antigens and Lewis antigens, as well as glycolipids [152, 159, 160]. Antibodies have been developed and are currently in clinical trials or have been employed for the treatment of diseases. Antibodies have also been used for the diagnostic applications in disease, with one example being an antibody that targets Sialyl Lewis A for detecting and monitoring of several cancers [161]. Many AGAs currently explored display low affinities for their target glycans as well as lacking specificity, recognising the family of glycan structures rather than a single glycan which is of interest.

The nature of many antibodies is characterised by the binding of antibodies to recombinant antigens in ELISA assays or western blotting of denatured complexes. These complexes could be from mammalian cells or cell extracts. Demonstrations have shown that anti–

GlcNAc antibody binding to bacterial cell wall peptidoglycan complexes is inhibited by soluble monomeric GlcNAc monosaccharide, but not its enantiomer GalNAc [162-164]. As a conclusion, these antibodies have shown to only bind identical or a very similar associated glycan epitope present in various molecular entities expressed by a wide range of living organisms.

The available AGAs cover a narrow set of glycan families, epitopes as well as many important O–glycans, N–glycans, glycosaminoglycans, they still lack a corresponding antibody [126]. There are still various opportunities in the development of new AGAs, as they lack the ability to distinguish specific amino acid residues (e.g. serine versus threonine). This will improve AGAs in the development of new diagnostic and therapeutic applications.

1.8 Artificial receptors

Efforts have been focused on designing artificial receptors that can mimic the role of antibodies and lectins as binding entities for several years. The efforts have focused on targeting monosaccharides, however there is a short list for receptors and targeting more complex systems. An example of a more complex system includes a set of ditopic diaminopyrrolic structures designed for the selective recognition of Manα(1–2)Man dimannosides [165].

Natural receptors previously mentioned provide an insight of some key features, and give rise to the selective recognition of carbohydrates. Unfortunately, the lack of application for

natural receptors remains an issue targeting biological relevance. Therefore, the next section discusses synthetic receptors for the application in biological settings. Examples of synthetic receptors include aptamers and boronic acid derivatives.

1.8.1 Aptamers

Aptamers are single stranded oligonucleotides and synthetically derived, that bind to non–oligonucleotide based targets. The method Systematic Evolution of Ligands by EXponential enrichment (SELEX) was first employed by Tuerk and Gold, and determined the sequence of aptamers [166]. Aptamers are typically constructed from less than 100 bases and interact with a variety of targets, ranging from small molecules to whole cells, with similar, if not improved, affinities than antibodies [167]. The literature on aptamers targeting glycans is very limited, with most sources identifying saccharide–binding sequences from the 1990s [168].

There is a lack of new developments, due to the limitations of the new options with regards to non–covalent binding interactions between sugars and oligonucleotides. An example includes the absence of charged groups and aromatic ring structures in simple sugars limits interactions to hydrophobic sites and hydrogen bonding [169].

Current advances have focused on aptamers that target sugars with charged moieties, these include sialic acids. These sugars are overexpressed in cancer cells, making aptamers ideal in cancer diagnostics and therapeutics [170]. An overview of the SELEX

process is shown in fig.14, demonstrating that the library is incubated with the target and some of the sequences bind to the sequence, while some do not [171].

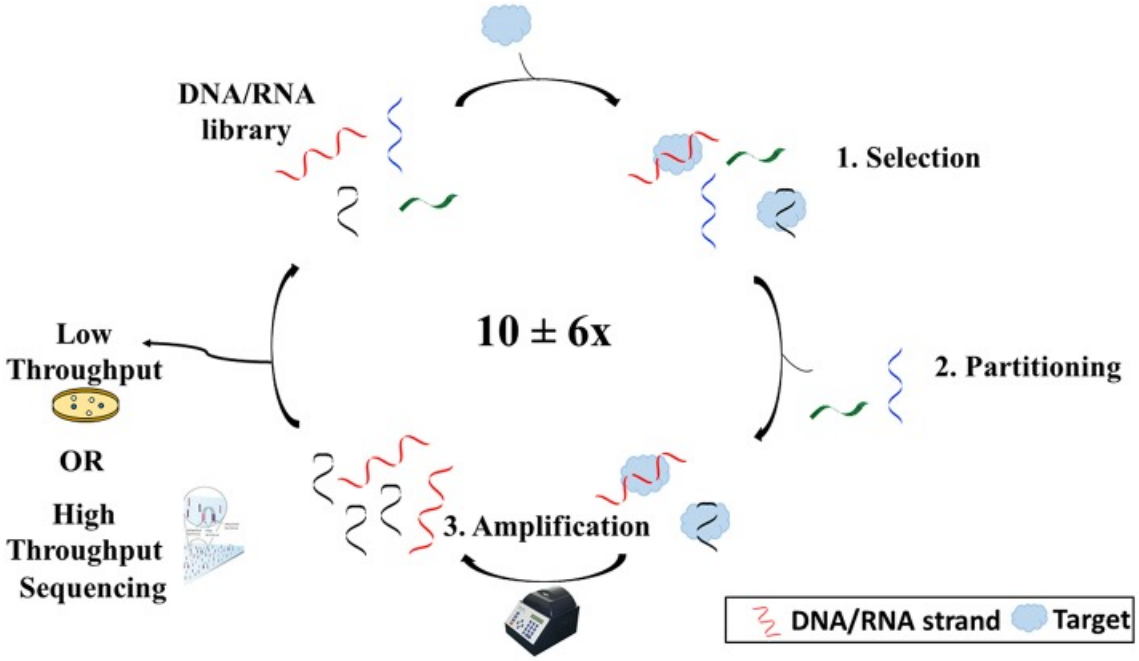

Figure 14: Overview of the SELEX process. SELEX begins with an oligonucleotide library consisting of ~10^{16} different sequences. The library is incubated with the target (1). Some sequences will bind to the target and others will not. Sequences that have bound to the target are then separated from those that have not (2). After separating the sequences from the target, the sequences are copied and amplified using polymerase chain reaction (3). Sequences are then reintroduced into the process several times before being sequenced via either high throughput or low throughput sequencing image taken from [172]].

The immobilisation of Neu5Ac has been directed to adopt a natural conformation. This was achieved by exposing the carboxylic acid group of the sugar which resulted in the

identification of an aptamer to be highly selective for both Neu5Ac alone and Neu5Ac modified glycans [173]. In addition to selectivity, the binding of the aptamer to Neu5Ac was also shown to prevent enzymatic hydrolysis of the sugar [174].

Another development for aptamers was target peptidoglycans and glycan regions of glycoproteins. One example is RNA aptamers which are selected against two classes of glycosaminoglycans, these classes are chondroitin and heparosan [175]. These glycosaminoglycan are non–immunogenic, making previous detection of biological samples using popular antibody–based technologies difficult. The selected RNA aptamers observed high affinities (K_D values in the range of 0.71–1.0 μM).

Aptamers face the challenge of lacking the interactions that can be established between the oligonucleotides and glycans. The easy adaptation of aptamers incorporates sugar–binding moieties such as boronic acids, to enhance interactions, is one way to overcome this limitation [176]. However, the biggest challenge of the use of aptamers as sensors for glycoconjugates is the lack of specificity towards glycan targets. Optimisation of aptamer selection process (such as SELEX methods) must be achieved, making aptamers potential sensors for glycans.

1.8.2 Boronic acids

Known for their ability to covalently bind to 2– and 1,3–diol groups found in carbohydrates, boronic acids binding interaction is both reversible as well as pH dependent [177], shown in fig. 15. Boronic acids can readily interconvert in aqueous

media from sp^2 to sp^3 hybridisation in the presence of a Lewis base, with the result of tetrahedral species in equilibrium with the neutral trigonal form [178]. In alkaline aqueous solutions, boronic acids and their reaction with diols result in the formation of boronate esters [179]. Therefore, these features make boronic acids interesting molecules for the realization of synthetic receptors for carbohydrate recognition, also named “boronolectins” [180].

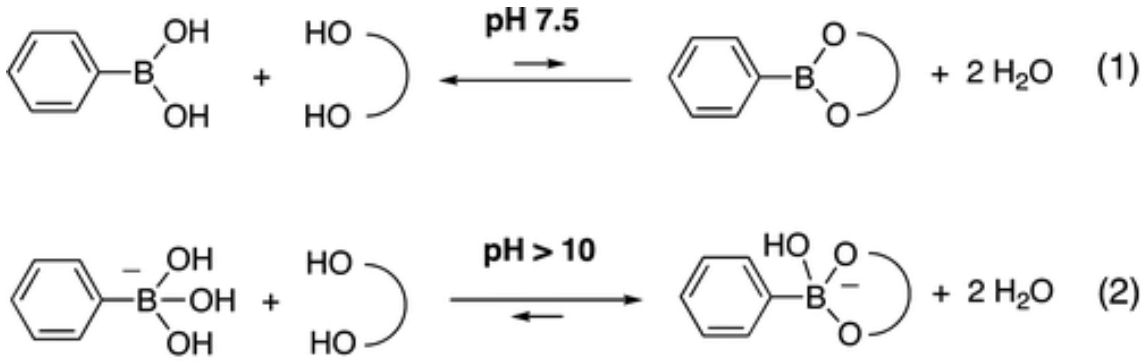

Figure 15: Complexation between arylboronic acids and diols in water [image taken from [181]].

Boronic acids are able to form boronic esters reversibly with polyols and sugars in water (eq 1, fig. 15) [182]. Boronic acids are one of the most promising approaches for the recognition of carbohydrate recognition, however as a limitation a high pH is generally required in order to favour the equilibrium toward the dialkoxyboronate anion (eq 2).

Reports have shown that phenylboronic acid–adamantane conjugates can form self–assembled monolayers on the surface of cyclodextrin vesicles in aqueous solution

[183]. The study had presented multiple boronic acid receptors on the surface and was found to bind monosaccharides with binding constants between 100 and 3000 M^{-1}. A previous study also developed a glucose selective sensor which was obtained by the formation of a self–assembled monolayer of bis–boronic acids on gold surfaces [184]. The binding of boronic acids and monosaccharide recognition and sensing has been well documented [184-188]. On the other hand, the recognition of glycans and glycoconjugate is still required. Promising results were obtained that act as fluorescent sensors with the use of boronic acid–functionalized peptidic receptors. An example of the fluorescent sensors is diboronic acid compounds, these are used to recognise cell surface cancer–associated glycans in situ, such as Sialyl Lewis X (sLe^x), with high specificity [185, 186]. Molecular imprinted polymers (MIP) are an effective way to create synthetic carbohydrate receptors. A successful and effective way to create synthetic carbohydrate receptors has been demonstrated by the use of molecular–imprinted polymers (MIP), with the use of boronic acids used as functional monomers [167, 189-195].

1.8.3 Benzoboroxoles

Derivatives of phenylboronic acids, benzoboroxoles have an intramolecular five membered–ring containing a boron atom. Benzoboroxoles were first reported in 1957 [196], but gained greater attention in the late 2000s due to their interesting biological activity and medical relevance becoming apparent.

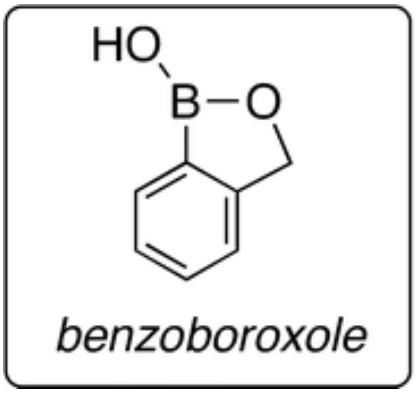

Figure 16: Generic structures of benzoboroxoles [image taken from [181]].

Benzoboroxoles show inhibitory activity against several enzymes, these include carbonic anhydrases and they are potential anti–tuberculosis agents [197, 198]. However, benzoboroxoles have drawn particular interest for their potential application as carbohydrate receptors, as they are able to bind sugars under physiological conditions [199]. Unlike their boronic acid counterparts, benzoboroxoles are able to bind sugars in their pyranose form and at physiological pH and, making them more suitable for biological systems (fig. 17). This ability makes benzoboroxoles attractive as potential candidates for the development of synthetic lectins for the recognition of glycans on cell surfaces and glycoproteins.

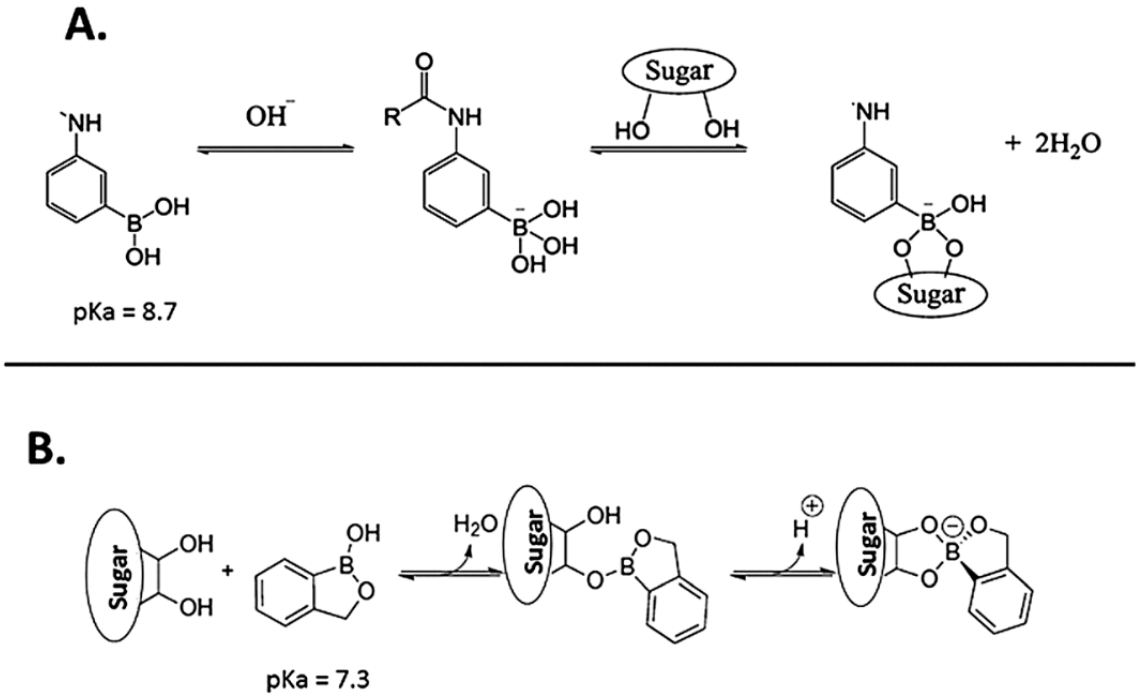

Figure 17: Reaction scheme showing how both benzoboroxoles (B) and aryl phenylboronics acids (A) bind the cis-diol moieties of carbohydrates. Theprimary difference lies in the lower pKa of the benzoboroxoles (B, pKa of 7.3) allowing for efficientcis-diol binding at physiological pH (pH: 7.4), as com-pared with phenylboronic acids (pKa = 8.7) [image taken from [200]]

Pal et. al. reported low molecular weight peptidyl bis(benzoboroxole) receptors and their ability to target cancer–related Thomsen–Friedenreich (TF) antigen. The receptors studied consisted of two benzoboroxoles which bound the two diol units of the TF antigen, a peptide backbone, with a tuneable length and rigidity, providing additional hydrogen bonding and hydrophobic/CH–π interactions (fig.18).

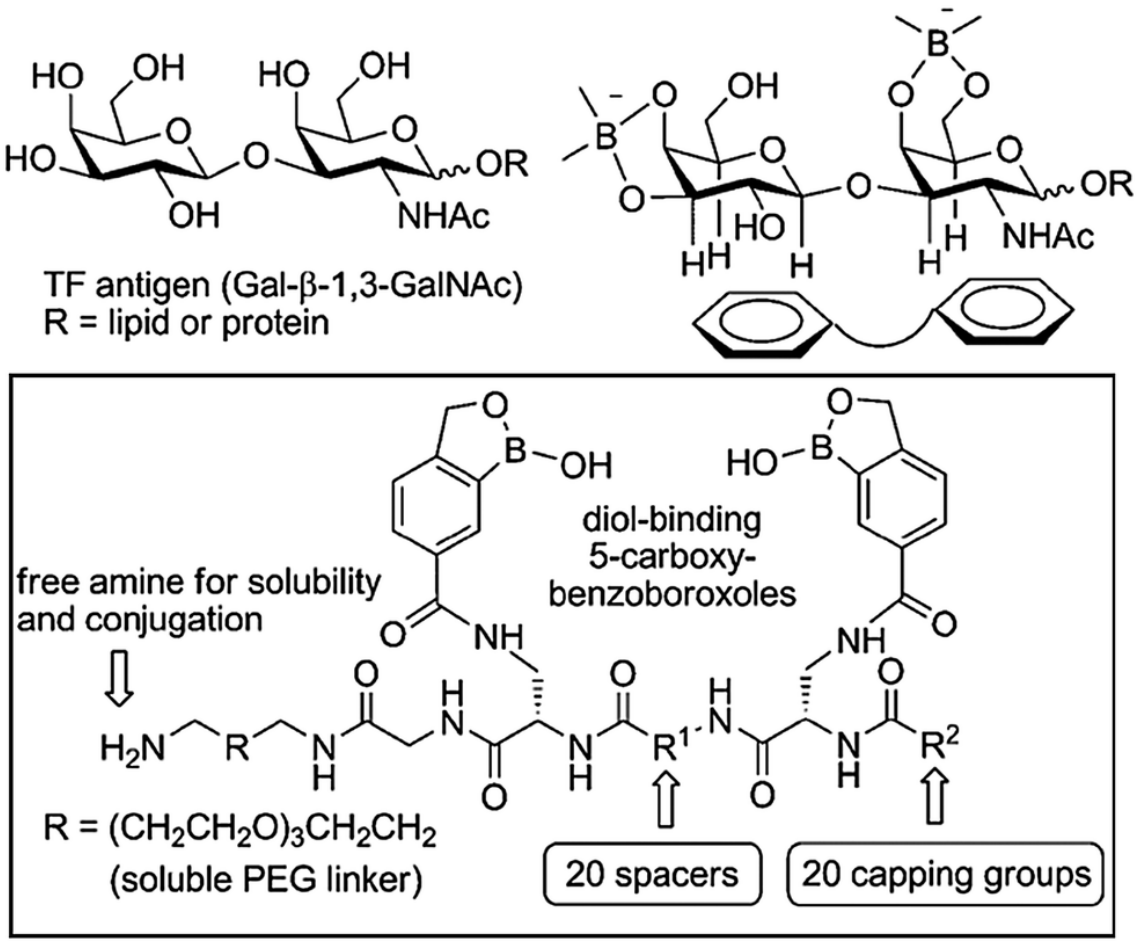

Figure 18: Design of peptidyl bis(benzoboroxoles) for the recognition of TF antigen; the library was generated by combining different spacers R1, natural and non–natural amino acids, and carboxylic acids as capping groups R2 [reproduced from [201]].

Small changes in the stereochemical configuration of the peptide spacer considerably affected the binding, highlighting the extent to which molecular recognition is sensitive to subtle variations. Using a competitive ELISA assay, the screening of the binding of TF antigen showed the most potent receptor exhibited an IC50 value (the concentration of inhibitor required to produce 50% inhibition of an enzymatic reaction at a specific substrate concentration) of 20 μM. Whilst only moderate affinities and selectivities were observed, the results were promising and encouraged future studies [202].

The binding properties of benzoboroxoles are attractive due to the recent development of a carbohydrate–binding ligand for specific enrichment of glycoproteins [203]. A benzoboroxole–modified ligand with a structure that mimics Trp and Phe (two amino acids that are frequently present in lectins) was immobilised on a Sepharose™ column. This mimicking approach allows the purification of glycoproteins from complex mixtures at neutral pH. Spiked into an E.coli supernatant, glucose oxidase (GOx) purified with benzoboroxole–modified column afforded GOx with a purity of 98%, retaining the protein's enzymatic activity. Thermo–responsive polymers functionalised with benzoboroxole units are also reported as promising sensing platforms for the detection of diols and polyols at physiological pH [204].

In addition, benzoboroxole–containing nanoparticles have turned out as promising options for immunological applications, such as internalisation of dendritic cells and controlled antigen release [205]. These nanoparticles are stable under physiological conditions and were obtained by mixing glycopolymers and a benzoboroxole–containing polymer. The formation of nanoparticles was promoted by the establishment of dynamic covalent bonds between the two complementary polymer chains. The study also reported that the nanoparticles could be internalised by dendritic cells which then dissociate when exposed to the acidic environment of the organelles, allowing the controlled release of a preloaded antigen upon internalization thus opening up new opportunities for applications in cancer immunotherapy. Although reaching high affinity and specificity is still a challenge within the field, benzoboroxoles are a very promising class of compounds for the development of synthetic receptors for glycans and their derivatives. In order to disclose the full potential of

synthetic glycan receptors, future efforts should focus on the fine control of the spatial arrangements of the ligands. Moreover, the promotion of additional secondary interactions, such as hydrogen bonding and CH–π interactions must be considered to achieve selective molecular recognition.

1.9 Self–assembly

The process of self–assembly is the organisation of components such as molecules, polymers or macroscopic particles, which are ordered functional structures as a consequence of local, specific interactions among the components themselves [206]. The technique of self–assembly is useful for the preparation of nanofibrous scaffolds, and is presented everywhere in nature [207]. By observing the transient interactions of chemical groups, predictions and formulations can be nanosized self–assembled structures. The design, implementation and outcome will be discussed in the following sub sections and used to inform our own biosensor design.

1.10 Self–assembled monolayers

Self–assembled monolayers (SAMs) have attracted considerable attention for over two decades , this is due to the potential of SAMs in applications in chemical and biological sensors [208] as well as modifying surfaces [209, 210]. An important route to the preparation of nanoscaled materials is the self–assembly of molecules on solid surfaces [211].

The chemisorbed SAM consists of three parts; an anchor providing a strong bond to the substrate, a tail group and a spacer, that separates the anchor and the tail group on the surface. Studies have presented alkanethiols [212-215], chainlike molecules with a sulphur anchor, a linear hydrocarbon chain and optional functional tail group. The sulphur atom present on the anchor, forms a chemical bond on metallic surfaces, such as Au, therefore thiolate SAMs are able to provide stable bonding onto the substrate surface, shown in fig.19.

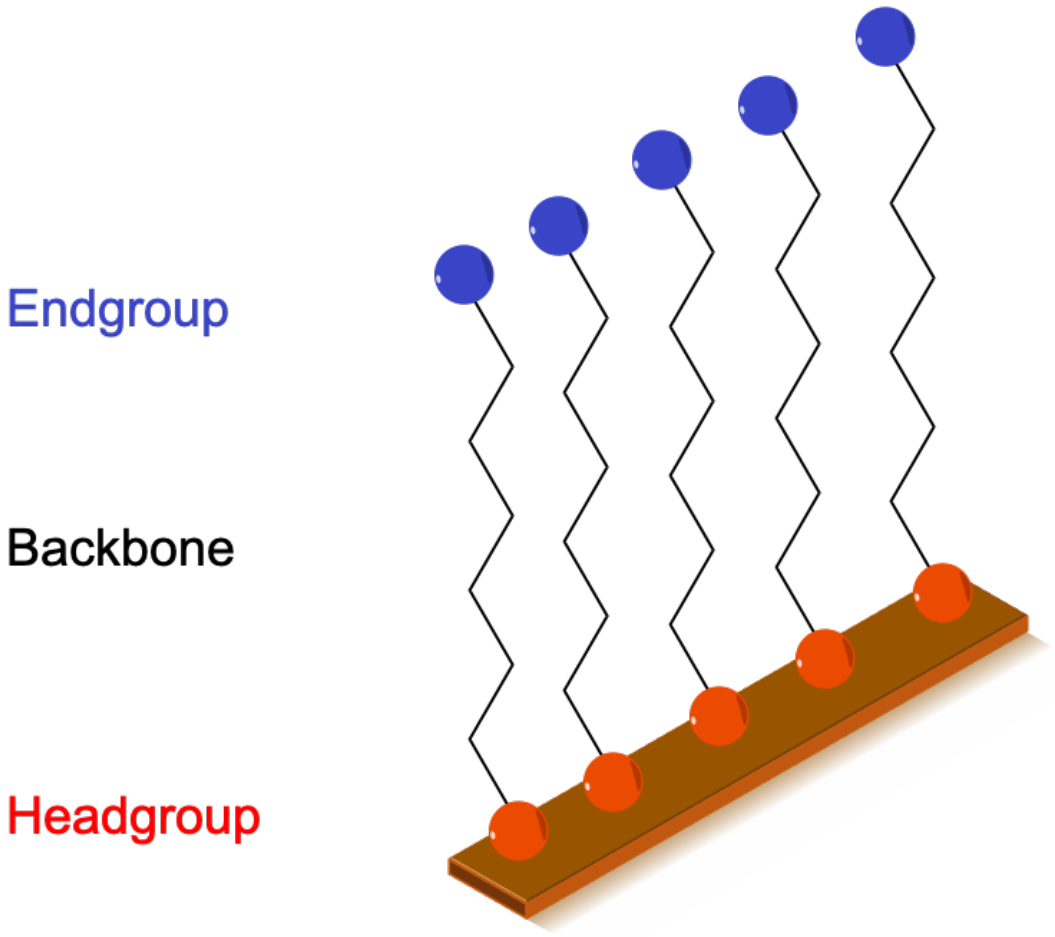

Figure 19: Representation of basic SAM structure.

The functional terminal groups of self–assembled monolayers (SAMs) govern surface properties such as wettability, friction and adhesion as well as providing anchoring sites for large complex ligands or molecules of biological or biochemical relevance [216]. The latter aspect is important because the synthesis of SAM–forming molecules such as alkanethiols that are coupled to biomolecules or other complex structures is often demanding [216]. A drawback of this aspect includes such molecules could be directly immobilized on surfaces like Au by self–assembly. However, if a SAM carries functional groups that undergo established coupling reactions, biomolecules can be attached after SAM formation.

Disulphides (R–S–S–R) and thiols (HS–R) adsorb strongly to Au surfaces but the nature of the event remains controversial. Generally, S–Au bonding occurs over two rapid physisorption of SAM compound to Au surface then slower chemisorption of S–Au bond formation [217] (Fig. 20). During the process of physisorption (shown labelled in fig. 20) SAM backbone groups form interactions with Au surface via Van de Waals interaction thus rapidly producing a ‘lying down’ arrangement of monomers [218]. Increasing the surface coverage, the SAM compounds present refrain from ‘lying–down’ to ‘standing up’. While changing configuration, the SAMs form a covalent bond between the Au–thiol species [219].

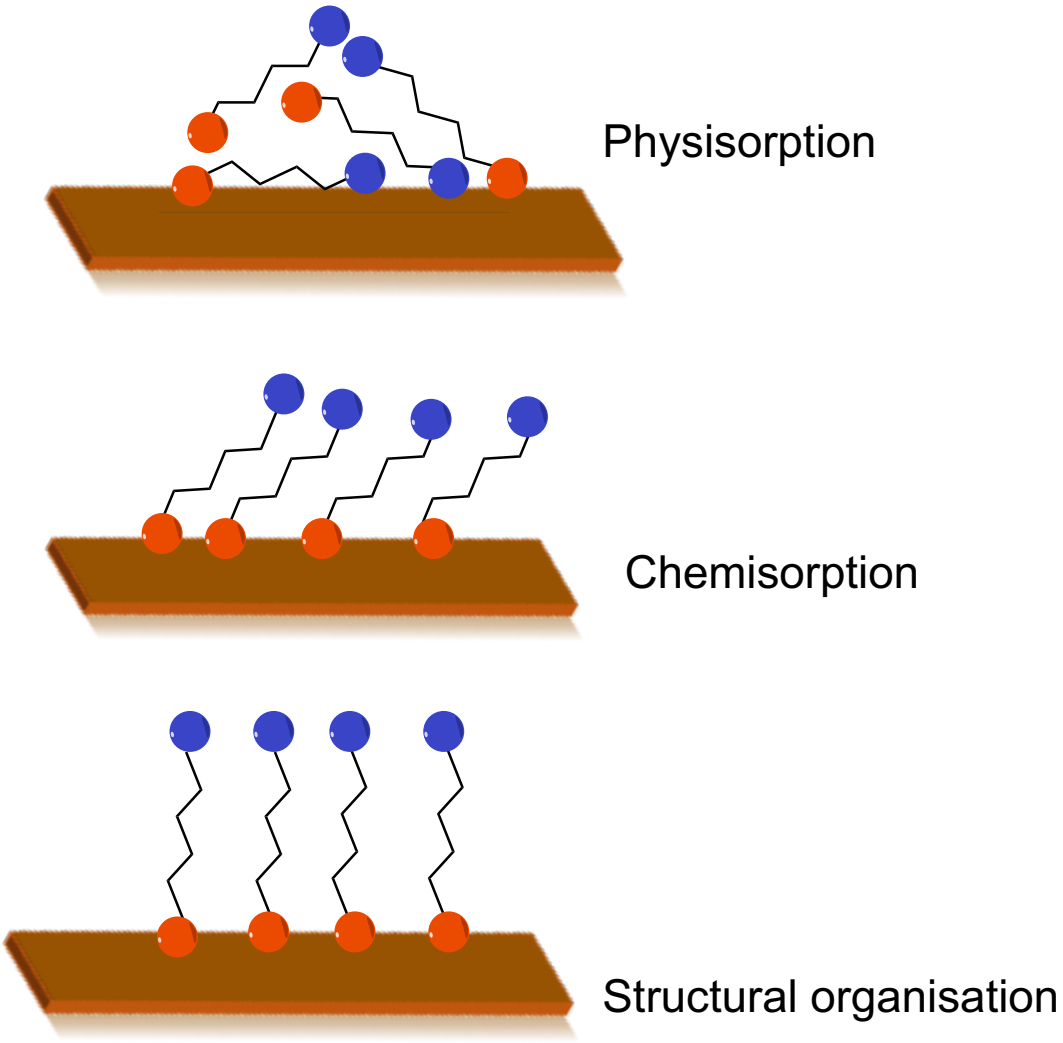

Figure 20: Preparation of SAMs. The substrate, Au on Si, is immersed into an ethanol solution of the desired thiol(s). Initial adsorption is fast (seconds); then an organization phase follows which should be allowed to continue for >15 h for best results.

It has been suggested that disulphides break into separate thiol species favouring the S–Au bond [220]. Disulphides provide several advantages over thiols for SAMs, including chemical stability, resistance to oxidation and no requirement for the protection of groups during synthesis procedures. This enables liberation of one end

of surface dithiol simultaneously chemisorbing the free dithiol thus producing typical substrate bound and free thiol groups at opposing terminus of the SAM monomer [221].

1.11 SAM defects

It is important to note that when discussing the formation of SAMs, the ideal scenario is being a well–packed and highly uniform monolayer free from contamination from other molecules and defects. However, defects are highly expected at varying degrees within the monolayer and the formation. Examples of defects are shown in the fig. 21, with examples including a) domain defects, b)pin–hole defects and c) disorder defects.

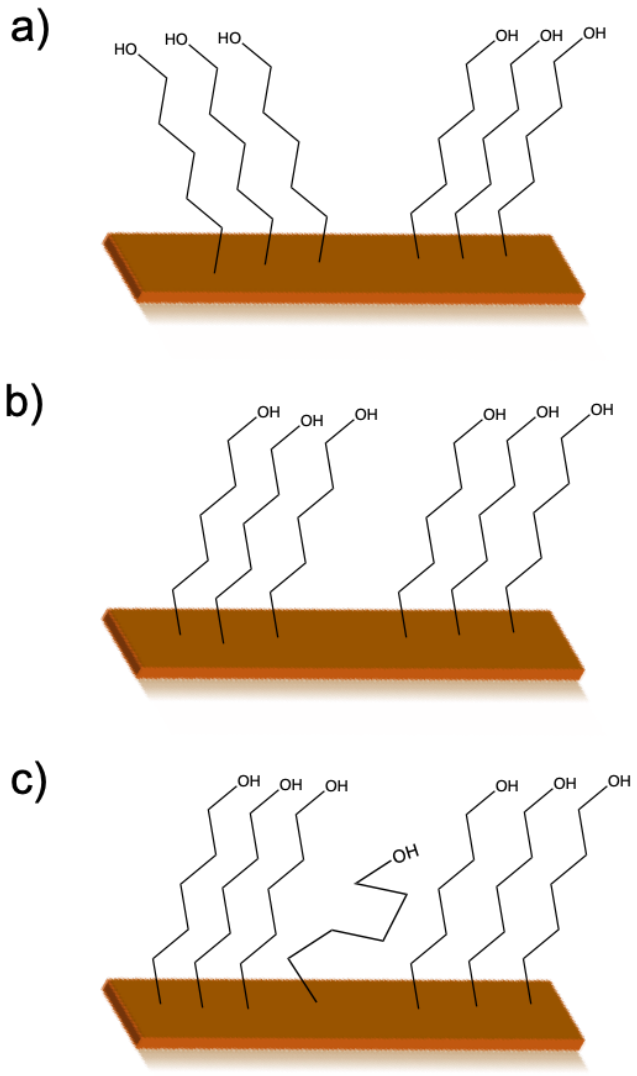

Figure 21: Schematic illustrating domains (a), pin–hole (b) and disorder (c) SAM defects.

Imperfections in the frontier of the underlying lattice. are known as domain defects, with SAMs presenting themselves on the substrate and arrange themselves in more than one orientation [222]. Pin–hole defects occur due to the failure of the alkanethiol to bind to a vacant site on the substrate causing isolated islands of monolayers to form [222]. Disordered defects are caused by disordered conformations of alkanethiol

chains unable to be fully stretched, for example a gauche defect [223]. The number of these defects on the substrate is influenced by the chain length of the alkanethiol and the terminal head group functionality [224]. Therefore, SAM protocols are optimised to produce monolayers with as limited defects as possible, providing the best possible SAM substrate.

1.12 Molecular imprinting

Molecular imprinting is an outstanding and favourable route generating customised affinity pockets in a cross–linked polymer matrix targeting molecules [225]. A general method of molecular imprinting includes the imprint molecule, also known as the template, added along functional monomers as well as high proportions of cross–linker, under optimised and appropriate conditions. During the reaction, polymeric chains organise around the imprint through functional groups interactions. The imprint molecules are removed from the polymer matrix, resulting in the development of binding pockets which are highly adapted. Fig. 22 shows a schematic representation of the molecular imprinting method described [226].

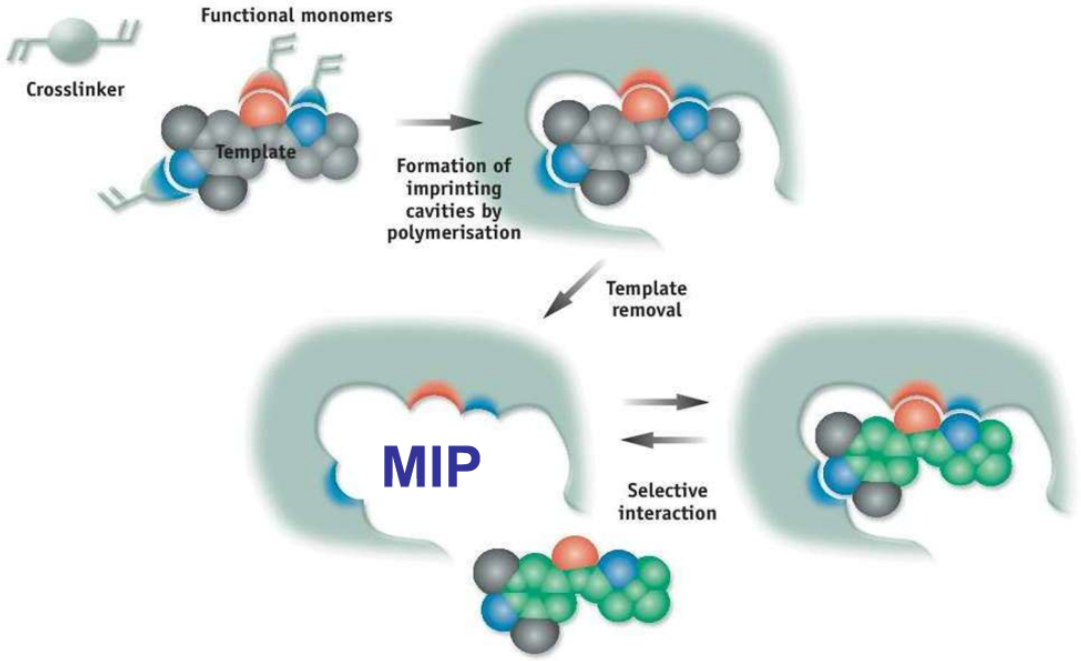

Figure 22: The schematic route of the synthesis of MIPs, demonstrating the template molecule is directed to the interaction of designed functional monomers [image taken from [227]].

1.13 The History of Imprinting

Molecular imprinting was studied in organic materials, in the 1930s, Polyakov was considered the first associated with the concept of molecular imprinting, with the synthesis of silica gel and its adsorption properties for imprint dyes [228]. Pauling et al proposed the formation of natural antibodies that take place in the presence of specific antigens. These antibodies function as template models and lead to the concept of template–induced interaction centres in antibodies that are responsible for unmatched selectivity as a result [229]. In 1950, the application of molecular imprinting arose with particular interest in the separation of organic molecules with different configurations, i.e., enantioselectivity occurred. The application was used when Patrikeev incubated

bacteria in silica gel, observing the resulting imprinted silica facilitates bacterial growth substantially compared with control silica [230]. Until the early 1970s, Wulff extended this approach to organic matrices. The contribution of Wulff and coworkers led the foundation of MIPs as biomimetic catalysts and holds the largest share of all [231-233].

Molecular imprinting is established as one of the most promising techniques for the introduction of molecular recognition features in a variety of material [234]. With this in mind, molecular imprinting remains a growing interest with numerous groups studying the different types of template models and imprinting strategies for different applications such as pharmaceutical selective drug delivery [235, 236].

1.14 MIP and artificial antibodies

To form a molecularly imprinted polymer (MIP), the template molecule is mixed with both mono–functional and difunctional monomers, to enable them to associate either covalently or non–covalently with areas of the template before triggering the polymerisation reaction to form a polymer matrix around the template involved. Subsequently, the cavity formed is complementary to the size, shape and chemical functionalities to the template formed. Following the removal of the template from the cavity, the imprinted scaffold can rebind a fresh target analyte. Ideally, MIPs should exhibit high selectivity and specificity for the target, with low affinities shown for competing molecules [237].

Current technologies such as mass spectrometry and multiplex immunoassays are extensively used in the diagnosis and prognosis of diseases, as well as the monitoring of response to therapy [238-240]. Although these technologies are very accurate and well developed, they require an exhaustive and time consuming sample preparation. Some advantages of this novel technology offered in sensing applications are the ease, rapid, and the inexpensive production of the applications.

The design of imprints needs to be carefully considered with different parameters to be taken into account. These parameters include; the monomer selection, relative ratios and the chemical functionalities [241]. Factors including incubation solvent and polymerisation time need to be also carefully considered, as these can drastically affect selectivity and sensitivity of the molecular imprint [242]. Imprints are created and use one of two methods; non–covalent imprinting and covalent imprinting. Non–covalent imprinting uses electrostatic interactions, hydrogen bonds, Van der Waals forces, or ionic bonds to form interactions between the monomer(s) and the template. However, covalent imprinting relies on covalently binding a ligand, such as a saccharide binding to a benzoboroxole. Covalent imprinting requires the covalent bond to be broken to free the template molecule using a washing step (e.g.an acidic or basic wash), but the removal of the template in non–covalent protocols requires much milder conditions [243].

Boronic acids are used as the functional monomers, with the approach being based on the formation of a polymer network around a template molecule (i.e. a glycoprotein).

This will create artificial binding sites and upon removal of the template can be occupied by their target [244]. Boronic acids used in MIPs can allow the realization of lectin–like surfaces for the specific recognition of glycoproteins, with the controlled orientation of the receptors around the glycoprotein enabling the creation of epitopes for specific fragments [190, 191, 245]. The approaches mentioned are both versatile and efficient, providing surfaces with high specificities along with strong affinities.

A sensor platform for the detection of prostate–specific antigen (PSA) when compared with other glycoproteins was studied. A pre–formed complex of PSA–acrylamido boronic acids was attached onto a functionalized gold surface and had provided immobilization of the synthetic receptors in spatial arrangements specific for the target glycoprotein. With the use of surface plasmon resonance (SPR), binding studies were conducted. These studies helped observe specificity of PSA, providing high affinity value of K_D in the micromolar range (1.8 μM), as well as detecting at the nanomolar concentrations [246]. Below is a figure which is a representation of the strategy, fabricating of glycoprotein–imprinted surfaces.

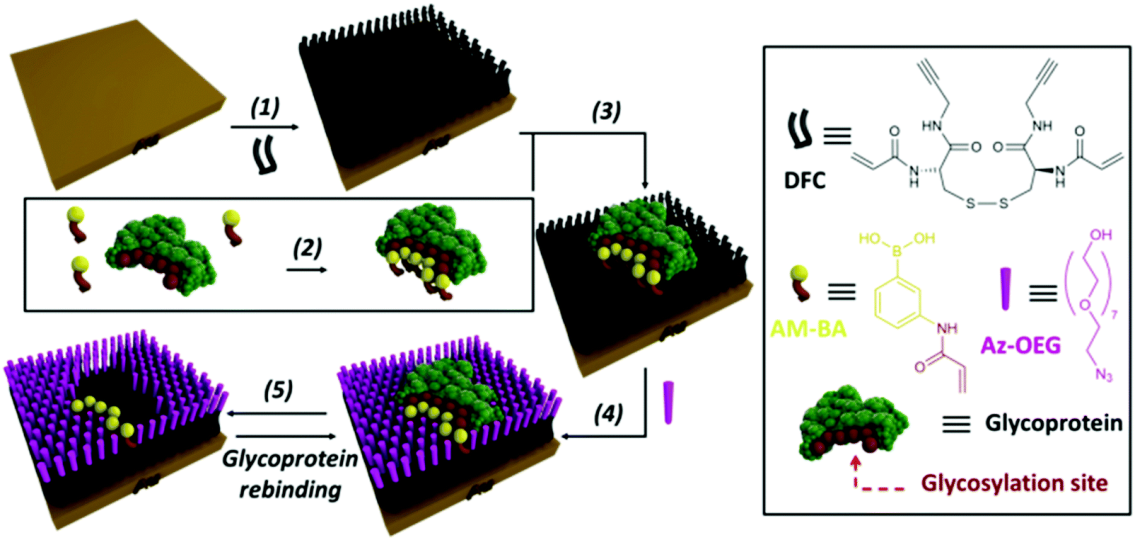

Figure 23: Strategy for the fabrication of glycoprotein–imprinted surfaces using acrylamido–boronic acids (AM–BAs); (step 1) self–assembled monolayer (SAM) formation on a gold surface with DFC molecule; (step 2) incubation of the AM–BA receptors with the template target glycoprotein; (step 3) grafting of the preformed boronic acid–glycoprotein complex on the SAM via acrylamide co–polymerization; (step 4) azide–terminated oligoethylene glycol (Az–OEG) functionalization to provide glycoprotein–shaped cavities; (step 5) removal of the template protein, affording a nanocavity specific for the target glycoprotein [image taken from [247]].

In addition, a surface–initiated controlled radical polymerisation is integrated with supramolecular templating and molecular imprinting to yield highly reproducible synthetic recognition sites on surfaces with dissociation constants (K_D). The K_D values were in the low micromolar range for target glycoproteins and minimal binding to nontarget glycoproteins. From the studies, it was shown that glycosylated and non–glycosylated forms of the same glycoproteins could be distinguished, giving a >5–fold difference in the binding affinity of the glycoprotein.

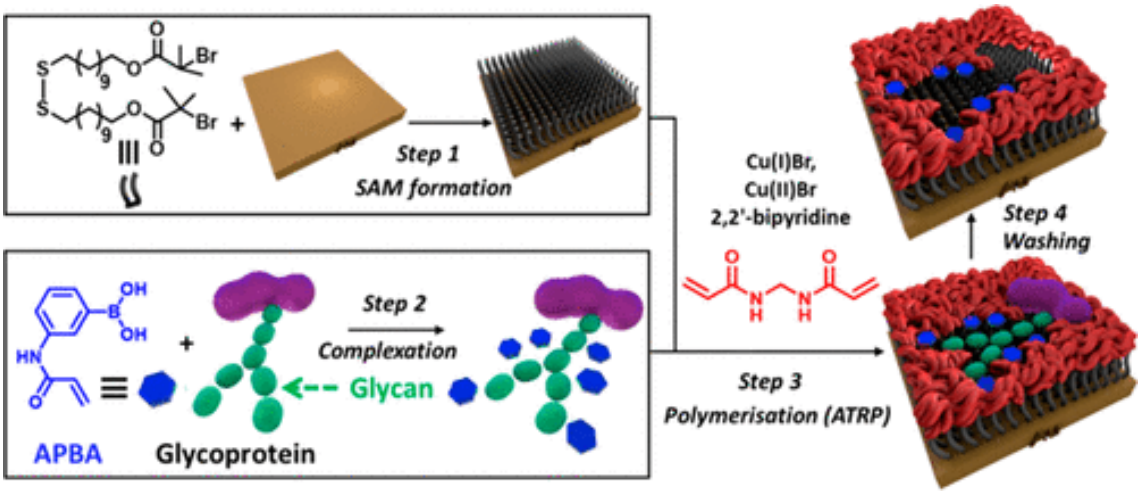

Figure 24: A schematic (not to scale) illustration of the molecular imprinting process involving pre complexation of BA–based carbohydrate receptors with the target glycoprotein and surface–initiated Atom transfer radical polymerization (ATRP) polymerization to form highly selective molecular cavities [image taken from [248]].

1.15 Concluding Remarks

The role of glycosylation in the development of disease is increasingly understood, but it is clear that there is a need for strategies that can detect changes in N– and O–glycosylation. For PCa, it is known that N–glycan changes occur to its glycoprotein biomarker with the progression of the disease and it is paramount that the sensing methods to enable the detection of these changes is to be realised. Current methods adopted to detect biomolecule glycan changes include HPLC and capillary electrophoresis (CE) coupled with mass spectrometry and are satisfactorily sensitive, however they require expensive and large set–ups [249-251]. On the other hand, the use of lectins in ELISA and agglutination assays are significantly cheaper than

previous methods, however both of these techniques are hindered by the weak affinities of lectins that lead to poor sensitivities for target saccharide molecules [252, 253].

1.16 Aims and Objectives

The overall aim of the thesis is the development of a novel recognition platform which has capability in the detection of saccharides. The oligosaccharides used are stachyose, nystose and man5. To create the platform, the surface must be homogeneous and crosslinking of the benzoboroxole must be successful. To target the oligosaccharides of interest selectively, a molecular imprinting system must incorporate functional benzoboroxole monomer within its design.

The strategy to achieve such a goal is outlined in a four stage process as shown in fig. 25. The first stage of the project is to create a foundation layer on a gold surface in which the benzoboroxole can crosslink to.

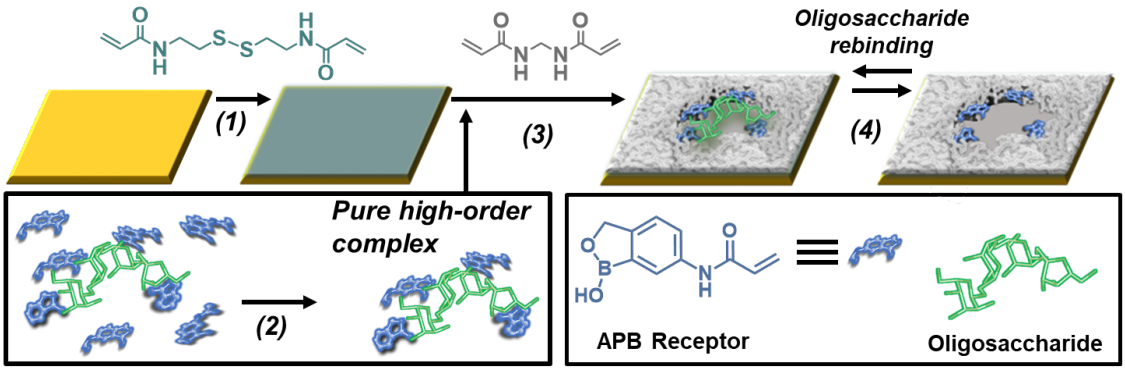

Figure 25: Method for creating synthetic materials with superselective oligosaccharide recognition. 1) Acrylamide-terminated monolayer formation using N,N′-bis(acryloyl)cystamine; 2) pure, high-order oligosaccharide: 5-acrylamido-2-(hydroxymethyl)phenylboronic acid cyclic monoester (APB) complex formation; 3) fixation of the complex on the surface and construction of molecular scaffold around the oligosaccharide template using N,N′-methylenebisacrylamide; 4) removal of the oligosaccharide template

The first step of the project will be to form an acrylamide-terminated monolayer using N,N′-bis(acryloyl)cystamine. This will be optimised using contact angle, ellipsometry and x–ray photochemical spectroscopy (XPS).

The second step of the project will be the complexation between saccharides and benzoboroxoles. In the initial case, stachyose will be used as the tetrasaccharide, with AABOB. The two species will be mixed together to create a complex that will then be used as the template to form the stachyose compatible imprint. The conditions to encourage the complexation will be investigated to ensure this binding is optimised.

The third step will bring steps 1 and 2 together, creating the molecular imprint. ATRP will be employed to crosslink the complex and the initiator SAM surfaces at room temperature in biocompatible conditions. A scaffold around the oligosaccharide template using N,N'–methylenebisacrylamide was also incorporated, enabling a pocket–like structure be present on the surface.

The final step is to begin to look into the oligosaccharide binding and rebinding process. Different oligosaccharides are used in comparison to determine if selectivity of the target molecule is observed when compared to other non–targets. Binding affinity values are calculated, R_{max} and K_D. R_{max} is determined by the relative molecular weight ratio between ligand and analyte and the amount of immobilized ligand [254] and K_D is the dissociation constants, the interactions with its ligands [255], giving a true understanding if the molecular imprint has potential to selectively and sensitively bind.

CHAPTER 2 – SURFACE CHARACTERISATION TECHNIQUES

Abstract: *In order to understand the physicochemical properties of the surfaces formed, different characterisation techniques are used. The techniques used include contact angle, ellipsometry, X–ray photoelectron spectroscopy (XPS) and surface plasmon resonance (SPR). In this section, all these techniques are briefly described and the reasoning behind their use for the SAM characterisation is discussed.*

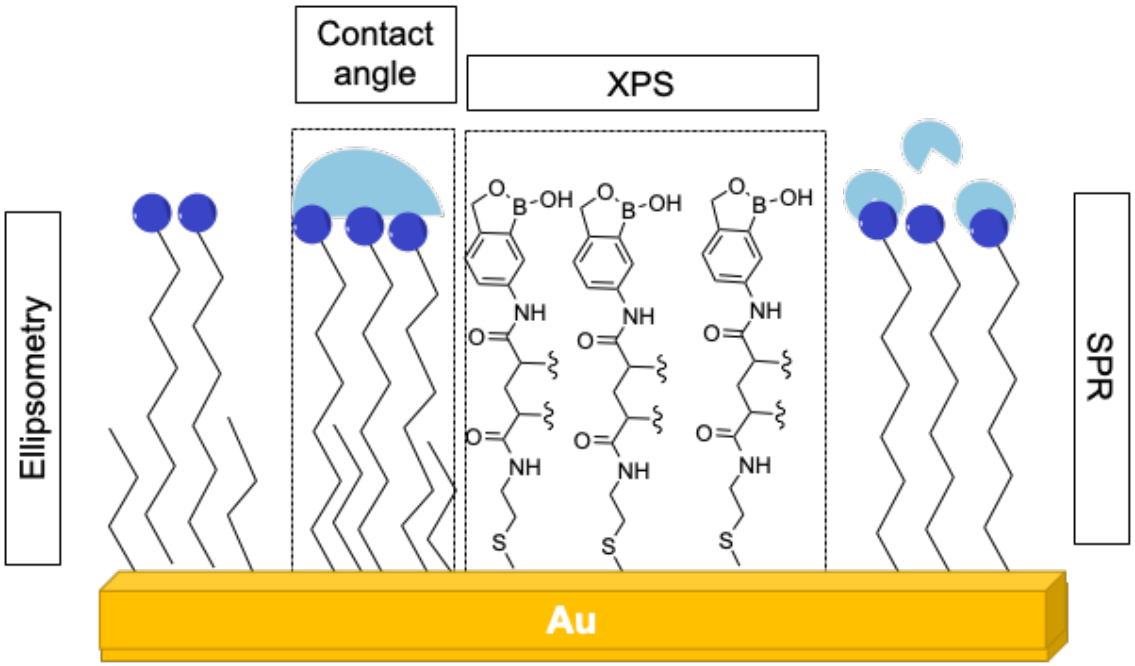

Figure 26: Overview of the methods used in this research work for studying thickness (ellipsometry), wettability (contact angle), elemental composition (XPS) and ligand interaction respectively (SPR).

2.1 Dynamic Contact Angle

In 1805, Thomas Young identified the measurement of the angle between solid–liquid and liquid–air interface can be a useful determinant of the properties of a surface [256]. The contact angle is defined as the angle that is formed by the intersection of the liquid–solid interface and the liquid–vapour interface [257]. Based on the Young–Dupree equation, the contact angle is calculated by the equation shown below:

Eq. 1 $$\gamma_{LV} \cos\theta_C = \gamma_{VS} - \gamma_{LS}$$

where γ is the surface interfacial tension, and VL, VS, and LS refer to vapour–liquid, vapour–solid, and liquid–solid interfaces [258].

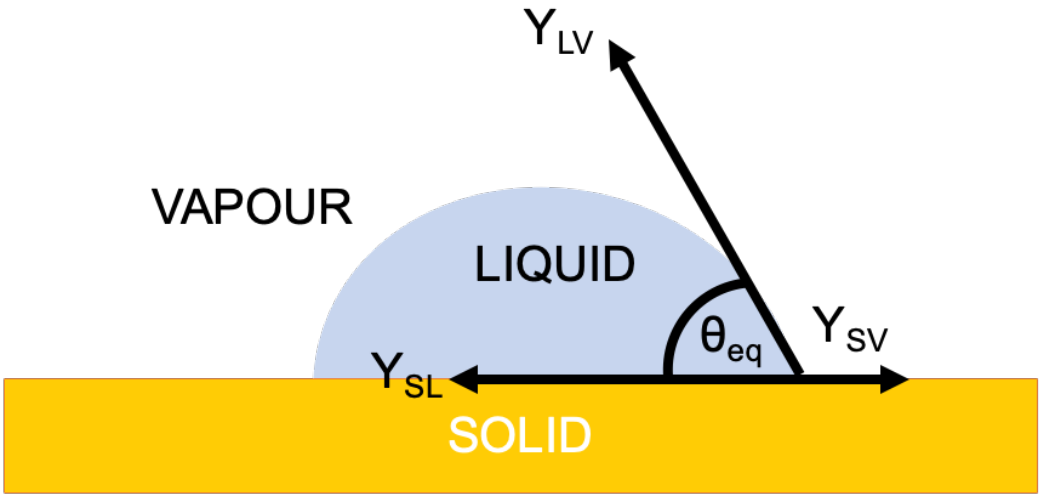

Figure 27: Equilibrium contact angle and interfacial energy relationship (SV: solid–vapour, SL: solid–liquid, LV: liquid–vapour).

This is geometrically acquired by applying a tangent line from the liquid–vapour contact point in the droplet profile. Contact angle is between the solid and the liquid and is dependent on the nature of the liquid as well as the characteristics of the solid [259]. Contact angles that are less than 90° are spread over the surface, whilst contact angles more than 90° will form a bead–like structure on the surface [259, 260].

The contact angle measurements allow the evaluation of the character of the surface and whether the surface is hydrophilic or hydrophobic. The technique is based on the principle that a liquid is in contact with a surface, in this case a gold functionalised surface, to form an angle θ, which can be measured with a contact angle apparatus, as shown in fig.28. The solvent, for example water, is deposited onto the surface from a syringe.

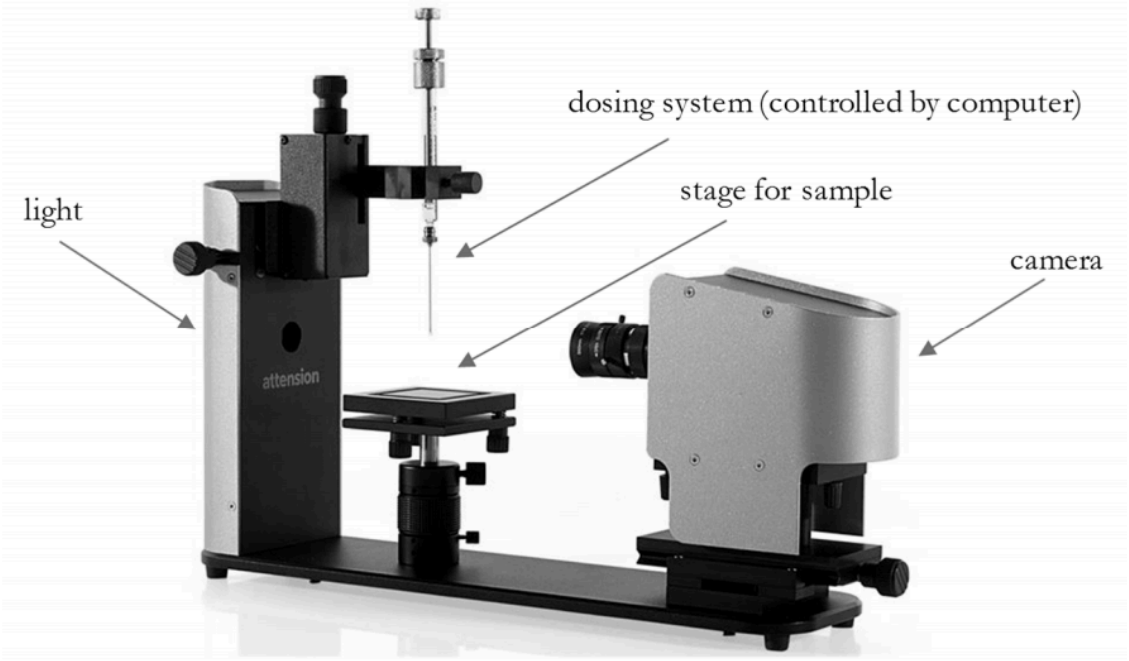

Figure 28: Diagram of the contact angle set up, by Biolin Scientific.

Once a liquid droplet is placed onto the surface, contact angles are formed by the expansion and contraction of the liquid. The advancing angle is frequently preferred when investigating solid surfaces, and is measured at a surface which is freshly wetted. The receding contact angle, θ_r, can be measured when a previously formed sessile drop on the substrate surface is contracted by applying a suction of the drop liquid through the needle. Precise measurement of θ_r is very difficult [261]. The angles obtained fall within a range, whereby the advancing as well as the receding angles reach a maximum. The difference between these two measurements is known as the hysteresis (H);

Eq. 2 $$H = \theta a - \theta r$$ [262]

Where a and r are advancing and receding contact angles, respectively.

Advancing and receding angles, shown in fig. 29, are taken over a period of time. With this in mind, an average is taken for both contact angle measurements. If the advancing and receding angles are similar, or the same, it is suggested that the monolayer surface is very well ordered. If the angles are similar throughout the surface, as multiple measurements are taken (in practice a minimum of three) the surface is considered as homogeneous [263].

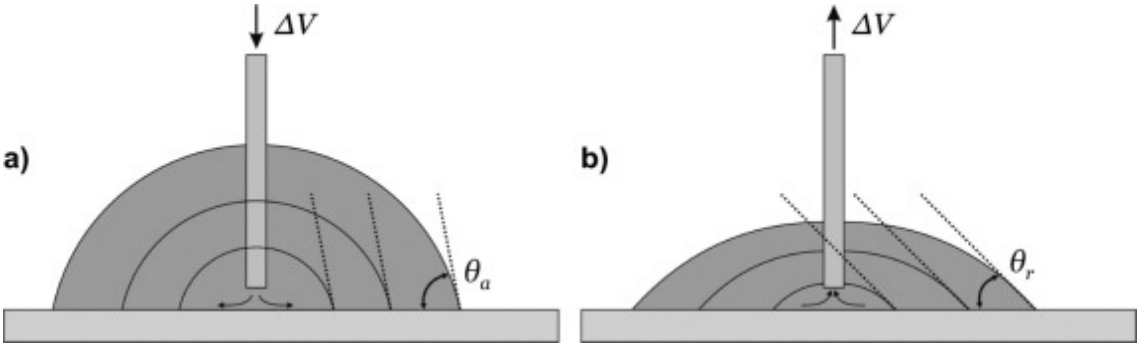

Figure 29: A diagram demonstrating a) advancing and b) receding angles on a surface [image taken from [264]].

Consequently, of both surface chemistry and homology can be analysed when using hysteresis. Hysteresis can provide information on both the homogeneity and the roughness of the surface in question.

2.2 Ellipsometry

The method of ellipsometry was first discovered in 1887 by Drude. The method probes the dielectric function of metals [265]. Ellipsometry is an optical technique used to measure both the transmission and the reflection properties after light is incident on a surface. Since the 1960s, ellipsometry developed a sensitive necessary measure of nanoscale layers with today allowing a convenient and accurate determination of the thickness as well as the refractive indexes of thin films [266].

Maxwell's theory explains how light is an electromagnetic wave consisting of two vectors: an electric field, E and a magnetic field, H. These field vectors are perpendicular as well as being perpendicular to the propagation direction of light, as given by the wave vector, k [267]. Both the E and H vectors themselves are formed

from two components – a parallel component, ‘s’, and a perpendicular component, ‘p’. In fig. 30, H is demonstrated as a blue wave whilst E is a red wave.

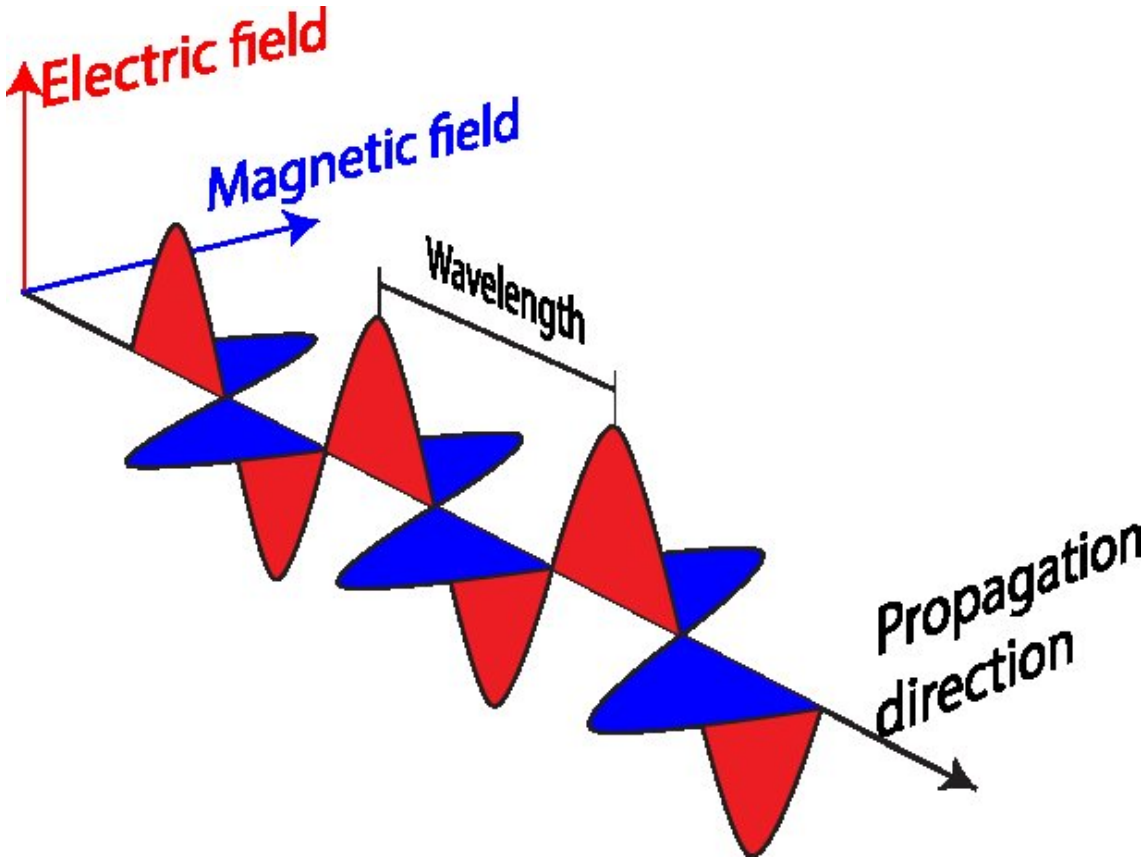

Figure 30: Illustration of light as an electromagnetic wave traveling in the propagation direction [268].

For non–polarized light, E and H oscillate in random directions (i.e. in a number of planes). However, for linearly polarized light, E oscillates in the same direction as H (i.e. oscillation occurs in a single plane). Therefore, ellipsometry takes advantage of these principles by measuring the changes that occur to the ‘s’ and ‘p’ components of the E vector of linearly polarised light upon reflection from a surface due to refraction by the surface molecules.

Applying these principles onto a system whereby linearly polarised light is shone at a defined angle onto a surface which has been functionalised, for example with a self–assembled monolayer (SAM), the light will resolve into the p ‘s’ and ‘p’ components due to its refraction by the SAM molecules (fig. 31).

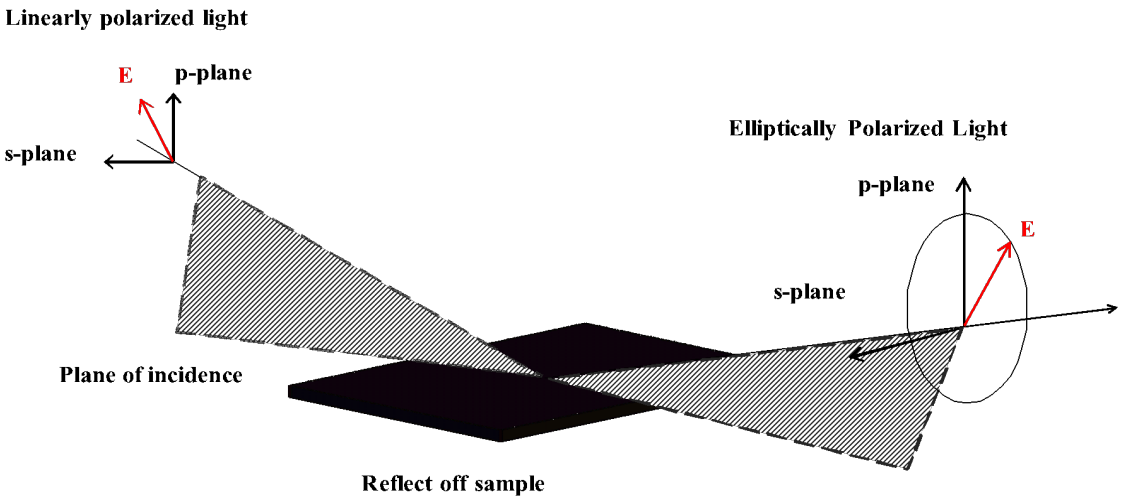

Figure 31: Schematic of a basic ellipsometry measurement gathering.

The change observed in both the phase and amplitude of the ‘s’ and ’p’ components produces elliptically polarized light and these changes can be measured and quantified using an ellipsometer to derive information about a surface, such as the adsorbed SAMs thickness. A typical ellipsometer setup is shown in figure 32.

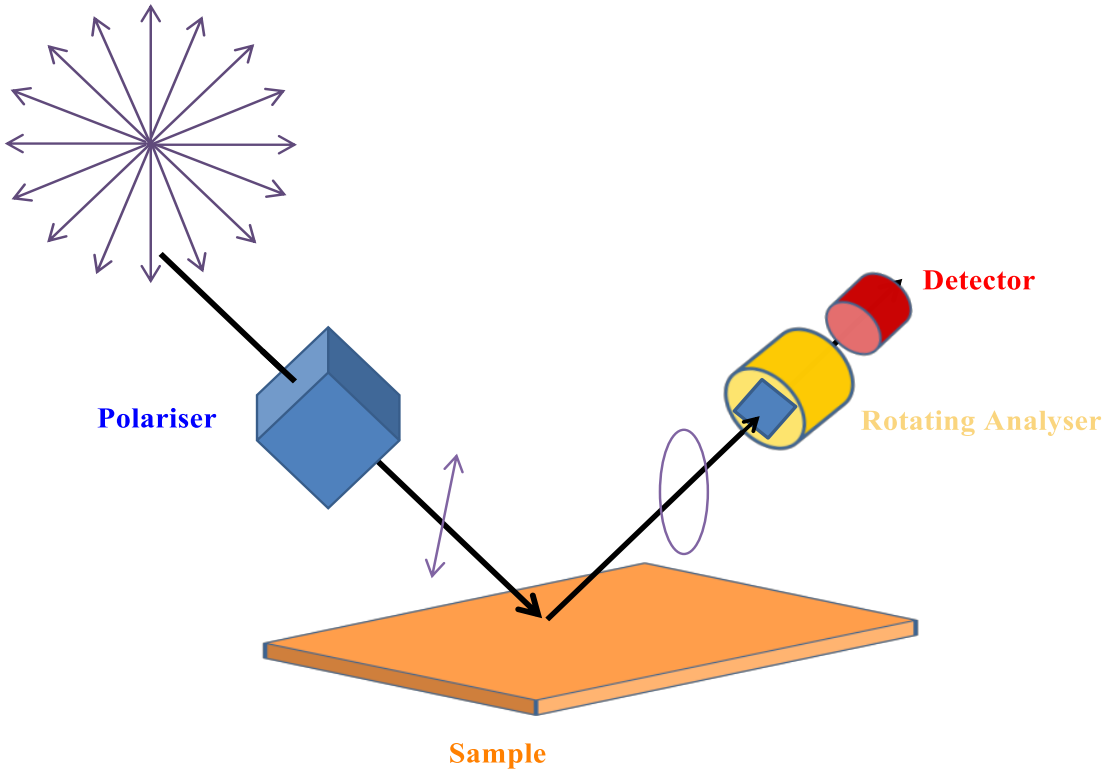

Figure 32: The schematic of a basic ellipsometry measurement gathering.

The configuration of the rotating analyser is shown in the fig. 32. Unpolarised light is produced from a light source and is sent through the polariser. Allowing the light of the preferred electric field orientation to pass, the polariser axis is oriented between both the s– and the p– plane, where both arrive at the sample surface. Reflecting from the sample surface, the linearly polarised light becomes elliptically polarised and travels through a continuously rotating polariser (referred to as the rotating analyser in the figure). The amount of light allowed to pass will be dependent on the polariser orientation. The final stage is where the detector converts the light transmitted to an electronic signal to determine the reflected polarisation. The data obtained is compared to the known input polarisation, determining the polarisation change caused

by the gold sample. Thus, this is the ellipsometry measurement of both Psi (ψ) and Delta (Δ).

Primarily, the method is interested in the change in s– and p– components upon reflection or transmission with respect to each other. The reference beam has a vital part in the experiment as a known polarisation is reflected or transmitted from the sample. It is the output polarisation which is what is measured. Commonly, the change in polarisation is written as:

$$\boldsymbol{\rho = \tan(\psi)\, e^{i\Delta}}$$

The incident light is linear with both s– and p– components, while the reflected light has undergone amplitude and the phase changes for both of the s– and p– polarised light. It is this change in polarised light that ellipsometry measures. The ψ and Δ parameters are calculated by applying a least–squared minimization iterative process incorporating the Fresnel equations whereby the unknown optical constants are varied. The collection of data includes the following primary tools: light source, a polarisation generator, the gold sample, polarisation analyser and the detector. Both, the polarisation generator and analyser are constructed of optical components which manipulate the polarisation; the polarisers, compensators and the phase modulators [269].

Since ellipsometry is an indirect method of determining the optical constants of a material, such as for SAMs a Cauchy model is used where the SAM layer is assumed to be transparent (k=0) with a refractive index of 1.49 [270]. The resulted thickness

value is then selected from the value with the lowest Chi squared value (χ^2) to indicate the best agreement between the measured and calculated ψ and Δ parameters.

2.3 X–ray Photoelectron Spectroscopy (XPS)

X–ray photoelectron spectroscopy (XPS) is a surface analysis technique used to both identify and measure the concentration of elements which are present at a surface. The basis behind the technique is to use monochromatic X–rays to bombard a material in a ultra–high vacuum (UHV) and cause atoms of the elements that are present near the surface examined to release electrons that are detected and thus analysed for their kinetic energy and intensity. The basic set up of a XPS spectrophotometer is shown in fig. 33 [271].

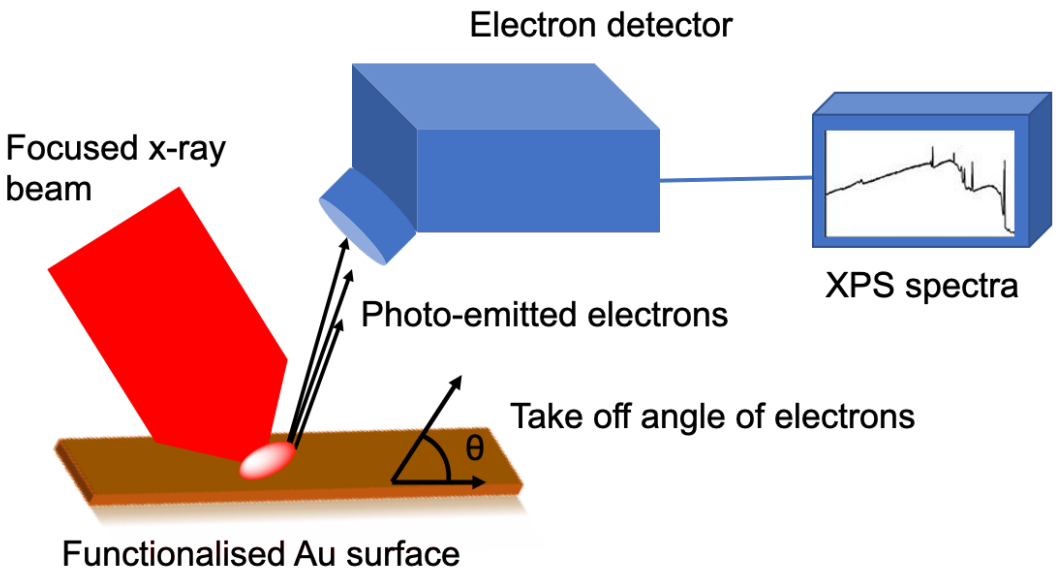

Figure 33: Schematic of an XPS system. The sample is mounted onto a platform within the UHV chamber that is then bombarded with Kα X–rays produced from a Mg or Al probe. The photoelectrons released from the sample are then collected by the detector to generate the XPS spectra.

A sample, shown here as a functionalised Au substrate, is mounted upon a stainless steel platform within the UHV chamber. X–rays excite the specific area of the specimen, releasing photoelectrons. Once an X–ray photon hits the electron of an atom, as shown in fig. 34, it causes this electron to be emitted into the photoelectron process [272].

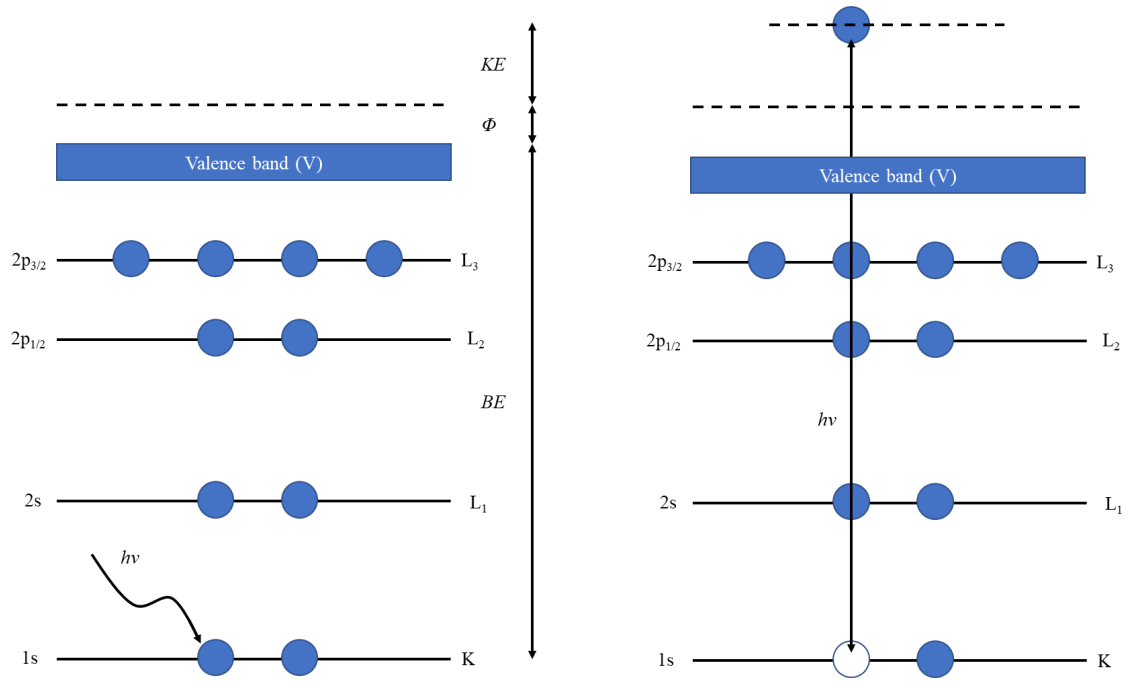

Figure 34: Schematic of photoelectron emission from the core shell of an atom.

In this technique, the sample is irradiated with X–ray beams while the kinetic energy and number of electrons that escape from the surface of the material are simultaneously measured [273]. The balance between hv and the kinetic energy of a photoelectron, $E_{k,}$ is expressed as;

$$E_K = h\nu - E_B$$

Where by the E_B is the binding energy of the electron to nucleus relative to the Fermi level. The E_B value and the chemical shift are utilised for the identification of an element and are the estimation of its chemical bonding state within a specimen [274].

2.4 Surface plasmon resonance (SPR)

Surface plasmon resonance (SPR) is an optical sensing technique that was widely used in this research work. The change in refractive index (RI) of a dielectric surface interface is utilised in the method. SPR has become widely used for studying the interaction between surface–used biomolecular binding of ligands to the target analytes, measuring the binding of an analyte in real time [275]. Advantages of SPR include the ease to set up, low running costs and the real–time measurements of both binding affinities and kinetics [276].

Before discussing the typical set–up of the SPR, the surface plasmon wave (SPW) from a dielectric surface interface must be mentioned. The monochromatic 'p' polarised light is fixed at a wavelength and shone at a particular angle (θ_i) through a glass prism with a high refractive index (RI). This glass prism is in contact with a thin conducting metal surface approximately 50 nm, such as Au or Ag, and a SPW is generated. The SPW is generated because of the total internal reflection (TIR) of the incident, enabling the excitation of free electrons of the metal thus generating photon–plasmon surface electromagnetic waves. This is shown in the fig. 35 [277]:

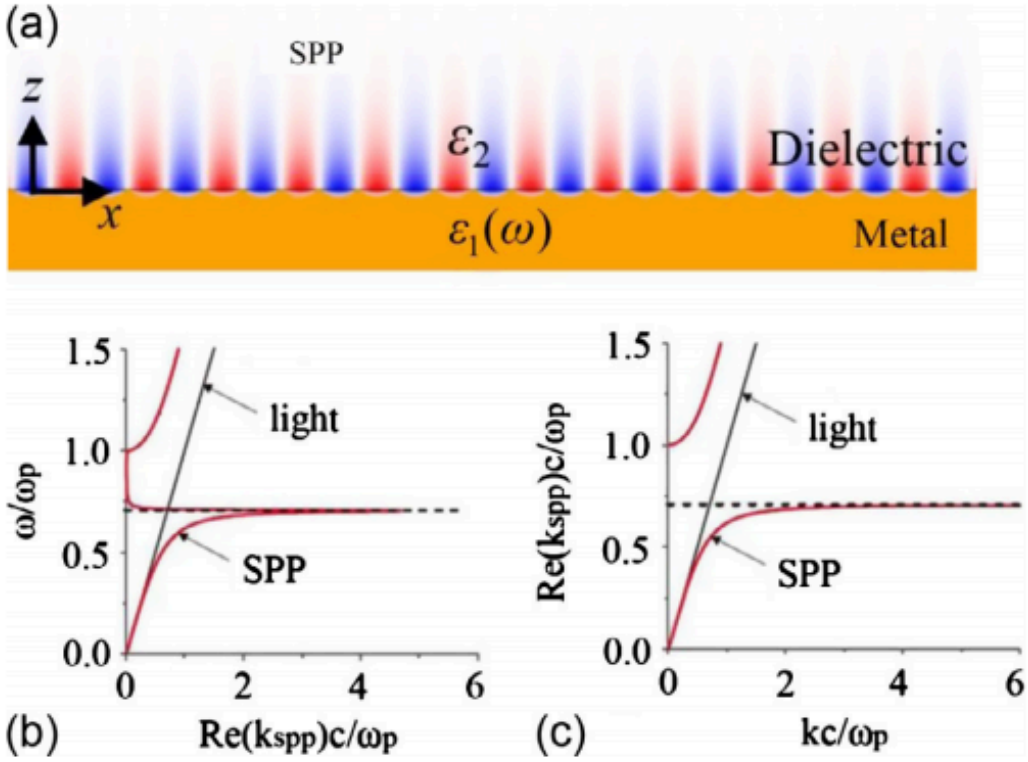

Figure 35: (a) Schematic of propagating SPPs on a metal-dielectric interface. Dispersion of SPPs propagating along a metal-air interface for (b) real frequency and complex wave vector, and (c) complex frequency and real wave vector. The flat asymptote dashed line represents the non-retarded surface plasmon solution.

Changes in RI within the immediate area of the dielectric interface can be detected. This is possible by measuring the change in the angle of the intensity minimum resonance angle (θ_rA to θ_rB) of the reflected light when a resonance change occurs. Reflected angle changes ($\Delta\theta$) can be detected by a photodiode and can be monitored in real time using an SPR set up [278].

Here, the system is first prepped by the equilibrium of a sensor chip. This sensor chip is fabricated from Au sputted onto a glass slide and placed on the top of the prism with

the presence of buffer (fig. 36, a). Equilibrium of buffer must be established before the analyte of interest is injected into the flow channel and pumped through and meets the surface (fig. 36, b). Following a change of RI occurs once the analyte binds to the surface, a change in reflected angle intensity minimum (θ_rA to θ_rB) is caused (fig. 36, c). These changes are recorded and the binding kinetics of the injected analyte are measured and analysed (fig. 36, d).

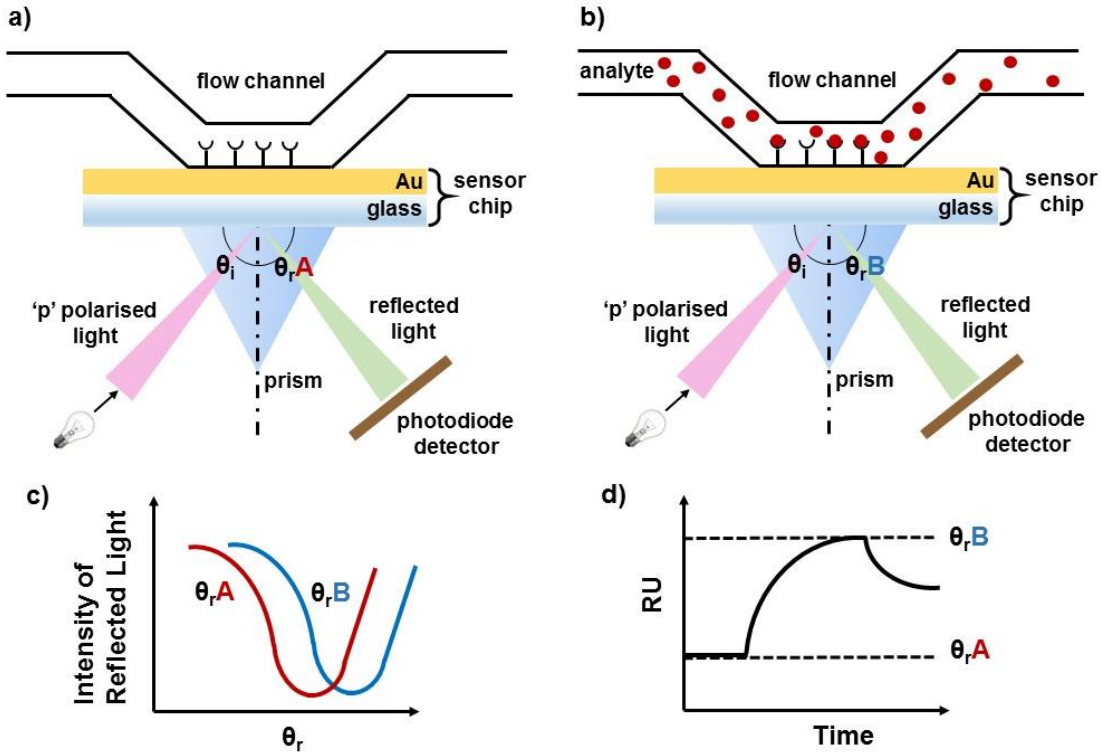

Figure 36: Schematic diagram of an SPR measurement using the Kretschmann set up. The functionalised Au/glass sensor chip is placed on–top of the prism and exposed to the flow channel. (a). When analyte is introduced and binds to the chip surface this causes a change in the RI (b). This change causes the intensity of the refracted light to dip (c) associated with the change in the angle (θ_rA) relates to the mass bound. The angle shifts to (θ_rB) when all the available mass has bound. These changes are

monitored using a sensorgram (d) that is a plot of the resonance angle versus time [image reproduced using [279]].

CHAPTER 3 – THE FORMATION AND CHARACTERISATION OF THE DSA SAM AND THE CROSS–LINKING OF AABOB ONTO A DSA SAM.

Abstract: *This chapter details the development of the N',N'–bis(acryloyl cystamine), abbreviated to DSA, monolayer. The surface is characterised using contact angle, ellipsometry and XPS. In addition, control surfaces, benzyl–terminated and a benzoboroxole–modified surface are created. Control surfaces were optimised to determine whether binding to sugars is possible and if so, binding affinities can be generated. Radical polymerisation is used to successfully crosslink the benzoboroxole carbohydrate receptors and the DSA monolayer. The optimal conditions will be later used to continue the development of the surfaces for molecular imprinting in chapter four.*

3.1 Introduction

Known as the most effective as well as versatile strategy for surface functionalisation, self–assembled monolayers (SAMs) can be a robust approach to fine–tune the surface of interest [280]. The formation of a SAM requires chemisorption on a surface which is followed by the spontaneous organization into 2D–crystalline long–range molecularly ordered domains [281]. SAMs have been seen across a variety of fields, including biomedical implants and applications [282, 283], corrosion inhibition [284] and of concern to this research, biosensors [285, 286].

Free–radical polymerisation is the most economical process for use with monomers due to the fact that reaction mixture does not require the high–purity reactants but does require rigorous exclusions of air, moisture and other impurities for successful operation [287]. The research conducted in this thesis looks at free–radical polymerisation with ammonium persulfate (APS) acting as a free–radical initiator and tetramethylethylethyendiamine (TEMED) used to catalyse the polymerisation [288].

Benzoboroxole–functionalised monomers have been incorporated to aid the detection of other diseases, with HIV as an example [289]. This chapter investigates the formation of SAMs, some containing benzoboroxoles, to understand whether or not successful saccharide binding can occur. This will be compared with non–benzoboroxole containing monomers, to determine if high selectivity can be observed.

3.1.1 Objectives:

The objectives of the work in this chapter can be broken down as follows:

- Create a high quality SAM with DSA.
- Use XPS to determine the optimum DSA concentration to be used.
- Successfully cross–link AABOB to DSA and confirm the surface physicochemical properties with the contact angle, ellipsometry and XPS techniques.
- Prepare control SAMs to be used later for comparison, namely benzoboroxole–modified surface as well as control benzyl–terminated SAM.

3.2 Cleaning of the bare Au surface

3.2.1 Introduction

Evaporated gold films are frequently used as substrates for the study of biomolecular adsorbates, nanoparticle systems and full monolayer films. These studies often benefit from a predeposition cleaning of the surface that removes adventitiously adsorbed material from laboratory contaminants [283]. However, the removal of surface contaminants is critical to all processes where the surface must be modified in some manner, such as deposition of thin films. Both organic and inorganic contaminants can cause unreliable bonding or even prevent continuous bonding required for SAMs [290]. The use of wet and dry cleaning techniques are well established for the removal of surface contaminants.

Wet cleaning techniques such as piranha acid solution can be used to clean substrates such as gold (Au). Piranha solutions are used to clean materials used in various fabrication processes. The most common is acid piranha: a 7:3 mixture of concentrated sulfuric acid (H_2SO_4) with 30% hydrogen peroxide (H_2O_2), which is used to remove organic residues from substrates. Piranha acid solution is used for the removal of any trace amounts of organic residues, such as photoresist, from the substrates [284]. Unfortunately, piranha cleaning has its drawbacks, such as the leading of extensive and uncontrolled etching of the surface as well as the severe disruption of surface topography [289].

A dry cleaning treatment is used for the removal of hydrocarbon contamination and is used for a number of substrates involving complex composition or geometries [285]. An example of a dry cleaning treatment is UV cleaning. The use of UV cleaning has been found to be attractive and there have been a few detailed studies of the cleaning of multicomponent surfaces consisting of metals, metal oxides, and other compounds [286–288]. The effects of relative cleaning rates and cross–contamination are particularly important in the application to cleaning of microelectronic device surfaces. The UV cleaning has the advantage of no damage to the surface, hence the process can be used on parts with delicate surfaces. On the other hand, UV cleaning is limited mainly to removal of biodegradable hydrocarbon contaminants. Most inorganic contaminants, large particles, and other debris cannot be removed. Particles and inorganic contaminants cannot be removed as these are not amenable to photosensitive oxidation [291].

The initial surface, bare Au, for the use of SAM surfaces must be thoroughly cleaned with no or limited combination present. If untreated or not cleaned, the monolayer formation can be disrupted, preventing whether the SAM can form onto the surface. Piranha cleaned Au as well as UV cleaned Au are compared, using contact angle, to determine if one of the techniques is considered more favourable than the other.

3.2.2 Results and discussion

To determine if the cleaning of the bare Au substrates with piranha acid solution varies in comparison with UV cleaning, the contact angles of both cleaning procedures with bare Au are shown in fig. 37.

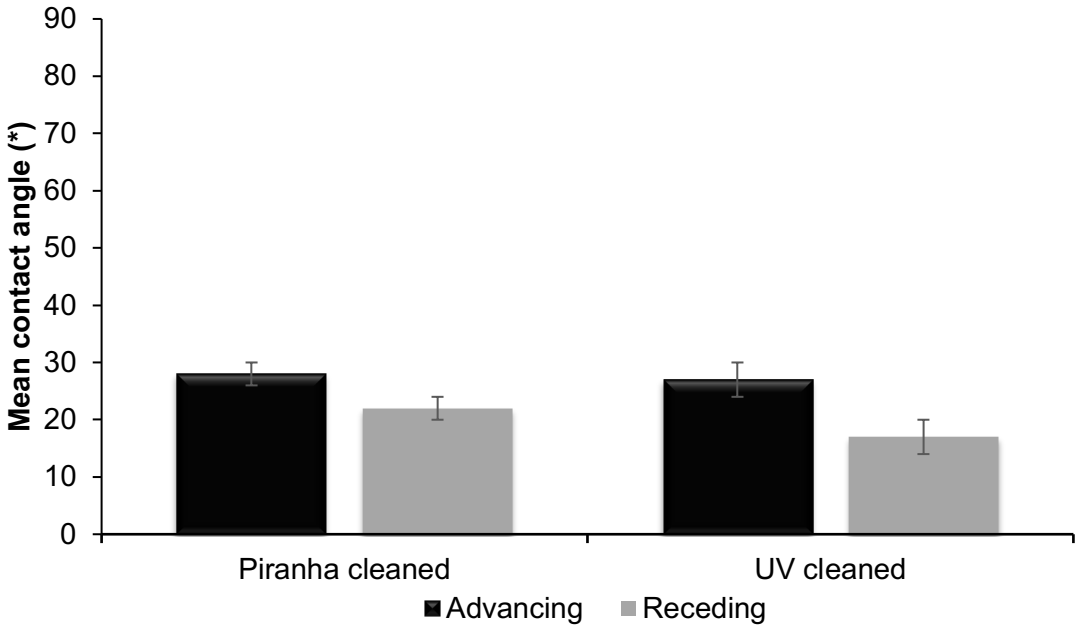

Figure 37: Contact angle data of Au surfaces that were cleaned under UV or cleaned using piranha acid solution.

The advancing angle obtained with the cleaning procedures were shown to be 27° and 28°, for UV and piranha cleaned Au respectively. The receding angles are 17° and 22°, for the UV cleaned Au and the piranha cleaned Au respectively. The contact angles concluded that the hysteresis of piranha solution was 6° and the UV cleaned Au was 10°. Both surface chemistry and surface topology are known to influence the contact angle and consequently the contact angle hysteresis [292]. Cleaning is to be effective in the removal of heavy metal contaminants, manifestation of cleaning is a reduced contact angle for water [293]. Contact angles at 0° are considered very clean, and any observed contact angle would suggest contamination, such as oxygen species, to the surface [294]. Therefore, the lower the variation of contact angles, resulting in the hysteresis value, the less contaminated the surface is. This is ideal for the initial surface for the formation of SAM.

3.2.4 Conclusion of cleaning of the bare Au surface

No evident difference was observed with the cleaning changes of gold surfaces, although piranha solution cleaned Au was shown to have a lower standard deviation than those values obtained with the UV ozone cleaned chips. Due to the consideration of both time and cost of resources, piranha solution was to remain the standard protocol for the cleaning of the Au surfaces. Piranha solution is advantageous due to the treatment resulting in low residual carbon present [295], which will prevent any contamination when forming the SAMs on the surface. The next stage was to consider the DSA SAM and the optimisation of the monolayer.

3.3 N'N' – bis(acryoyl) cystamine SAM

3.3.1 Introduction

The use of self–assembled monolayers (SAMs) is rapidly growing in different fields. Many biomedical fields are able to apply SAMs as an interface–layer between a metal surface and a solution or vapour. The formation of SAMs is dependent on concentration of thiol derivative, immersing time and incubation solvent [287], each individually explored in this sub–section. The studies started with investigations on the formation of SAMs based on the N, N' bis(acryoyl) cystamine, abbreviated to DSA, which the structure is shown in fig. 38.

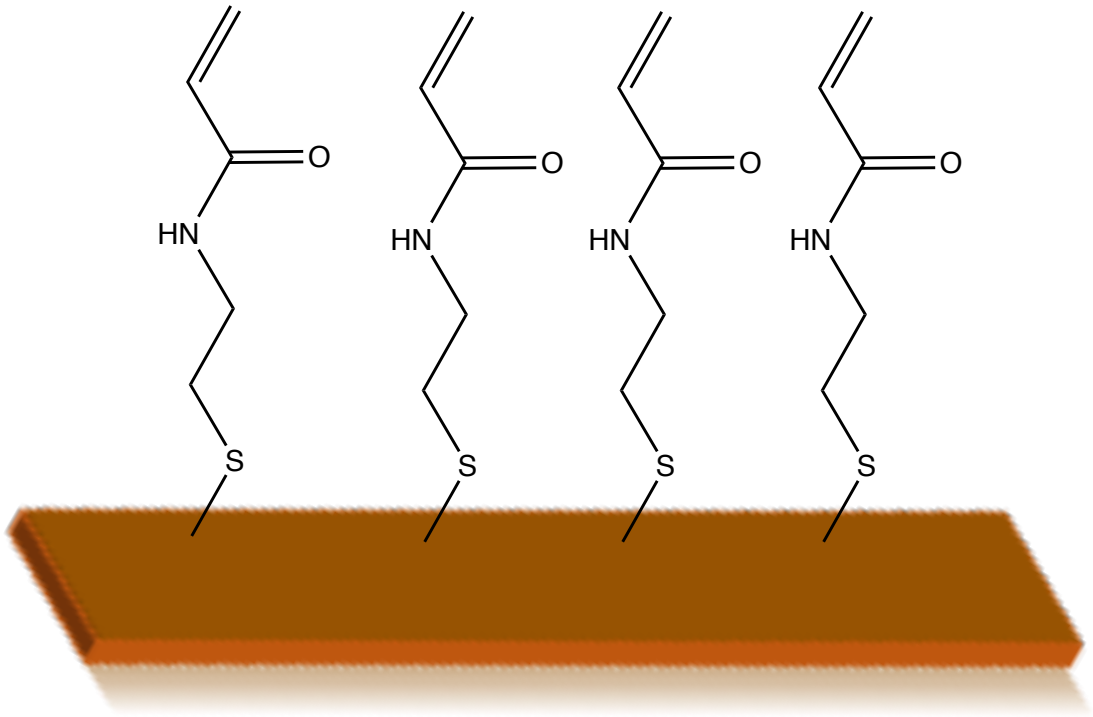

Figure 38: Schematic illustrating the structure of DSA SAM on gold

The strength of the gold–sulphur (Au–S) interaction formed between thiols and gold surfaces and provides the basis of fabricated robust SAMs for diverse applications

[220]. DSA is commercially available, making the SAM ideal for the research. As shown, DSA is a symmetric molecule and an excellent polymerisable compound because of conjugation of double bond and carbonyl bond. The conditions were each used to optimise the formation of the SAM with the use of different techniques. The techniques used were contact angle, ellipsometry and XPS. Contact angle along with ellipsometry determine whether or not the monolayer is well–formed, before the use of XPS demonstrating the successful chemical absorption on the Au surface.

3.3.2 The formation and optimisation of the DSA SAM

Formation as well as the optimisation of the surface is required, allowing for the DSA molecule to form a thiolate bond with Au and form a well–organised monolayer [296, 297]. Firstly, the DSA SAM formation needs to be optimised to create a single layered surface. The SAMs were created by first cleaning the ~1 cm^2 gold substrates using piranha solution for 7 minutes following which they were then washed with water and HPLC ethanol. The cleaned chips were then immersed in a solution of HPLC ethanol or methanol containing DSA in varying concentrations as stated in the results. The Au chips were incubated for 24 h at room temperature, before being washed with an excess of ethanol and UHQ water before finally dried under a stream of argon.

3.3.3 Contact angle of the optimisation of DSA monolayer

The DSA monolayer is first characterised with dynamic water contact angle to assess the surface's wettability. As shown in table 2, different concentrations of DSA were

used to form the SAMs, and contact angle measured to demonstrate whether the monolayer was considered hydrophilic or hydrophobic. If the contact angle is shown to be <90°, the surface is classed as hydrophilic with a high wettability [298]. The two concentrations used initially, were 0.1 mM and 1.0 mM at two different incubation solvents, methanol and ethanol. Advancing (θ_{adv}) as well as receding angles (θ_{rec}) were measured on the surface, before the hysteresis ($\theta_{adv} - \theta_{rec}$) was calculated.

Table 2: Contact angle analysis on different concentrations of DSA.

DSA Concentration (mM)	Solvent	Advancing angle (º)	Receding angle (º)	Hysteresis (°)
0.1	Ethanol	78.1 ± 4	61.7 ± 3	16.4
	Methanol	61.5 ± 3	40.6 ± 3	20.9
1.0	Ethanol	68.5 ± 3	59.9 ± 3	8.6
	Methanol	55.6 ± 3	44.7 ± 3	10.9

From the data obtained, all angles were <90º, suggesting that the surface is hydrophilic. The hysteresis was smaller when DSA was incubated in ethanol than that of methanol, shown in the fifth column of the table above. The advancing contact angle for the 0.1 mM DSA incubated in HPLC ethanol was shown to be 78.1 ± 4°. However,

the receding angle was 61.7 ± 3°, calculating a hysteresis of 16.4°. Contact angle hysteresis arises from the chemical and topographical heterogeneity of the surface, the swelling of the surface, rearrangement of the SAM or the alteration of the surface by the solvent [299]. Despite the seemingly simple application of the hysteresis, it has still been observed on smooth homogeneous surfaces as well [300]. The large hysteresis of the contact angles was reported on the 0.1 mM DSA in ethanol. It is suggested that there is low surface organisation observed as the hysteresis >10° [301]. In addition to the 0.1 mM DSA in ethanol, methanol used as an incubation solvent for the formation of the DSA SAM, the hysteresis was greater for the use of 0.1 mM DSA. The hysteresis was calculated as 20.9°, also suggesting low surface organisation. The increase in concentration of DSA was to allow for more SAM to be well organised on the surface, however the hysteresis calculated was still high.

Therefore, another consideration was made for the incubation solution to include trifluoroacetic acid (TFA) at a low concentration. The involvement of the acid is to prevent hydrogen bonding between the acrylamide immobilised on the surface and those in solution [302]. Hydrogen bonding between the acrylamide can affect creating a monolayer, and thus may create a double layer on the surface, which is not a favourable condition in this situation.

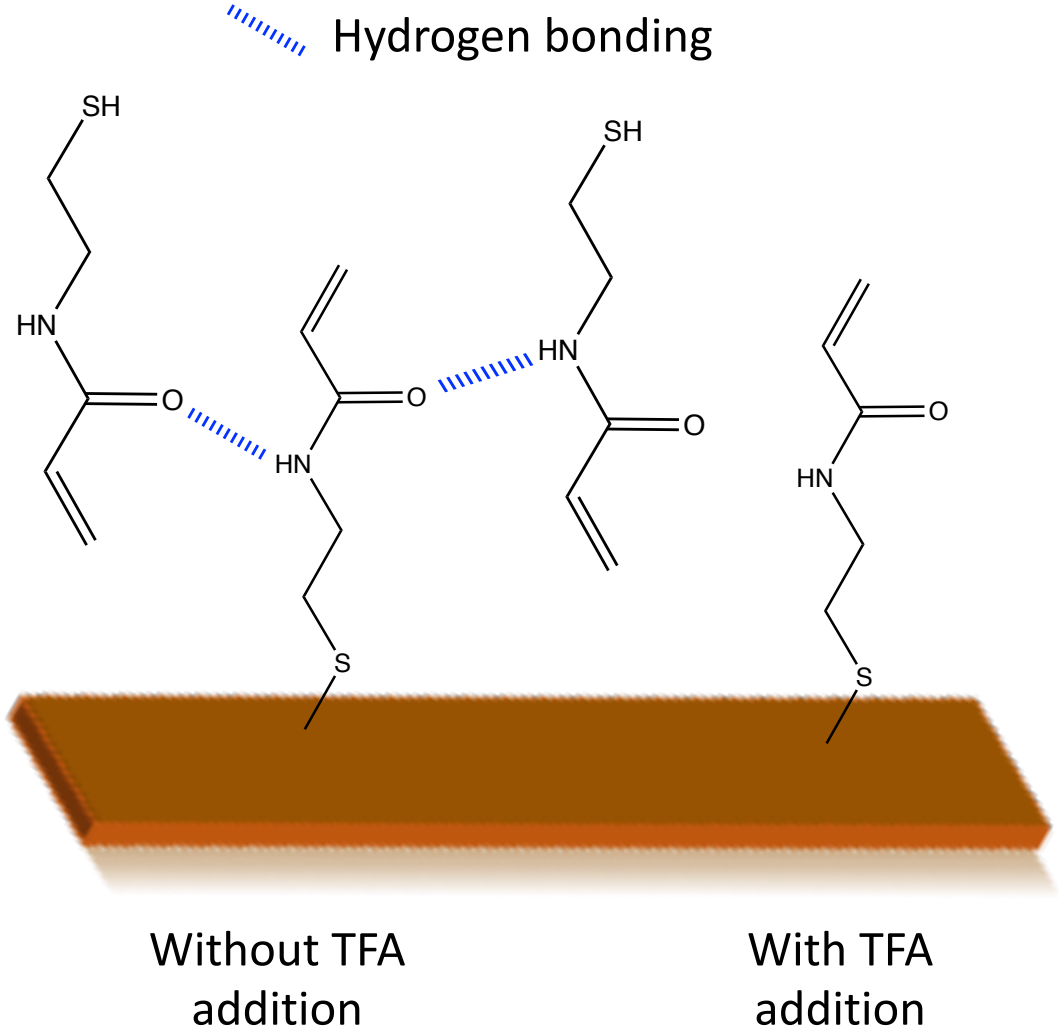

Figure 39: A schematic of the hydrogen bonding which would occur without the presence of TFA.

From fig. 39, it is clear where the hydrogen bonding could occur on the DSA molecule, disrupting the monolayer and potentially causing double layering to occur [303]. As the DSA molecule has both the presence of an O group as well as an H attached to N. This means that two potential sites available for hydrogen bonding to occur.

Table 3: CA analysis for 2% TFA in incubation solvents at varied concentrations of DSA.

Concentration (mM)	Incubation Solvent	Advancing Angle (°)	Receding Angle (°)	Hysteresis (°)
0.1	MeOH in 2% TFA	59.3 ± 3	52.2 ± 3	6.8
	EtOH in 2% TFA	54.9 ± 1	52.7 ± 1	2.2
0.5	MeOH in 2% TFA	62.3 ± 3	54.6 ± 3	7.7
	EtOH in 2% TFA	56.9 ± 1	54.7 ± 1	2.2
1.0	MeOH in 2% TFA	61.2 ± 3	57.1 ± 3	4.1
	EtOH in 2% TFA	51.3 ± 2	47.4 ± 2	3.9

The contact angles were analysed for the various concentrations of DSA and shown in table 3. The table demonstrates the difference between three varied concentrations, 0.1 mM, 0.5 mM and 1 mM and the use of two incubation solvents, ethanol with 2% TFA and methanol with 2% TFA. The results were shown to be very different, dependent on the solvent used for incubation. Firstly with the methanol with 2% TFA

used as an incubation solvent, the advancing (θ_{Adv}) and receding (θ_{Rec}) contact angles for DSA at 0.1 mM concentration were shown to be 59.3 ± 3° and 52.2 ± 3° respectively. The hysteresis was shown to be 6.8°, suggesting that the surface is not well–packed . 0.5 mM DSA was shown to have a contact angle of 62.3 ± 3° and 54.6 ± 3° respectively. The hysteresis was calculated as 7.7°, also suggesting slightly disorganised surfaces. 1 mM DSA has an advancing and receding angle of 61.2 ± 3° and 57.1 ± 3°, calculating the hysteresis to be 4.1°. Large hysteresis values are suggested to have created a certain roughness on the surface [304]. The next comparison was the use of ethanolic conditions with the presence of 2% TFA.

For ethanol with 2% TFA used as an incubation solvent, θ_{Adv} and θ_{Rec} contact angles for DSA at 0.1 mM concentration were 54.9 ± 1° and 52.7 ± 1°, respectively. The hysteresis is calculated as 2.2°, consistent with high surface organisation [305]. Hysteresis values <5° are considered to be low–surface–tension surface, so ultra–low hysteresis values make the conditions chosen more favourable [306]. The hysteresis was also calculated as 2.2 for the 0.5 mM DSA SAM, indicating a more densely packed SAM [307]. Therefore, the smaller concentration of DSA (0.1 mM) is to be used for the formation of the DSA SAM.

3.3.4 Incubation time

The incubation time for SAM formation can affect the physical formation of a SAM on a surface. Longer incubation times result in lower performance of immobilisation and in the formation of SAMs [308]. The incubation time of incubation was compared to further optimise the DSA monolayer and is explored in the next sub–section. The formation of a self–assembled monolayer is illustrated below (fig. 40).

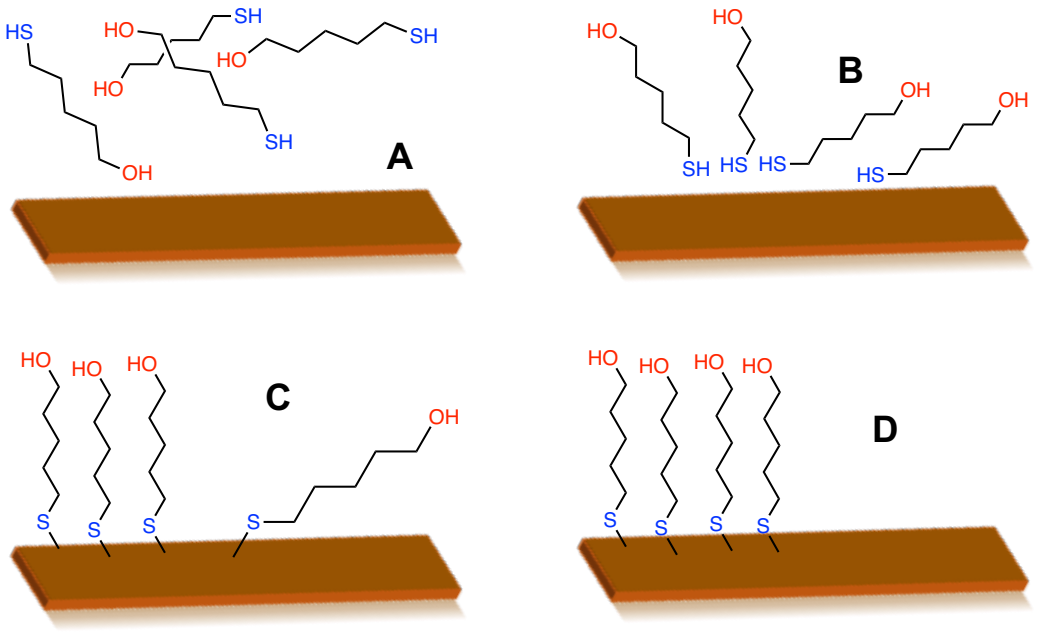

Figure 40: Schematic of the process of self–assembly. The alkanethiols in solution **A** physisorption onto an Au (III) substrate **B** The molecules then chemisorption onto the surface to form covalent bonds with the Aug via their sulfur head groups **C** Finally, through reorganisation of the surface a well–ordered monolayer is formed **D**.

To determine whether the incubation time could have an effect on the formation of SAMs, 24 and 48 h incubation times were compared. SAMs are usually formed within

6–18 h [309], however the increase in time may benefit the reorganisation of the surface.

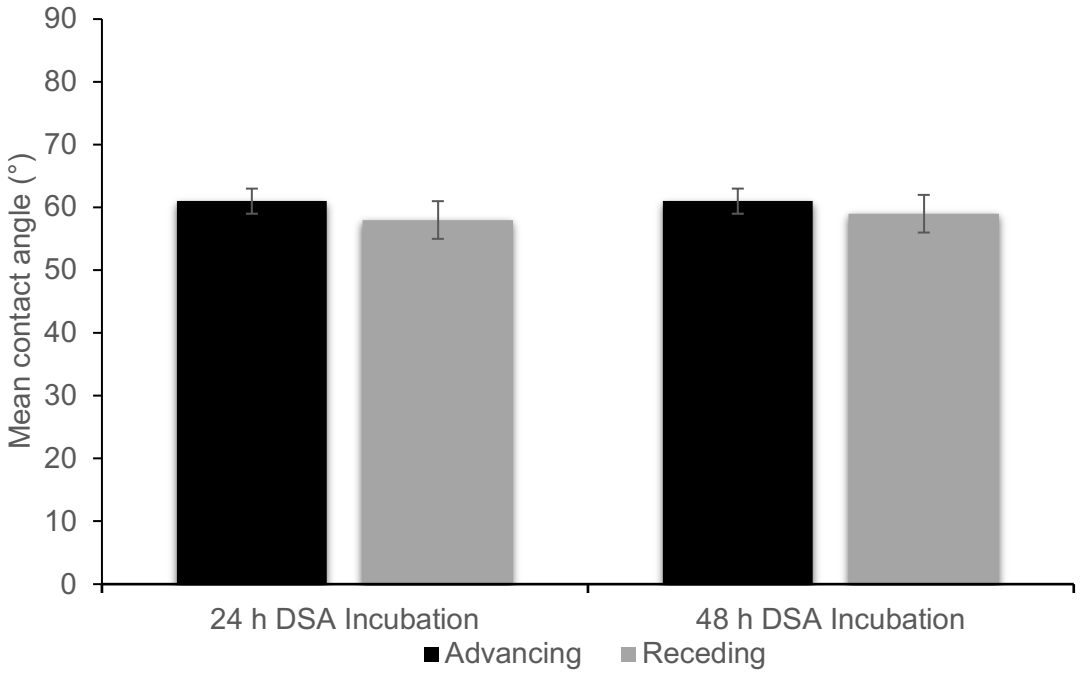

Figure 41: Contact angle data of 0.1 mM DSA in 2% TFA in EtOH under 24 and 48 hr incubation for SAM formation.

24 h incubation times prepare the SAM to avoid multistep surface reactions [310]. Increasing the incubation time to 48 h may create uneven surfaces as well as creating surface and SAM formation defects. The contact angle of the incubation of 0.1 mM DSA in 2% TFA in EtOH was similar whether incubated for 24 hr or 48 hr. From the data, there was no evidence that the increase in incubation time had a positive impact on the formation of SAMs. The next sub–section was to explore the ellipsometry of the DSA monolayer. Ellipsometry is a non–destructive technique that is used frequently

for measuring the thickness of thin film structures [311]. Ellipsometry analysis of the DSA SAM is explored, demonstrating the purpose of the TFA incubation.

3.3.5 Ellipsometry of the DSA monolayer

Ellipsometry is essentially used for finding the optical constants (refractive index n and extinction coefficient k) and the constants are used to determine the thickness of thin films as well as their interfaces [312]. Following the dynamic contact angle measurements, the thickness of the DSA SAMs was examined using the technique. Ellipsometry utilises extensive modelling principles and requires some available information related to the film structures. Table 4 demonstrates the thickness values observed for the three varied concentrations of DSA, 0.1 mM and 0.5 mM and different incubation solvents, ethanol (EtOH) and methanol (MeOH) with the presence of 2% TFA. The Chem Bio 3D Ultra software was used to calculate the expected thickness. The value obtained was 0.7 nm (7 Å), the distance between the Au–S and the furthest C on the SAM.

Ellipsometry allows for users to know about material properties including film thickness, optical constants, surface roughness, gradients in films and the bandgap of the material. Ψ and Δ changes are measured and are useful indicators of a change in a material [313, 314]. The development of a model is to mimic the experimental system. The modelled values of Ψ and Δ are compared to the measured ones, giving a mean squared error (MSE) value. The smaller the MSE value gives a measure of how well the modelled data matches the experimental data [315].

Due to variation of gold samples and surface defects, bare samples are used as the model for samples less than 10 nm. Developed to be an alternative to direct fits, B–spline layers combines the benefits of reduced number of fit parameters, complete flexibility in optical constants for any material, and remove the guesswork of where to place oscillators and what type to choose [316].

A b–spline layer is created with the bare gold samples (shown in fig. 42) and then a Cauchy model is generated on top to allow for the thickness values to be analysed for the gold sample incubated with the SAM (fig. 43). To determine an approximate film thickness as well as refractive index, region of the measured spectral range where the film is transparent (or nearly so) should be found. Due to the SAM being transparent, the following assumptions can be made;

- k=0
- Ψ , Δ and refractive index (n) for the two unknowns of film thickness are measured.

The Ψ and Δ fits to the experimental data are shown below and the refractive index is described using the Cauchy dispersion relation:

$$n(\lambda)=A+B/\lambda^2+C/\lambda^4$$

As the assumptions $n(\lambda)=A+B/\lambda^2+C/\lambda^4$, and $k(\lambda)=0$ are made, A, B and C are all fit coefficients, with λ is the wavelength in microns [317]. Below, the figures show the experimental data improvement against the model fit, and is more acceptable and closer to the experimental data obtained [318].

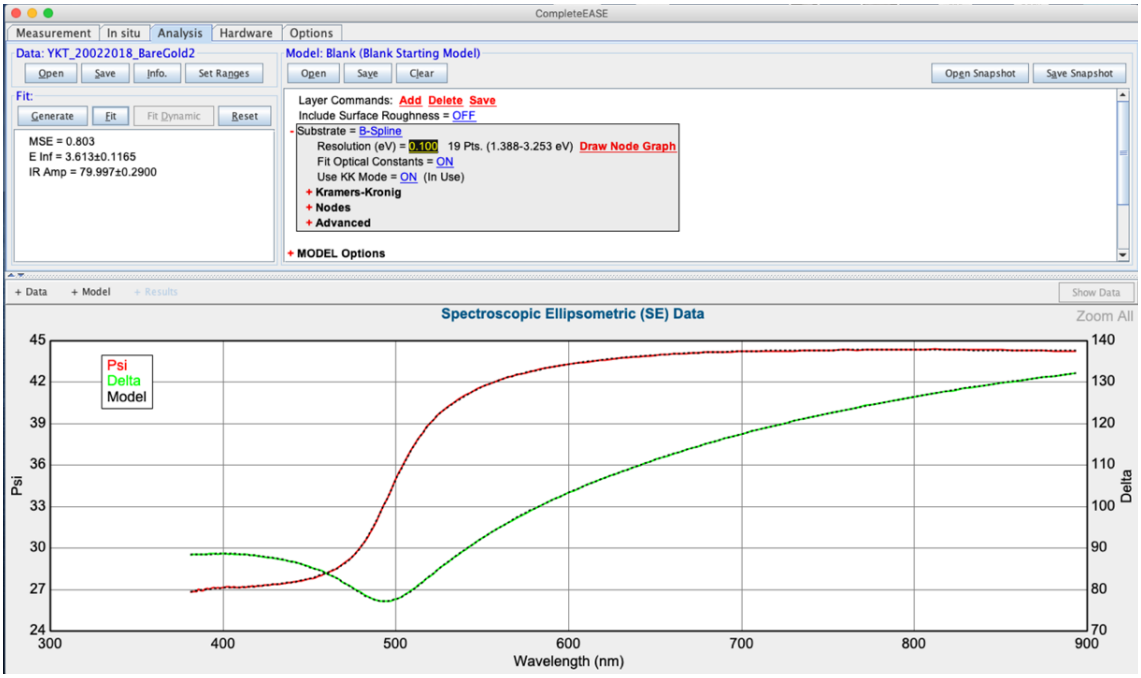

Figure 42: B–spline model of the bare gold sample at 70 degrees.

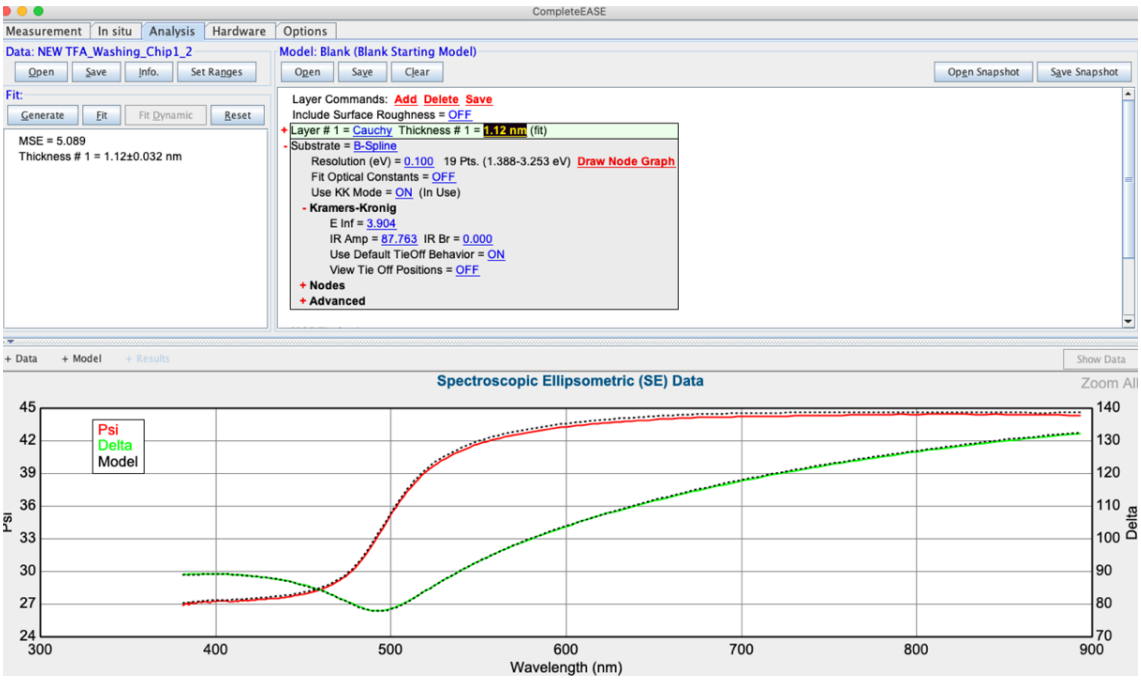

Figure 43: Cauchy model with the b–spline model of the SAM, as an example.

From the examination of the intensity transmission data, the transparent region is determined. Once an acceptable fit is achieved, this being dependent on the MSE values generated, the spectral range is extended and includes both longer and shorter wavelengths. The Cauchy model presented above is useful for obtaining an approximate film thickness and set of optical constants.

Table 4: Ellipsometry data for the addition and absence of 2% TFA in the incubation solvents at varied concentrations of DSA.

Concentration of DSA (mM)	Incubation Solvent	Thickness Observed (nm)
0.1	MeOH	1.32 ± 0.1
	2% TFA in MeOH	1.04 ± 0.04
	EtOH	1.12 ± 0.1
	2% TFA in EtOH	0.56 ± 0.06
0.5	MeOH	1.43 ± 0.2
	2% TFA in MeOH	1.26 ± 0.05
	EtOH	1.56 ± 0.3
	2% TFA in EtOH	0.90 ± 0.1

The ellipsometry results confirms with the contact angle data that MeOH as an incubation solvent does not demonstrate positive results for the formation of a DSA SAM. The thickness values obtained were 1.04 ± 0.04 nm for 0.1 mM DSA and 1.26 ± 0.05 nm for 0.5 mM, larger than the expected thickness of 0.7 nm. Previous studies were conducted by Dai et al. and have reported that the solvent parameters (such as polarity) can affect the quality of the SAMs [319, 320]. Methanol is more polar than

ethanol meaning that the packing of the SAM may be compromised. The next condition used was 2% TFA in ethanoic conditions. The thickness of 0.1 mM DSA with the incubation solvent as EtOH in 2% TFA was shown to be 0.43 nm, slightly lower than the expected thickness of 0.7 nm, which can be attributed to a slight tilt of the SAMs on the surface of the gold [184, 321]. 0.5 mM DSA SAMs with and without the addition of TFA are shown to be slightly greater than that of the expected thickness, suggesting that the SAM formation is creating a double layer and therefore the conditions are not optimal [322]. Ethanoic conditions with the presence of TFA was concluded to be proved, based on contact angle and ellipsometry measurements, to be more suitable and used for the foreseeable future of the formation and optimisation of the DSA SAM.

3.3.6 XPS of the DSA monolayer

Following the contact angle and ellipsometry measurements, the elemental composition and chemical environments of the DSA SAM were examined with the use of XPS. The XPS survey scan of the DSA SAM first revealed the presence of the expected Au, C, S, O and N elemental species on the surface. The high resolution scans as shown in fig. 44 then further confirmed the expected chemical environments for each of these elements.

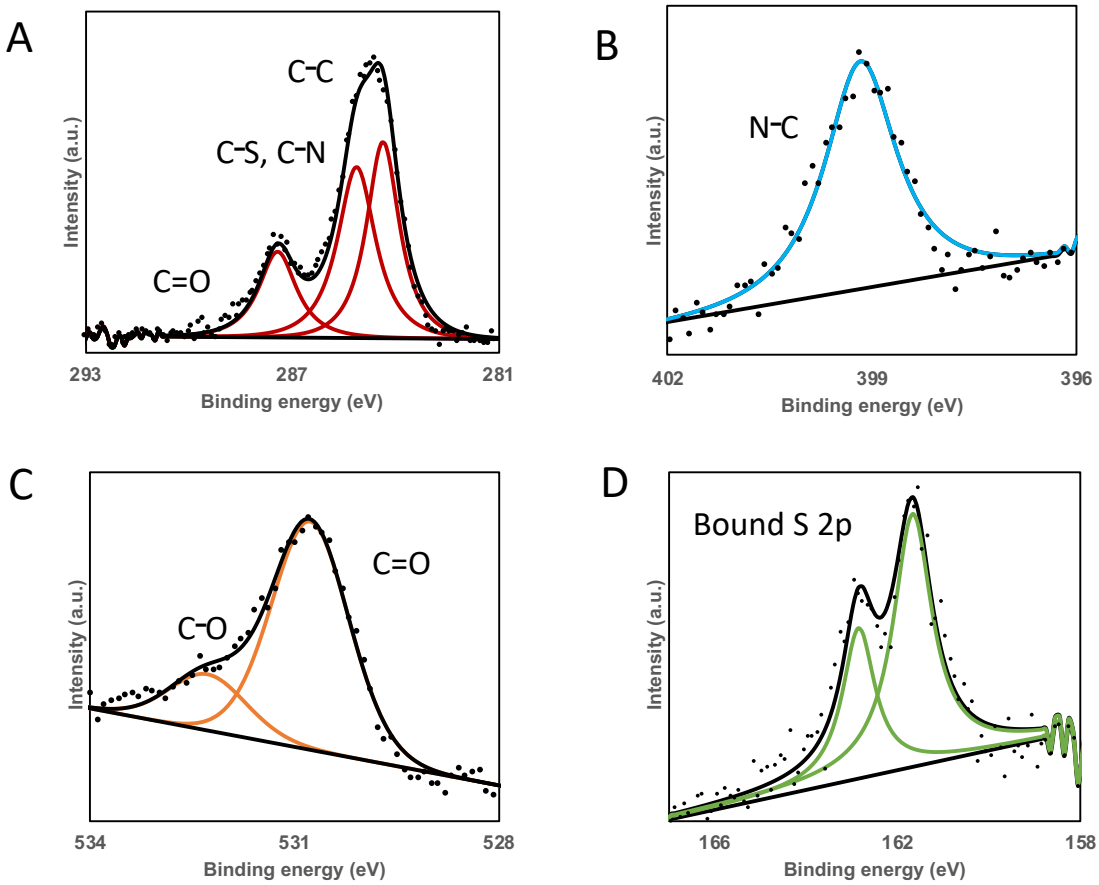

Figure 44: XPS peaks of 0.1 mM DSA with the Gaussian background, A C(1s), B O (1s), C N (1s) and D S (2p).

Next, deconvolution of the C (1s) spectra (figure fig. 44) had shown two carbon species as expected. The first is a sharp, singlet at 285.6 eV corresponding to the C–C of the alkanethiol main chain and the second is found at a higher binding energy of 287.9 eV consistent with the C–O of the terminal hydroxyl group. The second peak has a doublet demonstrating the C=O environment [323].

The next spectra analysed was O (1s), shown in orange. The O (1s) spectra likewise shows two oxygen environments by the peaks at 531.8 eV suggesting C=O and 532.9

eV consistent with the C–O environment. DSA only has a carbonyl group present, so the C–O peak provides indication of potential contamination. This can be contamination which is present during transportation or the incubation of the SAM.

The S 2p peak shown in green contains a doublet peak. The S 2p peak corresponds to the S $2p_{3/2}$ and S $2p_{1/2}$ orbitals of bound S (at the lower binding energies). The S (2p) spectra shows only one environment consisting of a doublet that corresponds to the S $2p_{3/2}$ and S $2p_{1/2}$ orbitals at 161.7 and 162.9 eV, respectively. The presence of S peaks show that the DSA alkanethiols have covalently bound to the Au substrate as expected [221].

In blue, the N (1s) peak is shown at 399.8 eV, suggesting that the N–C environment is present and bound to the surface [324]. This environment is expected from the expected structure of DSA, which contains one N atom.

In addition to 0.1 mM DSA with 2% TFA in ethanoic conditions, a higher concentration of 0.5 mM was used to be compared. This was to determine whether an increase in DSA on the monolayer could be a positive impact in the formation of a monolayer or work negatively when characterised with XPS. The XPS survey scan of the 0.5 mM DSA SAM first revealed the presence of the expected Au, C, S, O and N elemental species on the surface. The high resolution scans are shown in fig. 45 then further confirmed the expected chemical environments for each of these elements, to indicate successful functionalisation of the surface.

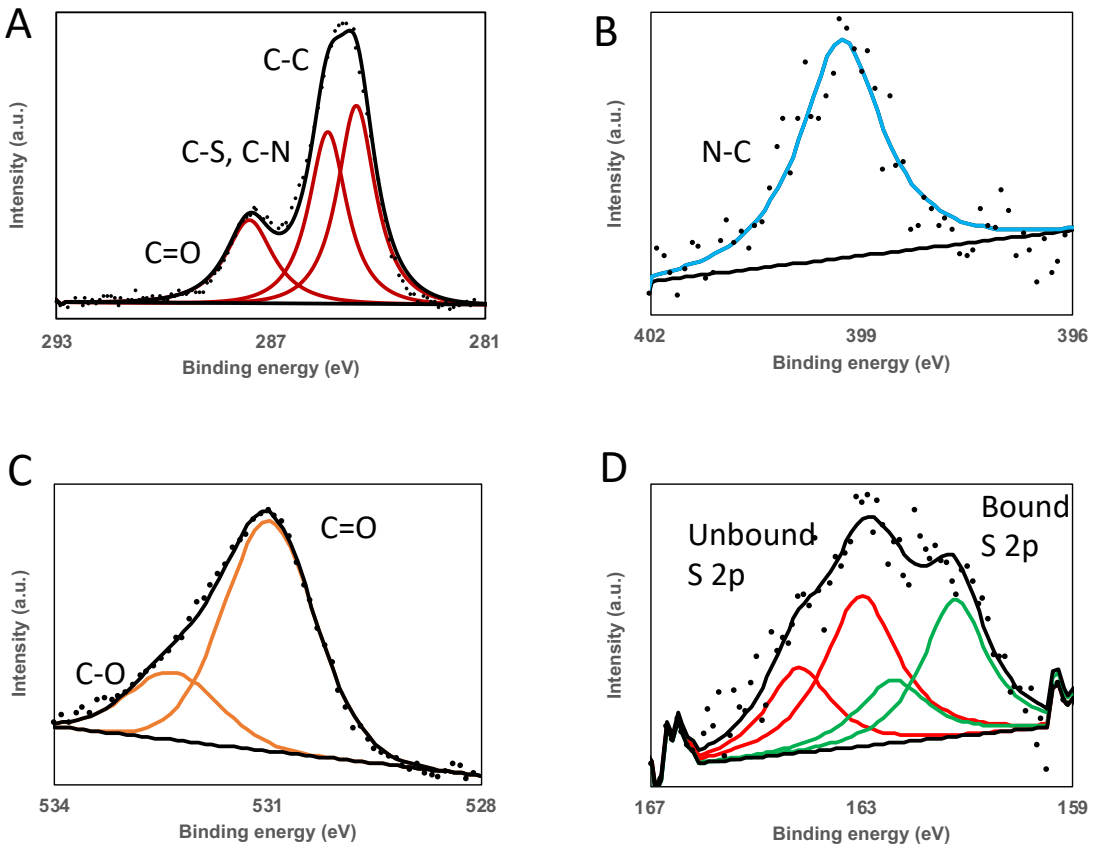

Figure 45: XPS peaks of 0.5 mM DSA with the Gaussian background, A C(1s), B O (1s), C N (1s) and D S (2p).

The S 2p peak shown in green and red contains two doublet peaks. With respect to the 0.5 mM DSA SAM, the S $2p_{3/2}$ doublet at 161.6 and 162.8 eV is smaller compared to the S $2p_{1/2}$ doublet at 163.2 eV and 164.1 eV, suggesting that the 0.5 mM DSA SAM presents more unbound sulphur than bound.

Peak fitting using 10% Lorentzian/90% Gaussian peaks indicated that the 0.1 mM DSA SAM had a bound: unbound sulphur ratio of 100% to 0% respectively, However, 0.5

mM DSA SAM had a percentage ratio of 51% to 49% respect to bound and unbound sulphur. These unbound thiol molecules could be either lying on top of the SAM or partially penetrating into the SAM [325, 326]. The SAMs were extensively rinsed with HPLC grade ethanol before being wrapped and submitted for XPS analysis, however a large amount of unbound thiol remains as shown from the high resolution S spectra. With these results in mind, the preferable condition for the formation of the DSA SAM is 0.1 mM as no unbound sulphur is present.

The other peaks, C (1s), N (1s) and O (1s) did not show any clear and understandable varied peaks to that of the 0.1 mM DSA SAM, suggesting that the DSA molecule has successfully bound to the substrate, whether completely bound to the surface or not.

The use of XPS analysis suggests that although using 0.5 mM concentration of DSA was potentially ideal, the sulphur peaks did not demonstrate to show adequate binding to the surface, which can later cause problems when cross–linking other compounds onto the surface. In addition to problems with cross–linking, the unbound sulphur also suggests that the monolayer is not particularly stable, another factor which is critical for molecular imprinting.

3.3.7 Conclusion of the optimisation of the DSA monolayer

Ellipsometry, contact angle and XPS were used to enable optimisation of the DSA surface. The ellipsometry and contact angle analysis both individually enabled the wettability of the surface as well as to measuring the thickness of the surface when

compared with the expected thickness of the surface, measured with the use of Chem Bio 3D Ultra. The use of trifluoroacetic acid was shown to be positive, avoiding hydrogen bonding on the surface [327]. From the XPS data presented, 0.1 mM DSA in 2% TFA demonstrated no unbound sulphur present on the surface and ideal thickness values with a small standard deviation suggesting the variation between surfaces is minute. No significant difference was observed when the incubation time was increased and the change in cleaning protocols. For the ellipsometry, the extinction coefficient of bare gold chips and the thickness values for the surfaces were obtained. XPS analysis demonstrated that 0.5 mM SAM had unbound sulphur peaks, suggesting that a partial double layer is present on the gold surface. Therefore, with the results from the dynamic contact angle, ellipsometry and XPS analysis, we can conclude the optimisation of the DSA SAM as 0.1 mM DSA in 2% TFA in EtOH.

3.4 The cross–linking of AABOB and DSA

3.4.1 Introduction

Benzoboroxoles are able to form reversible covalent complexes with diols [177], a common chemical moiety in saccharides such as fructose, glucose and mannose. Boronic acids and their derivatives such as benzoboroxoles, undergo a well–known condensation reaction with 1,2– or 1,3–diols to form five or six member cyclic boronate esters. This condensation reaction is reversible and is highly influenced by the pH and chemical structure of the boronic acid and diols [328, 329]. The conversion of the boronic acid to the charged boronate tetrahedral conformation yields is readily

reversible. As a result, benzoboroxole containing constructs are currently being exploited in glycoprotein detection [330, 331].

Free radical polymerization is one of the most commonly used processes amongst the different strategies developed to prepare cross–linked polymer networks [332]. The wide variety of molecules that can be polymerized and cross–linked by free–radical polymerization, ranging from thermosetting acrylate–based adhesives to hydrophilic monomers for contact lenses [333, 334]. Additionally, by choosing the appropriate amount of monomers along with the right amount and suitable type of initiator(s), the rate of polymerization can be well controlled [335].

As the DSA monolayer has been optimised earlier in the chapter, the next step was to modify the structural surface by cross–linking a benzoboroxole compound onto the DSA. Different conditions were examined to determine whether the cross–linking was successful. The successful condition would be determined with the analysis of XPS, demonstrating a boron peak before further analysis would be defined such as C (1s), N (1s), O (1s) and S (2p). Successful crosslinking of DSA and AABOB enables the conditions for further work with complexes in the research.

3.4.2 XPS of cross–linking attempts

In fig. 46, the schematic of the cross–linking of DSA and AABOB is shown. This sub–section looks into the XPS spectra of numerous different conditions, before being able

to successfully demonstrate the optimised conditions needed for the reaction to be suitable.

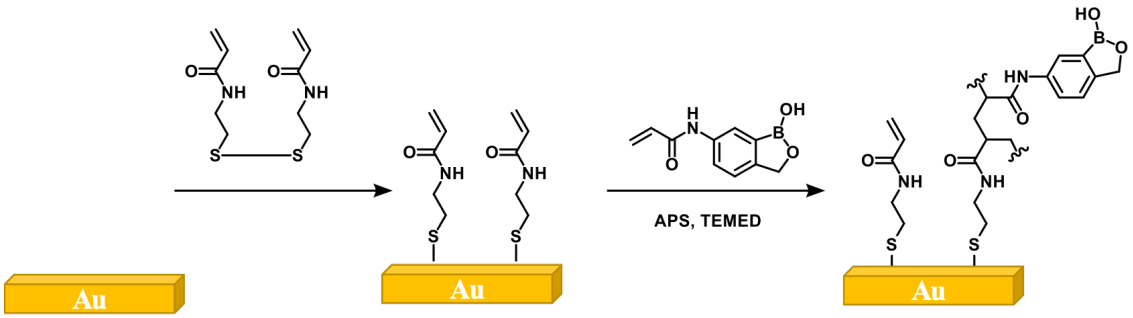

Figure 46: DSA monolayer cross–linking AABOB.

XPS can conclude if boron was present on the surface after cross–linking conditions were attempted. Each of the conditions shown were under the use of UHQ water. Numerous different conditions were implemented with unsuccessful results, some conditions were tabulated in table 5 to show some of those conditions and why they were deemed unsuccessful.

Table 5: Possible conditions used for the crosslinking of DSA and AABOB.

Conditions	Successful? (Y or N)
900 µl 0.5 mM AABOB 100 µl APS 1 µl TEMED 10 mins	N
900 µl 0.5 mM AABOB 100 µl APS 1 µl TEMED 30 mins	N
900 µl 0.5 mM AABOB 100 µl APS 1 µl TEMED 60 mins	N

XPS was conducted on the condition of 10 minutes incubation time with DSA and AABOB, showing high–resolution peaks, C (1s), B (1s), S (2p), N (1s) O (1s), each shown in the fig. 46. Each of the peaks are discussed below, helping understand whether or not the cross–linking was indeed successful.

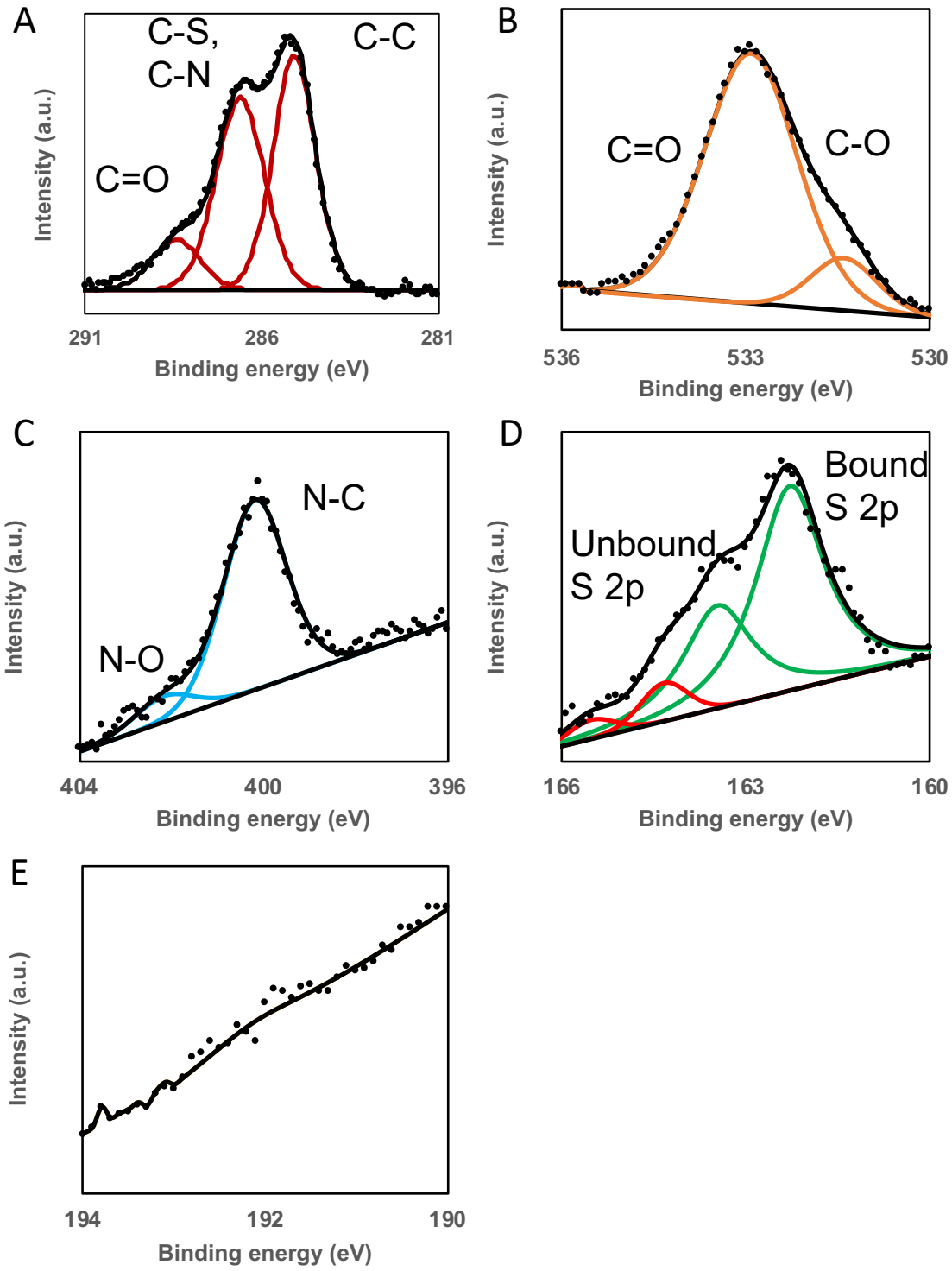

Figure 47: XPS spectra of the cross–linking of 0.1 mM DSA and 0.5 mM AABOB for 10 mins; A carbon , B oxygen, C nitrogen, D sulphur and E boron.

The XPS spectra was taken in several binding energy ranges to help identify the elemental species present on the surface. Two environments were shown in the N (1s) spectra, which are labelled in fig. 47. The first environment was assigned to amine/amide which was found at 400.5 eV [336]. The later environment is observed as the N (1s) region with higher binding energy of 402.9 eV [337]. The binding energy is known to be as the assigned NO^- species as the adsorption of NO on CeO_2 surfaces was reported by Overbury et al [338].

The C (1s) spectra (figure fig. 47) had shown three carbon species as expected. The first is a sharp, singlet at 285.6 eV corresponding to the C–C of the alkanethiol main chain and the second is found at a higher binding energy of 287.9 eV consistent with the C–S and C–N species. The second peak had demonstrated the C=O species, similar to that demonstrated by the DSA SAM. The species discussed suggest contamination with the polymerisation process.

The C=O and C–O environments are shown and labelled in the figure. The two environments are expected when the structure is demonstrated.

The S 2p peak shown in green and red contains two doublet peaks. The S $2p_{3/2}$ doublet at 161.6 and 162.8 eV and the S $2p_{1/2}$ doublet was shown at 163.2 eV and 164.1 eV, suggesting the presence of unbound sulphur as well as bound sulphur. Peak separation between the bound S $2p_{1/2}$ and unbound S $2p_{3/2}$ (separation 0.1 eV) is below the energy resolution of the XPS instrument (0.5 eV). With this in mind, we

cannot confirm reliably this species. Despite this, presence of unbound S $2p_{1/2}$ provides sufficient evidence for presence of the unbound S $2p_{3/2}$ peak given the expected S $2p_{3/2}$ and S $2p_{1/2}$ separation of 1.18 eV. The observation of unbound S on the surface may be due to insufficient rinsing of SAM [339].

Boron is known to be very difficult to detect in XPS. Boron is difficult to confidently assign B1s peak for low concentrations, when no secondary peak observed [340]. Since no B was detected, the next protocol was to increase the time of incubation to 30 minutes, also stated in table 5 and shown in fig. 48, unfortunately, similar to the previous experiment, boron was still absent on the XPS analysis confirming that the cross linking of DSA and AABOB were unsuccessful.

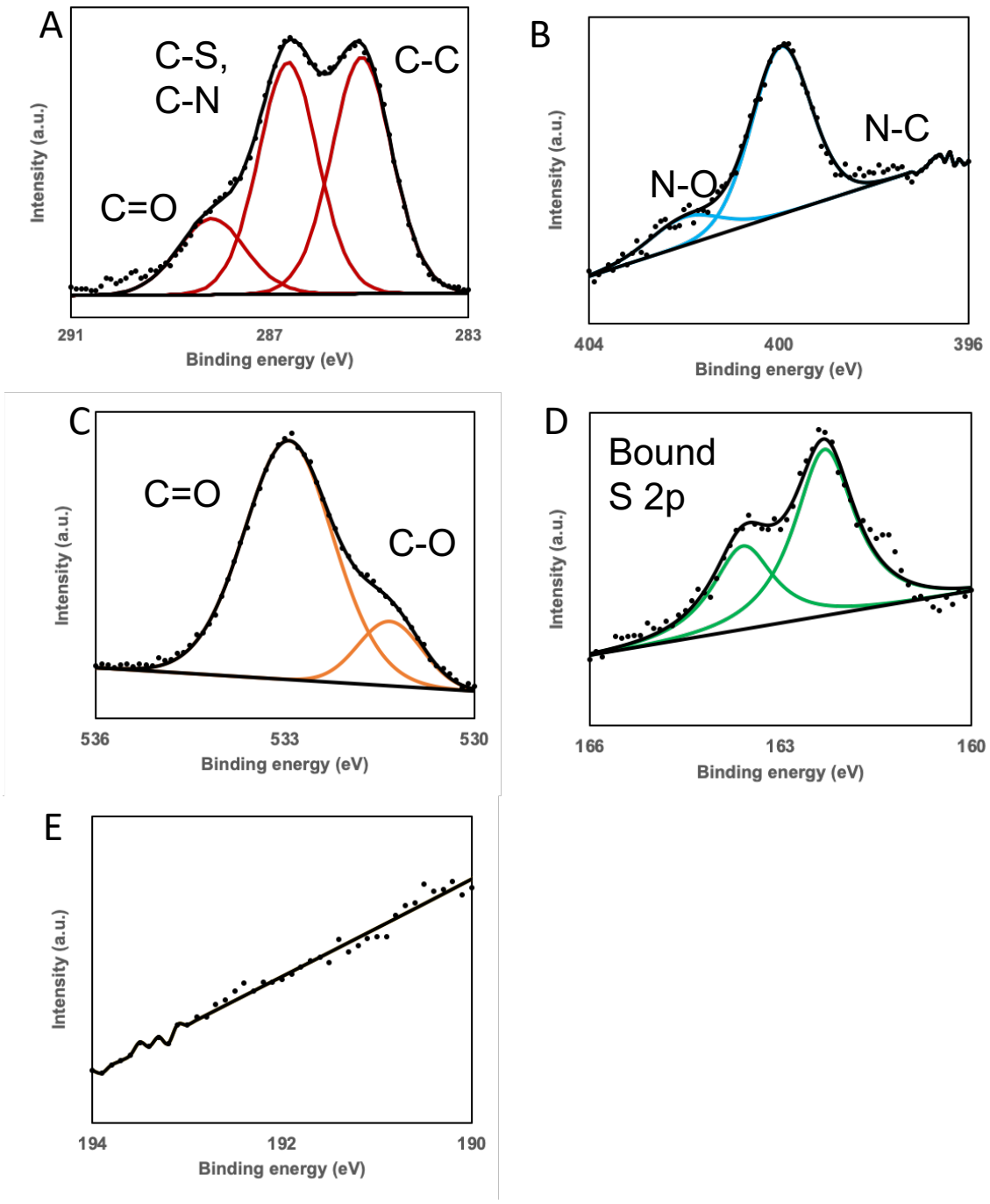

Figure 48: XPS spectra of the cross–linking of 0.1 mM DSA and 0.5 mM AABOB for 30 mins; A carbon, B nitrogen, C oxygen, D sulphur and E boron.

The increase in incubation time was shown to be unsuccessful too. The XPS spectra was analysed to demonstrate the ineffective conditions for the cross–linking of AABOB to a DSA SAM.

Similar to that of 10 mins of incubation for the DSA monolayer and AABOB, two environments was also shown in the N (1s) spectra (fig. 48). The first species was assigned as N (1s) was found at 400.5 eV and was also assigned to amine/amide as expected. The later environment assigned the presence of aqueous solutions in contact with the surface [341, 342]. The next elemental species analysed was carbon, looking at the C (1s) spectra.

In addition to the optimisation of the DSA SAM, the S 2p peak is shown in green, containing one doublet peak. The S $2p_{3/2}$ doublet at 161.6 and 162.8 eV, demonstrates the presence of only bound sulphur on the Au surface. However, no presence of a boron (B (1s)) peak was found on the analysis of the crosslinking condition. Therefore summarising that the cross–linking was indeed unsuccessful. The next condition was to increase the incubation time from 30 minutes to 60 minutes. The increase in time could account for the cross–linking of AABOB onto the DSA to occur [343].

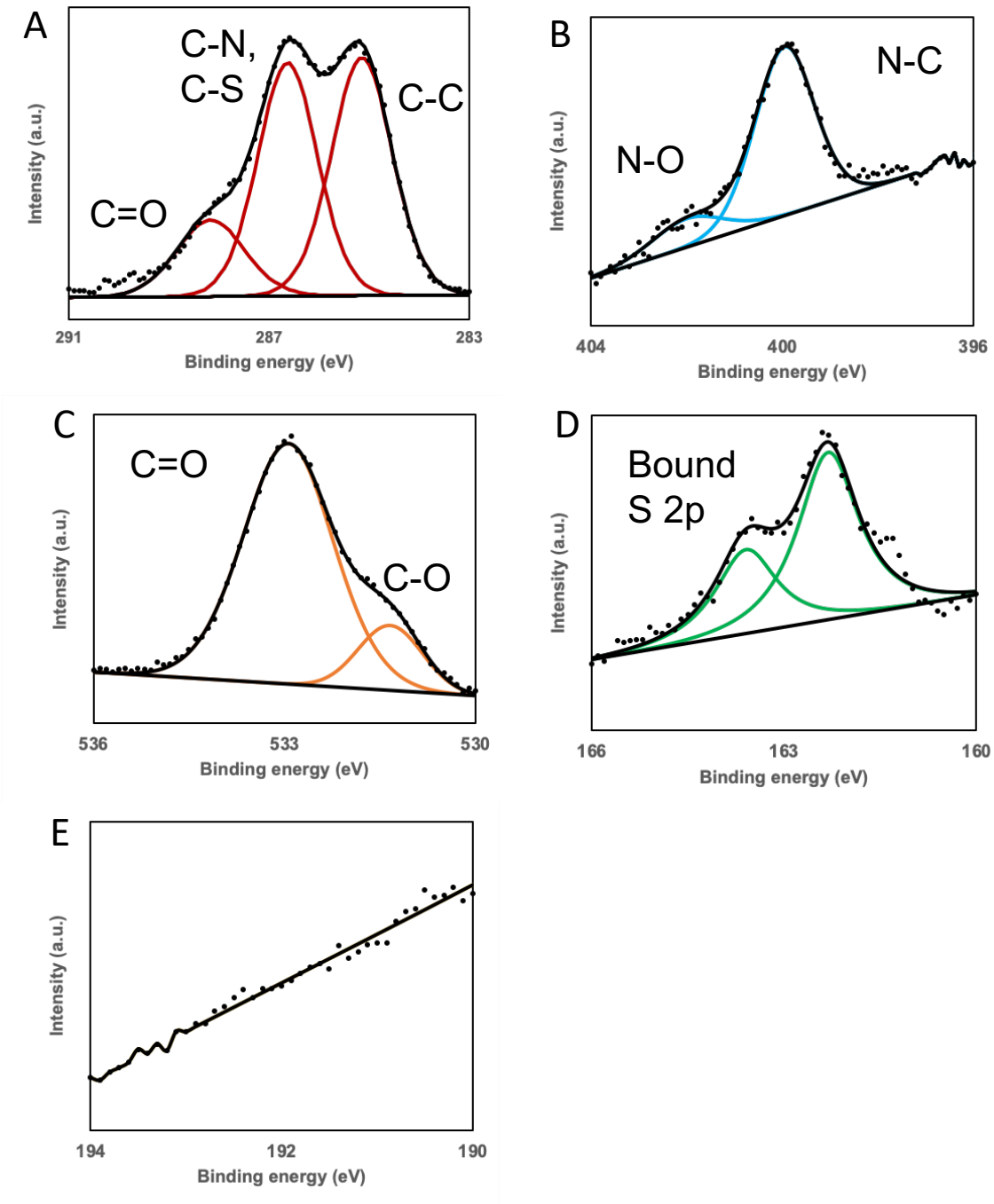

Figure 49: XPS spectra of the cross–linking of 0.1 mM DSA and 0.5 mM AABOB for 60 mins; A carbon, B nitrogen, C oxygen, D sulphur and E boron.

B (1s) peak was still not present, suggesting that the cross–linking of a benzoboroxole was not successfully bound to the DSA SAM. Further studying of the XPS analysis had

shown that the S (2p) doublet was bound, suggesting the SAM may still present and bound to the surface. Therefore, studies for optimisation were required and raised the concern of whether or not the initiators could affect the initial surface. The XPS spectra of APS and TEMED incubation with 0.1 mM DSA in 2% TFA in EtOH for 10 mins was conducted to determine whether APS and TEMED are in fact damaging the surface or whether the lack of success in cross–linking causes contamination to the surface and new initiators are required.

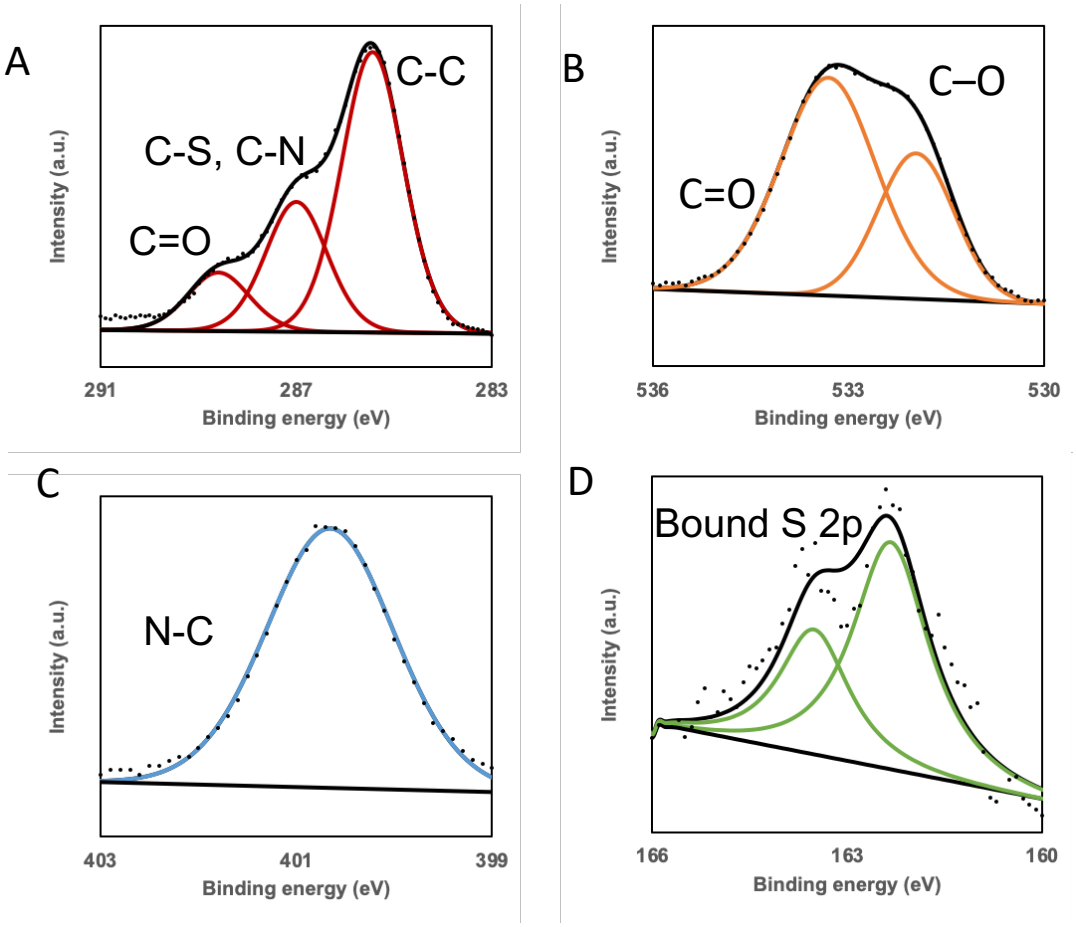

Figure 50: XPS spectra of the of APS and TEMED incubation with 0.1 mM DSA in 2% TFA in EtOH for 10 mins; A carbon, B oxygen, C nitrogen and D sulphur.

The XPS spectra shown in fig. 50 did not shown any damaging effects related to the presence and incubation of APS and TEMED for the DSA monolayer. The S (2p)

doublet is positioned at 162.0 and 163.2 eV, suggesting that DSA is still chemisorbed onto the surface. The further conclusion is the spectra does not demonstrate the sulphur is in an oxidised state, suggesting that APS or TEMED does not disrupt the surface, i.e. it does not oxidise the sulphur present on the surface [344]. To further determine if the presence of initiators and buffer affects the surface, the elemental ratios of the DSA SAM alone were calculated and compared with the expected ratios in table 6.

Table 6: Expected and observed elemental ratios to be observed for the DSA–APS/TEMED/water surface with the absence of AABOB.

Element	Expected Ratio	Observed Ratio.
C/S	5	6.2
O/S	1	1.5
N/S	1	0.9

The elemental expected ratios are determined using the structure shown in fig. 50 and the observed ratios were calculated using CASA XPS. The additional carbon and oxygen may be due to the presence of contamination and thus should be taken lightly in the sense of ratios. The ratio of N/S suggests that the DSA SAM is still present on the gold surface and the addition of imitators and buffer are not damaging to the surface.

Maintaining the pH is vital in the cross–linking process, which is required to cross–link AABOB onto a DSA surface [345]. However, the water used in the previous experiments is very difficult to maintain when adding reactants such as APS and TEMED. Therefore, to prevent pH fluctuation within the solution, a buffer was used to maintain the pH. The purpose of a buffer in the cross–linking of benzoboroxoles and the amide surface is to successfully maintain the pH of the incubation solution for the reaction.

In addition to the control over pH, oxygen–free cross–linking has been successful in previous studies for the free–radical polymerization [346]. The removal of oxygen is required as oxygen–free conditions are used to aid the cross–linking of AABOB and the DSA SAM surface. Argon–filled balloons were present for the duration of the cross–linking which took place in a vial.

The conditions used were the following:

- 240 min cross–linking
- 0.1 mM DSA SAM surface
- 0.5 mM AABOB solution in phosphate buffer
- Argon balloon inserted to prevent the involvement of oxygen

XPS was conducted on the surface to determine whether or not boron was indeed present on the surface, shown in fig. 51. The XPS survey scan of the cross–linked surface attempt first revealed the presence of the expected Au, C, S, O, N and

B elemental species on the surface. The high resolution scans of C (1s), O (1s), N (1s), S (2p) and B (1s) are shown to further confirm the expected chemical environments for each of these elements, indicating successful functionalisation of the surface.

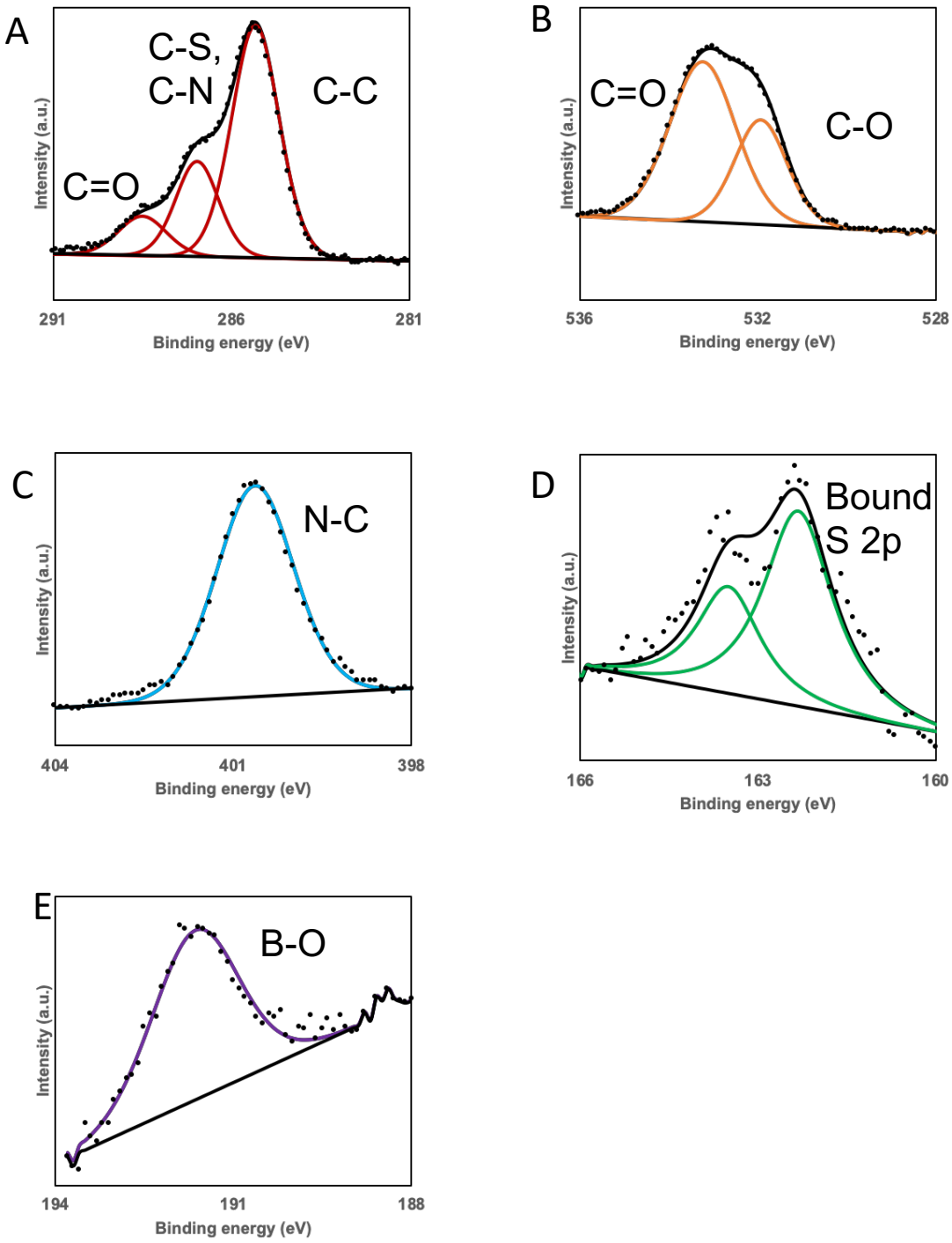

Figure 51: XPS spectra of the cross–linking of 0.1 mM DSA and 0.5 mM AABOB for 240 mins in oxygen–free conditions; A carbon, B oxygen, C nitrogen, D sulphur and E boron.

The high resolution B (1s) scan had confirmed the presence of a boron peak, labelled as B–O as previously reported at 190.8 eV [347]. The expected elemental ratios are determined using the structure shown in fig. 51 and the observed ratios were calculated using CASA XPS (table 7). From the table below comparing both the observed and expected ratios, the slight variation may be due to the contamination of the experimental protocol or the transportation of the chips to conduct the XPS analysis. However, the decreased ratio observed to expected may be due to the peak fitting preventing the numbers to be closer to the expected ratios. As only two chips were conducted for all the XPS analysis, more chips should be used to provide an observed ratio closer to that of the expected ratio.

Table 7: Expected and observed elemental ratios to be observed for the DSA– AABOB surface.

Element	Expected Ratio	Observed Ratio.
C/S	15	12.8
O/S	4	3.6
N/S	2	1.7
B/S	1	0.7

The conditions were deemed successful due to the presence of the B (1s) peak along with bound S 2p peaks. With this is mind, the reaction conditions were stated as these conditions and used later on.

3.4.2 Conclusion of the cross–linking of AABOB and DSA

The cross–linking of DSA and AABOB was shown to be a challenge in this thesis, with many conditions and XPS analysis demonstrating the absence of boron, confirming that the cross–linking protocol is yet to be optimised. The follow–up of XPS analysis with the oxygen–free conditions helps the progression of the DSA–AABOB surface, allowing the progression of the research to resume. The optimisation of the DSA–AABOB surface has been successfully determined, with the presence of boron. Controls of both benzoboroxole modified SAMs as well as benzyl–terminated SAM will enable further clarification of whether the use of benzoboroxoles may be used for the selective binding of target molecules.

3.5 Optimisation of the control surfaces

3.5.1 Introduction

Aryl boronic acids are well–known for their ability to bind to cis–diols by undergoing an esterification reaction [348, 349]. Easily formed at higher pH values, cyclic boronic acid esters are formed due to a hybridization change of the boron atom after coordination with a hydroxyl ion from solution [350]. As a result, the binding of saccharides to boronic acids at physiological pH values, i.e. pH 7.4, has been described to be

sufficient for saccharides exhibiting a high binding strength like fructose [351]. To shift the binding pH between saccharides and boronic acids toward physiologically relevant pH values two different strategies can be followed [352]. The electron–withdrawing groups present in boronic acids lowers the pKa of the boronic acid. As a result, binding to cis–diol containing substances can also take place at lower pH values [353]. Hall et. al. screened different ortho–substituted boronic acids and found that O–hydroxymethyl phenylboronic acid (benzoboroxole) has the ability to conveniently be used for glycopyranoside binding at pH 7.4 [354]. An approach used was by Tung et. al. in which they make use of the higher acidity of the formed saccharide/benzoboroxole ester in combination with a pH sensitive cyanine–based fluorochrome, monitoring the binding of fructose and glucose to the benzoboroxole [355].

Controls are needed and used in the research to determine whether or not benzoboroxoles are in fact suitable for oligosaccharide binding at surfaces. In this section, two controls are used, a benzoboroxole modified SAM along with a control benzyl–terminated SAM which is a phenol based surface with no benzoboroxole group. Different solvents were used to determine the optimal conditions for the formation of SAMs on the gold surface. Both molecules were synthesised and used to prepare SAMs. These SAMs were then to be successfully characterised with techniques including contact angle, ellipsometry and XPS. A schematic of both SAMs is shown in fig. 52, and this section will confirm the conditions required for creating high–quality SAMs.

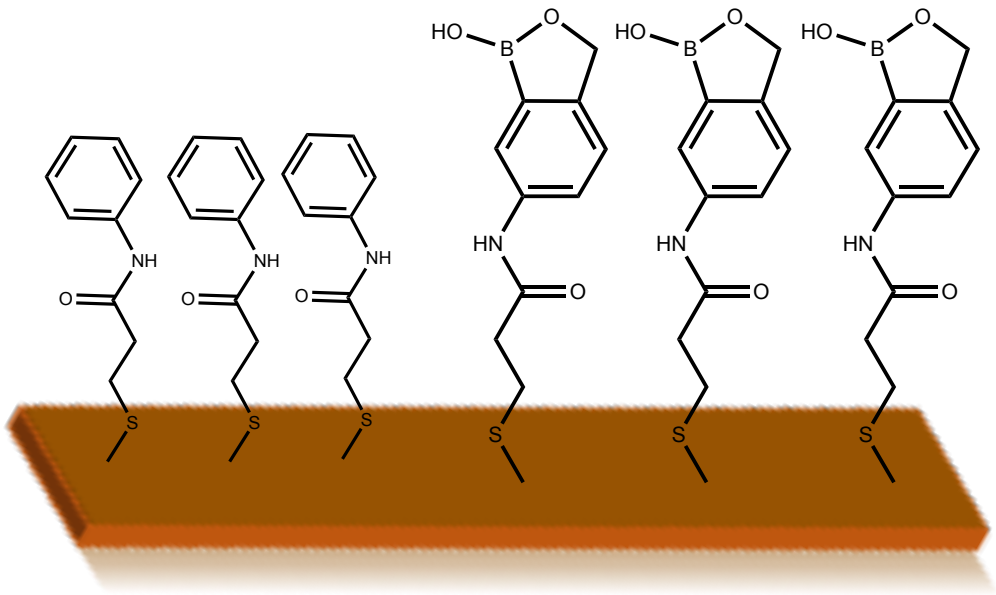

Figure 52: Control SAMs on an Au surface; left: benzyl terminated SAM and right: benzoboroxole modified surface.

3.5.2 Contact angle of the control SAMs

Calculations of the hysteresis was followed to further analyse the surfaces formed. Three different incubation solvents were compared by contact angle analysis, similar to that of the DSA SAM. These solvents and the results are tabulated below (table 8):

Table 8: The contact angle analysis of 0.1 mM benzyl–terminated SAMs using different solvents.

Incubation solvent	CA analysis		
	Advancing angle (º)	Receding angle (º)	Hysteresis (°)
MeOH	60.9 ± 0.09	55.3 ± 0.08	5.6
EtOH	66.2 ± 2	59.3 ± 3	6.9
2% TFA in EtOH	85.2 ± 4	75.3 ± 4	9.9

Contact angle measurements provide important information about the surface roughness as well as the hydrophilicity of the surface [356]. Water was used as the droplet solvent to determine the wettability of the surface. The advancing as well as the receding contact angles were smaller than 90°, confirming that the surface formed was hydrophilic. The hysteresis calculated for each of the solvents for the incubation of the SAMs were 5.6° for methanol, whilst the other two incubation solvents used were 6.9° and 9.9°, ethanol and 2% TFA in EtOH respectfully. Before any conclusion could be made, ellipsometry and XPS shall be used to confirm the suitability of the incubation solvents used. The standard deviations were calculated from three measurements on three different surfaces. The smaller the standard deviation, the less variation of the contact angles between different surfaces formed. The solvent which observed the smallest standard deviation between surfaces was methanol.

Similar to that of the benzyl–terminated control SAM, three different incubation solvents were used to compare the wettability of the surfaces. These incubation solvents were the same as benzyl–terminated SAM and DSA SAM; methanol (MeOH), ethanol (EtOH), and EtOH with 2% TFA. The results are tabulated below.

Table 9: The contact angle analysis of 0.1 mM Benzoboroxole–modified surfaces.

Incubation solvent	**CA analysis**		
	Advancing angle (°)	**Receding angle (°)**	**Hysteresis (°)**
MeOH	70.9 ± 3	65.3 ± 3	5.6
EtOH	65.2 ± 2	62.4 ± 3	2.8
2% TFA in EtOH	75.3 ± 9	55.8 ± 5	19.5

The hysteresis of the three incubation solvents were calculated as 5.6° for methanol, 2.8° for ethanol and 19.5° for 2% TFA in ethanol. Advancing and receding angles should be as identical as possible [357]. From the contact angle analysis, EtOH was to be used due to the closer advancing and receding angles as well as the standard deviations. If the hysteresis is not near to similar values, this is due to the existence of surface heterogeneity and defects [358]. With these values tabulated, the ideal solvent for the incubation of the benzoboroxole–modified surface is ethanol due to the near identical contact angles and the small standard deviation values.

3.5.3 Ellipsometry of the benzyl terminated SAM

As the contact angle suggested a possible optimal solvent for the incubation of the control, ellipsometry was also used to conclude the ideal incubation solvent. The expected thickness of the control SAM was 0.9 nm (9 Å), estimated with the software Chem Bio 3D Ultra. The expected thickness takes into account the bond between the Au–S and the furthest bond. This bond was identified as the carbon bond present in the aromatic ring. The incubation solvents compared were; methanol (MeOH), ethanol (EtOH), and EtOH with 2% TFA, the same solvents used in the contact angle studies. The results are tabulated below:

Table 10: 0.1 mM benzyl–terminated control SAM and the ellipsometry analysis.

Incubation solvent	Ellipsometry thickness (nm)
MeOH	0.70 ± 0.1
EtOH	0.58 ± 0.3
2% TFA in EtOH	1.2 ± 0.5

The ellipsometry studies help measure the observed thickness of the control surface as well as Chem Bio 3D Ultra determining the expected thickness of the surface. From the three incubation solvents, methanol had the lowest standard deviation when three measurements per sample were measured. The lower thickness value obtained accounts for the expectation of monomers to adopt a degree of tilt. The solvent used

for the incubation of the benzyl–terminated control SAM was methanol. XPS of the benzyl–terminated SAM.

The incubation solvent used to conduct XPS analysis was methanol due to the optimisation discussed previously. The XPS survey scan of the control surface first revealed the presence of the expected Au, C, S, O and N elemental species on the surface. The high resolution scans are shown (fig. 53) to further confirm the expected chemical environments for each of these elements and to indicate successful functionalisation of the surface (table 11).

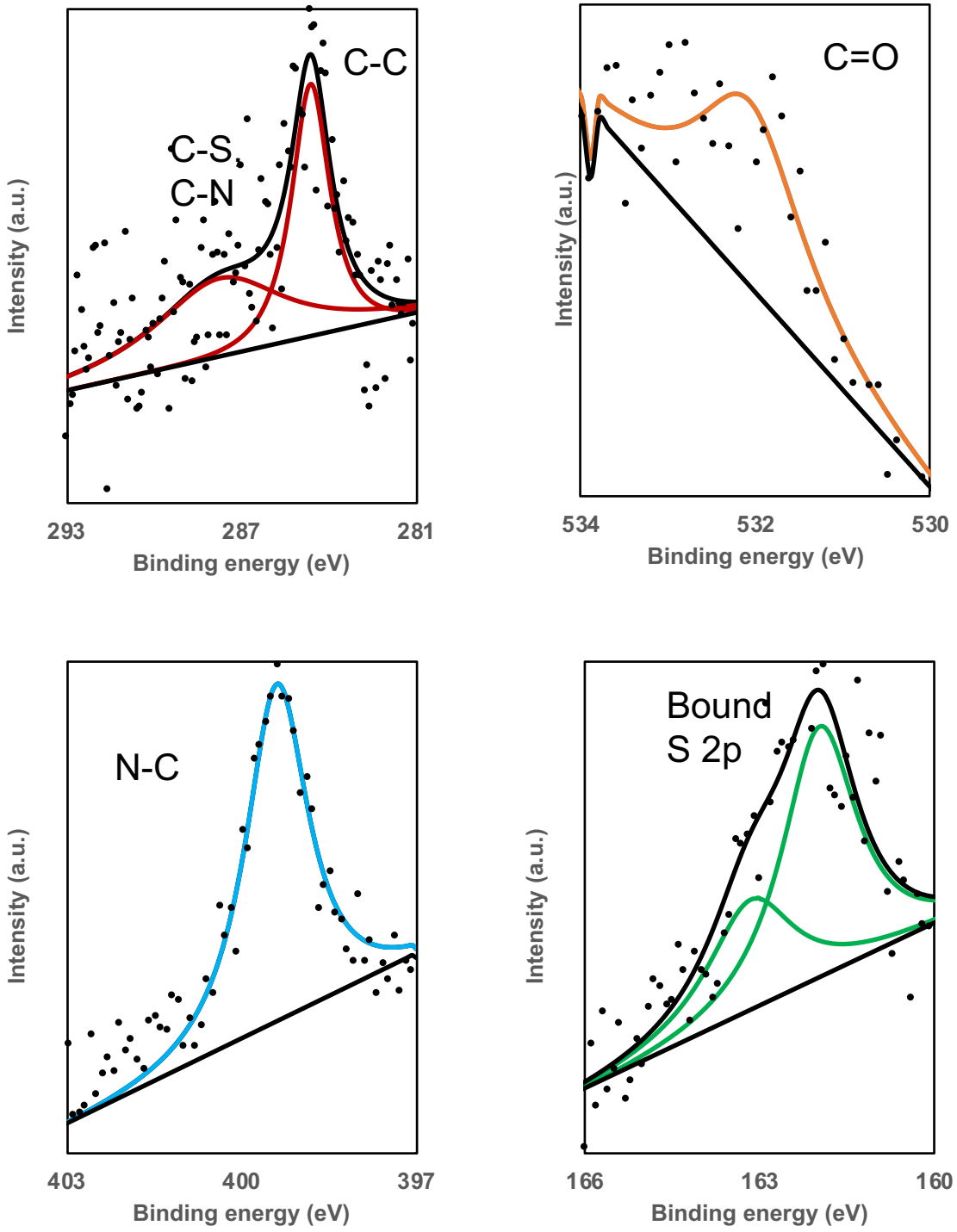

Figure 53: The XPS spectra of the control surface. Red (top left) is C 1s, orange (top right) is O 1s, blue (bottom left) is N 1s and green (bottom right) is S 2p.

Table 11: Expected and observed elemental ratios of the XPS analysis of the 0.1 mM benzyl–terminated control SAM control surface.

Ratio	Expected	Observed
C/S	7	5.2
N/S	1	1.2
O/S	1	0.5

From the XPS analysis shown in fig. 53, the S (2p) doublet is positioned at 161.9 and 163.1 eV, indicating the sulphur is chemisorbed bound on the gold surface [359]. The N (1s) peak can be assigned to a single peak which is centred at 399.4 eV, recognised as the amide group present in the benzyl–terminated control SAM. The observed ratio of oxygen: sulphur and carbon: sulphur are slightly lower than the expected ratio. To conclude the optimisation of the benzyl–terminated SAM was optimal when using 0.1 mM concentration in the incubation solvent of methanol. Further studies were conducted which displayed the SPR responses of varied sugars. These sugars were stachyose, nystose, melezitose and raffinose, saccharides which are continually used from hereon.

3.5.3 Benzoboroxole modified surface

A benzoboroxole modified surface enables to determine whether the benzoboroxole can form a SAM and whether or not the benzoboroxole group can bind to the sugars.

The control SAM is characterised using ellipsometry, contact angle and XPS. Ellipsometry and contact angle were initially used, determining the most suitable solvent, before XPS confirmation.

3.5.3.1 Ellipsometry of benzoboroxole modified surface

The expected thickness of the control SAM was 1.1 nm (11 Å), estimated with the software Chem Bio 3D Ultra. The expected thickness takes into account the bond between the Au–S and the furthest bond, which is the oxygen bond present in the aromatic ring. The results are tabulated below:

Table 12: The ellipsometry analysis of 0.1 mM Benzoboroxole–modified surfaces.

Incubation solvent	Ellipsometry thickness (nm)
MeOH	0.70 ± 0.1
EtOH	0.91 ± 0.04
2% TFA in EtOH	1.21 ± 0.6

The thickness values obtained vary dependent on the solvent used to incubate the benzoboroxole control. Methanol and ethanol only studies show a small standard deviation, suggesting that the multiple surfaces are very similar to each other [360]. 2% TFA in ethanol, the incubation solvent used for the DSA SAM, did not show a small standard deviation, suggesting a larger thickness value difference between surfaces

[361]. Therefore, the incubation solvent used for the benzoboroxole modified SAM surface was concluded as HPLC ethanol because the thickness value obtained was the closest to the theoretical value of the three solvents compared.

3.5.3.2 XPS of benzoboroxole modified surface

The optimal condition from the contact angle and ellipsometry analysis was ethanol for the incubation solvent. From the optimal conditions, XPS was conducted to determine whether or not the benzoboroxole thiol derivative was successfully bound to the surface as well as the ratios being as expected.

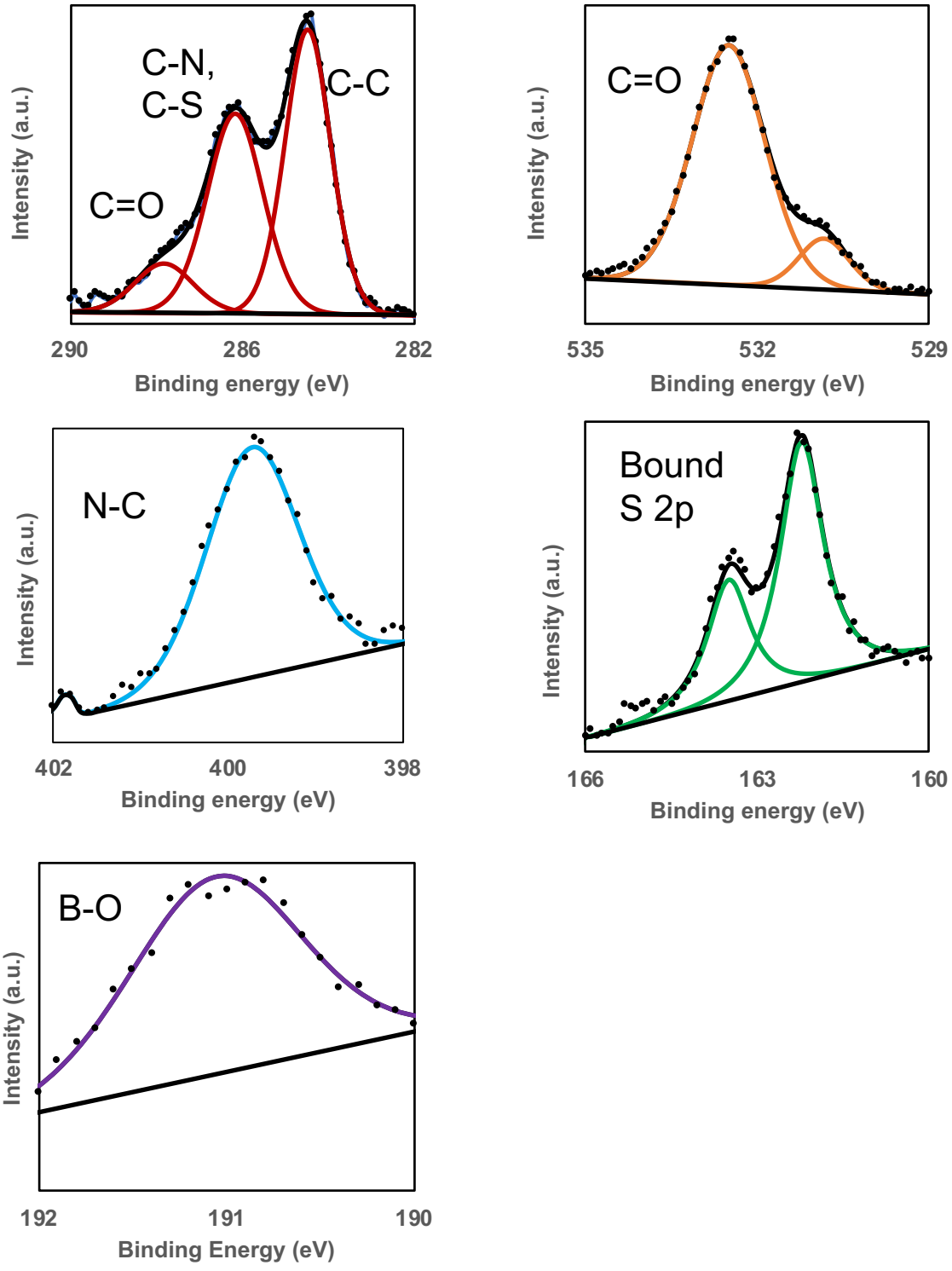

Figure 54: The XPS spectra of the benzoboroxole–modified surface. Red (top left) is C 1s, orange (top right) is O 1s, blue (middle left) is N 1s, green (middle right) is S 2p and purple (bottom left) is B 1s.

From the XPS analysis shown in fig. 54, the S (2p) doublet is positioned at 161.9 and 163.1 eV, indicating the sulphur is chemisorbed bound on the gold surface [359]. The N (1s) peak can be assigned to a single peak which is centred at 398.1 eV and is recognised as the amide group present in the benzoboroxole modified control SAM. B (1s) peak is shown at 190.8 eV, suggesting the XPS spectra of B–O and successfully demonstrating the presence of the benzoboroxole group [362].

Table 13: XPS analysis for the benzoboroxole–modified surface.

Ratio	Expected	Observed
C/S	10	7.2
B/S	1	0.9
O/S	3	3.1
N/S	1	1.1

The observed ratios of each of the elements are varied to that of the expected ratios The carbon: sulphur ratio is shown to be slightly lower than expected. This may be due to the distinguished a peak from the background and noise when using the reduced signal on offer at the lower pass energy [363]. This was shown to be the case of the B (1s) peak too, however boron is a sensitive peak and may be the reason for the small difference in the ratios [364].

3.5.3.3 SPR studies of the controls

The next stage of the chapter is to introduce surface plasmon resonance (SPR) studies and how the response of numerous sugars are able to bind to the complex on the Au surface. The propagation constant of a surface plasmon is sensitive to variations in the refractive index at the surface of a metal film supporting the surface plasmon [357].

In preliminary SPR studies conducted and shown hereafter, Stachyose, a tetrasaccharide, along with other sugars such as melezitose, raffinose and nystose were dissolved in 0.1 M phosphate buffer at pH 7.4, with varied concentrations from 0.25 mM to 20 mM. The structures of the four oligosaccharides used are shown in fig. 55.

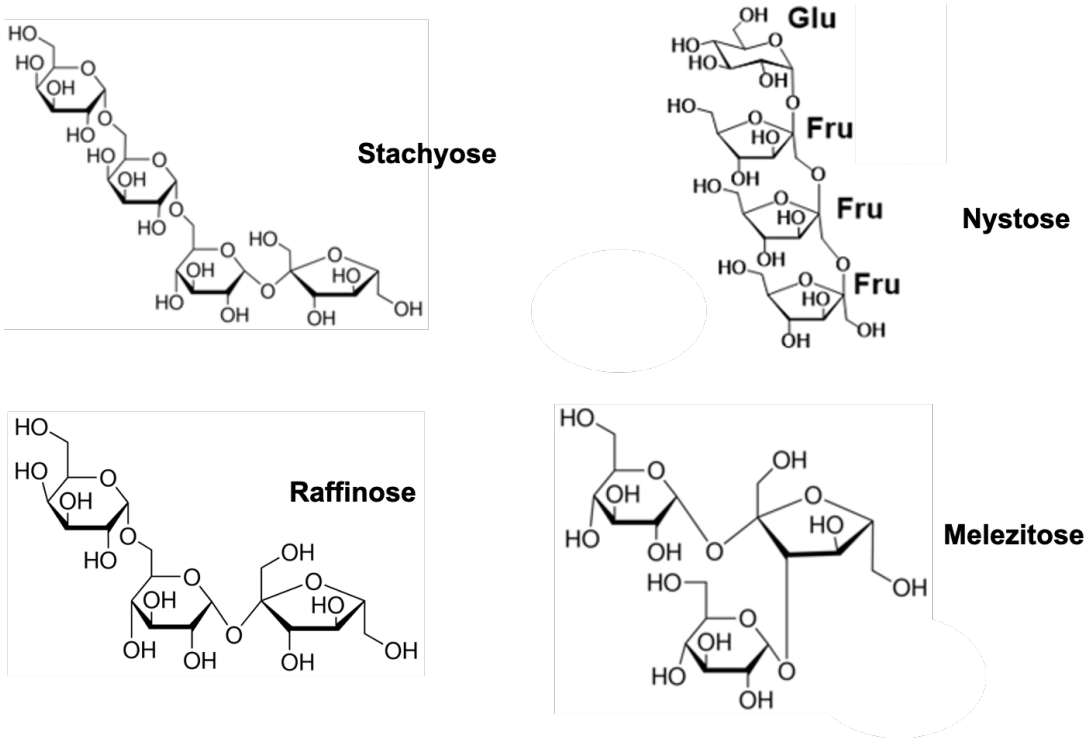

Figure 55: Chemical structures of stachyose, nystose, raffinose and melezitose.

3.5.3.4 SPR of the benzyl–terminated SAM

The data was to be obtained before further experiments were to be conducted and will account for the refractive index of the saccharides used throughout the work. Structures of the four used sugars are shown in fig. 56.

The four saccharide shown will be each flowed over the chips for SPR studies. The concentrations of the sugars will vary between 0.25 – 20 mM. These studies will enable the determination of the refractive index per saccharide.

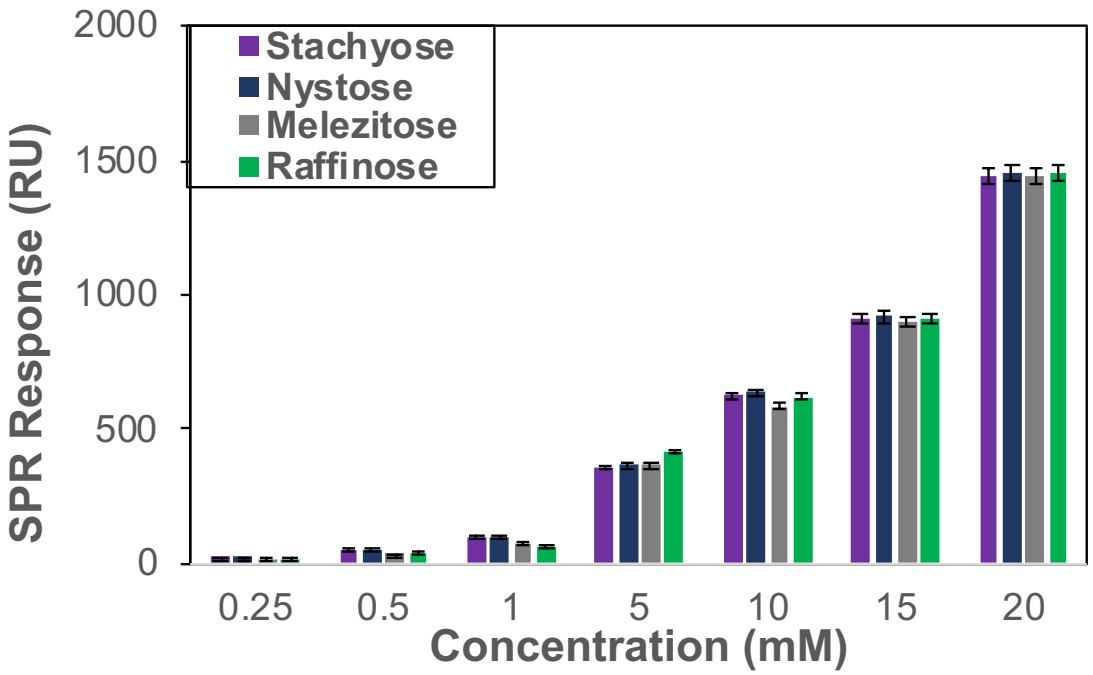

Figure 56: SPR studies of the benzyl–terminated control using pH 7.4 oligosaccharide solutions at different concentrations.

Stachyose, alongside the other saccharides used demonstrated similar SPR responses. Control surfaces are used when the analyte is injected over a surface it is

important, for two reasons, to perform a second injection with a control analyte [365]. The next stage was to record and analyse the benzoboroxole modified surface. This is to be formed and optimised similar to that of the benzyl–terminated surface, before examining the SPR responses.

3.5.3.5 SPR of benzoboroxole modified surface

In SPR sensors, the surface plasmon is excited at the interface between a metal film and a dielectric medium. The change in refractive index is observed and measured [366]. The optimum thickness of the Au layer used for the SPR studies is dependent on the wavelength used but typically is between 40 and 50nm [100]. Also, it is important to use an adhesive layer to bind the gold to the glass cover slip. Chromium and titanium are popular adhesive layers for this application; however, titanium was selected since leaching through the gold layer is less frequent than in chromium [101,102].

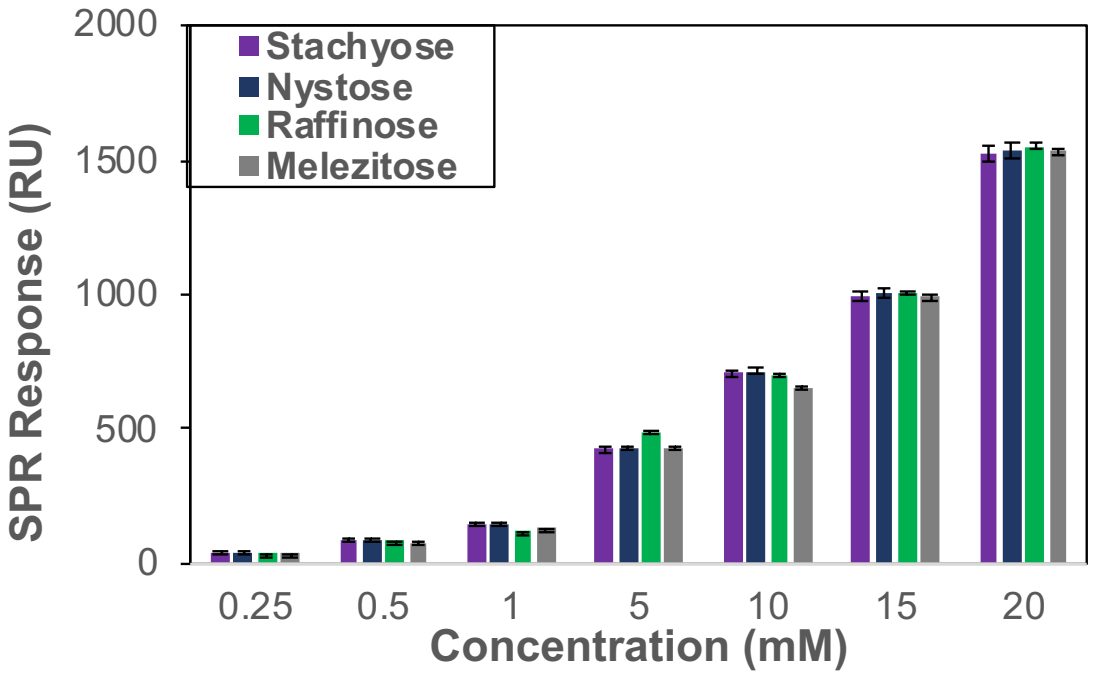

Figure 57: The SPR response obtained from the benzoboroxole modified SAM response. SPR studies using pH 7.4 running buffer and different concentrations of oligosaccharides.

The subtracted SPR response is shown in fig. 58 and is taken under different concentrations and a dissociation rate of 2.5 minutes, subtracting the SPR response obtained of the benzyl–terminated SAM and that of response of the benzoboroxole modified surface. The concentrations used are 0.25 mM to 20 mM, with the use of different sugars. The sugars used were stachyose, raffinose, melezitose and nystose.

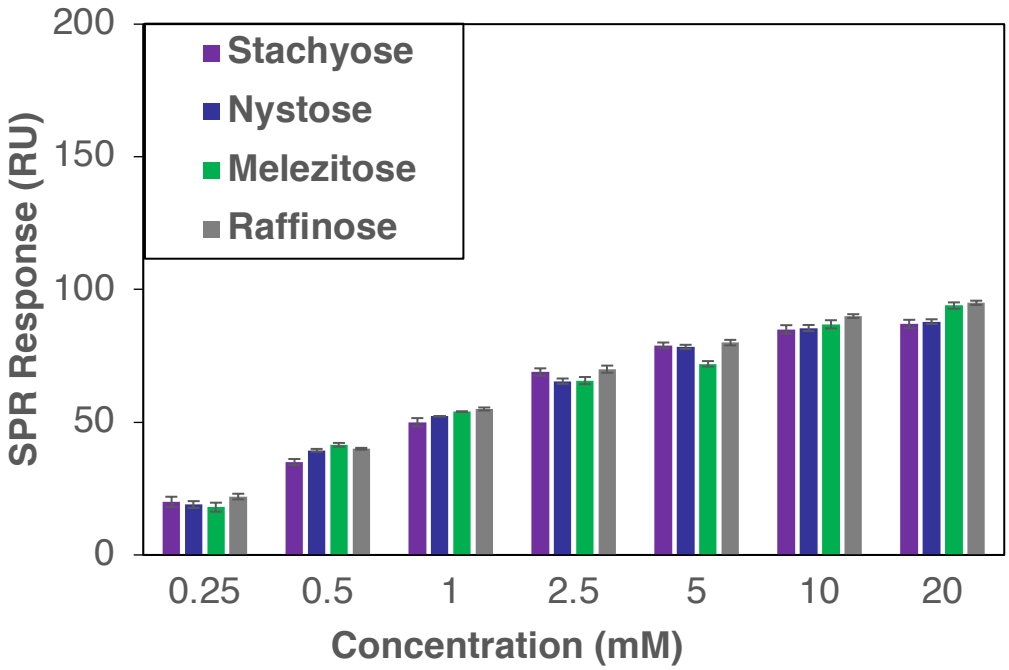

Figure 58: The benzyl–terminated SAM subtracted from the response obtained from the benzoboroxole modified SAM response. SPR studies using pH 7.4 oligosaccharide solutions at different concentrations.

The response obtained from the benzoboroxole modified SAM and the response from the benzyl–terminated SAM were subtracted. At different concentrations (0.25 – 20 mM) of sugars, the response was recorded once the response was at a plateau. This suggests that the presence of a benzoboroxole is able to specifically interact with sugars. The next analysis of the SPR data was to individually graph the data, and calculate the trend of each line.

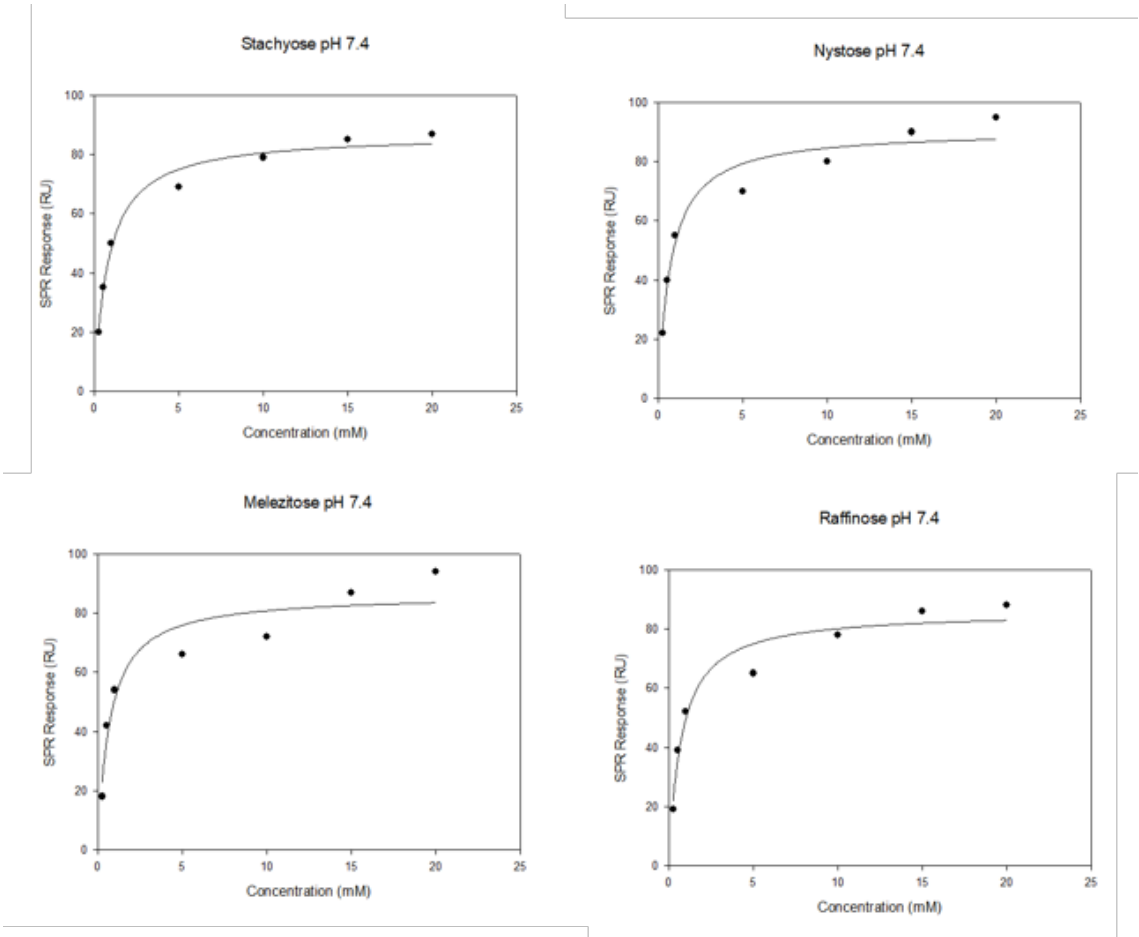

Figure 59: SPR subtracted response of the four oligosaccharides.

Rmax and K_D values are calculated from the hyperbolic curves shown in fig. 59. The hyperbolic functions are used to prove to be useful for expressing these concentration dependences [367]. R_{max} is defined as the maximum change in the SPR angle dependent on the total ligand concentration directly [368]. The K_D value is also known as the dissociation rate constant. The dissociation constants such as K_D are typically calculated from the ratio of the dissociation rate to the association rate, or from measurement of binding of the labelled ligand in the presence of increasing amounts of the unlabelled ligand [369].

From the curves shown above, the hyperbolic trend line was used for the calculation of both K_D and Rmax which are tabulated below. The hyperbolic regression analysis is an effective method for fitting experimental data points obtained from a variety of experiments in molecular biology, including enzyme kinetics [370].

$$R_{eq} = \left(\frac{C_p}{C_p + K_D}\right) R_{max}$$

The R^2 value of each of the saccharides and their curves is also tabulated. The regression of the data must be the nearest to 1, demonstrating the accuracy of the fit of the data [371].

Table 14: K_D and Rmax values obtained for the different oligosaccharides used.

Saccharide	Rmax (RU)	K_D (mM)	R^2 value
Stachyose	94.32	1.86	0.998
Nystose	92.24	1.61	0.997
Melezitose	92.84	1.58	0.996
Raffinose	98.26	1.71	0.995

K_D values are reported for fructose, glucose and methyl α–d– galactopyranoside of 2.95, 32.3, and 34.5 × 10^{-3} M, respectively [372]. As found to be in similar millimolar (mM) range, the K_D values shown in the table are similar to those in solutions. Affinity

in the mM range for monovalent interactions is concluded as low affinity when compared to antibody- protein K_D values in the nM range. This low K_D is typically counteracted by multivalency of the protein-glycan interaction [373]. As Rmax values reported are alike, the conclusion of the Rmax values is that the affinity observed are analogous regardless of the saccharides used. Interactions consist of hydrogen bonding within defined grooves alongside additional Van Der Waals interactions however, dependent on nearby amino acid functional groups i.e. methyl or carboxyl, ionic or hydrophobic interactions may also deliver or alter the binding.

3.6 Conclusion of the optimisation of controls

The optimisation of both a benzoboroxole–modified control SAM and control benzyl–terminated SAM was discussed in the chapter. The characterisation of the control benzoboroxole modified SAM confirms successful XPS data stating the presence of boron. The preliminary SPR studies are demonstrating that the benzoboroxole group is binding to sugars when compared with the control benzyl–terminated surface. The control benzyl–terminated surface will be used for future work when subtracting the SPR responses of any SPR studies conducted. This will be to account for the refractive index of the sugars used.

3.7 Overall conclusion of the formation and characterisation of DSA SAM and the cross–linking of AABOB onto a DSA SAM.

This chapter demonstrates the formation of the N, N' bis(acryoyl) cystamine SAM, which is abbreviated to DSA SAM for the research. The optimisation was determined with the use of ellipsometry and contact angle before further looking at the elemental configuration with XPS analysis. As previously described in the chapter, ellipsometry and contact angle data obtained suggested DSA SAM formed densely packed SAMs when incubated in ethanoic conditions with the presence of trifluoroacetic acid (TFA). Conversely, no contamination was observed on the 0.1 mM DSA incubated in ethanoic conditions with 2% TFA SAM, suggesting polar amide and carbonyl were likely to be bound onto the surface.

Cross–linking of AABOB and DSA on a gold surface required the optimisation with the use of XPS analysis. Boron (B1s) along with Sulfur (2p), Carbon (1s), Nitrogen (1s) and Oxygen (1s) allows the conditions used for the cross–linking to be successfully confirmed. The XPS spectra was analysed throughout the chapter to observe a boron peak on the surface. The conditions which confirmed successful cross–linking of AABOB on the DSA SAM were 0.1 mM DSA SAM surface and 0.5 mM AABOB solution in phosphate buffer, this is to be incubated for 240 mins. Argon balloon is inserted to prevent the involvement of oxygen, as oxygen may disrupt the cross–linking procedure [374].

Control SAMs were synthesised and determined whether benzoboroxoles were able bind to the DSA SAM surface successfully. The control benzyl–terminated SAM is to be used to observe the refractive index of sugars, whereas the benzoboroxole modified SAM can be used to compare the K_D values of the four oligosaccharides used as well as the R_{max} values. The control benzyl–terminated SAM will be used later in the research to subtract the response from any SPR response obtained by the complexes. This subtraction will account for the refractive index observed on the surfaces.

CHAPTER 4 – COMPLEXATION AND MOLECULAR IMPRINTING

Abstract: *This chapter is taken from the paper "Tommasone, S.,* ***Tagger, Y. K.****, Mendes, P. M., Targeting Oligosaccharides and Glycoconjugates Using Superselective Binding Scaffolds. Adv. Funct. Mater. 2020, 30, 2002298". A unique modular, synthetic strategy allows for the creation of artificial binding sites with precise spatial positioning of multiple carbohydrate receptors, enabling the remarkable ability to distinguish a target oligosaccharide over closely related carbohydrate structures.* ***Co-first author in the publication documented above****

4.1 Introduction

Oligosaccharides, which often occur as glycoconjugates, play essential roles within a multitude of biological processes, including fertilisation, cell differentiation, cell signalling, and host–pathogen interactions [375-378]. Furthermore, they are emerging as important biomarkers for a wide range of diseases, including immune deficiencies, hereditary disorders, neurodegenerative and cardiovascular diseases, as well as many types of cancers [379-381]. Thus, materials with highly specific oligosaccharide recognition are key for advancing glycobiology research and producing new opportunities to diagnose and treat diseases.

However, the approaches used today, rely on anticarbohydrate antibodies [382], lectins [383], aptamers [384], and synthetic carbohydrate receptors [385], are limited in their capabilities to discriminate between a large repertoire of carbohydrate structures, including closely related isomers [386]. For instance, natural and recombinant lectins exhibit specificity only toward a particular carbohydrate motif or structural feature and are available in a very limited number when compared with the striking variety of oligosaccharide structures [387]. On the other hand, oligosaccharides are poorly immunogenic, posing major hurdles in the development of highly selective anti–carbohydrate antibodies [388]. Synthetic carbohydrate receptors, including boronic acid moieties, which form reversible covalent complexes with diols, have been combined with molecular imprinting to obtain carbohydrate binding sites on polymer matrices [167, 389]. However, the available synthetic approaches are

incapable to encode the binding sites with precise molecular complementarity to target oligosaccharides.

Here, we will report on a modular synthetic approach that can harness both the construction of high–yield, complex oligosaccharide–synthetic carbohydrate receptor assemblies and the precise generation of surface–confined templated binding sites (fig. 60), thereby creating recognition sites of unparalleled oligosaccharide discrimination. Benzoboroxoles are employed as carbohydrate receptors since, in contrast to their boronic acids analogues, benzoboroxoles can bind nonreducing hexopyranosides at pH values compatible with biological systems [390].

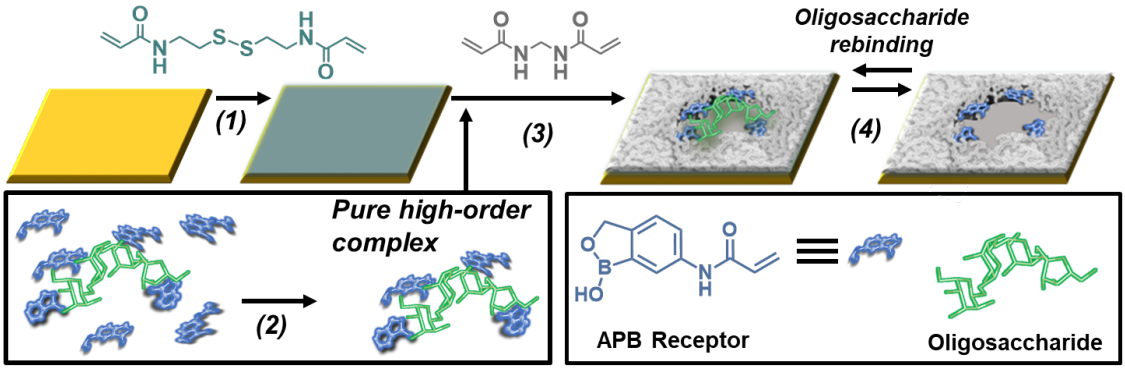

Figure 60: Method for creating synthetic materials with superselective oligosaccharide recognition.

4.2 Objectives

The objectives of the work in this chapter can be broken down as follows:

- Synthesise the complexation between saccharides and benzoboroxoles.
- To conduct SPR studies with the complexation, obtaining the R_{max} and K_D values.
- To create the molecular imprint. ATRP will be employed to crosslink the complex and the initiator SAM surfaces at room temperature in biocompatible conditions.
- Incorporate N,N'–methylenebisacrylamide, to form a scaffold around the oligosaccharide template enabling a pocket–like structure be present on the surface.
- To look into the oligosaccharide binding and rebinding process. Different oligosaccharides will be used in comparison to determine if selectivity of the target molecule is observed when compared to other non–targets.
- Further analyse the complexation with RNase B and MBA.

4.3 Complexation

The creation of stable and high–order complexes between oligosaccharides and benzoboroxoles was to be achieved by using two model oligosaccharides, stachyose and nystose. The structure of the benzoboroxole and the two model oligosaccharides used in the studies are each shown in fig. 61. The composition of stachyose is Gal(α1-6)Gal(α1-6)Glc(α1-2β)Fru whereas the composition of nystose is three fructose

molecules joined by a glucose molecule [391, 392]. This section was carried out by Stefano Tommasone.

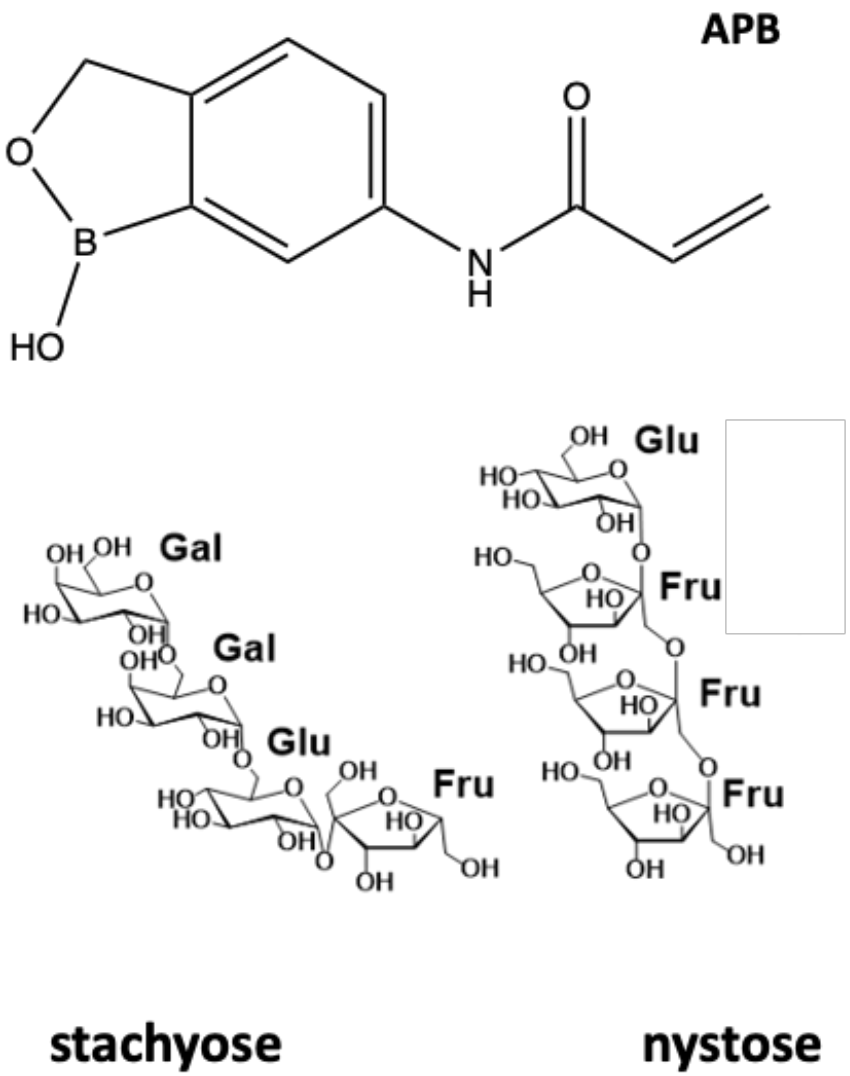

Figure 61: The chemical structure of 5–acrylamido–2–(hydroxymethyl) phenylboronic acid cyclic monoester (APB), stachyose and nystose.

The optimal complexation conditions were achieved by stirring for 24 h a mixture of an excess of 2–(hydroxymethyl)phenylboronic acid cyclic monoester (8.0 equivalents per sugar unit) and oligosaccharide in dioxane:acetonitrile (6:1 v/v) at 90°C with molecular sieves (3Å) to remove H_2O which is formed during this condensation reaction producing the APB complex. On the removal of the target oligosaccharide, a unique print would remain surrounded by APB–oligosaccharide complex forming a binding pocket.

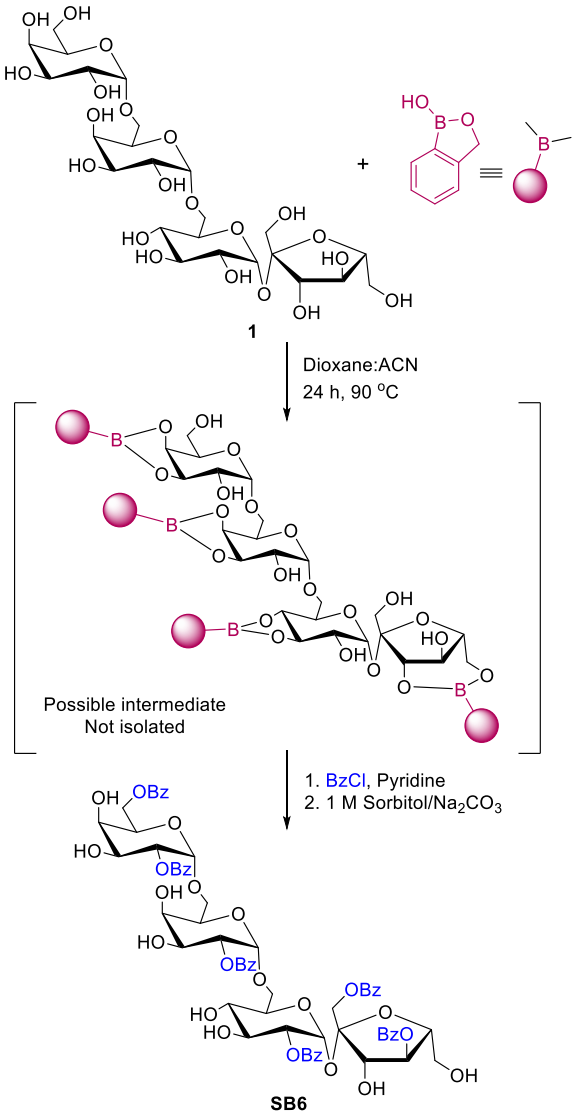

Figure 62: Indirect approach to assess the degree of complexation.

Following complexation, the resulting complex was treated with benzoyl chloride in pyridine for 5 h, in order to functionalize the OH groups that are not involved in any bond with the boron. This was conducted because the degree of complexation could not be characterised otherwise. Afterward, the boronate esters were hydrolysed by treatment with 1 M aqueous solution of sorbitol/Na_2CO_3 and ethyl acetate (EtOAc), and the product was finally recovered by several washings with EtOAc [393]. Together

with the known binding mechanism of boronic acid derivatives with diols [372, 394] the analysis of the resulting product gave us insight into the efficiency of the complexation and the structure of the complexes formed. These analyses demonstrated that the highest–order complexes were preferentially formed. For instance, stachyose can interact with benzoboroxoles to form complexes with stoichiometry ranging from 1:1 up to 1:4. However, the results indicate that stachyose was able to form complexes with benzoboroxoles in high 1:3 and 1:4 stoichiometric ratios, with a greater proportion of 1:4 (80%) than 1:3 (20%) complex. Structures of the benzoylated derivatives with stachyose and nystose compounds with an odd number of benzoyl groups B derive from complexes where the boron is bound to the sugar S via only one OH group are shown below.

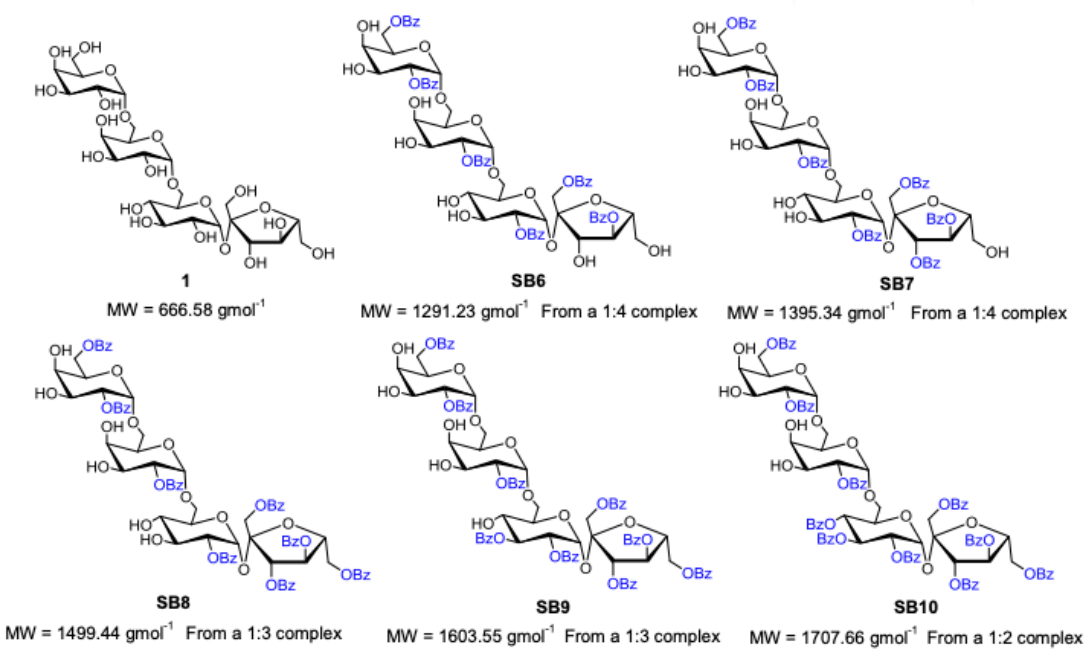

Figure 63: Benzoylated derivatives with stachyose **1**: compounds with an odd number of benzoyl groups B derive from complexes where the boron is bound to the sugar S via only one OH group.

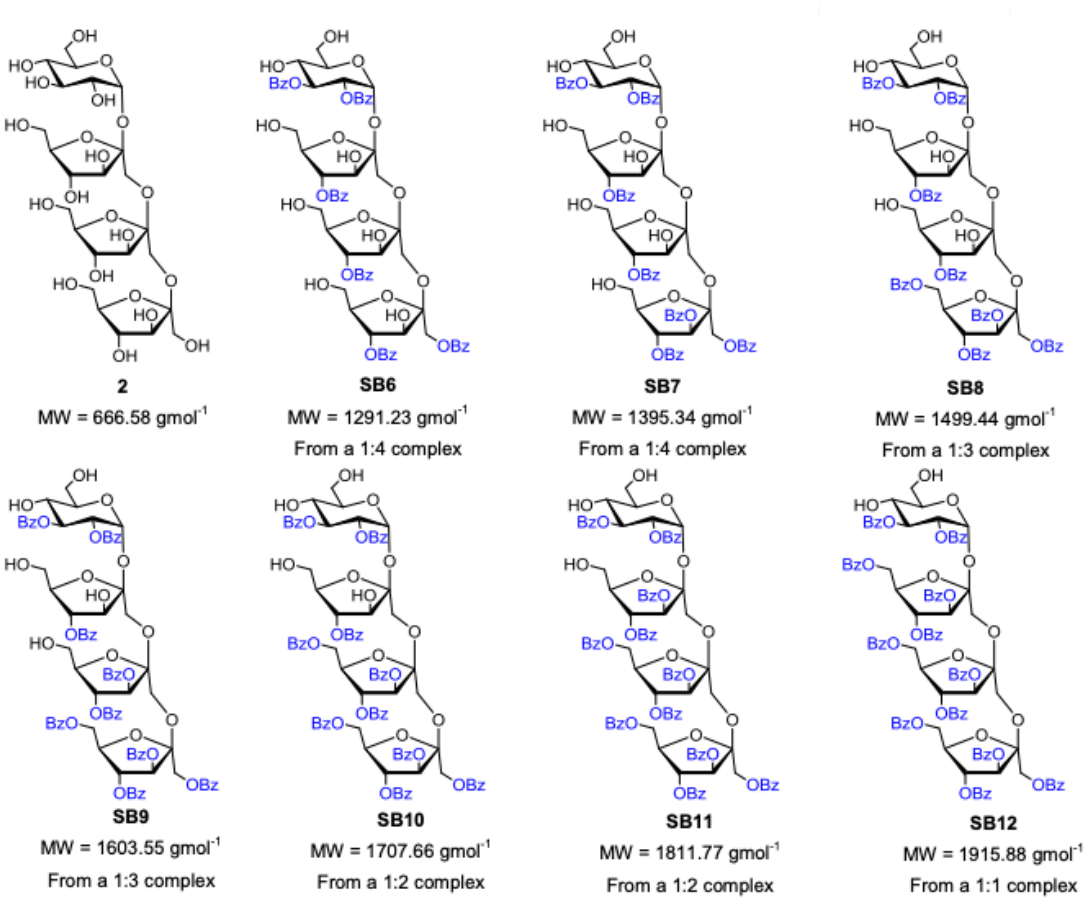

Figure 64: Benzoylated derivatives with nystose 2: compounds with an odd number of benzoyl groups B derive from complexes where the boron is bound to the sugar S via only one OH group.

Table 15: Degree of complexation of different oligosaccharides, stachyose and nystose with 2–(hydroxymethyl)phenylboronic acid cyclic monoester. Relative ratios (%) of complexes derived by the MALDI spectra of the products.

Substrate	Sugar Units	1:5	1:4	1:3	1:2	1:1
Stachyose	4	–	80	20	0	0
Nystose	4	–	15	69	16	0

Binding scaffolds were constructed to determine whether the response observed under SPR studies is indeed selective to the target oligosaccharide and not to non–target oligosaccharides. The first target oligosaccharide used in this research was stachyose as a template MIP. The construction of the oligosaccharide binding scaffolds was initiated by immersing clean gold substrates in a 0.1 mM ethanolic solution of N,N′–bis(acryloyl)cystamine with 2% trifluoracetic acid (TFA) for 24 h, as previously discussed and explained in chapter 3. This demonstrates that our approach can push the formation of boronate esters even when the conditions are less favourable, as well as being of general applicability since it affords high–order complexes with oligosaccharides with different sizes and stereochemistry.

4.4 Stachyose–template surface

The oligosaccharide and 2–(hydroxymethyl)phenylboronic acid cyclic were suspended in a mixture of dioxane and acetonitrile. For practical purposes, the commercially available 2–(hydroxymethyl)phenylboronic acid cyclic monoester rather than the synthetic derivative 5–acryalmido–2–(hydroxymethyl)phenylboronic acid cyclic monoester was used. This allowed us to scale up the process and work with a more tangible amount of sugar. The reaction mixture was stirred at 90 ºC for 24 h under argon atmosphere in presence of activated molecular sieves 3Å. The solvent was removed under reduced pressure and the crude was dissolved in pyridine. Benzoyl chloride was added at 0 ºC and the reaction mixture was stirred at room temperature for 5 h. The reaction mixture was diluted in toluene and filtered through celite. The solvent was removed under reduced pressure and the crude was dissolved in an equal measurement of both EtOAc and a solution of 1 M sorbitol/Na_2CO_3 and was stirred for 1 h. The two phases were then separated and the aqueous layer was washed three times with EtOAc. The organic phases were combined, dried over $MgSO_4$ and concentrated under reduced pressure.

Stachyose, along with other saccharides were to be compared to observe the SPR response created between the sugars. The SPR response of four saccharides was analysed and the analysis conducted is shown in fig. 65. The subtraction of the control benzyl–terminated SAM was conducted using Microsoft Excel and the concentration of the saccharides are plotted with a hyperbolic trendline. This subtraction is to avoid

the bulk refractive change of the used saccharides. From the hyperbolic trend line, the K_D and R_{max} values can be determined.

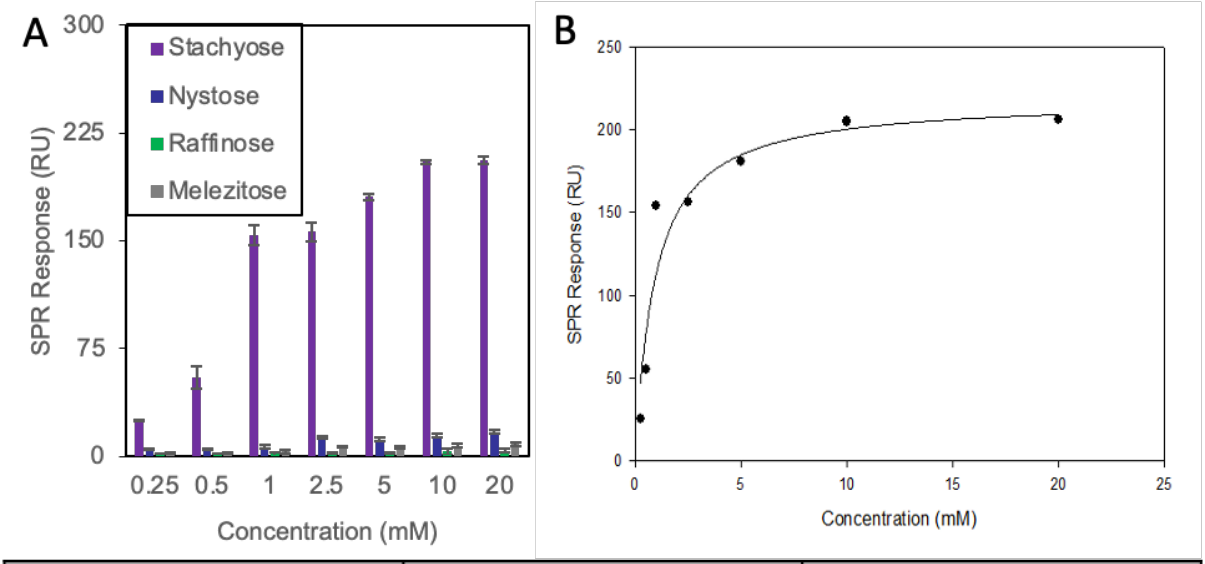

Rmax (RU)	K_D (mM)	R^2 value
220 ± 18	0.93 ± 0.1	0.84

Figure 65: **A** The stachyose complex with the binding responses of the four saccharides used at pH 7.4 studies, **B** is the hyperbolic trendline of the stachyose SPR response and **table** documents the K_D and Rmax values calculated from the hyperbolic trendline shown.

From the hyperbolic trendline, the K_D as well as the R_{max} are calculated. From the responses obtained, the surface shows superselectivity with stachyose (fig. 65 A). The other saccharides used for the studies demonstrated negligible binding, concluding that the other saccharides, namely raffinose, nystose and melezitose, did not selectively bind to the complex [395]. From the trendline (fig. 65 B), the R^2 value is

calculated along with the K_D value of the stachyose response. The dissociation constants (K_D) of benzoboroxoles for monosaccharides are largely dependent on their structure, with reported K_D values for fructose, glucose and methyl α–d–galactopyranoside of 2.95, 32.3, and 34.5 × 10^{-3} M, respectively [372]. Thus, the surface–confined binding scaffolds resulted in 5–50–fold higher binding affinity for the target oligosaccharide as compared to monosaccharides. The binding affinity is a measure of how tightly the target oligosaccharide binds to the scaffold architecture. There is an inverse relationship between the K_D and affinity. The smaller the K_D, the greater the affinity of the scaffold. The behaviour shown suggests that multivalent interactions are occurring between multiple benzoboroxoles receptors incorporated in the binding site with multiple hydroxyl groups within the oligosaccharide chain. While the binding affinity is comparable to that of oligosaccharide antibodies and lectins with dissociation constants in the low mM range [396, 397].

The R^2 value or coefficient is a statistical measure of how close data points are to the line of best fit (regression line) [398]. The R^2 value was calculated using Sigmaplot as 0.84, suggesting the R^2 value did not demonstrate the data points fitting to the hyperbolic trendline. Low sensitivity is reflected in the low R^2 values for the complexation [399] and hence we can summarise that other agents must be used.

4.5 N,N'–Methylenebisacrylamide

The N,N'–Methylenebisacrylamide (MBA) is a crosslinking agent and is used to allow building a molecular scaffold around the template [400, 401]. MBA defines the pocket shape and size of the oligosaccharide used as a template, enhancing to some extent its binding affinity. Apart from creating a shape complementary to the template, MBA can provide additional weak interactions with carbohydrates (i.e. hydrogen bonds) which could enhance the affinity for the target template. The structure of MBA is shown below:

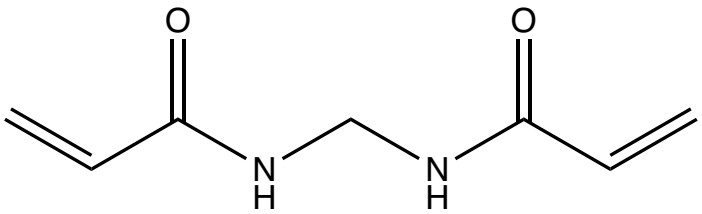

Figure 66: Chemical structure of N,N'–Methylenebisacrylamide (MBA).

In order to understand the contribution of the MBA to the saccharide binding, experiments were conducted to determine if the addition of MBA on a surface did have some effect, whether positive or negative. DSA was crosslinked with 5 mM MBA at pH 7.4 and the SPR response are shown below with the four oligosaccharides used in the studies.

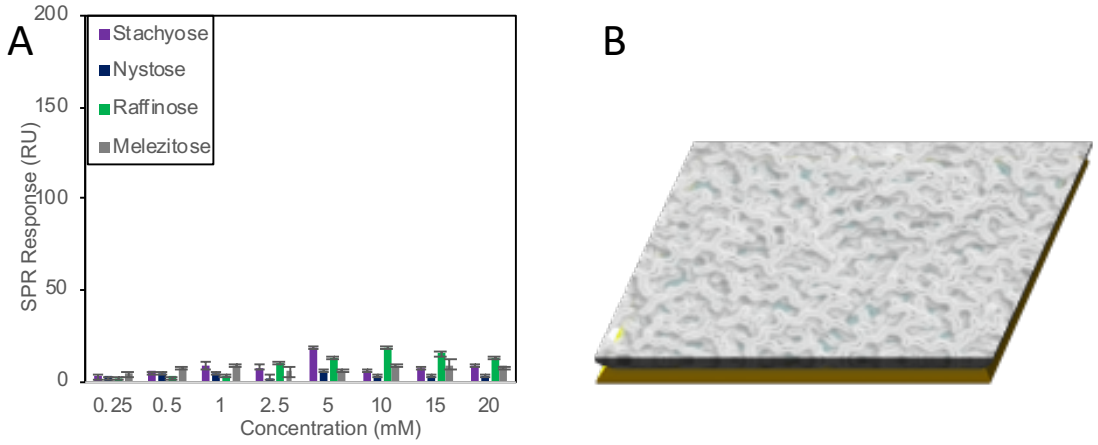

Figure 67: **A** The SPR response of a DSA-MBA only surface subtracted by the benzyl–terminated control SAM. The SPR studies were conducted using pH 7.4 oligosaccharide solutions. B the representation of the MBA surface.

Fig. 67 demonstrates the subtracted SPR response of the surface once different concentrations of saccharides are flowed over the surface. The subtracted response should be as minimal as possible, indicating that the presence of the MBA has a limiting effect on the surface before any complex is added. It was clear that the presence of MBA did not demonstrate any significant binding of the four oligosaccharide solutions used for the study. In conclusion, as negligible binding was observed the presence of the cross–linker was considered to not impact the surface before any complex was bound.

4.6 Stachyose template MIP

Following its complexation with APB, the stachyose complex and free APB were separated by precipitation followed by centrifugation. This protocol enabled us to remove the excess of unreacted APB, which otherwise would have had a detrimental effect in creating precise recognition sites for oligosaccharides. The next step was to optimise the incubation time of the MBA and whether or not the incubation should occur simultaneously or separately. The studies were conducted on one concentration, 5 mM stachyose and 5 mM MBA and the subtracted SPR response is shown.

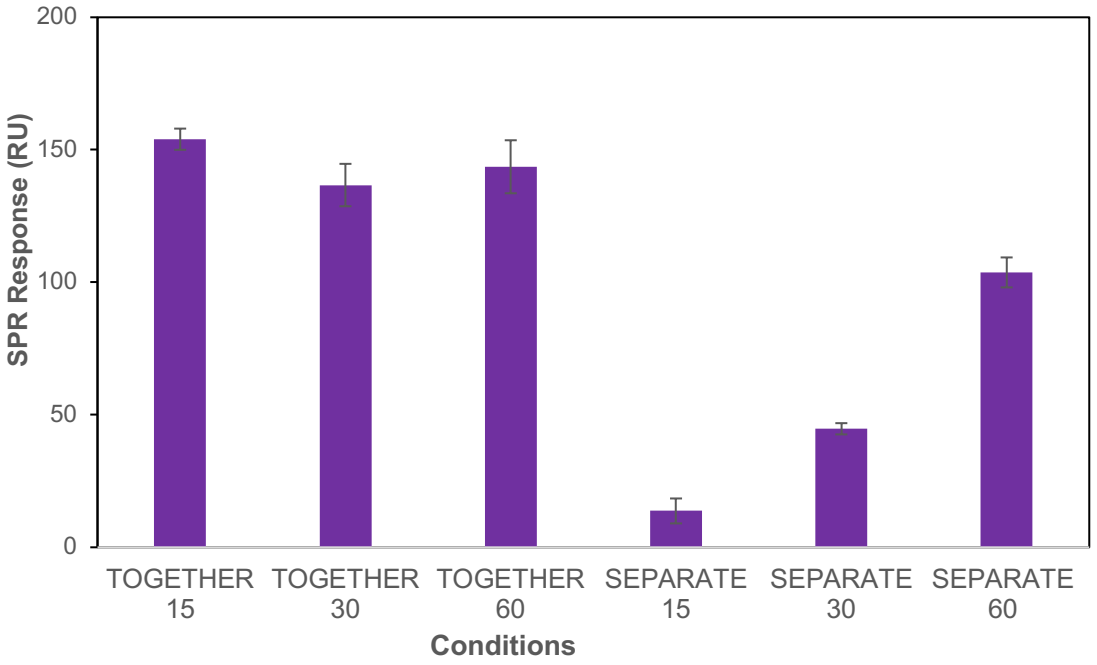

Figure 68: Different conditions and the use of MBA at varied times against the subtracted SPR response obtained.

From the figure shown, it was clear that incubating the complex and the MBA separately did not demonstrate a positive condition as SPR responses shown were reduced when compared with the complex and MBA incubated simultaneously. Hence, the binding scaffolds were prepared by grafting simultaneously MBA and the high–order complexes between stachyose and APB onto the DSA SAM for numerous different times, both simultaneously and separately incubated. It was clear that the numerous different incubation times generated very different SPR responses. Incubating the complex together with MBA had shown to be successful, as the SPR response does increase. The optimal incubation time was defined to be 15 minutes and will be used in the future studies.

Following dissociation of the oligosaccharide from the surface under pH studies, the binding affinity and selectivity of the stachyose–binding scaffolds were evaluated using SPR spectroscopy. To study pH effect on the imprinted surface, saccharide concentrations were prepared and compared in three different pH values. Physiological pH was used as benzoboroxoles are known to be work well at physiological pH (7.4), in addition, pH 10 was studied. Alkaline conditions is promoted for boronic acids and here we will be looking if such alkaline conditions make any difference with the benzoboroxoles that works quite effectively at neutral pH. Finally, pH 4 is explored to demonstrate whether or not the benzoboroxoles work under acidic conditions.

4.7 Physiological pH 7.4

It would be hard to overstate the importance of proteins in the human body. They make up ion channels, carry necessary lipophilic substances throughout our mostly lipophobic body, and participate in innumerable biological processes. For proteins to complete necessary functions, they must be in the proper configuration. The charges on proteins are what allow their proper shape to exist. When pH is altered outside of the physiological range, these charges are altered. The proteins are denatured leading to detrimental changes in architecture that cause a loss of proper function [402].

Benzoboroxoles are found to bind specifically to the cis–diol groups of carbohydrates at physiological pH and it is known to have superior affinity to that of any other Wulff–type boronic acid [403]. Different concentrations of the four oligosaccharides were used, from 0.25 mM to 20 mM.

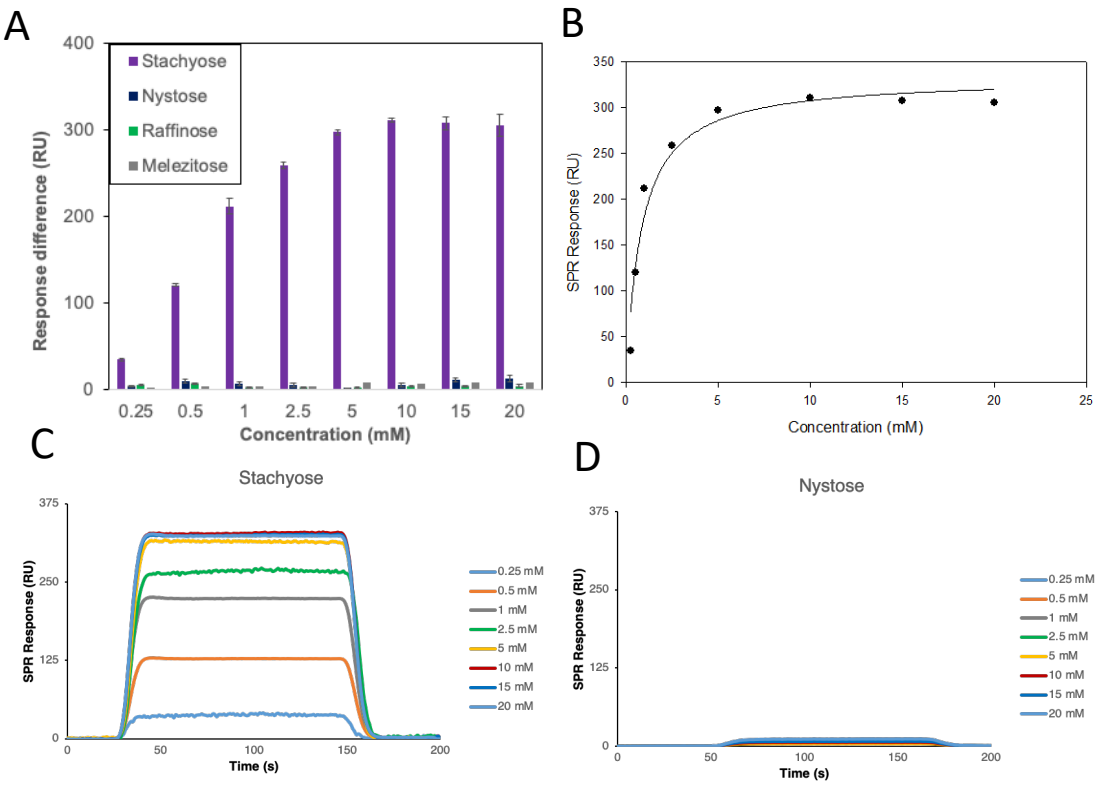

Figure 69: **A** The SPR response of a Stachyose template MIP surface subtracted by the benzyl–terminated control SAM. The SPR studies were conducted using pH 7.4 oligosaccharide solutions. **B** the analysis to determine the R_{max} and K_D values. **C** SPR sensograms of the stachyose (target) SPR response and **D** nystose (non–target) SPR sensograms.

The SPR response differences (fig. 69, A) demonstrate the differences of the SPR response from the control benzyl–terminated SAM for the varied concentrations of stachyose (target molecule). The differences accounts for the response obtained by what is bound on the surface, as previously mentioned in chapter 3. The SPR sensorgrams reveal a striking difference in binding between the target stachyose

oligosaccharide (fig. 69, C) and non–target oligosaccharides (fig. 69, D), with the formed binding sites allowing for a great degree of subtlety in recognizing stachyose.

From the differences obtained, the average of the SPR responses were plotted against the concentration. The points plotted were recorded against a hyperbolic trendline, similar to that of the other SPR studies conducted in this work (table 18).

Table 16: The K_D and R_{max} values calculated from the hyperbolic trendline shown in fig. 69, B.

Rmax (RU)	K_D (mM)	R^2 value
333 ± 15	0.83 ± 0.02	0.98

SPR binding analysis show that stachyose binds to the stachyose–binding scaffolds with a dissociation constant (K_D) of 0.83 mM ± 0.02, whilst no or negligible binding was observed for the non–target oligosaccharide, as an example nystose, and as a result the K_D was unable to be calculated. However, in our case only a slight increase in the binding affinity was observed (K_D of 0.83×10^{-3} M with MBA vs 0.93×10^{-3} M without MBA). This is probably because either the thickness of the polymer layer is too small and does not allow the MBA to have a significant effect on the overall binding or the crosslinker does not make the surface rigid enough to affect the properties of the binding site. Following the studies under physiological pH, the next stage was to consider pH 10. Stachyose–binding scaffolds was in the range of ~0.3

ng/mm^2 where 100 response units (RUs) = 0.1 ng.mm^2 [404]. This corresponds to 1 oligosaccharide per 4–6 nm^2. Assuming a footprint of approximately 2–3 nm^2 for a tetrasaccharide [405], an estimated 50% surface coverage by oligosaccharide can be achieved. The remaining surface area comprises crosslinked MBA, which defines the pocket shape and size of the oligosaccharide used as template, enhancing to some extent its binding affinity.

4.1.1 pH 10 studies

The reversible five–membered or six–membered ester ring formation between the phenylboronic acid and the cis–diols on the glycoproteins requires an alkaline pH [354]. Alkaline conditions are promoted for boronic acids and here we will be looking if such alkaline conditions make any difference with the benzoboroxoles that works quite effectively at neutral pH. To determine whether or not the binding of the complex can be used at pH 10, SPR studies are conducted. The SPR response of the stachyose–template MIP is subtracted from the control benzyl–terminated SAM as previously mentioned.

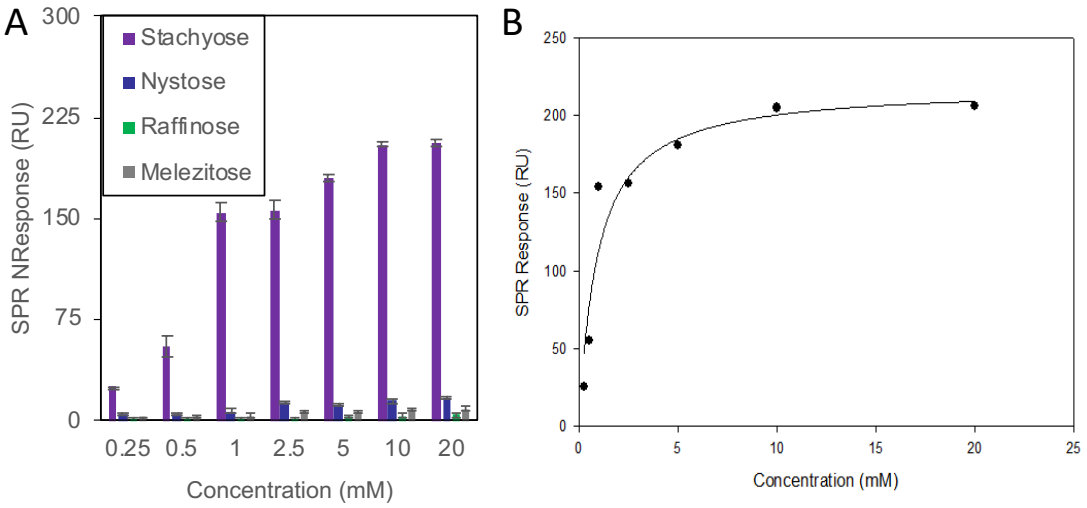

Rmax (RU)	K_D (mM)	R^2 value
220 ± 18	0.93 ± 0.1	0.84

Figure 70: **A** SPR sensorgrams of stachyose and nystose solutions on the stachyose–template MIP. Solutions are between 0.25 – 20 mM, under pH 10. **B** the analysis to determine the R_{max} and K_D values and table reporting the R_{max} and K_D values.

The stachyose–binding scaffolds displayed similar binding behaviour towards stachyose at and pH 10 (K_D= 0.82± 0.02, Fig. 70) when compared to pH 7.4 (K_D= 0.83 ± 0.02). When the SPR subtracted responses are compared, nystose, melezitose and raffinose still did not reveal selectivity of the molecular imprint.

4.1.2 pH 4 studies

Under acidic conditions, benzoboroxoles affinity to saccharides is greatly reduced [406]. The SPR analysis of the stachyose template MIP was conducted with the four oligosaccharides, all under pH 4 solutions.

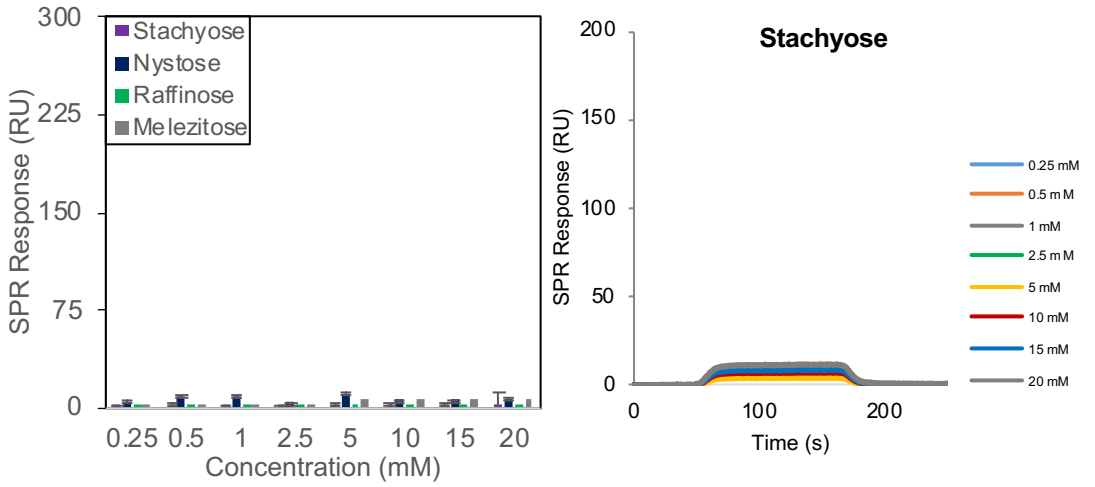

Figure 71: Left SPR sensorgrams of oligosaccharide solutions on the stachyose–template MIP. Solutions are between 0.25 – 20 mM, under pH 4 and right SPR sensogram of the stachyose (target) SPR response at pH 4.

One–site binding needs to show a smooth hyperbolic dependence of the concentration of the receptor–ligand complex on the free ligand concentration when calculating affinity [407]. The SPR responses for all of the four oligosaccharides did not demonstrate a hyperbolic trend, suggesting that no one–site binding occurred at acidic solutions. To conclude, the data obtained for the stachyose template MIP at pH 4 (fig. 71) demonstrated how the complexation previously discussed did not display a selective response for any of the oligosaccharides, target (stachyose) and non–target saccharides. No binding occurred at pH 4 since boronate ester formation is less favourable in acidic conditions.

4.8 Conclusion of stachyose MIP

Our findings provided evidence of the importance of precise and multivalent spatial pattern recognition to achieve super-selective oligosaccharide binding. When we take into consideration that stachyose is a higher homolog of raffinose and an all–or–nothing binding occurs between them, it indicates that the nature of the superselective behaviour is likely associated with a threshold in binding stability. The precise spatial arrangement of the receptors promotes the establishment of multiple interactions with the target oligosaccharide, stabilising the binding event with consequent enhanced K_D values, which is otherwise not possible with oligosaccharides that do not match the binding site. Although raffinose could potentially fit the binding sites of stachyose–binding scaffolds, it is probably not able to establish enough interactions to overcome the energetic requirements to reach an observable binding. The next study was to demonstrate whether a different complexation formed on the surface could create similar affinity and selectivity as shown by stachyose–template MIP.

4.9 Nystose template MIP

With nystose, the formation of high–order complexes was also observed, as we found evidence of a 1:3 adduct and some 1:4 (maximum degree of complexation). Instead, nystose has three fructose units and a glucose unit, unlike stachyose's singular fructose.

Similar to that of stachyose–template MIP, nystose template MIP was synthesised and used to determine the affinity of nystose as well as compare with other saccharides. Different concentrations of the four oligosaccharides were used, from 0.25 mM to 20 mM.

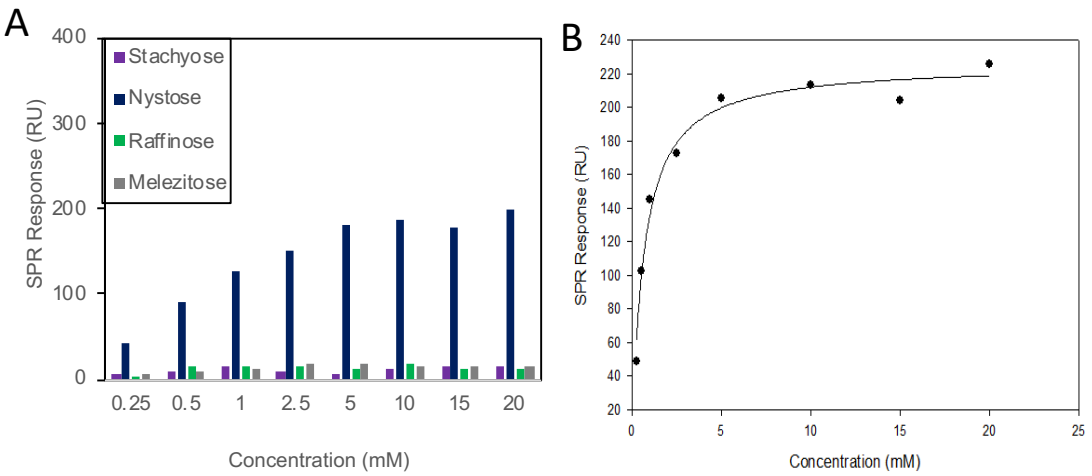

Rmax (RU)	K_D (mM)	R^2 value
238 ± 8	0.65 ± 0.08	0.97

Figure 72: A Nystose–binding scaffolds, from which K_D and R_{max} values have been obtained. B and C The K_D and R_{max} values calculated from the hyperbolic trendline.

In creating a nystose–binding scaffold, the selectivity is reversed and instead the recognition sites can only bind nystose, with a K_D value of 0.65×10^{-3} M. A possible explanation is that the binding takes place via the OH in position 3 and 6, which are in a sin–periplanar relationship [408]. Similar to that of stachyose, nystose demonstrates selectivity of the target oligosaccharide when compared to non–target saccharides.

Nystose–binding scaffolds was in the range of ~0.2 ng/mm^2 where 100 response units (RUs) = 0.1 ng.mm^2. Similar to that calculated of stachyose template MIP, a conclusion of an assumption a footprint of approximately 2–3 nm^2 for a tetrasaccharide [405], an estimated 50% surface coverage by oligosaccharide can be achieved. The remaining surface area comprises crosslinked MBA, which defines the pocket shape and size of the oligosaccharide used as template, enhancing to some extent its binding affinity was made.

The superselectivity of our system could find some analogy in a mechanism previously proposed [27], where the binding energy is not a linear function of the number of bonds but grows more rapidly. In fact, we were able to distinguish between a ligand that can form three bonds (raffinose) and one that can form four (stachyose), with an all–or–nothing behaviour. However, we believe that the superselectivity of our system also accounts for an additional contribution, which could be related to geometrical factors. A fine control of the shape complementarity of the binding site could explain why we can also discriminate between oligosaccharides with the same number of ligands (stachyose and nystose). Another point to consider is that benzoboroxoles have different binding affinities for different carbohydrates (Gal, Glu, and Fru), therefore each sugar unit of the oligosaccharides interacts with the receptors in a different way. To further demonstrate the capability of the novel binding scaffolds to bind specifically their glycoconjugates, Man_5 is to be explored and used.

4.10 RNase B template MIP

RNase B contains a single glycosylation site of high–mannose type with 5–9 mannose residues, Man5–Man9 [409]. The structure of the Man5 glycoform of RNase B is shown below.

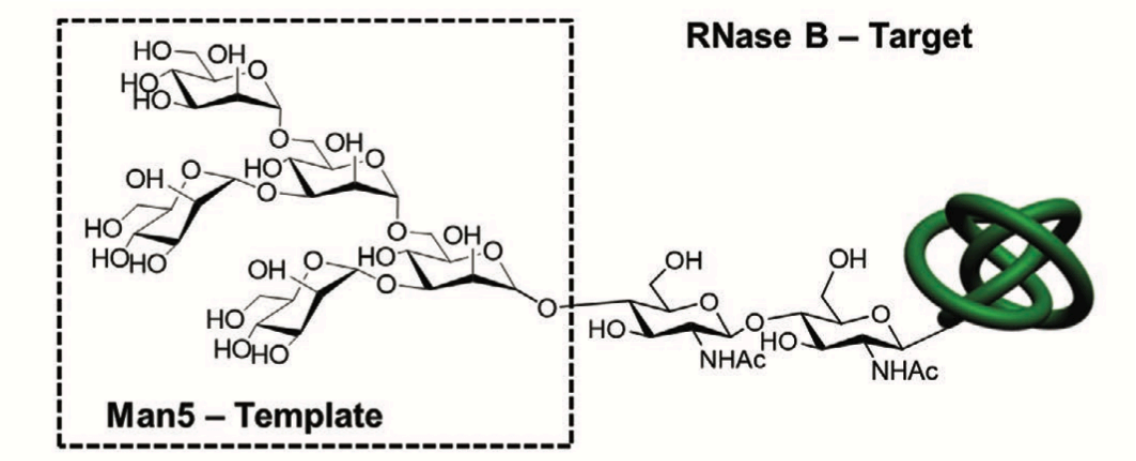

Figure 73: The oligosaccharide structure of the Man5 glycoform of RNase B, of which Man5 was used as a template for the generation of the binding scaffolds. The Man6–Man9 RNase B glycoforms contain further mannose units, which are added to the outer three mannose residues in Man5.

The other glycoproteins used for comparison were RNase A, α1–acid glycoprotein (AGP) and horseradish peroxidase (HRP). The non–glycosylated RNase form is RNase A and is composed of three α helices and seven β strands arranged in two "lobes". RNase A is thought to be divided into two halves: an N–terminal, predominantly α–helical half (residues 1–60) and a C–terminal, predominantly β–sheet half (residues 65–124) [410]. AGP and HRP are two highly glycosylated glycoproteins. AGP is a 41–43–kDa glycoprotein and the peptide moiety is a single chain of 183

amino acids (human) with two disulfide bridges [411]. AGP (45% glycosylation) possesses complex–type glycans that are strongly sialylated [412] and is one of the major acute phase proteins in humans, rats, mice, along with other species [413]. Whereas, HRP is an enzyme that catalyzes the oxidation of diaminobenzidine, and is 21% glycosylation and consists predominantly of the oligosaccharide (Xyl)Man3(Fuc)GlcNAc2, containing only low levels of the high mannose–type glycan [414, 415].

Using SPR, the selectivity of the complex is compared to the four glycoproteins described previously. The response is subtracted from the control benzyl–terminated SAM and is shown below for different concentrations of RNase B, RNase A, AGP and HRP. The concentrations were 0.1 – 10 mM at pH 7.4.

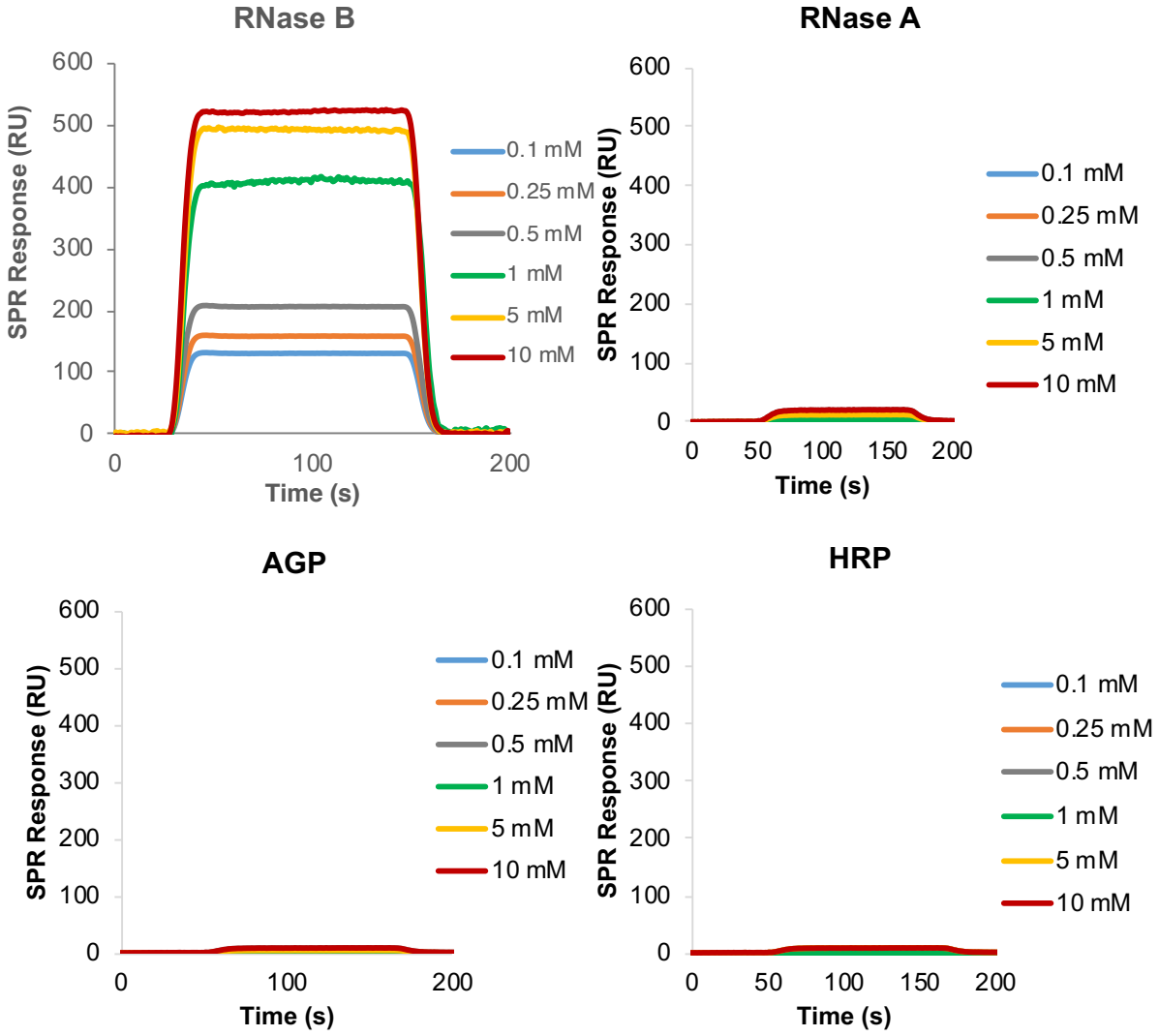

Figure 74: SPR sensorgram traces performed with Man5–imprinted surfaces on the SPR chip and different concentrations of RNase B, RNase A, AGP and HRP flowed over the surface.

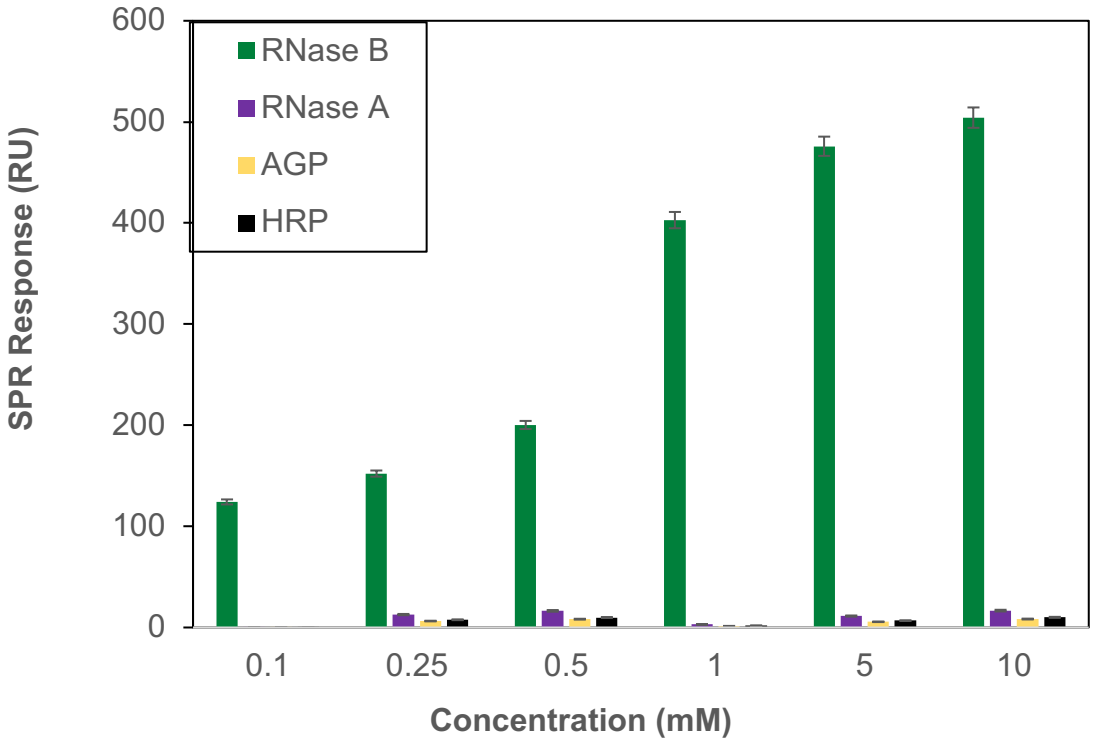

Figure 75: SPR responses at equilibrium against the concentration of injected protein, RNase B, RNase A, AGP, and HRP using Man5–binding scaffolds, from which K_D and R_{max} values have been obtained.

Table 17: The K_D and Rmax values calculated from the hyperbolic trendline.

Rmax (RU)	K_D (mM)	R^2 value
537 ± 4	0.55 ± 0.01	0.98

It was clear that the subtracted response had shown selectivity of the RNase B glycoprotein and very negligible binding of that for the other three glycoproteins. The hyperbolic trendline analysis of the points made with different concentrations of RNase B. With this in mind, analysis to determine the K_D and R_{max} values was conducted. The

K_D value was also in the millimolar range, similar to that of previous SPR studies. The Rmax demonstrated increased affinity of RNase B when compared with other oligosaccharides used. When compared with the previous template MIP, RNase B revealed to have very similar affinity of the target molecule than that of stachyose MIP with stachyose or nystose template MIP when binding nystose. The power of the methodology further demonstrated the capability of the novel binding scaffolds to bind specifically their glycoconjugates. It also confirmed the superselectivity of RNase B when compared to the other three glycoproteins used to compare the SPR response.

4.11 Overall conclusion of complexation and molecular imprinting

In conclusion, a unique modular strategy, which harnesses supramolecular assembly and well–controlled chemistry, was developed to create robust and highly reproducible template–induced oligosaccharide recognition sites on synthetic scaffolds. Our findings show that our approach has a remarkable ability to deliver synthetic receptors capable of highly specifically targeting oligosaccharides whether they occur in free form or as components of glycoproteins. These results go beyond the scope of the oligosaccharides described here, with the modularity of the synthetic strategy lending itself to adaptivity and incorporation into technologies for diagnostics, biotechnology, and glycobiology research.

CHAPTER 5 – OVERALL CONCLUSIONS AND FUTURE WORK

Abstract: *This chapter discusses the overall conclusions made from the work conducted throughout this project, mentioning any insights that were made accompanying the individual studies. Further work is stated that is needed for project to continue and successfully progress.*

5.1 Conclusions

In this thesis we proposed a modular synthetic approach that will harness both the construction of high–yield, complex oligosaccharide–synthetic carbohydrate receptor assemblies and the precise generation of surface–confined templated binding sites. This approach was successful as the complex was selective in the detection of the oligosaccharides in question.

Initially, the first stage was to successfully produce a SAM that will be used throughout the receptor production. This is documented in chapter three, systematically describing the solvent(s) used for the incubation and the time in which the incubation was used.

From the characterisation methods, namely ellipsometry, contact angle and XPS, it was clear that 2% TFA had a positive impact in the formation of the DSA SAM on a clean gold surface. XPS demonstrated that the S–Au bond was indeed present and bound to the surface as well as successful ratios confirming the presence of the DSA SAM.

Successful cross–linking of DSA and AABOB conditions were shown with XPS. The cross–linking was shown to be difficult as boron was unable to be detected in the XPS. As a sensitive element, boron has many challenges [416], and numerous conditions were chosen to attempt cross–linking AABOB onto the DSA surface. Oxygen is shown to negatively affect the cross–linking of benzoboroxole along with other diol–containing polymers [417], so conducting the cross–linking with oxygen–free conditions was the

way forward. In addition to the DSA SAM, controls SAMs were characterised and optimised to successfully show the presence of the SAM on a clean gold surface as well as showing bound S–Au bond.

The second results chapter demonstrates the formation of the complex before later describing the selectivity that is shown. The complexation is composed of the saccharides stachyose and nystose. The SPR studies conclude selectivity of the target saccharide that bind to the imprinted surface and the non–target saccharides do not bind selectively to the imprinted surface. The non–target saccharides include melezitose and raffinose, both 3–sugar unit saccharides. The use of a smaller saccharide was to determine whether or not the pocket formed on the surface is able to bind only target molecules.

In addition to nystose and stachyose complexes, a glycoprotein is also used to successfully demonstrate the selectivity shown in this project. Man5 is a large glycoprotein [418] and small saccharides were used to see whether successful and selective binding could be shown with SPR studies. The SPR studies had shown that the imprinted surface was only selective for the target (Man5) when compared with other glycoproteins.

Dissociation constants (k_D) were in the millimolar range (mM), suggesting that they were not as sensitive as reported [200]. To continue with the project, further studies must be conducted with other glycoproteins, demonstrating selectivity as well as

sensitivity for target molecules. To improve the affinity (dissociation constant) of the complexation in this thesis, further studies will need to be thoroughly studied. If we could demonstrate specificity and selectivity for one particular glycoform over another through the elegant arrangement of the boronic acid moieties within the MIP cavities we could then use this system to imprint clinically relevant glycoproteins such as PSA.

5.2 Future work

As selective recognition is arising from the expression of motifs, the use of SAMs can be further explored with surface roughness analysis. Surface roughness can be measured by using several different methods and different sampling areas and atomic force microscopy (AFM) is often used for surface roughness studies [419]. Conducting AFM on both bare gold as well as SAMs will enable us to obtain a quantitative conclusion whether the roughness of surfaces varies dependent on the cleaning of the surface. There are several parameters which are able to be used to describe the surface morphology. This is in terms of roughness parameters, amplitude or height parameters, functional or statistical parameters and spatial parameters [420]. In addition to surface roughness, other analytical tools which are well-suited for the analysis of individual particles can be used to help demonstrate what and how is bound to the surface. Transmission Electron Microscopy (TEM) and Scanning Electron Microscopy (SEM) but are conventional methods for direct imaging of particles providing size, shape, and morphological information [421].

A substantial amount of research exists on both SAMs and molecular imprinting but biosensing technology is still required to develop and successfully produce a clinically approved assay. Remaining dominated by ELISA assays, biomedical laboratories have already deciphered selective binding of biological ligands. There is an element of fragility to their design which extends to both liable disposition of antibodies to their environment i.e. pH, temperature, solvation etc., but also to some ligand binding affinities as observed for anti–glycan antibodies. Unfortunately, the complexity of glycan structures and glycosylation pathways complicates detection and quantification of potential glycan biomarkers. Approaches of glycoprofiling have been successful in isolation (i.e. through electrophoresis or chromatography) and in analysis through mass spectroscopy and lectin arrays [422]. Regardless of the current advances, the clinical utility of glycan biomarkers is still lacking. This is due to the clinical impracticality of the glycoprofiling techniques. As such, it is essential that new simple and reproducible glycan detecting technologies are developed to make use of this new wealth of information. The glycoprofile is recognised as an important diagnostic tool which overcomes factors such as weak affinity and low selectivity in carbohydrate ligands. With the principle of adaptability and biocompatibility in mind, we report here a method for producing selective oligosaccharide recognition on a SAM through extensive use of the benzoboroxole cross–linking reaction. This is achieved at a physiological pH, ideal for clinical assays. Although not sensitive as the K_D values obtained were not in a nanorange, the complexes shown are super–selective to the target oligosaccharide, with K_D values in the low millimolar range. Exchanging the oligosaccharide template for PSA, the MIP

described in this thesis could readily be applied to glycoprotein detection with further optimisation.

The current problem of PCa diagnosis needs to be addressed as current screening has a cut–off value of >4 ng/mL. PSA presents low clinical specificity and sensitivity. However, the detection of PSA glycoforms represents a true marker of cellular malignancy thus potentially offers significantly higher clinical specificity and sensitivity [423]. This thesis only demonstrated Man_5 with selectivity of RNase B, so further work would need to be achieved. Higher affinity of the MIP could further be induced with the inclusion of additional functional moieties i.e. carboxy, sulfonate or amine groups allowing interaction with exposed amino acid residues on the glycoprotein [424].

In addition to the explored MIPs, different glycan biomarkers can be studied and used. Whilst a small number of clinically relevant assays exist (i.e. CA125 ELISA for ovarian cancer or aPTT for monitoring heparin therapy), demand is currently outstripping supply with the myriad of new glycan disease markers now available [425-427]. As well as cancers, glycan biomarkers are novel in the diagnosis of cardiovascular diseases. GlycA, a biomarker of protein glycan N-acetyl groups, is related to incident cardiovascular disease (CVD) [428]. Apart from CVD, glycan biomarkers are able to identify neurodegenerative disease. Neurodegenerative disease is the umbrella term for a range of conditions which are characterized by the progressive loss of structure or function of neurons in the human brain leading to the cognitive and physical

impairments, including the death of neurons [429]. The expression of the P-glycoprotein has also been investigated inr the diagnosis of Alzheimer's Disease [430].

While we have demonstrated selective oligosaccharide detection in solution, quantification of specific glycoprotein glycan moieties in complex biological media would require pre-isolation of glycan biomarkers to prevent binding of structurally similar saccharides. Therefore, significantly increased sensitivity in SPR would be expected on the other glycans discussed throughout the thesis, arising from larger perturbation to surface plasmon than with smaller biomolecule binding. This therefore provides additional signal amplification to only small concentrations of detected PCa glycans further enhancing this assay design

CHAPTER 6 – MATERIALS AND METHODS

Abstract: *The materials used throughout the project as well as the methods used explained. This section was obtained from "Tommasone, S., Tagger, Y. K., Mendes, P. M., Targeting Oligosaccharides and Glycoconjugates Using Superselective Binding Scaffolds. Adv. Funct. Mater. 2020, 30, 2002298".*

6.1 Materials

Commercially available solvents were purchased from Sigma–Aldrich and used without further purification. All the chemicals were purchased from Sigma–Aldrich with the exception of Verbascose, purchased from Carbosynth Limited and 5–amino–2–(hydroxymethyl)phenylboronic acid cyclic monoester, purchased from Tokyo Chemical Industry UK Ltd. RNase B from bovine pancreas, RNase A from bovine pancreas, α1–acid glycoprotein from bovine plasma and HRP from horse radish root were all purchased from Sigma Aldrich. Polycrystalline gold substrates were purchased from George Albert PVD, Germany. The gold substrates consist of a 100 nm gold layer deposited onto glass, which are covered with a 5 nm layer of chromium as an adhesion layer. These gold substrates were used for ellipsometry, XPS and contact angle analysis. The polycrystalline gold substrates which were employed in SPR experiments were purchased from Reichert Technologies, USA. The gold substrates consist of 49 nm gold with 1 nm chromium.

6.2 Synthetic procedures

The synthetic procedures documented below were kindly provided by Dr Stefano Tommasone for the experiments conducted.

6.2.1 Synthesis of 5–acrylamido–2–(hydroxymethyl) phenylboronic acid cyclic monoester (APB) [431]

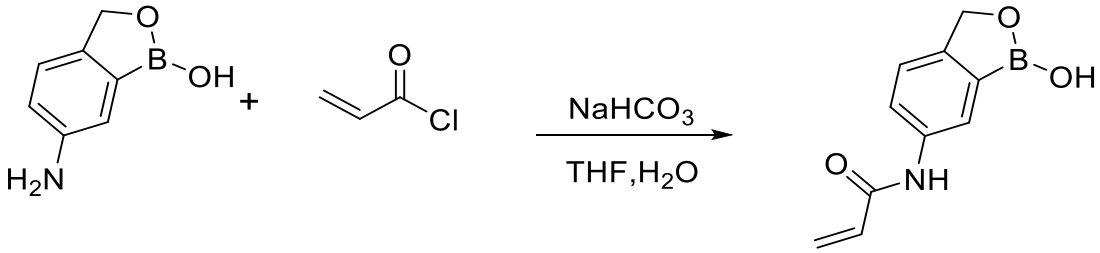

5–Amino–2–(hydroxymethyl)phenylboronic acid cyclic monoester (0.50 g, 3.35 mmol) was dissolved in a mixture of THF:H_2O (1:1, 11.6 ml). The solution was cooled with an ice–bath and sodium carbonate (1.12 g, 13.40 mmol) and acryloyl chloride (0.54 ml, 6.71 mmol) were then added. The reaction mixture was stirred at room temperature for 5 h. The solvent was removed under reduced pressure and the product was recovered by crystallization from water:methanol (0.30 g, y = 44%). The NMR analysis was in agreement with the literature.[431] ^{1}H NMR (400 MHz, 298K, DMSO–d6): δ 4.93 (s, 2H), 5.75 (dd, J_1 = 10.0 Hz, J_2 = 2.0 Hz, 1H), 6.26 (dd, J_1 = 16.8 Hz, J_2 = 2.0 Hz, 1H), 6.46 (dd, J_1 = 16.8 Hz, J_2 = 10.0 Hz, 1H), 7.35 (bd, J_1 = 8.0 Hz, J_2 = 0.4 Hz, 1H) 7.69 (dd, J_1 = 8.4 Hz, J_2 = 2 Hz, 1H), 8.06 (s,1H), 9.22 (s,1H), 10.19 (s,1H).

6.2.2 Synthesis of control SAM molecule (5) – 3,3'–disulfanediylbis (N–phenylpropanamide) [432]

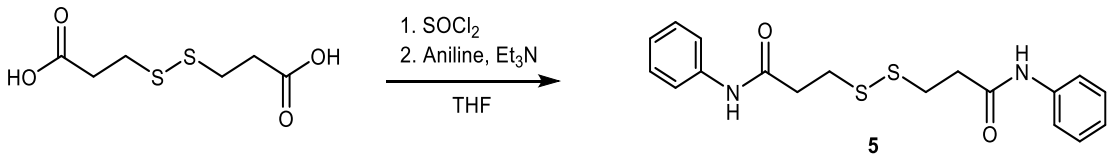

A solution of 3,3'–dithiopropionic acid (500 mg, 2.38 mmol) in THF (5 ml) was cooled in an ice bath and $SOCl_2$ (0.67 ml, 9.27 mmol) was added dropwise. The reaction mixture was stirred overnight at room temperature. After cooling the solution with an ice bath, aniline (0.84 ml, 9.27 mmol) and Et_3N (1.29 ml, 9.27 mmol) were slowly added. The reaction mixture was allowed to warm at room temperature and stirred for 4 h. Water was added to quench the reaction and the product was extracted with CH_2Cl_2. The organic phase was washed with water, dried over $MgSO_4$ and concentrated. The product was purified by column chromatography with silica gel (CH_2Cl_2:MeOH, 98:2) (73 mg, yield = 8%). ^{1}H NMR (400 MHz, 298K, DMSO–d_6) δ: 2.74 (t, J = 6.8 Hz, 4H), 3.01 (t, J = 7.2 Hz, 4H), 7.03 (t, J = 7.2 Hz, 2H), 7.30 (t, J = 7.6 Hz, 4H), 7.58 (d, J = 7.6 Hz, 4H), 10.02 (s, 2H); ^{13}C NMR (101 MHz, 298K, DMSO–d_6) δ: 33.5, 36.0, 119.1, 123.1, 128.7, 139.1, 169.1.

6.2.3 Synthesis of benzoboroxole terminated SAM molecule (6) – 3,3'–disulfanediylbis(N–(1–hydroxy–1,3–dihydrobenzo [c][1,2] oxaborol–6–yl) propanamide)

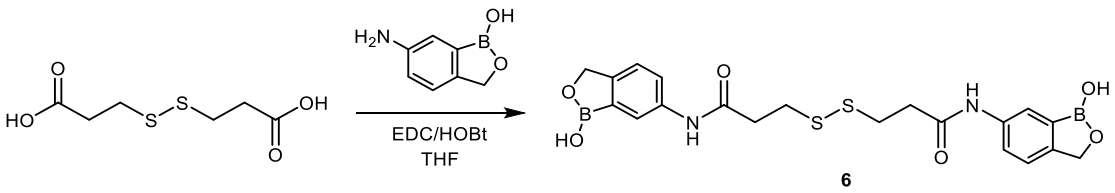

6

3,3'–dithiopropionic acid (58 mg, 0.28 mmol) was dissolved in THF (2.8 ml). EDC (128 mg, 0.67 mmol) and HOBt (90 mg, 0.67 mmol) were added and the reaction mixture was stirred at room temperature for 30 min. Afterwards, 5–amino–2–(hydroxymethyl)phenylboronic acid cyclic monoester (100 mg, 0.67 mmol) was added and the reaction mixture was stirred overnight. The solvent was then removed under reduced pressure and water (10 ml) was added, affording a precipitate that was filtered and dried. The crude was suspended in CH_2Cl_2 and the precipitated was filtered and dried. Finally, the product was suspended in methanol and the white solid obtained was filtered and dried, affording the pure product (55 mg, yield = 42%). ^{1}H NMR (400 MHz, 298K, DMSO–d_6) δ: 2.76 (t, J = 6.4 Hz, 4H), 3.03 (t, J = 6.4 Hz, 4H), 4.92 (s, 4H), 7.31 (d, J = 8 Hz, 2H), 7.61 (d, J = 7.6 Hz, 2H), 7.99 (s, 2H), 9.22 (s, 2H), 10.06 (s, 2H); ^{13}C NMR (101 MHz, 298K, DMSO–d_6) δ: 33.6, 36.0, 69.7, 121.0, 121.5, 122.3, 137.9, 148.6, 169.0. ESI(+) MS m/z 495.10 $[M–Na]^+$. HRMS (ESI) m/z $[M–Na]^+$ calcd for $C_{20}H_{22}B_2N_2O_6S_2Na$ 495.1010, found 495.1009.

6.3 Complex formation and indirect approach to access degree of complexation

The oligosaccharide (20.0 mg, 0.030 mmol for stachyose and nystose, 0.024 mmol for verbascose) and 2–(hydroxymethyl)phenylboronic acid cyclic monoester (8.0 eq/sugar unit, 128 mg, 0.96 mmol) were suspended in a mixture of dioxane (2.4 ml) and acetonitrile (0.4 ml). For practical purposes, the commercially available 2–(hydroxymethyl)phenylboronic acid cyclic monoester rather than the synthetic derivative 5–acryalmido–2–(hydroxymethyl)phenylboronic acid cyclic monoester was used. This allowed us to scale up the process and work with a more tangible amount of sugar. The reaction mixture was stirred at 90 ºC for 24 h under argon atmosphere in presence of activated molecular sieves 3Å. The solvent was removed under reduced pressure and the crude was dissolved in pyridine (0.5 ml). Benzoyl chloride (50 μl, 0.41 mmol) was added at 0 ºC and the reaction mixture was stirred at room temperature for 5 h. The reaction mixture was diluted in toluene and filtered through celite. The solvent was removed under reduced pressure and the crude was dissolved in a mixture of EtOAc (5 ml) and a solution of 1 M sorbitol/Na_2CO_3 (5 ml) and stirred for 1 h. The two phases were then separated and the aqueous layer was washed three times with EtOAc. The organic phases were combined, dried over $MgSO_4$ and concentrated under reduced pressure. The crude was then purified by column chromatography on silica gel (DCM:MeOH 99:1 – 90:10). The fractions collected were analysed by MALDI–MS.

6.4 Methods

6.4.1 SAM Preparation

The gold substrates were cleaned by immersion in piranha solution (70% H_2SO_4, 30% H_2O_2) at room temperature for 7 minutes, rinsed with Ultra High Quality (UHQ) water and then HPLC grade ethanol thoroughly for 1 min. (Caution: Piranha solution reacts violently with all organic compounds and should be handled with care). Immediately after rinsing, the substrates were immersed for 24 h in ethanolic 0.1 mM solutions of N,N'–bis(acryloyl) cystamine containing 2% trifluoroacetic acid (TFA). The substrates were rinsed with HPLC EtOH and dried under a stream of Ar. The control benzyl–terminated SAMs were prepared in a similar way, by immersing the clean gold substrates in 0.1 mM ethanolic solutions for 24 h whilst the benzoboroxole control SAM was incubated in 0.1 mM methanolic solutions, followed by rinsing and then drying in a stream of Ar.

6.4.2 Contact Angle

Contact angle measurements were conducted on an Attension Theta contact angle meter from Biolin Scientific. The dynamic contact angles were recorded as an automated micro–syringe was used to add liquid onto the functionalized gold surface (advancing) or remove liquid from the drop deposited on the gold surface (receding). A video camera recorded images at an acquisition rate of 32 frames per second that were subsequently analysed using the OneAttension software to obtain the contact

angles of the drops at the three–phase intersection. Averages and standard deviations were determined from six measurements for each type of SAM.

6.4.3 Ellipsometry

The thickness of the deposited monolayers was determined by spectroscopic ellipsometry using an Alpha–SE ellipsometer from J.A. Woollam. The ellipsometric data acquired at angles of incidence of 65°, 70° and 75° was processed using the CompleteEASE software. The thickness calculations were based on a three–phase ambient/SAM/Au model, in which the SAM was assumed to be isotropic and assigned a refractive index of 1.50. The thickness reported is the average of six measurements taken on each SAM, with the errors reported as standard deviation.

6.4.4 X–ray photoelectron spectroscopy (XPS)

XPS experiments were carried out using a Thermo Scientific K–Alpha XPS system and a monochromatic Al Kα X–ray source (1486.7 eV) at a take–off angle of 90° to the surface plane. High–resolution scans of C (1s), O (1s), N (1s) and S (2p) were recorded using a pass energy of 40 eV at a step size of 0.1 eV. Fitting of XPS peaks was performed using CasaXPS processing software. Sensitivity factors used in this study were: C (1s) 1.00; O (1s) 2.93; N (1s), 1.80; S (2p), 1.68. The S doublet was constrained to have a peak separation of 1.18 eV, a 2:1 area ratio ($2p_{3/2}$: $2p_{1/2}$) and equal FWHM.

6.5 Formation of binding scaffold and surface plasmon resonance studies

6.5.1 Complex formation

In a 25 ml round bottom glass flask, stachyose or nystose (6.67 mg, 10.01 μmol) and 5–acrylamido–2–(hydroxymethyl)phenylboronic acid cyclic monoester (65.0 mg, 320 μmol, 8.0 eq/sugar unit) were suspended in a mixture of dioxane (2 ml) and acetonitrile (0.34 ml). Man5 (8.29 mg, 10.01 μmo l) and 5–acrylamido–2–(hydroxymethyl)phenylboronic acid cyclic monoester (81.2 mg, 400 μmol, 8.0 eq/sugar unit) were suspended in a mixture of dioxane (2.49 ml) and acetonitrile (0.41 ml). The reaction mixture was stirred at 90 °C for 24 h under argon atmosphere in presence of activated molecular sieves 3Å. The solvent was removed under reduced pressure and the crude was treated with acetonitrile (0.6 ml) in order to afford a white precipitate. The suspension was transferred in a 1 ml Eppendorf and centrifuged. The supernatant was collected and the precipitate was re–suspended in acetonitrile (0.6 ml) for a second centrifugation. Subsequently, the supernatant was removed, the precipitate was dried and dissolved in a 1.6 ml solution of phosphate buffer (pH 7.4).

6.5.2 Formation of binding scaffold

The gold substrates functionalized with N',N'–bis(acryloyl)cystamine SAMs were added to individual polymerisation solutions containing 800 μL of the complex prepared as described in section 6.1, 100 μL of ammonium persulfate (40 mg/mL) and 100 μL of a 5 M N,N′–methylenebis(acrylamide) solution. 1 μL of

tetramethylethylenediamine (TEMED) was subsequently added to initiate the polymerization under argon. After 15 min, the modified gold surfaces were removed from the solution, rinsed with UHQ water, ammonium acetate (pH 6), ethanol and dried under a stream of argon. Bisacrylamide only studies were conducted with 800 μL of a 0.1 M phosphate buffer saline solution, 100 μL ammonium per sulphate (40 mg/mL) and 100 μL of a 5 M N,N′–methylenebis(acrylamide) before adding 1 μL TEMED for 15 minutes.

6.6 Surface Plasmon Resonance (SPR)

The SPR experiments were performed on a Reichert SR7000DC Dual Channel Spectrometer (NY, USA) at 25°C. A baseline was established for each surface by running degassed 0.1 M ammonium acetate at pH 10 over the sample at 25 μl/min until baseline stabilization was achieved. SPR sensorgrams were acquired by injecting solutions of either an oligosaccharide or protein diluted in the running buffer (i.e. 1 M ammonium acetate at pH 10) for 2 min at a flow rate of 25 μl/min, following by 5 min dissociation in the running buffer and 5 min regeneration using 1 M ammonium acetate at pH 6. For each concentration, 2 measurements from 2 individual chips were taken (n=4) from which the average and standard deviation values were then calculated.

Data sets were analysed using Scrubber 2 (BioLogic Software, Campbell, Australia). In order to correct for bulk refractive index contributions arising from the oligosaccharides and proteins, SPR responses from the control 3,3'–disulfanediylbis(N–phenylpropanamide) (5) SAM were subtracted from those obtained

from the surfaces containing the oligosaccharide–binding sites. The corrected SPR responses at equilibrium (Req) were plotted against the concentration of the injected oligosaccharide or protein (C_p) and fitted to a 1:1 steady–state model using Scrubber 2. The model uses a non–linear least–squares regression method to fit data to the Langmuir adsorption isotherm, with K_D being the dissociation constant and R_{max} the maximum analyte binding capacity of the surface.

e.

CHAPTER 7 – REFERENCES

1. Arens, U., *Authorised EU health claim for carbohydrates and maintenance of normal brain function*, in *Foods, Nutrients and Food Ingredients with Authorised EU Health Claims*. 2018. p. 229-236.
2. Fairclough, S.H. and K. Houston, *A metabolic measure of mental effort.* Biol Psychol, 2004. **66**(2): p. 177-90.
3. Niaz, K., F. Khan, and M.A. Shah, *Analysis of carbohydrates (monosaccharides, polysaccharides)*, in *Recent Advances in Natural Products Analysis*. 2020. p. 621-633.
4. Alonso, J.L., et al., *The conformational behaviour of freed-glucose—at last.* Chem. Sci., 2014. **5**(2): p. 515-522.
5. Dilworth, L.L., C.K. Riley, and D.K. Stennett, *Plant Constituents*, in *Pharmacognosy*. 2017. p. 61-80.
6. Aparicio, S., *A systematic computational study on flavonoids.* International journal of molecular sciences, 2010. **11**(5): p. 2017-2038.
7. Amchra, F., et al., *Effect of Stevia rebaudiana, sucrose and aspartame on human health: A comprehensive review.* Journal of Medicinal Plants Studies, 2018. **102**: p. 102-108.
8. Berg, J.M., J.L. Tymoczko, and L. Stryer, *Biochemistry, Fifth Edition*. 2002: W.H. Freeman.
9. Weishaupt, M., S. Eller, and P.H. Seeberger, *Chapter Twenty-Two - Solid Phase Synthesis of Oligosaccharides*, in *Methods in Enzymology*, M. Fukuda, Editor. 2010, Academic Press. p. 463-484.

10. P.M, V., *STARCH-BASED BIONANOCOMPOSITES: PROCESSING AND PROPERTIES Polysaccharide Building Blocks: A Sustainable Approach to the Development of Renewable Biomaterials, First Edition. Edited By*. 2014.

11. Springer, S.A. and P. Gagneux, *Glycomics: revealing the dynamic ecology and evolution of sugar molecules.* Journal of proteomics, 2016. **135**: p. 90-100.

12. Zhang, L., S. Luo, and B. Zhang, *Glycan analysis of therapeutic glycoproteins.* mAbs, 2015. **8**.

13. Rini, J., J. Esko, and A. Varki, *Glycosyltransferases and Glycan-processing Enzymes*, in *Essentials of Glycobiology*, A. Varki, et al., Editors. 2009, Cold Spring Harbor Laboratory Press

14. Cole, L. and P.R. Kramer, *Chapter 5.1 - Macronutrients*, in *Human Physiology, Biochemistry and Basic Medicine*, L. Cole and P.R. Kramer, Editors. 2016, Academic Press: Boston. p. 157-164.

15. Muthana, S.M., C.T. Campbell, and J.C. Gildersleeve, *Modifications of glycans: biological significance and therapeutic opportunities.* ACS chemical biology, 2012. **7**(1): p. 31-43.

16. Reily, C., et al., *Glycosylation in health and disease.* Nature reviews. Nephrology, 2019. **15**(6): p. 346-366.

17. Batra, J. and A. Rathore, *Glycosylation of Monoclonal Antibody Products: Current Status and Future Prospects.* Biotechnology progress, 2016. **32**.

18. Lanctot, P.M., F.H. Gage, and A.P. Varki, *The glycans of stem cells.* Curr Opin Chem Biol, 2007. **11**(4): p. 373-80.

19. Hudak, Jason E. and Carolyn R. Bertozzi, *Glycotherapy: New Advances Inspire a Reemergence of Glycans in Medicine.* Chemistry & Biology, 2014. **21**(1): p. 16-37.

20. Vasconcelos-Dos-Santos, A., et al., *Biosynthetic Machinery Involved in Aberrant Glycosylation: Promising Targets for Developing of Drugs Against Cancer.* Front Oncol, 2015. **5**: p. 138.

21. Westhoff, C.M. and B.H. Shaz, *Lewis, I, P1PK and GLOB Blood Group Systems*, in *Transfusion Medicine and Hemostasis*. 2013. p. 171-176.

22. Westhoff, C.M., J.R. Storry, and B.H. Shaz, *Chapter 110 - Human Blood Group Antigens and Antibodies*, in *Hematology (Seventh Edition)*, R. Hoffman, et al., Editors. 2018, Elsevier. p. 1687-1701.

23. Shaz, B.H., *Chapter 26 - Lewis, I and P Blood Group Systems*, in *Transfusion Medicine and Hemostasis*, C.D. Hillyer, et al., Editors. 2009, Academic Press: San Diego. p. 139-144.

24. Shan, M., et al., *Chapter Four - Fucosylation in cancer biology and its clinical applications*, in *Progress in Molecular Biology and Translational Science*, L. Zhang, Editor. 2019, Academic Press. p. 93-119.

25. J, B., *The Role of Glycosylation in Receptor Signaling*, in *Glycosylation*. 2012.

26. J, B., *The Role of Glycosylation in Receptor Signaling*. 2012, InTech.

27. Solá, R.J. and K. Griebenow, *Glycosylation of therapeutic proteins: an effective strategy to optimize efficacy.* BioDrugs : clinical immunotherapeutics, biopharmaceuticals and gene therapy, 2010. **24**(1): p. 9-21.

28. Moremen, K.W., M. Tiemeyer, and A.V. Nairn, *Vertebrate protein glycosylation: diversity, synthesis and function.* Nature reviews. Molecular cell biology, 2012. **13**(7): p. 448-462.

29. Gonzalez, M.W. and M.G. Kann, *Chapter 4: Protein interactions and disease.* PLoS computational biology, 2012. **8**(12): p. e1002819-e1002819.

30. Upreti, R.K., M. Kumar, and V. Shankar, *Bacterial glycoproteins: functions, biosynthesis and applications.* Proteomics, 2003. **3**(4): p. 363-79.

31. Audagnotto, M. and M. Dal Peraro, *Protein post-translational modifications: In silico prediction tools and molecular modeling.* Computational and structural biotechnology journal, 2017. **15**: p. 307-319.

32. Jarrell, K.F., et al., *N-Linked Glycosylation in Archaea: a Structural, Functional, and Genetic Analysis.* Microbiology and Molecular Biology Reviews, 2014. **78**(2): p. 304.

33. Varki, A., *Biological roles of oligosaccharides: all of the theories are correct.* Glycobiology, 1993. **3**(2): p. 97-130.

34. Opdenakker, G., et al., *Concepts and principles of glycobiology.* Faseb j, 1993. **7**(14): p. 1330-7.

35. Sheta, R. and D. Bachvarov, *Role of aberrant glycosylation in ovarian cancer dissemination.* Biomedical reviews, 2014. **25**: p. 83-92.

36. Breitling, J. and M. Aebi, *N-Linked Protein Glycosylation in the Endoplasmic Reticulum.* Cold Spring Harbor perspectives in biology, 2013. **5**.

37. Burda, P. and M. Aebi, *The dolichol pathway of N-linked glycosylation.* Biochimica et Biophysica Acta (BBA) - General Subjects, 1999. **1426**(2): p. 239-257.

38. Gavel, Y. and G.V. Heijne, *Sequence differences between glycosylated and non-glycosylated asn-x-thr/ser acceptor sites: Implications for protein engineering.* Protein Engineering, Design and Selection, 1990. **3**(5): p. 433-442.

39. Kornfeld, R. and S. Kornfeld, *Assembly of asparagine-linked oligosaccharides.* Annual Review of Biochemistry, 1985. **VOL. 54**: p. 631-664.

40. Hirschberg, C.B. and M.D. Snider, *Topography of glycosylation in the rough endoplasmic reticulum and Golgi apparatus.* Annual review of biochemistry, 1987. **56**: p. 63-87.

41. Verbert, A., R. Cacan, and R. Cecchelli, *Membrane transport of sugar donors to the glycosylation sites.* Biochimie, 1987. **69**(2): p. 91-99.

42. Trimble, R.B. and M.F. Verostek, *Glycoprotein oligosaccharide synthesis and processing in yeast.* Trends Glycosci. Glycotechnol., 1995. **7**(33): p. 1-30.

43. Herscovics, A. and P. Orlean, *Glycoprotein biosynthesis in yeast.* FASEB Journal, 1993. **7**(6): p. 540-550.

44. Abeijon, C. and C.B. Hirschberg, *Topography of glycosylation reactions in the endoplasmic reticulum.* Trends in Biochemical Sciences, 1992. **17**(1): p. 32-36.

45. Lubas, W.A., et al., *O-Linked GlcNAc transferase is a conserved nucleocytoplasmic protein containing tetratricopeptide repeats.* J Biol Chem, 1997. **272**(14): p. 9316-24.

46. Hart, G.W., et al., *O-GlcNAcylation of key nuclear and cytoskeletal proteins: reciprocity with O-phosphorylation and putative roles in protein multimerization.* Glycobiology, 1996. **6**(7): p. 711-6.

47. Belanger, A., et al., *Molecular mass and carbohydrate structure of prostate specific antigen: studies for establishment of an international PSA standard.* Prostate, 1995. **27**(4): p. 187-97.

48. Furmanek, A. and J. Hofsteenge, *Protein C-mannosylation: facts and questions.* Acta Biochim Pol, 2000. **47**(3): p. 781-9.

49. Kegley, N.R., et al., *Identifying C-Mannosylated Proteins in RAW264.7 Cells.* The FASEB Journal, 2019. **33**(1_supplement): p. 798.8-798.8.

50. Kong, L., W. Smith, and D. Hao, *Overview of RAW264.7 for osteoclastogensis study: Phenotype and stimuli.* Journal of cellular and molecular medicine, 2019. **23**(5): p. 3077-3087.

51. Uddin, M.S. and G. Ashraf, *Quality Control of Cellular Protein in Neurodegenerative Disorders*. 2020.

52. Muñiz, M. and H. Riezman, *Trafficking of glycosylphosphatidylinositol anchored proteins from the endoplasmic reticulum to the cell surface.* Journal of lipid research, 2016. **57**(3): p. 352-360.

53. Menon, A.K., et al., *Phosphatidylethanolamine is the donor of the terminal phosphoethanolamine group in trypanosome glycosylphosphatidylinositols.* The EMBO journal, 1993. **12**(5): p. 1907-1914.

54. Galian, C., et al., *Efficient glycosylphosphatidylinositol (GPI) modification of membrane proteins requires a C-terminal anchoring signal of marginal hydrophobicity.* The Journal of biological chemistry, 2012. **287**(20): p. 16399-16409.

55. Barz, W.P. and P. Walter, *Two Endoplasmic Reticulum (ER) Membrane Proteins That Facilitate ER-to-Golgi Transport of Glycosylphosphatidylinositol-anchored Proteins.* Molecular Biology of the Cell, 1999. **10**(4): p. 1043-1059.

56. Spiro, R.G., *Protein glycosylation: nature, distribution, enzymatic formation, and disease implications of glycopeptide bonds.* Glycobiology, 2002. **12**(4): p. 43R-56R.

57. Schiller, B., et al., *Complicated N-linked glycans in simple organisms.* Biological chemistry, 2012. **393**(8): p. 661-673.

58. Franke, M., T. Braulke, and S. Storch, *Transport of the GlcNAc-1-phosphotransferase α/β-subunit precursor protein to the Golgi apparatus requires a combinatorial sorting motif.* The Journal of biological chemistry, 2013. **288**(2): p. 1238-1249.

59. Mehta, D.P., et al., *A lysosomal cysteine proteinase from Dictyostelium discoideum contains N-acetylglucosamine-1-phosphate bound to serine but not mannose-6-phosphate on N-linked oligosaccharides.* J Biol Chem, 1996. **271**(18): p. 10897-903.

60. Moss, J., et al., *Characterization of a Novel GDP-mannose:Serine-protein Mannose-1-phosphotransferase from Leishmania mexicana.* The Journal of biological chemistry, 1999. **274**: p. 6678-88.

61. Varki, A., *Biological roles of glycans.* Glycobiology, 2017. **27**(1): p. 3-49.

62. Lowe, J.B. and J.D. Marth, *A Genetic Approach to Mammalian Glycan Function.* Annual Review of Biochemistry, 2003. **72**(1): p. 643-691.

63. Adamczyk, B., T. Tharmalingam, and P.M. Rudd, *Glycans as cancer biomarkers.* Biochimica et Biophysica Acta (BBA) - General Subjects, 2012. **1820**(9): p. 1347-1353.

64. Delves, P.J., *The Role of Glycosylation in Autoimmune Disease.* 1998. **27**(4): p. 239-253.

65. Lyons, J.J., J.D. Milner, and S.D. Rosenzweig, *Glycans Instructing Immunity: The Emerging Role of Altered Glycosylation in Clinical Immunology.* Frontiers in Pediatrics, 2015. **3**: p. 54.

66. Kanninen, K., et al., *Glycosylation changes in Alzheimer's disease as revealed by a proteomic approach.* Neuroscience Letters, 2004. **367**(2): p. 235-240.

67. Ercan-Herbst, E., et al., *A post-translational modification signature defines changes in soluble tau correlating with oligomerization in early stage Alzheimer's disease brain.* Acta Neuropathologica Communications, 2019. **7**(1).

68. Liu, F., et al., *Aberrant glycosylation modulates phosphorylation of tau by protein kinase A and dephosphorylation of tau by protein phosphatase 2A and 5.* Neuroscience, 2002. **115**(3): p. 829-37.

69. De Strooper, B., T. Iwatsubo, and M.S. Wolfe, *Presenilins and γ-secretase: structure, function, and role in Alzheimer disease.* Cold Spring Harbor perspectives in medicine, 2012. **2**(1): p. a006304.

70. Schedin-Weiss, S., B. Winblad, and L.O. Tjernberg, *The role of protein glycosylation in Alzheimer disease.* FEBS Journal, 2014. **281**(1): p. 46-62.

71. Frenkel-Pinter, M., et al., *Interplay between protein glycosylation pathways in Alzheimer's disease.* Science advances, 2017. **3**(9): p. e1601576-e1601576.

72. Stowell, S.R., T. Ju, and R.D. Cummings, *Protein glycosylation in cancer.* Annual review of pathology, 2015. **10**: p. 473-510.

73. Hakomori, S.-i., *Aberrant glycosylation in tumors and tumor-associated carbohydrate antigens*, in *Advances in cancer research*. 1989, Elsevier. p. 257-331.

74. Hakomori, S.-i., *Tumor malignancy defined by aberrant glycosylation and sphingo (glyco) lipid metabolism.* Cancer research, 1996. **56**(23): p. 5309-5318.

75. Cuello, H.A., et al., *Aberrant O-glycosylation modulates aggressiveness in neuroblastoma.* Oncotarget, 2018. **9**(75): p. 34176-34188.

76. Sharma, P., K. Zargar-Shoshtari, and J. Pow-Sang, *Biomarkers for prostate cancer: present challenges and future opportunities.* Future Science OA, 2015. **2**.

77. Rittenhouse, H.G., et al., *Human Kallikrein 2 (hK2) and Prostate-Specific Antigen (PSA): Two Closely Related, but Distinct, Kallikreins in the Prostate.* Critical Reviews in Clinical Laboratory Sciences, 1998. **35**(4): p. 275-368.

78. Madu, C.O. and Y. Lu, *Novel diagnostic biomarkers for prostate cancer.* Journal of Cancer, 2010. **1**: p. 150-177.

79. Ilyin, S.E., S.M. Belkowski, and C.R. Plata-Salamán, *Biomarker discovery and validation: technologies and integrative approaches.* Trends in biotechnology, 2004. **22**(8): p. 411-416.

80. Pannek, J. and A.W. Partin, *The role of PSA and percent free PSA for staging and prognosis prediction in clinically localized prostate cancer.* Semin Urol Oncol, 1998. **16**(3): p. 100-5.

81. Catalona, W.J., et al., *Comparison of Digital Rectal Examination and Serum Prostate Specific Antigen in the Early Detection of Prostate Cancer: Results of a Multicenter Clinical Trial of 6,630 Men.* J Urol, 2017. **197**(2s): p. S200-s207.

82. Hudak, S.J., J. Hernandez, and I.M. Thompson, *Role of 5 alpha-reductase inhibitors in the management of prostate cancer.* Clinical interventions in aging, 2006. **1**(4): p. 425-431.

83. Tajiri, M., C. Ohyama, and Y. Wada, *Oligosaccharide Profiles of the Prostate Specific Antigen in Free and Complexed Forms from the Prostate Cancer Patient Serum and in Seminal Plasma: a Glycopeptide Approach.* Glycobiology, 2007. **18**(1): p. 2-8.

84. Hatakeyama, S., et al., *Recent progress and perspectives on prostate cancer biomarkers.* International Journal of Clinical Oncology, 2017. **22**(2): p. 214-221.

85. Yoneyama, T., et al., *Measurement of aberrant glycosylation of prostate specific antigen can improve specificity in early detection of prostate cancer.*

Biochemical and Biophysical Research Communications, 2014. **448**(4): p. 390-396.

86. Llop, E., et al., *Improvement of Prostate Cancer Diagnosis by Detecting PSA Glycosylation-Specific Changes.* Theranostics, 2016. **6**(8): p. 1190-1204.

87. Ohyama, C., et al., *Carbohydrate structure and differential binding of prostate specific antigen to Maackia amurensis lectin between prostate cancer and benign prostate hypertrophy.* Glycobiology, 2004. **14**(8): p. 671-679.

88. Li, F. and J. Ding, *Sialylation is involved in cell fate decision during development, reprogramming and cancer progression.* Protein & Cell, 2019. **10**(8): p. 550-565.

89. Scott, E. and J. Munkley, *Glycans as Biomarkers in Prostate Cancer.* International journal of molecular sciences, 2019. **20**(6): p. 1389.

90. Zhang, Z., M. Wuhrer, and S. Holst, *Serum sialylation changes in cancer.* Glycoconjugate journal, 2018. **35**(2): p. 139-160.

91. Tabarés, G., et al., *Different glycan structures in prostate-specific antigen from prostate cancer sera in relation to seminal plasma PSA.* Glycobiology, 2005. **16**(2): p. 132-145.

92. Kammeijer, G.S.M., et al., *An In-Depth Glycosylation Assay for Urinary Prostate-Specific Antigen.* Analytical chemistry, 2018. **90**(7): p. 4414-4421.

93. Haga, Y., et al., *Identification of Multisialylated LacdiNAc Structures as Highly Prostate Cancer Specific Glycan Signatures on PSA.* Analytical Chemistry, 2019. **91**(3): p. 2247-2254.

94. Pihíková, D., P. Kasák, and J. Tkac, *Glycoprofiling of cancer biomarkers: Label-free electrochemical lectin-based biosensors.* Open chemistry, 2015. **13**(1): p. 636-655.

95. Hirabayashi, J., et al., *Lectin microarrays: concept, principle and applications.* Chemical Society Reviews, 2013. **42**(10): p. 4443-4458.

96. Mody, R., S.H.a. Joshi, and W. Chaney, *Use of lectins as diagnostic and therapeutic tools for cancer.* Journal of Pharmacological and Toxicological Methods, 1995. **33**(1): p. 1-10.

97. Feng, Y., et al., *Lectin-mediated in situ rolling circle amplification on exosomes for probing cancer-related glycan pattern.* Analytica Chimica Acta, 2018. **1039**: p. 108-115.

98. Teillet, F., et al., *The Two Major Oligomeric Forms of Human Mannan-Binding Lectin: Chemical Characterization, Carbohydrate-Binding Properties, and Interaction with MBL-Associated Serine Proteases.* The Journal of Immunology, 2005. **174**(5): p. 2870.

99. Stowell, S.R., et al., *Galectin-1, -2, and -3 exhibit differential recognition of sialylated glycans and blood group antigens.* J Biol Chem, 2008. **283**(15): p. 10109-23.

100. Bewley, C.A. and S. Otero-Quintero, *The Potent Anti-HIV Protein Cyanovirin-N Contains Two Novel Carbohydrate Binding Sites That Selectively Bind to Man8 D1D3 and Man9 with Nanomolar Affinity: Implications for Binding to the HIV Envelope Protein gp120.* Journal of the American Chemical Society, 2001. **123**(17): p. 3892-3902.

101. Dessen, A., et al., *X-ray Crystal Structure of the Soybean Agglutinin Cross-Linked with a Biantennary Analog of the Blood Group I Carbohydrate Antigen.* Biochemistry, 1995. **34**(15): p. 4933-4942.

102. Weis, W.I. and K. Drickamer, *STRUCTURAL BASIS OF LECTIN-CARBOHYDRATE RECOGNITION.* Annual Review of Biochemistry, 1996. **65**(1): p. 441-473.

103. Teillet, F., et al., *The two major oligomeric forms of human mannan-binding lectin: chemical characterization, carbohydrate-binding properties, and interaction with MBL-associated serine proteases.* J Immunol, 2005. **174**(5): p. 2870-7.

104. Wimmerová, M., et al., *Stacking Interactions between Carbohydrate and Protein Quantified by Combination of Theoretical and Experimental Methods.* PLOS ONE, 2012. **7**(10): p. e46032.

105. Madhusudan Makwana, K. and R. Mahalakshmi, *Implications of aromatic-aromatic interactions: From protein structures to peptide models.* Protein Sci, 2015. **24**(12): p. 1920-33.

106. Wimmerova, M., et al., *Stacking interactions between carbohydrate and protein quantified by combination of theoretical and experimental methods.* PLoS One, 2012. **7**(10): p. e46032.

107. Faller, C.E. and O. Guvench, *Terminal sialic acids on CD44 N-glycans can block hyaluronan binding by forming competing intramolecular contacts with arginine sidechains.* Proteins, 2014. **82**(11): p. 3079-89.

108. Pröpster, J.M., et al., *Structural basis for sulfation-dependent self-glycan recognition by the human immune-inhibitory receptor Siglec-8.* Proceedings of the National Academy of Sciences, 2016. **113**(29): p. E4170.

109. Weis, W.I., et al., *Structure of the calcium-dependent lectin domain from a rat mannose-binding protein determined by MAD phasing.* Science, 1991. **254**(5038): p. 1608.

110. Drickamer, K., *Two distinct classes of carbohydrate-recognition domains in animal lectins.* J Biol Chem, 1988. **263**(20): p. 9557-60.

111. McGreal, E.P., et al., *The carbohydrate-recognition domain of Dectin-2 is a C-type lectin with specificity for high mannose.* Glycobiology, 2006. **16**(5): p. 422-30.

112. Saijo, S., et al., *Dectin-2 recognition of alpha-mannans and induction of Th17 cell differentiation is essential for host defense against Candida albicans.* Immunity, 2010. **32**(5): p. 681-91.

113. Zhang, L., S. Luo, and B. Zhang, *The use of lectin microarray for assessing glycosylation of therapeutic proteins.* MAbs, 2016. **8**(3): p. 524-35.

114. Hu, S. and D.T. Wong, *Lectin microarray.* Proteomics. Clinical applications, 2009. **3**(2): p. 148-154.

115. Syed, P., et al., *Role of lectin microarrays in cancer diagnosis.* PROTEOMICS, 2016. **16**(8): p. 1257-1265.

116. Matsuda, A., et al., *Lectin Microarray-Based Sero-Biomarker Verification Targeting Aberrant O-Linked Glycosylation on Mucin 1.* Anal Chem, 2015. **87**(14): p. 7274-81.

117. Iizuka, D., et al., *Analysis of a lectin microarray identifies altered sialylation of mouse serum glycoproteins induced by whole-body radiation exposure.* J Radiat Res, 2019. **60**(2): p. 189-196.

118. Guo, Y., et al., *Lectin microarray and mass spectrometric analysis of hepatitis C proteins reveals N-linked glycosylation.* Medicine (Baltimore), 2018. **97**(15): p. e0208.

119. Swanson, M.D., et al., *Engineering a Therapeutic Lectin by Uncoupling Mitogenicity from Antiviral Activity.* Cell, 2015. **163**(3): p. 746-758.

120. Yamamoto, K., Y. Konami, and T. Osawa, *A Chimeric Lectin Formed from Bauhinia purpurea Lectin and Lens culinaris Lectin Recognizes a Unique Carbohydrate Structure1.* The Journal of Biochemistry, 2000. **127**(1): p. 129-135.

121. Kříž, Z., et al., *Engineering the Pseudomonas aeruginosa II lectin: designing mutants with changed affinity and specificity.* Journal of Computer-Aided Molecular Design, 2014. **28**(9): p. 951-960.

122. Matsumoto, A. and Y. Miyahara, *'Borono-lectin' based engineering as a versatile platform for biomedical applications.* Sci Technol Adv Mater, 2018. **19**(1): p. 18-30.

123. Hu, D., H. Tateno, and J. Hirabayashi, *Lectin engineering, a molecular evolutionary approach to expanding the lectin utilities.* Molecules, 2015. **20**(5): p. 7637-56.

124. Mahajan, S. and T.N.C. Ramya, *Nature-inspired engineering of an F-type lectin for increased binding strength.* Glycobiology, 2018. **28**(12): p. 933-948.

125. Ribeiro, J.P., et al., *Tailor-made Janus lectin with dual avidity assembles glycoconjugate multilayers and crosslinks protocells.* Chemical Science, 2018. **9**(39): p. 7634-7641.

126. Sterner, E., N. Flanagan, and J.C. Gildersleeve, *Perspectives on Anti-Glycan Antibodies Gleaned from Development of a Community Resource Database.* ACS Chem Biol, 2016. **11**(7): p. 1773-83.

127. Bovin, N., et al., *Repertoire of human natural anti-glycan immunoglobulins. Do we have auto-antibodies?* Biochim Biophys Acta, 2012. **1820**(9): p. 1373-82.

128. Xu, H., et al., *The in vitro and in vivo effects of anti-galactose antibodies on endothelial cell activation and xenograft rejection.* J Immunol, 2003. **170**(3): p. 1531-9.

129. Estrada, J.L., et al., *Evaluation of human and non-human primate antibody binding to pig cells lacking GGTA1/CMAH/β4GalNT2 genes.* Xenotransplantation, 2015. **22**(3): p. 194-202.

130. Makeneni, S., et al., *Predicting the Origins of Anti-Blood Group Antibody Specificity: A Case Study of the ABO A- and B-Antigens.* Front Immunol, 2014. **5**: p. 397.

131. Rieder, F., et al., *Characterization of changes in serum anti-glycan antibodies in Crohn's disease--a longitudinal analysis.* PLoS One, 2011. **6**(5): p. e18172.

132. Hirche, T.O., et al., *Increased levels of anti-glycan antibodies in patients with cystic fibrosis.* Eur J Med Res, 2011. **16**(9): p. 385-90.

133. Jacob, F., et al., *Serum antiglycan antibody detection of nonmucinous ovarian cancers by using a printed glycan array.* Int J Cancer, 2012. **130**(1): p. 138-46.

134. Pochechueva, T., et al., *Comparison of printed glycan array, suspension array and ELISA in the detection of human anti-glycan antibodies.* Glycoconj J, 2011. **28**(8-9): p. 507-17.

135. Pedersen, J.W., et al., *Seromic profiling of colorectal cancer patients with novel glycopeptide microarray.* Int J Cancer, 2011. **128**(8): p. 1860-71.

136. Wandall, H.H., et al., *Cancer biomarkers defined by autoantibody signatures to aberrant O-glycopeptide epitopes.* Cancer Res, 2010. **70**(4): p. 1306-13.

137. Haji-Ghassemi, O., et al., *Antibody recognition of carbohydrate epitopesdagger.* Glycobiology, 2015. **25**(9): p. 920-52.

138. Polonskaya, Z., et al., *T cells control the generation of nanomolar-affinity anti-glycan antibodies.* J Clin Invest, 2017. **127**(4): p. 1491-1504.

139. Kaltgrad, E., et al., *Anti-Carbohydrate Antibodies Elicited by Polyvalent Display on a Viral Scaffold.* ChemBioChem, 2007. **8**(12): p. 1455-1462.

140. MacKenzie, C.R., et al., *Analysis by surface plasmon resonance of the influence of valence on the ligand binding affinity and kinetics of an anti-carbohydrate antibody.* J Biol Chem, 1996. **271**(3): p. 1527-33.

141. Mammen, M., S.-K. Choi, and G.M. Whitesides, *Polyvalent Interactions in Biological Systems: Implications for Design and Use of Multivalent Ligands and Inhibitors.* Angewandte Chemie International Edition, 1998. **37**(20): p. 2754-2794.

142. Lundquist, J.J. and E.J. Toone, *The cluster glycoside effect.* Chem Rev, 2002. **102**(2): p. 555-78.

143. Calarese, D.A., et al., *Antibody domain exchange is an immunological solution to carbohydrate cluster recognition.* Science, 2003. **300**(5628): p. 2065-71.

144. Hoorelbeke, B., et al., *HIV-1 envelope trimer has similar binding characteristics for carbohydrate-binding agents as monomeric gp120.* FEBS Letters, 2013. **587**(7): p. 860-866.

145. Polonskaya, Z., et al., *High-affinity anti-glycan antibodies: challenges and strategies.* Current opinion in immunology, 2019. **59**: p. 65-71.

146. Cygler, M., *Recognition of carbohydrates by antibodies.* Res Immunol, 1994. **145**(1): p. 36-40.

147. Haji-Ghassemi, O., et al., *Antibody recognition of carbohydrate epitopes†.* Glycobiology, 2015. **25**(9): p. 920-52.

148. Villeneuve, S., et al., *Crystal structure of an anti-carbohydrate antibody directed against Vibrio cholerae O1 in complex with antigen: molecular basis for serotype specificity.* Proc Natl Acad Sci U S A, 2000. **97**(15): p. 8433-8.

149. Haji-Ghassemi, O., et al., *Groove-type recognition of chlamydiaceae-specific lipopolysaccharide antigen by a family of antibodies possessing an unusual variable heavy chain N-linked glycan.* J Biol Chem, 2014. **289**(24): p. 16644-61.

150. Rangappa, S., et al., *Effects of the multiple O-glycosylation states on antibody recognition of the immunodominant motif in MUC1 extracellular tandem repeats.* MedChemComm, 2016. **7**(6): p. 1102-1122.

151. Coelho, H., et al., *The Quest for Anticancer Vaccines: Deciphering the Fine-Epitope Specificity of Cancer-Related Monoclonal Antibodies by Combining*

Microarray Screening and Saturation Transfer Difference NMR. Journal of the American Chemical Society, 2015. **137**(39): p. 12438-12441.

152. Müller-Loennies, S., et al., *Characterization of high affinity monoclonal antibodies specific for chlamydial lipopolysaccharide.* Glycobiology, 2000. **10**(2): p. 121-30.

153. Lak, P., et al., *Specificity of furanoside-protein recognition through antibody engineering and molecular modeling.* Chemistry, 2015. **21**(3): p. 1138-48.

154. Lak, P., et al., *Specificity of furanoside-protein recognition through antibody engineering and molecular modeling.* Chemistry (Weinheim an der Bergstrasse, Germany), 2015. **21**(3): p. 1138-1148.

155. Müller-Loennies, S., et al., *Characterization of high affinity monoclonal antibodies specific for chlamydial lipopolysaccharide.* Glycobiology, 2000. **10**(2): p. 121-130.

156. Park, S., et al., *Carbohydrate microarrays.* Chemical Society Reviews, 2013. **42**(10): p. 4310-4326.

157. de Paz, J.L. and P.H. Seeberger, *Recent advances and future challenges in glycan microarray technology.* Methods Mol Biol, 2012. **808**: p. 1-12.

158. Karacosta, L.G., et al., *Preclinical Analysis of JAA-F11, a Specific Anti–Thomsen-Friedenreich Antibody via Immunohistochemistry and In Vivo Imaging.* Translational Oncology, 2018. **11**(2): p. 450-466.

159. Jeyakanthan, M., et al., *ABH-Glycan Microarray Characterizes ABO Subtype Antibodies: Fine Specificity of Immune Tolerance After ABO-Incompatible Transplantation.* Am J Transplant, 2016. **16**(5): p. 1548-58.

160. Ragupathi, G., et al., *Synthesis of sialyl Lewis(a) (sLe (a), CA19-9) and construction of an immunogenic sLe(a) vaccine.* Cancer Immunol Immunother, 2009. **58**(9): p. 1397-405.

161. Sawada, R., et al., *Human monoclonal antibodies to sialyl-Lewis (CA19.9) with potent CDC, ADCC, and antitumor activity.* Clin Cancer Res, 2011. **17**(5): p. 1024-32.

162. Shackelford, P.G., et al., *Human antibodies to group A streptococcal carbohydrate. Ontogeny, subclass restriction, and clonal diversity.* The Journal of Immunology, 1988. **140**(9): p. 3200-3205.

163. Kearney, J.F., et al., *Natural antibody repertoires: development and functional role in inhibiting allergic airway disease.* Annual review of immunology, 2015. **33**: p. 475-504.

164. Patel, P. and J.F. Kearney, *Immunological Outcomes of Antibody Binding to Glycans Shared between Microorganisms and Mammals.* Journal of immunology (Baltimore, Md. : 1950), 2016. **197**(11): p. 4201-4209.

165. Francesconi, O., et al., *Pyrrolic tripodal receptors for the molecular recognition of carbohydrates: ditopic receptors for dimannosides.* Chemistry, 2013. **19**(35): p. 11742-52.

166. Yang, F., et al., *Chapter Eleven - Establishing the Architecture of Plant Gene Regulatory Networks*, in *Methods in Enzymology*, S.E. O'Connor, Editor. 2016, Academic Press. p. 251-304.

167. Stephenson-Brown, A., et al., *Selective glycoprotein detection through covalent templating and allosteric click-imprinting.* Chemical Science, 2015. **6**(9): p. 5114-5119.

168. Tuerk, C. and L. Gold, *Systematic evolution of ligands by exponential enrichment: RNA ligands to bacteriophage T4 DNA polymerase.* Science, 1990. **249**(4968): p. 505-10.

169. Yang, X., et al., *Boronic acid-modified DNA that changes fluorescent properties upon carbohydrate binding.* Chemical Communications, 2010. **46**(7): p. 1073-1075.

170. Keefe, A.D., S. Pai, and A. Ellington, *Aptamers as therapeutics.* Nat Rev Drug Discov, 2010. **9**(7): p. 537-50.

171. Ruscito, A. and M.C. DeRosa, *Small-Molecule Binding Aptamers: Selection Strategies, Characterization, and Applications.* Frontiers in chemistry, 2016. **4**: p. 14-14.

172. Ruscito, A. and M.C. Derosa, *Small-Molecule Binding Aptamers: Selection Strategies, Characterization, and Applications.* Frontiers in Chemistry, 2016. **4**.

173. Fuster, M.M. and J.D. Esko, *The sweet and sour of cancer: glycans as novel therapeutic targets.* Nat Rev Cancer, 2005. **5**(7): p. 526-42.

174. Cho, S., et al., *In vitro selection of sialic acid specific RNA aptamer and its application to the rapid sensing of sialic acid modified sugars.* Biotechnology and Bioengineering, 2013. **110**(3): p. 905-913.

175. Kizer, M., et al., *RNA Aptamers with Specificity for Heparosan and Chondroitin Glycosaminoglycans.* ACS Omega, 2018. **3**(10): p. 13667-13675.

176. Li, M., et al., *Selecting aptamers for a glycoprotein through the incorporation of the boronic acid moiety.* J Am Chem Soc, 2008. **130**(38): p. 12636-8.

177. Springsteen, G. and B. Wang, *A detailed examination of boronic acid–diol complexation.* Tetrahedron, 2002. **58**(26): p. 5291-5300.

178. Hall, D., *Boronic Acids: Preparation and Applications in Organic Synthesis and Medicine*. 2006. p. 1-99.

179. Martínez-Aguirre, M.A., et al., *Examination of pinanediol–boronic acid ester formation in aqueous media: relevance to the relative stability of trigonal and tetrahedral boronate esters.* Organic & Biomolecular Chemistry, 2020. **18**(14): p. 2716-2726.

180. Yan, J., H. Fang, and B. Wang, *Boronolectins and fluorescent boronolectins: an examination of the detailed chemistry issues important for the design.* Med Res Rev, 2005. **25**(5): p. 490-520.

181. Bérubé, M., M. Dowlut, and D.G. Hall, *Benzoboroxoles as Efficient Glycopyranoside-Binding Agents in Physiological Conditions: Structure and Selectivity of Complex Formation.* The Journal of Organic Chemistry, 2008. **73**(17): p. 6471-6479.

182. Yan, J., et al., *The relationship among pKa, pH, and binding constants in the interactions between boronic acids and diols—It is not as simple as it appears.* Tetrahedron, 2004. **60**: p. 11205–11209.

183. Himmelein, S. and B.J. Ravoo, *A Self-Assembled Sensor for Carbohydrates on the Surface of Cyclodextrin Vesicles.* Chemistry, 2017. **23**(25): p. 6034-6041.

184. Stephenson-Brown, A., et al., *Glucose selective Surface Plasmon Resonance-based bis-boronic acid sensor.* Analyst, 2013. **138**(23): p. 7140-7145.

185. Guo, L.E., et al., *Proline-Based Boronic Acid Receptors for Chiral Recognition of Glucose.* J Org Chem, 2018. **83**(24): p. 15128-15135.

186. Wu, X., et al., *Selective sensing of saccharides using simple boronic acids and their aggregates.* Chemical Society Reviews, 2013. **42**(20): p. 8032-8048.

187. James, T.D., K.R.A.S. Sandanayake, and S. Shinkai, *Saccharide Sensing with Molecular Receptors Based on Boronic Acid.* Angewandte Chemie International Edition in English, 1996. **35**(17): p. 1910-1922.

188. Zhai, W., et al., *Boronic Acid-Based Carbohydrate Sensing.* Chem Asian J, 2015. **10**(9): p. 1836-48.

189. Mitchell, P., et al., *Precise Generation of Selective Surface-Confined Glycoprotein Recognition Sites.* ACS Appl Bio Mater, 2019. **2**(6): p. 2617-2623.

190. Li, L., et al., *Photolithographic boronate affinity molecular imprinting: a general and facile approach for glycoprotein imprinting.* Angew Chem Int Ed Engl, 2013. **52**(29): p. 7451-4.

191. Cieplak, M. and W. Kutner, *Artificial Biosensors: How Can Molecular Imprinting Mimic Biorecognition?* Trends Biotechnol, 2016. **34**(11): p. 922-941.

192. Zhao, T., et al., *One-step post-imprint modification achieve dual-function of glycoprotein fluorescent sensor by "Click Chemistry".* Biosens Bioelectron, 2017. **91**: p. 756-761.

193. Shen, F. and X. Ren, *Covalent molecular imprinting made easy: a case study of mannose imprinted polymer.* RSC Advances, 2014. **4**(25): p. 13123-13125.

194. Bonini, F., et al., *Surface imprinted beads for the recognition of human serum albumin.* Biosens Bioelectron, 2007. **22**(9-10): p. 2322-8.

195. Wulff, G. and S. Schauhoff, *Enzyme-analog-built polymers. 27. Racemic resolution of free sugars with macroporous polymers prepared by molecular imprinting. Selectivity dependence on the arrangement of functional groups versus spatial requirements.* The Journal of Organic Chemistry, 1991. **56**(1): p. 395-400.

196. Torssell, K., *Bromination of tolylboronic acids according to Wohl-Ziegler.* Ark. Kemi, 1957. **10**: p. 507-511.

197. Alterio, V., et al., *Benzoxaborole as a new chemotype for carbonic anhydrase inhibition.* Chemical Communications, 2016. **52**(80): p. 11983-11986.

198. Alam, M.A., et al., *Synthesis and evaluation of functionalized benzoboroxoles as potential anti-tuberculosis agents.* Tetrahedron, 2016. **72**(26): p. 3795-3801.

199. Berube, M., M. Dowlut, and D.G. Hall, *Benzoboroxoles as efficient glycopyranoside-binding agents in physiological conditions: structure and selectivity of complex formation.* J Org Chem, 2008. **73**(17): p. 6471-9.

200. Rowe, L., G. El Khoury, and C.R. Lowe, *A benzoboroxole-based affinity ligand for glycoprotein purification at physiological pH.* Journal of Molecular Recognition, 2016. **29**(5): p. 232-238.

201. Pal, A., M. Bérubé, and D.G. Hall, *Design, synthesis, and screening of a library of peptidyl bis(boroxoles) as oligosaccharide receptors in water: identification of a receptor for the tumor marker TF-antigen disaccharide.* Angew Chem Int Ed Engl, 2010. **49**(8): p. 1492-5.

202. Pal, A., M. Berube, and D.G. Hall, *Design, synthesis, and screening of a library of peptidyl bis(boroxoles) as oligosaccharide receptors in water: identification of a receptor for the tumor marker TF-antigen disaccharide.* Angew Chem Int Ed Engl, 2010. **49**(8): p. 1492-5.

203. Chen, C., et al., *A carbohydrate-binding affinity ligand for the specific enrichment of glycoproteins.* J Chromatogr A, 2016. **1444**: p. 8-20.

204. Couturier, J.P., et al., *Thermoresponsive Polymers and Inverse Opal Hydrogels for the Detection of Diols.* Langmuir, 2016. **32**(17): p. 4333-45.

205. Lin, M., et al., *Supramolecular Glyco-nanoparticles Toward Immunological Applications.* Small, 2015. **11**(45): p. 6065-70.

206. Varga, M., *Chapter 3 - Self-assembly of nanobiomaterials*, in *Fabrication and Self-Assembly of Nanobiomaterials*, A.M. Grumezescu, Editor. 2016, William Andrew Publishing. p. 57-90.

207. Ghalia, M.A. and Y. Dahman, *Chapter 6 - Advanced nanobiomaterials in tissue engineering: Synthesis, properties, and applications*, in *Nanobiomaterials in Soft Tissue Engineering*, A.M. Grumezescu, Editor. 2016, William Andrew Publishing. p. 141-172.

208. Allara, D.L., *Critical issues in applications of self-assembled monolayers.* Biosensors and Bioelectronics, 1995. **10**(9-10): p. 771-783.

209. Liu, H., et al., *Investigation of the adhesion, friction, and wear properties of biphenyl thiol self-assembled monolayers by atomic force microscopy.* Journal of Vacuum Science & Technology A: Vacuum, Surfaces, and Films, 2001. **19**(4): p. 1234-1240.

210. Zucchi, F., et al., *Inhibition of copper corrosion by silane coatings.* Corrosion Science, 2004. **46**(11): p. 2853-2865.

211. Tao, F. and S.L. Bernasek, *5.05 - Self-Assembled Monolayers*, in *Comprehensive Nanoscience and Technology*, D.L. Andrews, G.D. Scholes, and G.P. Wiederrecht, Editors. 2011, Academic Press: Amsterdam. p. 127-152.

212. Cyganik, P., et al., *Self-Assembled Monolayers of ω-Biphenylalkanethiols on Au(111): Influence of Spacer Chain on Molecular Packing.* Journal of Physical Chemistry B, 2004. **108**(16): p. 4989-4996.

213. Cyganik, P., et al., *Competition as a design concept: Polymorphism in self-assembled monolayers of biphenyl-based thiols.* Journal of the American Chemical Society, 2006. **128**(42): p. 13868-13878.

214. Cyganik, P., et al., *Influence of molecular structure on phase transitions: A study of self-assembled monolayers of 2-(aryl)-ethane thiols.* Journal of Physical Chemistry C, 2007. **111**(45): p. 16909-16919.

215. Camillone Iii, N., et al., *Substrate dependence of the surface structure and chain packing of docosyl mercaptan self-assembled on the (111), (110), and (100) faces of single crystal gold.* The Journal of Chemical Physics, 1993. **98**(5): p. 4234-4245.

216. Rohdenburg, M., et al., *Cisplatin as a Potential Platinum Focused Electron Beam Induced Deposition Precursor: NH3 Ligands Enhance the Electron-Induced Removal of Chlorine.* The Journal of Physical Chemistry C, 2019. **123**(35): p. 21774-21787.

217. Bilić, A., J.R. Reimers, and N.S. Hush, *The structure, energetics, and nature of the chemical bonding of phenylthiol adsorbed on the Au(111) surface: Implications for density-functional calculations of molecular-electronic conduction.* 2005. **122**(9): p. 094708.

218. Schreiber, F., *Structure and growth of self-assembling monolayers.* Progress in Surface Science, 2000. **65**(5): p. 151-257.

219. Gärtner, M., et al., *Understanding the Properties of Tailor-Made Self-Assembled Monolayers with Embedded Dipole Moments for Interface Engineering.* The Journal of Physical Chemistry C, 2018. **122**(50): p. 28757-28774.

220. Xue, Y., et al., *Quantifying thiol–gold interactions towards the efficient strength control.* Nature Communications, 2014. **5**(1).

221. Vericat, C., et al., *Self-assembled monolayers of thiols and dithiols on gold: new challenges for a well-known system.* Chemical Society Reviews, 2010. **39**(5): p. 1805-1834.

222. Vericat, C., M.E. Vela, and R.C. Salvarezza, *Self-assembled monolayers of alkanethiols on Au(111): surface structures, defects and dynamics.* Physical Chemistry Chemical Physics, 2005. **7**(18): p. 3258-3268.

223. Schreiber, F., *Structure and Growth of Self-Assembling Monolayers.* Progress in Surface Science - PROG SURF SCI, 2000. **65**.

224. Chen, J., et al., *Quantifying Gauche Defects and Phase Evolution in Self-Assembled Monolayers through Sessile Drops.* ACS Omega, 2017. **2**(5): p. 2072-2084.

225. Alexander, C., et al., *Molecular Imprinting Science and Technology: A Survey of the Literature for The Years Up to And Including 2003.* Journal of molecular recognition : JMR, 2006. **19**: p. 106-80.

226. Mujahid, A. and F.L. Dickert, *Molecularly Imprinted Polymers*. 2016, Elsevier. p. 79-101.

227. Technologies, M. *MIPs*. 2015; Available from: http://www.miptechnologies.com/mips/.

228. Polyakov, M.V. and Z. Khim, *Adsorption properties of silica gel and its structure.* Zhur Fiz Khim, 1931. **2**: p. 799-805.

229. Pauling, L., *Molecular Architecture and Biological Reactions.* Chemical & Engineering News Archive, 1946. **24**(10): p. 1375-1377.

230. Patrikeev, V.V., Z.S. Smirnova, and G.I. Maksimov, *SOME BIOLOGICAL PROPERTIES OF PECIFICALLY FORMED SILICA GEL.* DOKLADY AKADEMII NAUK SSSR, 1962. **146**(3): p. 707.

231. Mujahid, A. and F.L. Dickert, *5 - Molecularly Imprinted Polymers: Principle, Design, and Enzyme-Like Catalysis*, in *Molecularly Imprinted Catalysts*, S. Li, et al., Editors. 2016, Elsevier: Amsterdam. p. 79-101.

232. Wulff, G., A.W. Sarhan, and H. Sarhan, *Use of polymers with enzyme-analogous structures for the resolution of racemates.* 1972.

233. Wulff, G., A. Sarhan, and K. Zabrocki, *Enzyme-analogue built polymers and their use for the resolution of racemates.* Tetrahedron Letters, 1973. **14**(44): p. 4329-4332.

234. Vidyasankar, S. and F.H. Arnold, *Molecular imprinting: selective materials for separations, sensors and catalysis.* Current Opinion in Biotechnology, 1995. **6**(2): p. 218-224.

235. Wulff, G., *The role of binding-site interactions in the molecular imprinting of polymers.* Trends in biotechnology, 1993. **11**(3): p. 85-87.

236. Allender, C., et al., *Pharmaceutical applications for molecularly imprinted polymers.* International journal of pharmaceutics, 2000. **195**: p. 39-43.

237. Chen, L., et al., *Molecular imprinting: perspectives and applications.* Chemical Society Reviews, 2016. **45**(8): p. 2137-2211.

238. Powers, A.D. and S.P. Palecek, *Protein analytical assays for diagnosing, monitoring, and choosing treatment for cancer patients.* Journal of healthcare engineering, 2012. **3**(4): p. 503-534.

239. Kupcova Skalnikova, H., et al., *Advances in Proteomic Techniques for Cytokine Analysis: Focus on Melanoma Research.* International journal of molecular sciences, 2017. **18**(12): p. 2697.

240. Souf, S., *Recent advances in diagnostic testing for viral infections.* Bioscience Horizons: The International Journal of Student Research, 2016. **9**.

241. Yang, Y., et al., *Optimization of polymerization parameters for the sorption of oseltamivir onto molecularly imprinted polymers.* Analytical and bioanalytical chemistry, 2011. **400**: p. 3665-74.

242. Joshi, V., et al., *Effect of Solvents on Selectivity in Separation Using Molecularly Imprinted Adsorbents: Separation of Phenol and Bisphenol A.* Industrial & Engineering Chemistry Research - IND ENG CHEM RES, 1999. **38**.

243. Wulff, G., *Enzyme-like Catalysis by Molecularly Imprinted Polymers.* Chemical Reviews, 2002. **102**(1): p. 1-28.

244. Yang, W., et al., *The first fluorescent diboronic acid sensor specific for hepatocellular carcinoma cells expressing sialyl Lewis X.* Chem Biol, 2004. **11**(4): p. 439-48.

245. Xu, X.D., et al., *In situ recognition of cell-surface glycans and targeted imaging of cancer cells.* Sci Rep, 2013. **3**: p. 2679.

246. Bie, Z., et al., *Boronate-Affinity Glycan-Oriented Surface Imprinting: A New Strategy to Mimic Lectins for the Recognition of an Intact Glycoprotein and Its Characteristic Fragments.* Angew Chem Int Ed Engl, 2015. **54**(35): p. 10211-5.

247. Stephenson-Bron, A., et al., *Selective glycoprotein detection through covalent templating and allosteric click-imprinting.* Chem. Sci., 2015. **6**.

248. Mitchell, P., et al., *Precise Generation of Selective Surface-Confined Glycoprotein Recognition Sites.* ACS applied bio materials, 2019. **2**(6): p. 2617-2623.

249. Haab, B.B., *Using lectins in biomarker research: addressing the limitations of sensitivity and availability.* Proteomics Clin Appl, 2012. **6**(7-8): p. 346-50.

250. Haab, B.B., *Antibody-lectin sandwich arrays for biomarker and glycobiology studies.* Expert review of proteomics, 2010. **7**(1): p. 9-11.

251. Hirabayashi, J., *Concept, strategy and realization of lectin-based glycan profiling.* J Biochem, 2008. **144**(2): p. 139-47.

252. Ghazarian, H., B. Idoni, and S.B. Oppenheimer, *A glycobiology review: carbohydrates, lectins and implications in cancer therapeutics.* Acta Histochem, 2011. **113**(3): p. 236-47.

253. Hendrickson, O.D. and A.V. Zherdev, *Analytical Application of Lectins.* Crit Rev Anal Chem, 2018. **48**(4): p. 279-292.

254. Shu-Kun, L., *Physical Biochemistry: Principles and Applications. By David Sheehan.* Molecules, 2000. **5**.

255. Coombe, D.R. and C.R. Parish, *Editorial: Carbohydrates: The Yet to be Tasted Sweet Spot of Immunity.* Frontiers in immunology, 2015. **6**: p. 314-314.

256. Seveno, D., T.D. Blake, and J. De Coninck, *Young's Equation at the Nanoscale.* Physical Review Letters, 2013. **111**(9): p. 096101.

257. Dwivedi, C., et al., *Chapter 9 - Electrospun Nanofibrous Scaffold as a Potential Carrier of Antimicrobial Therapeutics for Diabetic Wound Healing and Tissue Regeneration*, in *Nano- and Microscale Drug Delivery Systems*, A.M. Grumezescu, Editor. 2017, Elsevier. p. 147-164.

258. Schrader, M.E., *Young-Dupre Revisited.* Langmuir, 1995. **11**(9): p. 3585-3589.

259. Kulkarni, V.S. and C. Shaw, *Chapter 2 - Surfactants, Lipids, and Surface Chemistry*, in *Essential Chemistry for Formulators of Semisolid and Liquid Dosages*, V.S. Kulkarni and C. Shaw, Editors. 2016, Academic Press: Boston. p. 5-19.

260. Yuan, Y. and T.R. Lee, *Contact Angle and Wetting Properties*, in *Surface Science Techniques*. 2013. p. 3-34.

261. Erbil, H.Y., *The debate on the dependence of apparent contact angles on drop contact area or three-phase contact line: A review.* Surface Science Reports, 2014. **69**(4): p. 325-365.

262. Extrand, C.W., *Remodeling of Super-hydrophobic Surfaces.* Langmuir, 2016. **32**(34): p. 8608-8612.

263. Guancheng, J., *Chapter 2 - Evaluation Methods and Influencing Factors of Gas Wettability*, in *Gas Wettability of Reservoir Rock Surfaces with Porous Media*, J. Guancheng, Editor. 2018, Gulf Professional Publishing. p. 29-84.

264. Rapp, B.E., *Chapter 20 - Surface Tension*, in *Microfluidics: Modelling, Mechanics and Mathematics*, B.E. Rapp, Editor. 2017, Elsevier: Oxford. p. 421-444.

265. Aspnes, D.E., *Spectroscopic ellipsometry—A perspective.* 2013. **31**(5): p. 058502.

266. McCrackin, F.L., et al., *Measurement of the Thickness and Refractive Index of Very Thin Films and the Optical Properties of Surfaces by Ellipsometry.* Journal of research of the National Bureau of Standards. Section A, Physics and chemistry, 1963. **67A**(4): p. 363-377.

267. Kerker, M., *CHAPTER 2 - Electromagnetic Waves*, in *The Scattering of Light and Other Electromagnetic Radiation*, M. Kerker, Editor. 1969, Academic Press. p. 8-26.

268. Dzebo, D., *Photon Upconversion through Triplet-Triplet Annihilation: Towards Higher Efficiency and Solid State Applications*. 2016.

269. Shribak, M., *Complete polarization state generator with one variable retarder and its application for fast and sensitive measuring of two-dimensional birefringence distribution.* Journal of the Optical Society of America A, 2011. **28**(3): p. 410-419.

270. Taqatqa, O. and H. Al Attar, *Spectroscopic ellipsometry investigation of azo dye and azo dye doped polymer.* The European Physical Journal Applied Physics, 2006. **37**(1): p. 61-64.

271. Huber, A.-K., et al., *In situ study of electrochemical activation and surface segregation of the SOFC electrode material La0.75Sr0.25Cr0.5Mn0.5O3±δ.* Phys. Chem. Chem. Phys., 2012. **14**(2): p. 751-758.

272. Breithaupt, J., *BOOK REVIEW: New Understanding Physics for Advanced Level.* Physics Education, 2000. **35**: p. 368-369.

273. Salouti, M. and F.K. Derakhshan, *Chapter 3 - Phytosynthesis of Nanoscale Materials*, in *Advances in Phytonanotechnology*, M. Ghorbanpour and S.H. Wani, Editors. 2019, Academic Press. p. 45-121.

274. Konno, H., *Chapter 8 - X-ray Photoelectron Spectroscopy*, in *Materials Science and Engineering of Carbon*, M. Inagaki and F. Kang, Editors. 2016, Butterworth-Heinemann. p. 153-171.

275. Yang, W., et al., *A novel type of fluorescent boronic acid that shows large fluorescence intensity changes upon binding with a carbohydrate in aqueous solution at physiological pH.* Bioorganic & Medicinal Chemistry Letters, 2003. **13**(6): p. 1019-1022.

276. Nguyen, H.H., et al., *Surface plasmon resonance: a versatile technique for biosensor applications.* Sensors (Basel, Switzerland), 2015. **15**(5): p. 10481-10510.

277. Zhao, C., J. Zhang, and Y. Liu, *Light manipulation with encoded plasmonic nanostructures.* EPJ Applied Metamaterials, 2014. **1**.

278. Jang, D., G. Chae, and S. Shin, *Analysis of Surface Plasmon Resonance Curves with a Novel Sigmoid-Asymmetric Fitting Algorithm.* Sensors, 2015. **15**: p. 25385-25398.

279. Hinman, S.S., K.S. McKeating, and Q. Cheng, *Surface Plasmon Resonance: Material and Interface Design for Universal Accessibility.* Analytical chemistry, 2018. **90**(1): p. 19-39.

280. Casalini, S., et al., *Self-assembled monolayers in organic electronics.* Chemical Society Reviews, 2017. **46**(1): p. 40-71.

281. Akiba, U. and M. Fujihira.

282. Freitas, S.C., et al., *Self-Assembled Monolayers for Dental Implants.* International journal of dentistry, 2018. **2018**: p. 4395460-4395460.

283. Vaithilingam, J., et al., *SURFACE MODIFICATION OF SELECTIVE LASER MELTED STRUCTURES USING SELF-ASSEMBLED MONOLAYERS FOR BIOMEDICAL APPLICATIONS*. 2012.

284. Caprioli, F., F. Decker, and V.D. Castro, *Durable Cu corrosion inhibition in acidic solution by SAMs of Benzenethiol.* Journal of Electroanalytical Chemistry, 2011. **657**(1): p. 192-195.

285. Chaki, N.K. and K. Vijayamohanan, *Self-assembled monolayers as a tunable platform for biosensor applications.* Biosens Bioelectron, 2002. **17**(1-2): p. 1-12.

286. Butterworth, A., et al., *SAM Composition and Electrode Roughness Affect Performance of a DNA Biosensor for Antibiotic Resistance.* Biosensors, 2019. **9**(1): p. 22.

287. Rudin, A. and P. Choi, *Free-Radical Polymerization*. 2013, Elsevier. p. 341-389.

288. Huang, S.H., et al., *Whispering gallery mode resonator sensor for in situ measurements of hydrogel gelation.* Optics Express, 2018. **26**(1): p. 51-62.

289. Jay, J.I., et al., *Multivalent Benzoboroxole Functionalized Polymers as gp120 Glycan Targeted Microbicide Entry Inhibitors.* Molecular Pharmaceutics, 2010. **7**(1): p. 116-129.

290. Kohli, R., *UV-Ozone Cleaning for Removal of Surface Contaminants*. 2015, Elsevier. p. 71-104.

291. Kohli, R., *Chapter 2 - UV-Ozone Cleaning for Removal of Surface Contaminants*, in *Developments in Surface Contamination and Cleaning*, R. Kohli and K.L. Mittal, Editors. 2015, William Andrew Publishing: Oxford. p. 71-104.

292. Makkonen, L., *A thermodynamic model of contact angle hysteresis.* The Journal of Chemical Physics, 2017. **147**(6): p. 064703.

293. Canning, J., I. Petermann, and K. Cook, *Surface treatment of silicate based glass: Base Piranha treatment versus 193nm laser processing.* Proc SPIE, 2012. **8351**: p. 89.

294. Gardner, J.R. and R. Woods, *The hydrophilic nature of gold and platinum.* Journal of Electroanalytical Chemistry and Interfacial Electrochemistry, 1977. **81**(2): p. 285-290.

295. Mark, J.E., B.R. Erman, and M. Roland, *The science and technology of rubber*. 2013.

296. Colorado, R. and T.R. Lee, *Thiol-based Self-assembled Monolayers: Formation and Organization*, in *Encyclopedia of Materials: Science and Technology*, K.H.J. Buschow, et al., Editors. 2001, Elsevier: Oxford. p. 9332-9344.

297. Park, J.-S., et al., *Systematic Control of the Packing Density of Self-Assembled Monolayers Using Bidentate and Tridentate Chelating Alkanethiols.* Langmuir, 2005. **21**(7): p. 2902-2911.

298. Sonia, T.A. and C.P. Sharma, *4 - Experimental techniques involved in the development of oral insulin carriers*, in *Oral Delivery of Insulin*, T.A. Sonia and C.P. Sharma, Editors. 2014, Woodhead Publishing. p. 169-217.

299. Yasuda, H., A.K. Sharma, and T. Yasuda, *Effect of orientation and mobility of polymer molecules at surfaces on contact angle and its hysteresis.* Journal of Polymer Science: Polymer Physics Edition, 1981. **19**(9): p. 1285-1291.

300. Starov, V., *Static contact angle hysteresis on smooth, homogeneous solid substrates.* Colloid and Polymer Science, 2013. **291**.

301. Briscoe, W.H. and J. Klein, *Friction and Adhesion Hysteresis between Surfactant Monolayers in Water.* The Journal of Adhesion, 2007. **83**(7): p. 705-722.

302. Wang, H., et al., *Improved method for the preparation of carboxylic acid and amine terminated self-assembled monolayers of alkanethiolates.* Langmuir, 2005. **21**(7): p. 2633-6.

303. Wang, H., et al., *Improved Method for the Preparation of Carboxylic Acid and Amine Terminated Self-Assembled Monolayers of Alkanethiolates.* Langmuir, 2005. **21**(7): p. 2633-2636.

304. Gittens, R.A., et al., *The roles of titanium surface micro/nanotopography and wettability on the differential response of human osteoblast lineage cells.* Acta biomaterialia, 2013. **9**(4): p. 6268-6277.

305. Dutz, S., et al., *Hysteresis losses of magnetic nanoparticle powders in the single domain size range.* Journal of Magnetism and Magnetic Materials, 2007. **308**: p. 305–312.

306. Golovin, K., et al., *Transparent, Flexible, Superomniphobic Surfaces with Ultra-Low Contact Angle Hysteresis.* Angewandte Chemie International Edition, 2013. **52**(49): p. 13007-13011.

307. Smith, M.B., et al., *Study of the Packing Density and Molecular Orientation of Bimolecular Self-Assembled Monolayers of Aromatic and Aliphatic Organosilanes on Silica.* Langmuir, 2007. **23**(2): p. 673-683.

308. Bahadır, E.B. and M.K. Sezgintürk, *A comparative study of short chain and long chain mercapto acids used in biosensor fabrication: A VEGF-R1-based immunosensor as a model system.* Artificial Cells, Nanomedicine, and Biotechnology, 2016. **44**(2): p. 462-470.

309. Bowers, C.M., et al., *Characterizing the Metal–SAM Interface in Tunneling Junctions.* ACS Nano, 2015. **9**(2): p. 1471-1477.

310. Bhattarai, J., et al., *Self-Assembled Monolayers of Carbohydrate Derivatives on Gold Surfaces*. 2017.

311. Kohli, S., et al., *Comparison of nanometer-thick films by x-ray reflectivity and spectroscopic ellipsometry.* Review of Scientific Instruments, 2005. **76**(2): p. 023906.

312. Podraza, N.J. and G.E. Jellison, *Ellipsometry☆*, in *Encyclopedia of Spectroscopy and Spectrometry (Third Edition)*, J.C. Lindon, G.E. Tranter, and D.W. Koppenaal, Editors. 2017, Academic Press: Oxford. p. 482-489.

313. Schweizer, T., *Handbook of Ellipsometry.* Applied Rheology, 2005. **15**: p. 10-11.

314. Mora, M.F., et al., *Investigating Protein Adsorption via Spectroscopic Ellipsometry.* Biological Interactions on Materials Surfaces: Understanding and Controlling Protein, Cell, and Tissue Responses, 2009: p. 19-41.

315. Woollam, J., et al., *Overview of Variable Angle Spectroscopic Ellipsometry (VASE), Part I: Basic Theory and Typical Applications.* Proceedings of SPIE - The International Society for Optical Engineering, 1999. **-1**: p. 3-28.

316. de Boor, C., *Package for Calculating with B-Splines.* SIAM Journal on Numerical Analysis, 1973. **14**: p. 57.

317. Alzaatreh, A., et al., *The generalized Cauchy family of distributions with applications.* Journal of Statistical Distributions and Applications, 2016. **3**(1): p. 12.

318. Canepa, M., et al., *Spectroscopic ellipsometry of self assembled monolayers: interface effects. The case of phenyl selenide SAMs on gold.* Physical Chemistry Chemical Physics, 2013. **15**(27): p. 11559-11565.

319. Hu, J., et al., *Theoretical Insights into the Solvent Polarity Effect on the Quality of Self-Assembled N-Octadecanethiol Monolayers on Cu (111) Surfaces.* Molecules, 2018. **23**(4): p. 733.

320. Dai, J., et al., *Study of the solvent effect on the quality of dodecanethiol self-assembled monolayers on polycrystalline gold.* Journal of Electroanalytical Chemistry, 2008. **624**(1): p. 315-322.

321. Bain, C.D., et al., *Formation of monolayer films by the spontaneous assembly of organic thiols from solution onto gold.* Journal of the American Chemical Society, 1989. **111**(1): p. 321-335.

322. Hu, K., et al., *In Situ Monitoring of Diffuse Double Layer Structure Changes of Electrochemically Addressable Self-Assembled Monolayers with an Atomic Force Microscope.* Langmuir, 1999. **15**(9): p. 3343-3347.

323. Malitesta, C., et al., *New findings on polypyrrole chemical structure by XPS coupled to chemical derivatization labelling.* Journal of Electron Spectroscopy and Related Phenomena, 1995. **76**: p. 629-634.

324. Yan, X., et al., *Preparation and characterization of electrochemically deposited carbon nitride films on silicon substrate.* Journal of Physics D: Applied Physics, 2004. **37**(6): p. 907-913.

325. Weidner, T., et al., *Tripodal Binding Units for Self-Assembled Monolayers on Gold: A Comparison of Thiol and Thioether Headgroups.* The Journal of Physical Chemistry C, 2009. **113**(45): p. 19609-19617.

326. Castner, D.G., K. Hinds, and D.W. Grainger, *X-ray Photoelectron Spectroscopy Sulfur 2p Study of Organic Thiol and Disulfide Binding Interactions with Gold Surfaces.* Langmuir, 1996. **12**(21): p. 5083-5086.

327. Arnett, E.M. and B. Chawla, *Thermometric titrations of substituted pyridines with trifluoroacetic acid in carbon tetrachloride. Hydrogen bonded ion pair systems.* Journal of the American Chemical Society, 1978. **100**(1): p. 217-221.

328. Singhal, R.P., et al., *New ligands for boronate affinity chromatography synthesis and properties.* Journal of chromatography, 1991. **543**(1): p. 17-38.

329. Yan, J., et al., *The relationship among pKa, pH, and binding constants in the interactions between boronic acids and diols—it is not as simple as it appears.* Tetrahedron, 2004. **60**(49): p. 11205-11209.

330. Sørensen, M.D., R. Martins, and O. Hindsgaul, *Assessing the terminal glycosylation of a glycoprotein by the naked eye.* Angewandte Chemie, 2007. **119**(14): p. 2455-2459.

331. Ricardo, A., et al., *2-Hydroxymethylboronate as a reagent to detect carbohydrates: application to the analysis of the formose reaction.* The Journal of Organic Chemistry, 2006. **71**(25): p. 9503-9505.

332. Selimis, A. and M. Farsari, *3.8 Laser-Based 3D Printing and Surface Texturing*, in *Comprehensive Materials Finishing*, M.S.J. Hashmi, Editor. 2017, Elsevier: Oxford. p. 111-136.

333. Khelifa, F., Y. Habibi, and P. Dubois, *Chapter 5 - Nanocellulose-Based Polymeric Blends for Coating Applications*, in *Multifunctional Polymeric Nanocomposites Based on Cellulosic Reinforcements*, D. Puglia, E. Fortunati, and J.M. Kenny, Editors. 2016, William Andrew Publishing. p. 131-175.

334. Maitz, M.F., *Applications of synthetic polymers in clinical medicine.* Biosurface and Biotribology, 2015. **1**(3): p. 161-176.

335. Su, W.-F., *Radical Chain Polymerization*, in *Principles of Polymer Design and Synthesis*, W.-F. Su, Editor. 2013, Springer Berlin Heidelberg: Berlin, Heidelberg. p. 137-183.

336. Zorn, G., et al., *X-ray Photoelectron Spectroscopy Investigation of the Nitrogen Species in Photoactive Perfluorophenylazide-Modified Surfaces.* The Journal of Physical Chemistry C, 2014. **118**(1): p. 376-383.

337. Baltrusaitis, J., P.M. Jayaweera, and V.H. Grassian, *XPS study of nitrogen dioxide adsorption on metal oxide particle surfaces under different environmental conditions.* Physical Chemistry Chemical Physics, 2009. **11**(37): p. 8295.

338. Overbury, S.H., et al., *Chemisorption and Reaction of Sulfur Dioxide with Oxidized and Reduced Ceria Surfaces.* The Journal of Physical Chemistry B, 1999. **103**(51): p. 11308-11317.

339. Mirsaleh-Kohan, N., A.D. Bass, and L. Sanche, *X-ray photoelectron spectroscopy analysis of gold surfaces after removal of thiolated DNA oligomers by ultraviolet/ozone treatment.* Langmuir : the ACS journal of surfaces and colloids, 2010. **26**(9): p. 6508-6514.

340. Hantsche, H., *Comparison of basic principles of the surface-specific analytical methods: AES/SAM, ESCA (XPS), SIMS, and ISS with X-ray microanalysis, and some applications in research and industry.* Scanning, 1989. **11**(6): p. 257-280.

341. Gericke, S.M., et al., *Water-polyamide chemical interplay in desalination membranes explored by ambient pressure X-ray photoelectron spectroscopy.* Physical Chemistry Chemical Physics, 2020. **22**(27): p. 15658-15663.

342. Ahmed, M. and O. Kostko, *From atoms to aerosols: probing clusters and nanoparticles with synchrotron based mass spectrometry and X-ray spectroscopy.* Physical Chemistry Chemical Physics, 2020. **22**(5): p. 2713-2737.

343. Schneider, M., A. Belsom, and J. Rappsilber, *Protein Tertiary Structure by Crosslinking/Mass Spectrometry.* Trends in biochemical sciences, 2018. **43**(3): p. 157-169.

344. Vericat, C., et al., *Self-assembled monolayers of thiols and dithiols on gold: new challenges for a well-known system.* Chemical Society Reviews, 2010. **39**(5): p. 1805.

345. Hu, X., et al., *Thiol and pH dual-responsive dynamic covalent shell cross-linked micelles for triggered release of chemotherapeutic drugs.* Polymer Chemistry, 2013. **4**(3): p. 695-706.

346. Aromaa, M.K. and P.K. Vallittu, *Delayed post-curing stage and oxygen inhibition of free-radical polymerization of dimethacrylate resin.* Dental Materials, 2018. **34**(9): p. 1247-1252.

347. Il'inchik, E., V. Volkov, and L. Mazalov, *X-ray photoelectron spectroscopy of boron compounds.* Journal of Structural Chemistry, 2005. **46**: p. 523-534.

348. Kuivila, H.G., A.H. Keough, and E.J. Soboczenski, *ARENEBORONATES FROM DIOLS AND POLYOLS1.* The Journal of Organic Chemistry, 1954. **19**(5): p. 780-783.

349. Mader, H.S. and O.S. Wolfbeis, *Boronic acid based probes for microdetermination of saccharides and glycosylated biomolecules.* Microchimica Acta, 2008. **162**(1-2): p. 1-34.

350. Marco-Dufort, B. and M.W. Tibbitt, *Design of moldable hydrogels for biomedical applications using dynamic covalent boronic esters.* Materials Today Chemistry, 2019. **12**: p. 16-33.

351. Schumacher, S., et al., *Benzoboroxole-modified nanoparticles for the recognition of glucose at neutral pH. Chem Sens 1:1-7.* Chemical Sensors, 2010. **1**: p. 1-7.

352. Jin, S., et al., *Carbohydrate recognition by boronolectins, small molecules, and lectins.* Medicinal research reviews, 2010. **30**(2): p. 171-257.

353. Brooks, W.L.A., C.C. Deng, and B.S. Sumerlin, *Structure–Reactivity Relationships in Boronic Acid–Diol Complexation.* ACS Omega, 2018. **3**(12): p. 17863-17870.

354. Dowlut, M. and D.G. Hall, *An Improved Class of Sugar-Binding Boronic Acids, Soluble and Capable of Complexing Glycosides in Neutral Water.* Journal of the American Chemical Society, 2006. **128**(13): p. 4226-4227.

355. Kim, Y., et al., *Sugar sensing based on induced pH changes.* Chemical Communications, 2007(22): p. 2299-2301.

356. Tran, P.A. and T.J. Webster, *Understanding the wetting properties of nanostructured selenium coatings: the role of nanostructured surface roughness and air-pocket formation.* International journal of nanomedicine, 2013. **8**: p. 2001-2009.

357. Bruel, C., et al., *Experimental methods in chemical engineering: Contact angles.* The Canadian Journal of Chemical Engineering, 2019. **97**(4): p. 832-842.

358. Hu, Y.-Z. and T.-B. Ma, *5.12 - Tribology of Nanostructured Surfaces☆*, in *Comprehensive Nanoscience and Nanotechnology (Second Edition)*, D.L. Andrews, R.H. Lipson, and T. Nann, Editors. 2019, Academic Press: Oxford. p. 309-342.

359. Reimers, J.R., et al., *Gold surfaces and nanoparticles are protected by Au(0)–thiyl species and are destroyed when Au(I)–thiolates form.* Proceedings of the National Academy of Sciences, 2016. **113**(11): p. E1424.

360. Cumming, G., F. Fidler, and D.L. Vaux, *Error bars in experimental biology.* The Journal of cell biology, 2007. **177**(1): p. 7-11.

361. Viitala, R., et al., *Device and method for measuring thickness variation of large roller element bearing rings.* Precision Engineering, 2019. **55**: p. 59-69.

362. Wu, X., et al., *Synthesis and catalytic activity of heteroatom doped metal-free single-wall carbon nanohorns.* 2016. **52**(31): p. 5391-5393.

363. Greczynski, G. and L. Hultman, *X-ray photoelectron spectroscopy: Towards reliable binding energy referencing.* Progress in Materials Science, 2020. **107**: p. 100591.

364. Lee, F.-Y., et al., *The chemical states and atomic structure evolution of ultralow-energy high-dose Boron implanted Si(110) via laser annealing.* Scientific Reports, 2017. **7**(1).

365. Drescher, D.G., N.A. Ramakrishnan, and M.J. Drescher, *Surface plasmon resonance (SPR) analysis of binding interactions of proteins in inner-ear sensory epithelia.* Methods in molecular biology (Clifton, N.J.), 2009. **493**: p. 323-343.

366. Homola, J., *Surface Plasmon Resonance Based Sensors*. Springer Series on Chemical Sensors and Biosensors. 2006: Springer Berlin Heidelberg.

367. Dixon, H.B.F., *Curves of ligand binding. The use of hyperbolic functions for expressing titration curves.* 1974. **137**(3): p. 443-447.

368. Sheehan, D., *Physical Biochemistry: Principles and Applications*. 2000: Wiley.

369. Prestwich, G.D., *14 - Chemical Studies of Pheromone Reception and Catabolism*, in *Pheromone Biochemistry*, G.D. Prestwich and G.J. Blomquist, Editors. 1987, Academic Press. p. 473-527.

370. Studnicka, G.M., *Hyperbolic regression analysis for kinetics, electrophoresis, ELISA, RIA, Bradford, Lowry, and other applications.* Bioinformatics, 1987. **3**(1): p. 9-16.

371. Motulsky, H. and A. Christopoulos, *Fitting Models to Biological Data Using Linear and Nonlinear Regression: A Practical Guide to Curve Fitting*. 2004: Oxford University Press.

372. Bérubé, M., M. Dowlut, and D.G. Hall, *Benzoboroxoles as efficient glycopyranoside-binding agents in physiological conditions: structure and selectivity of complex formation.* J Org Chem, 2008. **73**(17): p. 6471-9.

373. Kiessling, L.L., et al., *Multivalency in Protein–Carbohydrate Recognition*, in *Glycoscience: Chemistry and Chemical Biology*, B.O. Fraser-Reid, K. Tatsuta, and J. Thiem, Editors. 2008, Springer Berlin Heidelberg: Berlin, Heidelberg. p. 2483-2523.

374. Fu, M.X., et al., *Role of oxygen in cross-linking and chemical modification of collagen by glucose.* Diabetes, 1992. **41 Suppl 2**: p. 42-8.

375. Zhao, Y.Y., et al., *Functional roles of N-glycans in cell signaling and cell adhesion in cancer.* Cancer Sci, 2008. **99**(7): p. 1304-10.

376. Rudman, N., O. Gornik, and G. Lauc, *Altered N-glycosylation profiles as potential biomarkers and drug targets in diabetes.* FEBS Lett, 2019. **593**(13): p. 1598-1615.

377. Seppälä, M., et al., *Glycodelin: a major lipocalin protein of the reproductive axis with diverse actions in cell recognition and differentiation.* Endocr Rev, 2002. **23**(4): p. 401-30.

378. Miyamoto, S., et al., *Multiple Reaction Monitoring for the Quantitation of Serum Protein Glycosylation Profiles: Application to Ovarian Cancer.* J Proteome Res, 2018. **17**(1): p. 222-233.

379. Otvos, J.D., et al., *GlycA: A Composite Nuclear Magnetic Resonance Biomarker of Systemic Inflammation.* Clin Chem, 2015. **61**(5): p. 714-23.

380. Adamczyk, B., T. Tharmalingam, and P.M. Rudd, *Glycans as cancer biomarkers.* Biochim Biophys Acta, 2012. **1820**(9): p. 1347-53.

381. Tian, Y. and H. Zhang, *Glycoproteomics and clinical applications.* Proteomics Clin Appl, 2010. **4**(2): p. 124-32.

382. Polonskaya, Z., et al., *High-affinity anti-glycan antibodies: challenges and strategies.* Curr Opin Immunol, 2019. **59**: p. 65-71.

383. Syed, P., et al., *Role of lectin microarrays in cancer diagnosis.* Proteomics, 2016. **16**(8): p. 1257-65.

384. Sun, W., L. Du, and M. Li, *Aptamer-based carbohydrate recognition.* Curr Pharm Des, 2010. **16**(20): p. 2269-78.

385. Wu, X., et al., *Selective sensing of saccharides using simple boronic acids and their aggregates.* Chem Soc Rev, 2013. **42**(20): p. 8032-48.

386. Tommasone, S., et al., *The challenges of glycan recognition with natural and artificial receptors.* Chem Soc Rev, 2019. **48**(22): p. 5488-5505.

387. Wang, B. and G.-J. Boons, *Carbohydrate recognition: biological problems, methods, and applications*. Vol. 13. 2011: John Wiley & Sons.

388. Heimburg-Molinaro, J., et al., *Cancer vaccines and carbohydrate epitopes.* Vaccine, 2011. **29**(48): p. 8802-8826.

389. Li, L., et al., *Photolithographic boronate affinity molecular imprinting: a general and facile approach for glycoprotein imprinting.* Angewandte Chemie International Edition, 2013. **52**(29): p. 7451-7454.

390. Bérubé, M., M. Dowlut, and D.G. Hall, *Benzoboroxoles as efficient glycopyranoside-binding agents in physiological conditions: structure and selectivity of complex formation.* The Journal of organic chemistry, 2008. **73**(17): p. 6471-6479.

391. Zhang, J., et al., *Present status on removal of raff inose family oligosaccharides – a Review.* Czech Journal of Food Sciences, 2019. **37**: p. 141-154.

392. Correia, D.M., et al., *Dietary Sugars Analysis: Quantification of Fructooligossacharides during Fermentation by HPLC-RI Method.* Frontiers in nutrition, 2014. **1**: p. 11-11.

393. Mancini, R.S., J.B. Lee, and M.S. Taylor, *Boronic esters as protective groups in carbohydrate chemistry: processes for acylation, silylation and alkylation of glycoside-derived boronates.* Organic & Biomolecular Chemistry, 2017. **15**(1): p. 132-143.

394. Adamczyk-Woźniak, A., K.M. Borys, and A. Sporzyński, *Recent developments in the chemistry and biological applications of benzoxaboroles.* Chem Rev, 2015. **115**(11): p. 5224-47.

395. Neuber, T., et al., *Characterization and screening of IgG binding to the neonatal Fc receptor.* MAbs, 2014. **6**(4): p. 928-42.

396. Tommasone, S., et al., *The challenges of glycan recognition with natural and artificial receptors.* Chemical Society Reviews, 2019. **48**(22): p. 5488-5505.

397. Sterner, E., N. Flanagan, and J.C. Gildersleeve, *Perspectives on Anti-Glycan Antibodies Gleaned from Development of a Community Resource Database.* ACS Chemical Biology, 2016. **11**(7): p. 1773-1783.

398. Jung, P., S. Kang, and J. Lee, *Automated code-based test selection for software product line regression testing.* Journal of Systems and Software, 2019. **158**: p. 110419.

399. Das, C., et al., *Augmenting Sensitivity of Surface Plasmon Resonance (SPR) Sensors with the Aid of Anti-reflective Coatings (ARCs).* Photonics and Nanostructures - Fundamentals and Applications, 2019. **38**: p. 100760.

400. Paul, S.D., et al., *Chapter 12 - Novel gels: implications for drug delivery*, in *Nanostructures for Drug Delivery*, E. Andronescu and A.M. Grumezescu, Editors. 2017, Elsevier. p. 379-412.

401. Bhatia, S. and R. Dahiya, *Chapter 4 - Concepts and Techniques of Plant Tissue Culture Science*, in *Modern Applications of Plant Biotechnology in Pharmaceutical Sciences*, S. Bhatia, et al., Editors. 2015, Academic Press: Boston. p. 121-156.

402. Hopkins, E. and S. Sharma, *Physiology, Acid Base Balance*. 2019: StatPearls Publishing, Treasure Island (FL).

403. Rowe, L., G. El Khoury, and C.R. Lowe, *A benzoboroxole-based affinity ligand for glycoprotein purification at physiological pH.* J Mol Recognit, 2016. **29**(5): p. 232-8.

404. Lahiri, J., et al., *A Strategy for the Generation of Surfaces Presenting Ligands for Studies of Binding Based on an Active Ester as a Common Reactive Intermediate:A Surface Plasmon Resonance Study.* Analytical Chemistry, 1999. **71**(4): p. 777-790.

405. Ishii, T., et al., *Crystal structure of β-d,l-fructose.* Acta crystallographica. Section E, Crystallographic communications, 2015. **71**(Pt 10): p. o719-o720.

406. Di Pasquale, A., et al., *Cooperative Multipoint Recognition of Sialic Acid by Benzoboroxole-Based Receptors Bearing Cationic Hydrogen-Bond Donors.* The Journal of Organic Chemistry, 2020. **85**(13): p. 8330-8338.

407. Hulme, E.C. and M.A. Trevethick, *Ligand binding assays at equilibrium: validation and interpretation.* British journal of pharmacology, 2010. **161**(6): p. 1219-1237.

408. Norrild, J.C. and H. Eggert, *Boronic acids as fructose sensors. Structure determination of the complexes involved using 1JCC coupling constants.* Journal of the Chemical Society, Perkin Transactions 2, 1996(12): p. 2583-2588.

409. Joao, H.C. and R.A. Dwek, *Effects of glycosylation on protein-structure and dynamics in ribonuclease-b and some of its individual glycoforms.* European Journal of Biochemistry, 1993. **218**(1): p. 239-244.

410. Scheraga, H.A., W.J. Wedemeyer, and E. Welker, *[12] - Bovine Pancreatic Ribonuclease A: Oxidative and Conformational Folding Studies*, in *Methods in Enzymology*, A.W. Nicholson, Editor. 2001, Academic Press. p. 189-221.

411. Fournier, T., N. Medjoubi-N, and D. Porquet, *Alpha-1-acid glycoprotein.* Biochimica et Biophysica Acta (BBA) - Protein Structure and Molecular Enzymology, 2000. **1482**(1): p. 157-171.

412. Fernandes, C.L., R. Ligabue-Braun, and H. Verli, *Structural glycobiology of human α1-acid glycoprotein and its implications for pharmacokinetics and inflammation.* Glycobiology, 2015. **25**(10): p. 1125-1133.

413. Gruys, E., et al., *Acute phase reaction and acute phase proteins.* Journal of Zhejiang University. Science. B, 2005. **6**(11): p. 1045-1056.

414. Yang, B.Y., J.S.S. Gray, and R. Montgomery, *The glycans of horseradish peroxidase.* Carbohydrate Research, 1996. **287**(2): p. 203-212.

415. Zucker, R.S., D.M. Kullmann, and P.S. Kaeser, *Chapter 15 - Release of Neurotransmitters*, in *From Molecules to Networks (Third Edition)*, J.H. Byrne, R. Heidelberger, and M.N. Waxham, Editors. 2014, Academic Press: Boston. p. 443-488.

416. Escamilla, R. and L. Huerta, *X-ray photoelectron spectroscopy studies of non-stoichiometric superconducting NbB2+x.* Superconductor Science and Technology, 2004. **19**.

417. Figueiredo, T., et al., *Boronic acid and diol-containing polymers: how to choose the correct couple to form "strong" hydrogels at physiological pH.* Soft Matter, 2020. **16**(15): p. 3628-3641.

418. in *Essentials of Glycobiology*, A. Varki, et al., Editors. 2009, Cold Spring Harbor Laboratory Press

419. Jumelle, C., et al., *Comparison of four methods of surface roughness assessment of corneal stromal bed after lamellar cutting.* Biomedical optics express, 2017. **8**(11): p. 4974-4986.

420. Gadelmawla, E.S., et al., *Roughness parameters.* Journal of Materials Processing Technology, 2002. **123**: p. 133-145.

421. Köllensperger, G., et al., *Application of atomic force microscopy to particle sizing.* Fresenius' Journal of Analytical Chemistry, 1999. **363**(4): p. 323-332.

422. Patwa, T., et al., *Glycoprotein analysis using protein microarrays and mass spectrometry.* Mass spectrometry reviews, 2010. **29**(5): p. 830-844.

423. Filella, X., et al., *Emerging biomarkers in the diagnosis of prostate cancer.* Pharmacogenomics and personalized medicine, 2018. **11**: p. 83-94.

424. Bteich, M., *An overview of albumin and alpha-1-acid glycoprotein main characteristics: highlighting the roles of amino acids in binding kinetics and molecular interactions.* Heliyon, 2019. **5**(11): p. e02879-e02879.

425. Scholler, N. and N. Urban, *CA125 in ovarian cancer.* Biomarkers in medicine, 2007. **1**(4): p. 513-523.

426. Kailemia, M.J., D. Park, and C.B. Lebrilla, *Glycans and glycoproteins as specific biomarkers for cancer.* Analytical and bioanalytical chemistry, 2017. **409**(2): p. 395-410.

427. Gomes, A.M., et al., *Unique extracellular matrix heparan sulfate from the bivalve Nodipecten nodosus (Linnaeus, 1758) safely inhibits arterial thrombosis after photochemically induced endothelial lesion.* The Journal of biological chemistry, 2010. **285**(10): p. 7312-7323.

428. Akinkuolie, A.O., et al., *A Novel Protein Glycan Biomarker and Future Cardiovascular Disease Events.* Journal of the American Heart Association, 2014. **3**(5): p. e001221-e001221.

429. Przedborski, S., M. Vila, and V. Jackson-Lewis, *Neurodegeneration: what is it and where are we?* The Journal of clinical investigation, 2003. **111**(1): p. 3-10.

430. Jeynes, B. and J. Provias, *P-Glycoprotein Altered Expression in Alzheimer's Disease: Regional Anatomic Variability.* Journal of Neurodegenerative Diseases, 2013. **2013**: p. 1-7.

431. Lin, M., G. Chen, and M. Jiang, *Direct and indirect core–shell inversion of block copolymer micelles.* Polym. Chem., 2014. **5**(1): p. 234-240.

432. Lewis, S.N., et al., *Isothiazoles I: 4-isothiazolin-3-ones. A general synthesis from 3,3′-dithiodipropionamides.* Journal of Heterocyclic Chemistry, 1971. **8**(4): p. 571-580.

CHAPTER 8 – APPENDIX

Targeting Oligosaccharides and Glycoconjugates Using Superselective Binding Scaffolds

Stefano Tommasone, Yazmin K. Tagger, Paula M. Mendes

First published: 28 May 2020

https://doi.org/10.1002/adfm.202002298

The copyright line for this article was changed on 25 May 2020 after original online publication.

Abstract

Recognition of oligosaccharides is associated with very limited specificity due to their strong solvation in water and the high degree of subtle structural variations between them. Here, oligosaccharide recognition sites are created on material surfaces with unmatched, binary on–off binding behavior, sharply discriminating a target oligosaccharide over closely related carbohydrate structures. The basis for the superselective binding behavior relies on the highly efficient generation of a pure, high order complex of the oligosaccharide target with synthetic carbohydrate receptor sites, in which the spatial arrangement of the multiple receptors in the complex is preserved upon material surface incorporation. The synthetic binding scaffolds can easily be tailored to recognize different oligosaccharides and glycoconjugates, opening up a realm of possibilities for their use in a wide field of applications, ranging from life sciences to diagnostics.

1 Introduction

Oligosaccharides, which often occur as glycoconjugates, play essential roles within a multitude of biological processes, including fertilization, cell differentiation, cell signaling, and host–pathogen interactions.[1-4] Furthermore, they are emerging as important biomarkers for a wide range of diseases, including immune deficiencies, hereditary disorders, neurodegenerative and cardiovascular diseases, and many types of cancers.[5-7]Thus, materials with highly specific oligosaccharide recognition are key for advancing glycobiology research and producing new opportunities to diagnose and treat diseases. However, the approaches used today, that rely on anticarbohydrate antibodies,[8] lectins,[9]aptamers,[10] and synthetic carbohydrate receptors,[11] are limited in their capabilities to discriminate between a large repertoire of carbohydrate structures, including closely related isomers.[12] For instance, natural and recombinant lectins exhibit specificity only toward a particular carbohydrate motif or structural feature and are available in a very limited number when compared with the striking variety of oligosaccharide structures.[13] On the other hand, oligosaccharides are poorly immunogenic, posing major hurdles in the development of highly selective anticarbohydrate antibodies.[14] Examples of aptamers that evolved to recognize oligosaccharides are scarce owing to the limited number of noncovalent interactions that can be harnessed between carbohydrates and oligonucleotides.[15, 16] Synthetic carbohydrate receptors, including boronic acid moieties, which form reversible covalent complexes with diols, have been combined with molecular imprinting to obtain carbohydrate binding sites on polymer matrices.[17, 18] However, the available synthetic approaches are incapable to encode the binding sites with precise molecular

complementarity to target oligosaccharides. Here, we report on a modular synthetic approach that harnesses both the construction of high-yield, complex oligosaccharide–synthetic carbohydrate receptor assemblies and the precise generation of surface-confined templated binding sites (**Figure 1**), thereby creating recognition sites of unparalleled oligosaccharide discrimination. Benzoboroxoles are employed as carbohydrate receptors since, in contrast to their boronic acids analogs, benzoboroxoles can bind nonreducing hexopyranosides at pH values compatible with biological systems.[19]

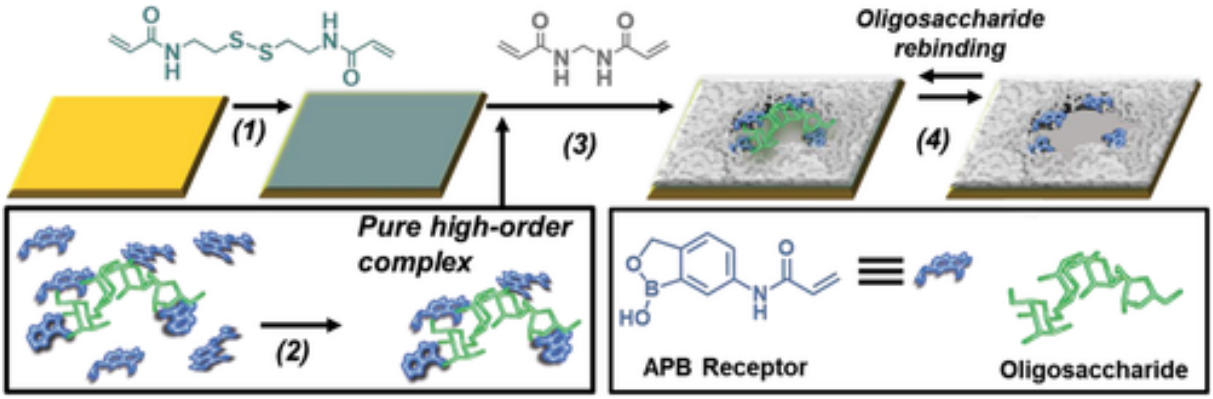

Figure 1 Method for creating synthetic materials with superselective oligosaccharide recognition. 1) Acrylamide-terminated monolayer formation using *N,N′*-bis(acryloyl)cystamine; 2) pure, high-order oligosaccharide: 5-acrylamido-2-(hydroxymethyl)phenylboronic acid cyclic monoester (APB) complex formation; 3) fixation of the complex on the surface and construction of molecular scaffold around the oligosaccharide template using *N,N′*-methylenebisacrylamide; 4) removal of the oligosaccharide template.

2 Results and Discussion

Initially, we demonstrated the feasibility of creating stable, high-order complexes between oligosaccharides and benzoboroxoles using three model oligosaccharides, namely, stachyose **1**, nystose **2**, and verbascose **3**. Optimum complexation conditions were achieved by stirring for 24 h a mixture of an excess of 2-(hydroxymethyl)phenylboronic acid cyclic monoester **4** (8.0 equivalents per sugar unit) and oligosaccharide in dioxane:acetonitrile (6:1 v/v) at 90 °C. These conditions provided the optimal compromise for both solubility and reaction temperature. An indirect method has been devised, using partial chemical benzoylation and mass spectrometry analysis, for obtaining a relative estimate of the different high-order complexes formed (Figure S1, Supporting Information). Following complexation, the resulting complex was treated with benzoyl chloride in pyridine for 5 h, in order to functionalize the OH groups not involved in any bond with the boron. Afterward, the boronate esters were hydrolyzed by treatment with 1 m aqueous solution of sorbitol/Na_2CO_3 and EtOAc, and the product was finally recovered by several washings with EtOAc.[20] Together with the known binding mechanism of boronic acid derivatives with diols,[19, 21] the analysis of the resulting product gave us insight into the efficiency of the complexation and the structure of the complexes formed (more details in Figures S2–S8 in the Supporting Information). These analyses demonstrated that the highest-order complexes were preferentially formed (**Table 1**). For instance, while stachyose **1** can interact with benzoboroxoles to form complexes with stoichiometry ranging from 1:1 up to 1:4, the results indicate that stachyose was able to form complexes with benzoboroxoles in high 1:3 and 1:4 stoichiometric ratios, with a greater

proportion of 1:4 (80%) than 1:3 (20%) complex. Benzoboroxoles usually bind fructose units in positions 2 and 3. However, according to the structure of nystose **2**, the hydroxyls in positions 2 are not accessible since they are involved in the formation of glycosidic bonds. Nevertheless, with nystose, we observed the formation of high-order complexes, as we found evidence of a 1:3 adduct and some 1:4 (maximum degree of complexation). A possible explanation is that the binding takes place via the OH in position 3 and 6, which are in a sin-periplanar relationship.[22] This demonstrates that our approach can push the formation of boronate esters even when the conditions are less favorable, as well as being of general applicability since it affords high-order complexes with oligosaccharides with different sizes and stereochemistry.

Table 1. Degree of complexation of different oligosaccharides, stachyose 1, nystose 2, and verbascose 3 with 2-(hydroxymethyl)phenylboronic acid cyclic monoester 4. Relative ratios (%) of complexes derived by the MALDI spectra of the products isolated after column chromatography following the approach in Figure S1 (Supporting Information)

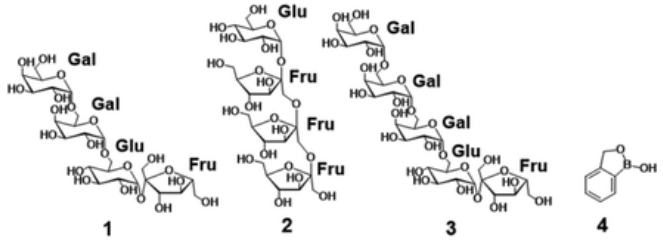

Oligosaccharide	Sugar units	Complex (%) 1:5	1:4	1:3	1:2	1:1
1	4	-	80	20	0	0
2	4	-	15	69	16	0
3	5	33	53	14	0	0

The construction of the oligosaccharide binding scaffolds was initiated by immersing clean gold substrates in a 0.1 × 10^{-3} m ethanolic solution of *N,N′*-bis(acryloyl)cystamine with 2% trifluoracetic acid (TFA) for 24 h. The formation of the

acrylamide-terminated self-assembled monolayers (SAMs) was confirmed by contact angle (advancing and receding contact angles of 78 ± 1° and 62 ± 2°, respectively), ellipsometry (thickness of 0.56 ± 0.06 nm), and X-ray photoelectron spectroscopy (XPS). XPS peaks (Figure S9, Supporting Information) account for the presence of C (1s), O (1s), N (1s), and S (2p), with the binding energies of the S (2p) peaks at 161.6 and 162.8 eV, indicating the chemisorption of the *N,N′*-bis(acryloyl)cystamine on the gold surface through S—Au bonds.

We initially created oligosaccharide-binding scaffolds using stachyose as the template. Following its complexation with 5-acrylamido-2-(hydroxymethyl)phenylboronic acid cyclic monoester (APB; Figure **1**), the complex and free APB were separated by precipitation followed by centrifugation. This protocol enabled us to remove the excess of unreacted APB, which otherwise would have had a detrimental effect in creating precise recognition sites for oligosaccharides. The binding scaffolds were prepared by grafting simultaneously *N,N′*-methylenebisacrylamide (MBA) and the high-order complexes between stachyose and APB onto the acrylamide-terminated SAMs for 15 min. Following dissociation of the oligosaccharide from the surface under acidic conditions, the binding affinity and selectivity of the stachyose-binding scaffolds was evaluated using surface plasmon resonance (SPR) spectroscopy. Stachyose and three structurally related oligosaccharides, namely, nystose, raffinose, and melezitose, were employed to evaluate the selectivity of the binding scaffolds. The SPR sensorgrams of the binding scaffolds prepared using stachyose as a template reveal a striking difference in binding between the target stachyose oligosaccharide (**Figure 2A**) and nontarget oligosaccharides (e.g., nystose; Figure **2B**), with the

formed binding sites allowing for a great degree of subtlety in recognizing stachyose. SPR binding analysis show that stachyose binds the stachyose-binding scaffolds with a dissociation constant (K_D) of 0.83 × 10^{-3} m, while no or negligible binding was observed for the nontarget oligosaccharides (Figure **2C**). In creating a nystose-binding scaffold, the selectivity is reversed and instead the recognition sites can only bind nystose, with a K_D of 0.65 × 10^{-3} m (Figure **2D**).

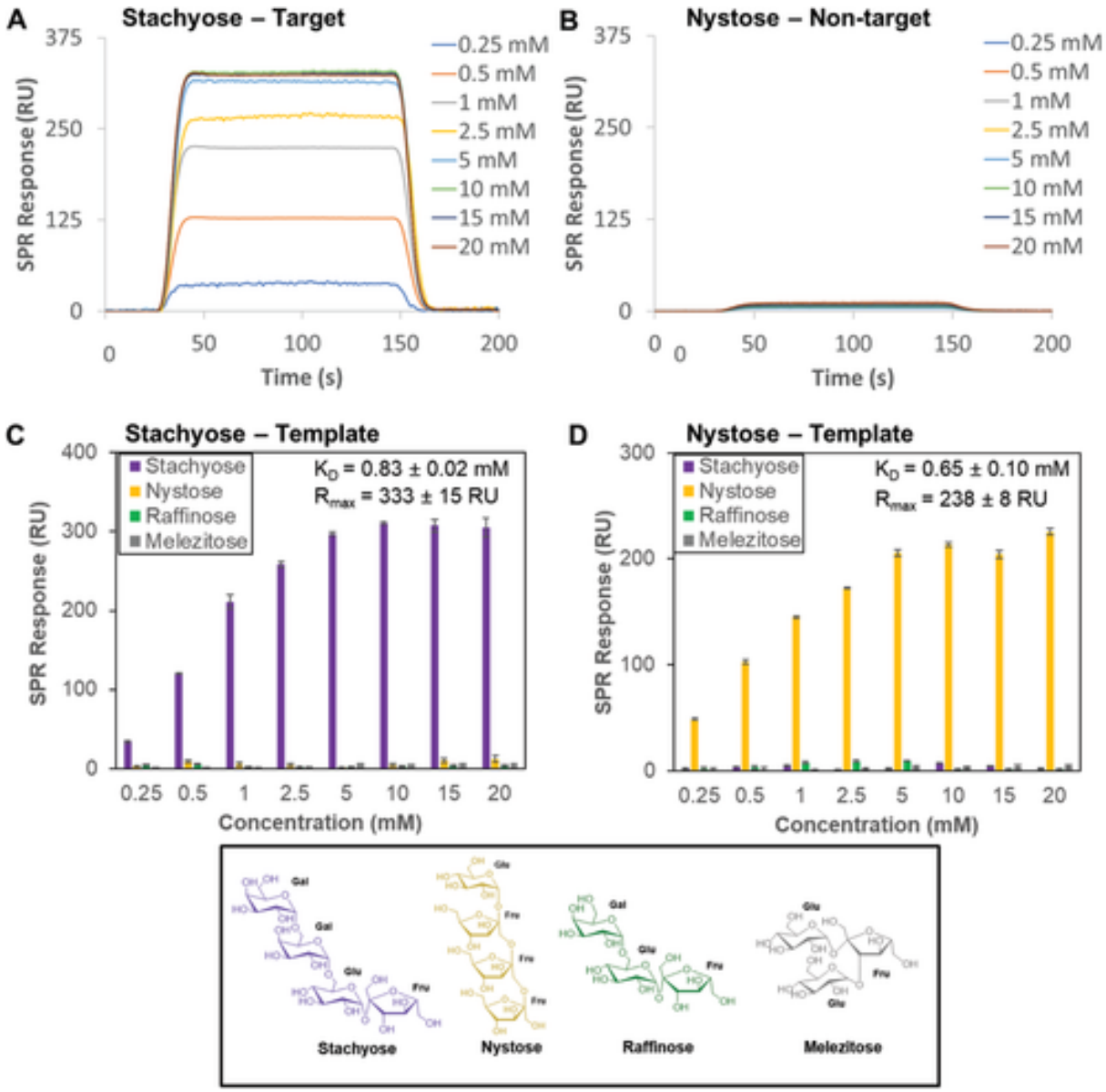

Figure 2 SPR sensorgram traces performed on binding scaffolds prepared on SPR chips using stachyose as a template and different concentrations of A) stachyose and B) nystose flowed over the surface at pH 7.4. SPR responses at equilibrium against the concentration of injected oligosaccharides, stachyose, nystose, raffinose and melezitose (shown at the bottom) using C) stachyose-binding scaffolds and D) nystose-binding scaffolds, from which K_D and R_{max} values have been obtained.

The dissociation constants of benzoboroxoles for monosaccharides are largely dependent on their structure, with reported K_D values for fructose, glucose and methyl α-d-galactopyranoside of 2.95, 32.3, and 34.5 × 10^{-3} m, respectively.[23] Thus, the surface-confined binding scaffolds resulted in 5–50-fold higher binding affinity for the target oligosaccharide as compared to monosaccharides. This behavior suggests that multivalent interactions are occurring between multiple benzoboroxoles receptors incorporated in the binding site with multiple hydroxyl groups within the oligosaccharide chain. While the binding affinity is comparable to that of oligosaccharide antibodies and lectins with dissociation constants in the low mm range,[12, 24] our oligosaccharide recognition sites exhibit an unprecedented binary on–off oligosaccharide binding behavior.

The achieved maximum binding capacity (R_{max}) for the stachyose- and nystose-binding scaffolds was in the range of 0.2–0.3 ng mm^{-2} (100 response units (RUs) = 0.1 ng mm^2[25]), corresponding to 1 oligosaccharide per 6–4 nm^2. Assuming a footprint of approximately 2–3 nm^2 for a tetrasaccharide,[26] an estimated 50% surface coverage by oligosaccharide can be achieved. The remaining surface area comprises crosslinked MBA, which defines the pocket shape and size of the oligosaccharide used

as template, enhancing to some extent its binding affinity. A control surface obtained by grafting only high-order complexes between stachyose and APB onto the acrylamide-terminated SAMs for 15 min (i.e., absence of MBA) has led to similar superselectivity for stachyose (**Figure 3A**), but a slightly higher K_D value of (0.93 ± 0.13) × 10^{-3} m. The MBA is a crosslinking agent that allows building a molecular scaffold around the template. Apart from creating a shape complementary to the template, MBA can provide additional weak interactions with carbohydrates (i.e., hydrogen bonds) which could enhance the affinity for the target template. However, in our case only a slightly increase in the binding affinity was observed (K_D of 0.83 × 10^{-3} m with MBA, Figure **2C** vs 0.93 × 10^{-3} m without MBA, Figure **3A**). This is probably because either the thickness of the polymer layer is too small and does not allow, the MBA to have a significant effect on the overall binding or the crosslinker does not make the surface rigid enough to affect the properties of the binding site.

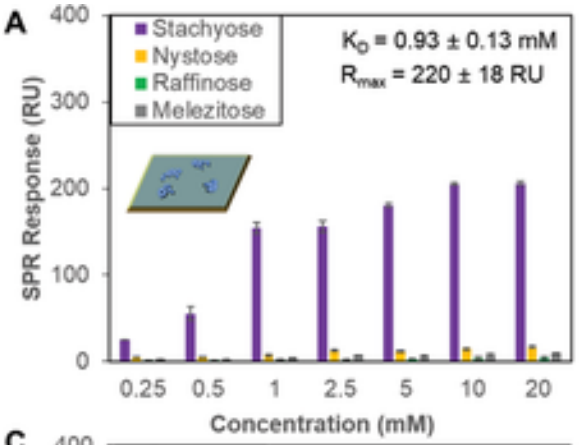

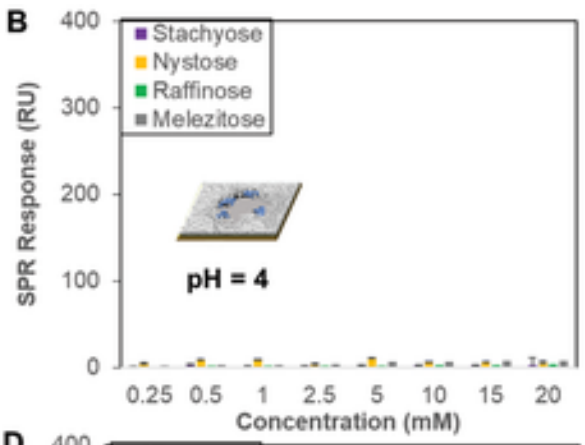

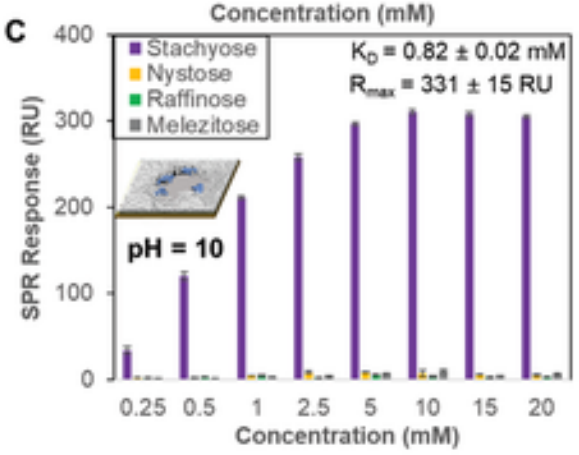

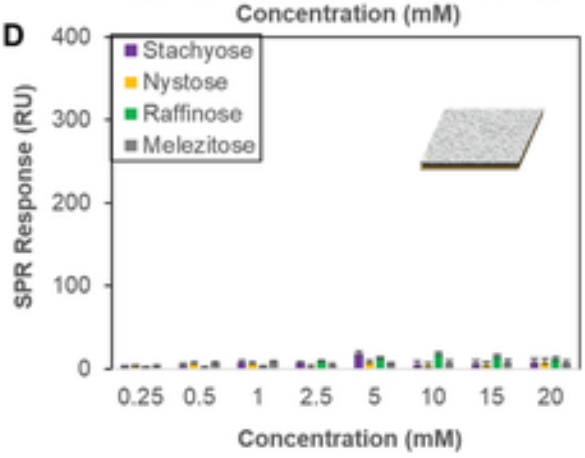

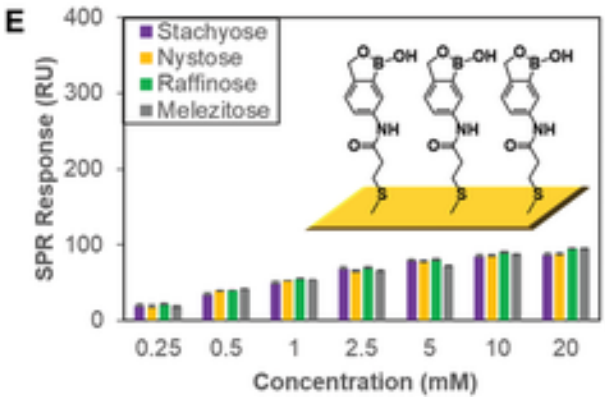

Oligosaccharide	K_D (mM)	R_{max} (RU)
Stachyose	1.85 ± 0.06	94 ± 8
Nystose	1.61 ± 0.05	92 ± 7
Raffinose	1.71 ± 0.08	98 ± 7
Melezitose	1.57 ± 0.05	93 ± 8

Figure 3 SPR responses at equilibrium against the concentration of injected oligosaccharides, stachyose, nystose, raffinose, and melezitose. A) Acrylamide-terminated SAMs with only high-order complexes between stachyose and APB grafted on it (i.e., absence of MBA) using pH 7.4 oligosaccharide solutions. B) pH 4 and C) pH 10 oligosaccharide solutions were employed to run SPR on stachyose-binding scaffolds. D) Surfaces prepared by copolymerizing MBA onto the acrylamide-

terminated SAMs using pH 7.4 oligosaccharide solutions. E) Benzoboroxole-terminated SAMs using pH 7.4 oligosaccharide solutions. The table illustrates the K_D and R_{max} values obtained for the different oligosaccharides used.

The presence of the benzoboroxole receptors in the recognition site is crucial to establish the selective binding for the target oligosaccharide. At pH 7.4, the binding scaffolds showed higher binding for the target oligosaccharide such as stachyose due to the benzoboroxole moieties forming boronate esters with stachyose, whereas no binding occurred at pH 4 (Figure **3B**) since boronate ester formation is less favorable in acidic conditions. While acidic conditions disrupt binding, the stachyose-binding scaffolds displayed similar binding behavior towards stachyose at pH 7.4 (K_D = 0.83± 0.02, Figure **2C**) and pH 10 (K_D = 0.82± 0.02, Figure **3C**). Furthermore, control experiments involving only the copolymerization of MBA onto the acrylamide-terminated SAMs have led to negligible binding to all the oligosaccharides (Figure **3D**), indicating that selectivity arises from the binding pockets containing the suitably spatially arranged benzoboroxole receptors.

Our findings provide evidence of the importance of precise and multivalent spatial pattern recognition to achieve superselective oligosaccharide binding. When we take into consideration that stachyose is a higher homolog of raffinose and an all-or-nothing binding occurs between them, it indicates that the nature of the superselective behavior is likely associated with a threshold in binding stability. The precise spatial arrangement of the receptors promotes the establishment of multiple interactions with the target oligosaccharide, stabilizing the binding event with consequent

enhanced K_D values, which is otherwise not possible with oligosaccharides that do not match the binding site. Although raffinose could potentially fit the binding sites of stachyose-binding scaffolds, it is probably not able to establish enough interactions to overcome the energetic requirements to reach an observable binding. This interpretation is supported by control experiments, wherein a surface comprising a monolayer of benzoboroxoles show similar binding for stachyose, nystose, raffinose and melezitose (Figure **3E**), with K_D values in the range (1.58–1.86) × 10^{-3}m. The presence of a high density of benzoboroxoles on the surface is not able to provide a specific spatial arrangement to regulate binding stability of target and nontarget oligosaccharides, with these surfaces allowing the binding of all the oligosaccharides. The superselectivity of our system could find some analogy in a mechanism previously proposed,[27] where the binding energy is not a linear function of the number of bonds but grows more rapidly. In fact, we were able to distinguish between a ligand that can form three bonds (raffinose) and one that can form four (stachyose), with an all-or-nothing behavior. However, we believe that the superselectivity of our system also accounts for an additional contribution, which could be related to geometrical factors. A fine control of the shape complementarity of the binding site could explain why we can also discriminate between oligosaccharides with the same number of ligands (stachyose and nystose). Another point to consider is that benzoboroxoles have different binding affinities for different carbohydrates (Gal, Glu, and Fru), therefore each sugar unit of the oligosaccharides interacts with the receptors in a different way.

The power of the methodology was further demonstrated by the capability of the novel binding scaffolds to bind specifically their glycoconjugates (**Figure 4**). Ribonuclease B

(RNase B) contains a single glycosylation site of high-mannose type with 5–9 mannose residues, Man5–Man9.[28] Binding scaffolds using Man5 as the template were shown to bind only RNase B and not the nonglycosylated RNase form, RNase A, and two highly glycosylated glycoproteins, α1-acid glycoprotein (AGP) and horseradish peroxidase (HRP). AGP (45% glycosylation) possesses complex-type glycans that are strongly sialylated,[29] while HRP (21% glycosylation) consists predominantly of the oligosaccharide (Xyl)Man3(Fuc)GlcNAc2, containing only low levels of the high mannose-type glycan.[30]

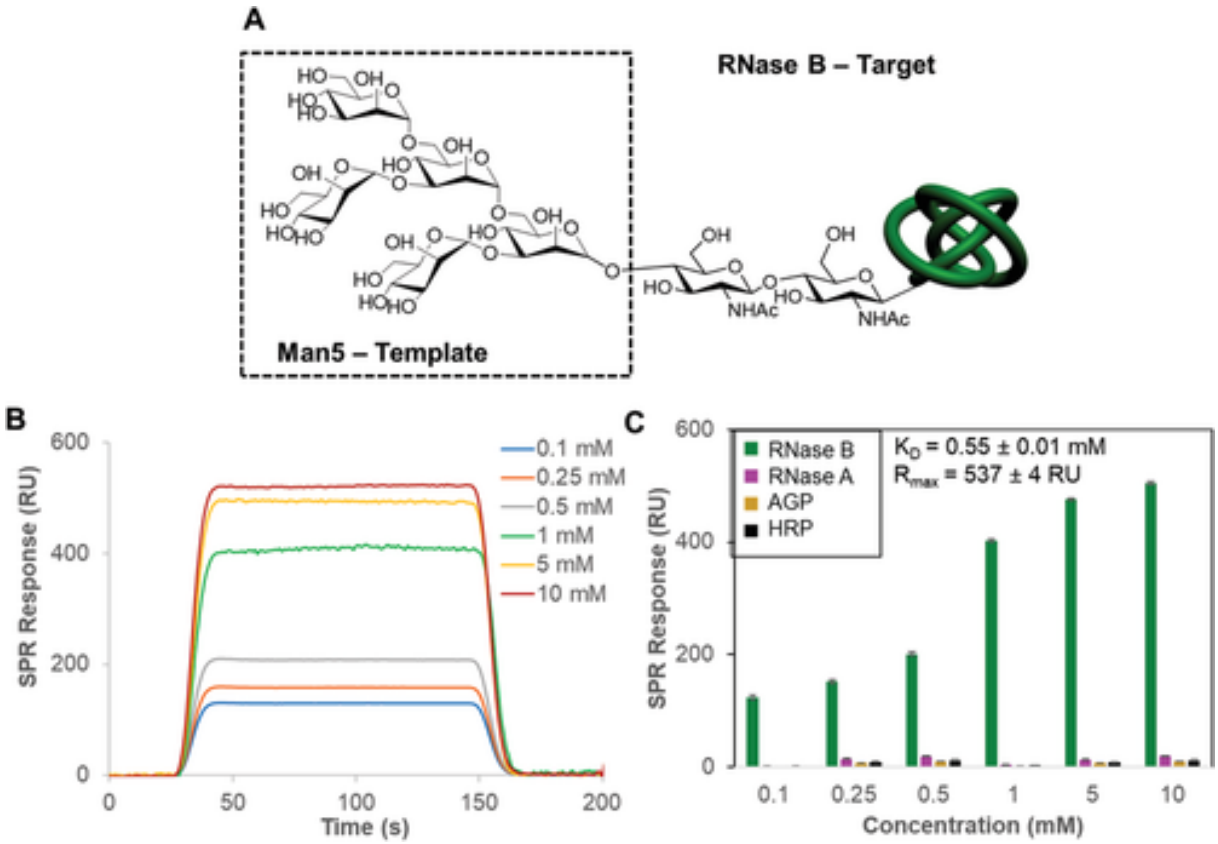

Figure 4 A) The oligosaccharide structure of the Man5 glycoform of RNase B, of which Man5 was used as a template for the generation of the binding scaffolds. The Man6–Man9 RNase B glycoforms contain further mannose units, which are added to the outer three mannose residues in Man5. B) SPR sensorgram traces performed with Man5-

binding scaffolds on the SPR chip and different concentrations of RNase B flowed over the surface. C) SPR responses at equilibrium against the concentration of injected protein, RNase B, RNase A, AGP, and HRP using Man5-binding scaffolds, from which K_D and R_{max} values have been obtained.

3 Conclusion

In conclusion, a unique modular strategy, which harnesses supramolecular assembly and well-controlled chemistry, was developed to create robust and highly reproducible template-induced oligosaccharide recognition sites on synthetic scaffolds. Our findings show that our approach has a remarkable ability to deliver synthetic receptors capable of highly specifically targeting oligosaccharides whether they occur in free form or as components of glycoproteins. These results go beyond the scope of the oligosaccharides described here, with the modularity of the synthetic strategy lending itself to adaptivity and incorporation into technologies for diagnostics, biotechnology, and glycobiology research.

Acknowledgements

S.T. and Y.K.T. contributed equally to this work. The authors thank Dr. Chi Tsang for technical assistance with mass spectrometry analysis. The authors also acknowledge financial support of this work by the EPSRC (EP/K027263/1), ERC (Consolidator Grant 614787), MRC (MC_PC_15032), and Prostate Cancer UK (RIA17-ST2-020). The other authors declare that they have no competing interests.

Conflict of Interest

A patent has been filled by the University of Birmingham related with the modular, synthetic strategy reported in this article under WO2015/118294. P.M.M is an author on the patent. The other authors declare that they have no competing interests.

References

Available online.